Endowing Organometallic Catalysts with a Genetic Memory: Artificial Metalloenzymes

Fabian Schwizer,[1,‡] Yasunori Okamoto,[1,‡] Tillmann Heinisch,[1,‡] Yifan Gu,[2,‡] Michela M. Pellioni,[1,‡] Vincent Lebrun,[1,‡] Raphael Reuter,[1,‡] Valentin Köhler,[1,‡] Jared C. Lewis[2,*] and Thomas R. Ward[1,*]

[1]Department of Chemistry, Spitalstrasse 51, University of Basel, CH-4056 Basel, Switzerland.
[2]Searle Chemistry Laboratory, University of Chicago, 5735 S. Ellis Ave., Chicago, IL 60637, USA.

‡ equal contribution
address correspondance to jaredlewis@uchicago.edu or thomas.ward@unibas.ch.

Acknowledgements. TRW thanks the Swiss National Science Foundation and more recently the NCCR "Molecular Systems Engineering" for generously funding his research on artificial metalloenzymes. JCL similarly thanks the David and Lucile Packard Foundation, the U.S. Army Research Office (62247-LS), and the NSF (CHE-1351991).

Yifan Gu received his B.S. in Chemistry from Peking University in 2011 under Professor Zhangjie Shi. He is a current Ph.D. student under Professor Jared C. Lewis at the University of Chicago. In 2016, he received the Eugene Olshansky Memorial Fellowship from the University of Chicago to continue his research on the use of artificial metalloenzymes in olefin polymerization and photoredox catalysis. His research interests also include cofactor design, artificial metalloenzymes construction, and biocatalysis.

Tillmann Heinisch obtained his PhD in Chemistry and Protein Crystallography at the University of Basel under Profs. T. Ward and T. Schirmer. After joining the group of Prof. Frances Arnold at Caltech for postdoctoral research, he returned to Basel for a second postdoc. His research interests include the structure-based engineering of artificial metalloenzymes.

Valentin Köhler studied chemistry at the University of Göttingen, Germany, followed by a PhD thesis with A. Pfaltz in asymmetric transition metal catalysis at the University of Basel. During his postdoctoral studies he focused first on oxidative biocatalysis in the groups of N. J. Turner and S. L. Flitsch (University of Manchester, United Kingdom) before combining synthetic transition metal catalysis and protein control in the investigation of hybrid catalyst systems with Prof. Ward. Since 2014 he holds a permanent position as a scientific coworker at the University of Basel which gratifyingly permits some independent research. His current research interests extend to protein modification and peptide design for unusual applications outside of catalysis.

Vincent Lebrun received his PhD in chemistry in 2014 from the University Grenoble Alpes under the guidance of Dr. O. Sénèque and Dr. J.-M. Latour. During this time, he worked

on peptidic models of zinc fingers. He currently is a postdoc fellow in the group of Prof. T. R. Ward, focusing on the use of peptides to control the activity of artificial metalloenzymes.

Jared C. Lewis received his B.S. in chemistry in 2002 from the University of Illinois, working with Eric Oldfield, and his Ph. D. in 2007 from the University of California, Berkeley under the direction of Jonathan Ellman and Robert Bergman. He carried out postdoctoral research in Frances Arnold's laboratory at the California Institute of Technology. He began his independent career in 2011 at the University of Chicago, where he is an Assistant Professor. His research involves engineering and evolving natural and artificial enzymes for selective catalysis.

Yasunori Okamoto received his Ph.D. from Osaka University (Japan) in 2014 under the supervision of Prof. T. Hayashi. During and after his Ph.D., he joined Prof. D. M. Kurtz's group at University of Texas at San Antonio (US) and Prof. S. Aono's group at National Institute of Natural Science (Japan). Since 2014 he is postdoctoral fellow in the group of Prof. T. R. Ward and was recently awarded a JSPS fellowship to implement artificial metalloenzymes in mamalian cells for therapeutic purposes.

Michela M. Pellioni received her B.S. degree in Pharmaceutical Biotechnology in 2009 and her M.S. degree in Biotechnology Medicine in 2011 from the University of Milan. She earned her PhD degree in Pharmaceutical Sciences from the University of Milan in 2015 on the development of hybrid systems based on new chiral aminophosphine and diamine ligands and their applications in asymmetric synthesis. She then joined the group of Prof. Ward to work on the development of new catalytic reactions and protein scaffold engineering for *in vivo* catalysis with ArMs.

Raphael Reuter was born in Weil am Rhein, Germany. He obtained his BSc and MSc in chemistry at the university of Basel and did his PhD from 2008 to 2011 in the group of Prof. Dr. Hermann A. Wegner, working on the synthesis and properties of macrocyclic oligoazobenzenes. From 2012 to 2016 he was a postdoctoral fellow in the group of Prof. Ward on *in vivo* olefin metathesis. He now works for Dottikon Exclusive Synthesis.

Fabian Schwizer received his M.Sc. in Chemistry from the University of Basel in 2013 on chemo-genetic engineering of artificial metalloenzymes. He then joined the Ward-group for a PhD and is interested to implement *in vivo* catalysis with artificial metalloenzymes in *E. coli* cells.

Thomas R Ward obtained his PhD in homogeneous catalysis from the ETHZ (1991). Following a postdoc with R. Hoffmann (Cornell University, theoretical chemistry) and C. Floriani (Univ. Lausanne, organometallic chemistry), he initiated his independent career at the University of Berne in 1993. In 2000, he moved to the University of Neuchâtel and initiated his research on artificial metalloenzymes. He moved to the University of Basel in 2008. Since 2016, he is the director of the National Compentence Center in Research

“Molecular Systems Engineering”. He was recently awarded an ERC advanced grant to realize his DrEAM: the Directed Evolution of Artificial Metalloenzymes for *in vivo* catalysis.

Abstract

The incorporation of a synthetic, catalytically competent metallocofactor into a protein scaffold to generate an artificial metalloenzyme (ArM) has been explored since the late 1970s. Progress in the ensuing years was limited by the tools available for both organometallic synthesis and protein engineering. Advances in both of these areas, combined with increased appreciation of the potential benefits of combining attractive features of both homogeneous catalysis and enzymatic catalysis, led to a resurgence of interest in ArMs starting in the early 2000s. Perhaps the most intriguing of potential ArM properties is their ability to endow organometallic catalysts with a genetic memory. Incorporating an organometallic catalyst into a genetically-encoded scaffold offers the opportunity to improve ArM performance by directed evolution. This capability could, in turn, lead to improvements in ArM efficiency similar to those obtained for natural enzymes, providing systems suitable for practical applications and greater insight into the role of second coordination sphere interactions in organometallic catalysis.

Since its renaissance in the early 2000s, different aspects of artificial metalloenzymes have been extensively reviewed and highlighted. Our intent is to provide a comprehensive overview of all work in the field to date, organized according to reaction class. Because of the wide range of non-natural reactions catalyzed by ArMs, this was done using a functional-group transformation classification. The review begins with a summary of the proteins and the anchoring strategies used to date for the creation of ArMs, followed by a historical perspective. Then follows a summary of the reactions catalyzed by ArMs and a concluding critical outlook. This analysis allows for comparison of similar reactions catalyzed by ArMs constructed using different metallocofactor anchoring strategies, cofactors, protein scaffolds, and mutagenesis strategies. These data will be used to construct a searchable website on ArMs that will be updated regularly by the authors.

Table of Contents

1. Introduction

Artificial metalloenzymes (ArMs) result from the incorporation of a catalytically competent metallocofactor into a protein scaffold. Initial attempts to construct ArMs were reported by Wilson and Whitesides as well as Kaiser and coworkers in the late 1970s.[1-2] Despite several fascinating aspects of these hybrid catalysts, Whitesides concluded his article by stating "the catalytic system (...) is not a practical asymmetric catalyst."[2] Unfortunately, following this pronouncement, relatively little progress was made toward ArM development until the new millennium. Setting aside the question of whether practicality should dictate the course of scientific inquiry, it is certainly the case that ArM construction in those early days was limited by the tools available for both organometallic synthesis and protein engineering. Significant progress in these areas contributed to the revival in ArM research that continues to this day.

The resurgence of interest in ArMs was also driven by increased appreciation of the potential benefits of combining attractive features of both homogeneous catalysis and enzymatic catalysis, Table 1. For example, the ArM secondary coordination sphere could interact with metal catalysts, substrates, or intermediates to facilitate reactions or to discriminate similarly reactive sites on substrates. ArMs could also be generated from protein scaffolds with inherent functionality (e.g. catalytic activity, substrate binding, redox properties, etc.) that could be used to augment ArM function. Perhaps more intriguingly, ArMs could endow organometallic catalysts with a genetic memory. Incorporating a organometallic catalyst within a genetically-encoded scaffold offers the opportunity to improve the ArM performance by mutagenesis. Ultimately, this could enable Darwinian evolution schemes for ArM optimization. Introduced in the early nineties by Frances Arnold and Pim Stemmer,[3-4] directed evolution has had a revolutionary impact on biotechnology,[5-

[7] leading to catalysts that have supplanted well-established large-scale processes based on homogeneous catalysts.[8] Similar optimization of ArMs could ultimately led to systems suitable for practical applications, and provide greater insight into the role of second coordination sphere interactions in organometallic catalysis.

Table 1. Comparison of homogeneous and enzymatic catalysts.

	Homogeneous Catalysts	**Enzymes**
Access to both enantiomers of product	straightforward	challenging
Solvent tolerance	mostly organic solvents	mostly aqueous
Reaction repertoire	broad	limited
Optimization	chemical	genetic
Second coordination sphere	ill-defined	well-defined
Catalyst lifetime	limited	extended
In vivo compatibility	limited	excellent

Four complementary strategies have been implemented to localize metallocofactors within a well defined second coordination sphere environment, provided by the host protein: i) covalent, ii) supramolecular, iii) dative and iv) metal substitution, Figure 1.

i) Covalent anchoring, reminiscent of the well-established bioconjugation techniques,[9] involves a high-yielding and irreversible reaction between cofactors bearing a reactive functional group and an amino acid side-chain on the protein scaffold. Common reactions used for ArM formation include: a) nucleophilic attack by cysteine or another uniquely activated residue on an electrophilic moiety (maleimide, α-halocarbonyl, etc.) on the cofactor, b) disulfide bond formation between cysteine and a cofactor substituted with an electrophilic sulfur moiety, and c) Huisgen [3+2]-cycloaddition between an unnatural amino acid bearing a terminal alkyne or azide with an azide- or alkyne-substituted cofactor.[10]

ii) Supramolecular anchoring exploits the high affinity that proteins may display for a limited set of non-covalent inhibitors, natural cofactors or substrates. Covalent

modification of these with the cofactor may, in some cases, maintain a high affinity, thus ensuring quantitative localization of the cofactor within the host protein.

iii) Dative anchoring relies on the coordination of a nucleophilic amino acid residue (His, Cys, Glu, Asp, Ser etc.) to a coordinately unsaturated metal center. This type of anchoring and activation of the metal often complements either covalent or supramolecular strategies.

iv) Metal substitution builds upon the unique reactivity of non-native metals combined with the exquisitely tailored active site of natural metalloenzymes. Upon substituting the metal, new-to-nature reactivities can be introduced in the ArM's repertoire.[11] This strategy builds upon the very elegant enzyme repurposing approach introduced by Frances Arnold in 2013.[12-14] A complete coverage of the enzyme repurposing strategy is presented by Fasan and coworkers in this issue of *Chemical Reviews*.

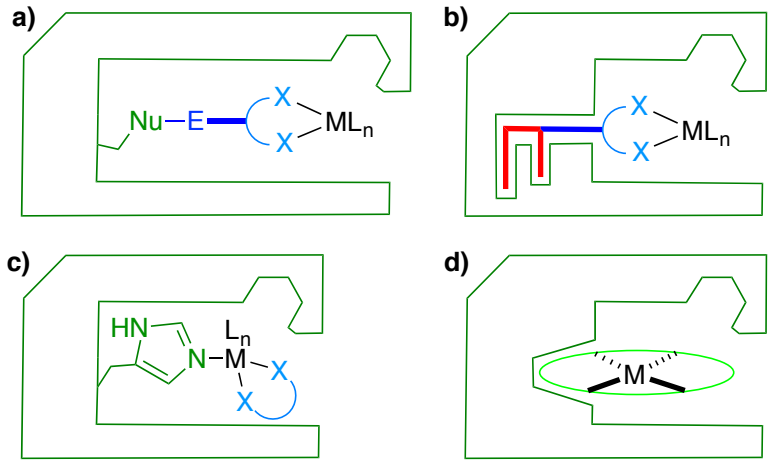

Figure 1. Four anchoring strategies allow to firmly localize an abiotic cofactor within a protein scaffold: a) covalent, b) supramolecular, c) dative, and d) metal substitution. The following colour codes apply: protein and natural cofactor (green), supramolecular anchor (red), variable spacer and ligand (blue) and abiotic metal (black).

Since its renaissance in the early 2000s, the field of artificial metalloenzymes has been extensively reviewed and highlighted.[15-95] With catalytic applications in mind, the present review summarizes the progress in ArM according to the reaction they catalyze.

The authors' initial intention was to classify the reactions according to the enzyme class system (EC) from the International Union of Biochemistry and Molecular Biology: oxidoreductase, transferase, hydrolase, lyase, isomerase and ligase. It rapidly became evident that the EC system is not best suited to ArM as the reactions these catalyze are often non-natural: in what EC would one assign to an artificial metathase or Suzukiase? We thus followed a more classical functional-group transformation classification.

In view of the focus on catalysis, artificial metalloproteins with no catalytic function are not covered comprehensively.[34-35] The same applies to the fascinating fields of DNA- and RNAzymes as well as metallopeptides with less than one hundred amino acids (an arbitrary length set for inclusion in this review). These DNA/RNAzymes and metallopeptides have been reviewed recently by key players in the field.[70, 96-98]

This review begins with a summary of the proteins and the anchoring strategies used to date for the creation of ArMs (chapter 2), followed by a historical perspective (chapter 3). Then follows a summary of the reactions catalyzed by ArMs (Reduction chemistry, C–C bond-formation, oxygen insertion and Hydration: chapters 4-7). This review ends with a critical outlook (chapter 8).

The authors have invested significant effort to cover *all* artificial metalloenzymes published to date, albeit with the restrictions outlined above. Despite the care for the detail and the search tools available, there is no doubt that we have missed some articles. We strive to apply a fair ethics of citation and thus wish to apologize for any unintentional omission.[99] In addition, this review served as a basis to set up a fully-searchable website on ArM that will be updated regularly by the authors.[100]

2. Protein Scaffolds

The table presented below summarizes all the protein scaffolds that have been used to date to create artificial metalloenzymes as well as relevant data including i) the anchoring strategy, ii) whether mutants have been tested, iii) the reaction that the resulting ArM catalyzes etc. Protein scaffolds that have been subjected to mutagenesis to optimize the performance of the ArMs are displayed throughout the article where most relevant.

Table 2 Summary of protein scaffolds reported to date for the creation of artificial metalloenzymes.

Entry	Name	PDB-code	Protein Fold[a]	Oligomeric state[b]	M_w [kDa]	Anchoring Mode[c]	PI[d]	Native Function	Stability[e]	Mutants tested[f]	Reactions[g]
1	α_3D peptide	2A3D	Designed single chain three-helix bundle	Monomer	8	D	5.8	*De novo*-designed protein	n.d	+	H2O
2	α-chymotrypsin	1YPH	Trypsin-like serine protease	Homo dimer	25	D, C	8.7	Endopeptidase	+/++	WT	DO, M
3	ß-lactamase	2FU7	Metallo-hydrolase/oxido reductase	Monomer	29	D	6.2	Hydrolysis of ß-lactams	+/++	+	CO, H20
4	ß-lactoglobulin	3NPO	Lipocalins	Monomer	18	S, C	4.8	Transport	++	WT	TH, SO
5	6-Phospho-gluconolactonase (6-PGLac)	4TM8	NagB/RpiA/CoA transferase-like	Monomer	27	D	4.7	Hydrolase	++	+	PE
6	Adipocyte lipid binding protein (ALBP)	1A18	Lipocalins	Homo dimer	15	C	8.6	lipid binding protein	+/++	+	HYD, TA
7	Alcohol dehydrogenase (ADH)	5ENV	GroES-like	Homo tetramer	141	D	5.4	Oxidoreductase	+/++	WT	DO

Entry	Name	PDB-code	Protein Fold[a]	Oligomeric state[b]	M_w [kDa]	Anchoring Mode[c]	PI[d]	Native Function	Stability[e]	Mutants tested[f]	Reactions[g]
8	Antibody 03-1	n.d	Immunoglobulin like ß sandwich	n.d	n.d	S	n.d	Immune response	n.d	WT	PE
9	Antibody 12E11G	n.d	Immunoglobulin like ß sandwich	n.d	n.d	S	n.d	Immune response	n.d	WT	PE
10	Antibody 13G10	4AMK	Immunoglobulin like ß sandwich	Hetero dimer	46	S	8.1	Immune response	n.d	WT	PE
11	Antibody 14H7	4AT6	Immunoglobulin like ß sandwich	Hetero dimer	45	S	6.5	Immune response	n.d	WT	PE
12	Antibody 1G8	n.d	Immunoglobulin like ß sandwich	n.d	n.d	S	n.d	Immune response	n.d	WT	H
13	Antibody 28F11	n.d	Immunoglobulin like ß sandwich	Hetero dimer	45	S	n.d	Immune response	n.d	WT	PEP
14	Antibody 2B4	n.d	Immunoglobulin like ß sandwich	n.d	n.d	S	n.d	Immune response	n.d	WT	PE
15	Antibody 33F12	1AXT	Immunoglobulin like ß sandwich	Hetero dimer	47.5	C	8.5	Immune response	+/++	WT	ALD
16	Antibody 38C2[m]	n.d	Immunoglobulin like ß sandwich	n.d	n.d	C	n.d	Immune response	+/++	WT	ALD, HYD
17	Antibody 3A3	n.d	Immunoglobulin like ß sandwich	n.d	n.d	S	n.d	Immune response	n.d	WT	PE, SO, PN
18	Antibody 7A3	n.d	Immunoglobulin like ß sandwich	n.d	n.d	S	n.d	Immune response	n.d	WT	PE, SO, EO

Entry	Name	PDB-code	Protein Fold[a]	Oligomeric state[b]	M_w [kDa]	Anchoring Mode[c]	PI[d]	Native Function	Stability[e]	Mutants tested[f]	Reactions[g]
19	Antibody 7G12	n.d	Immunoglobulin like ß sandwich	n.d	n.d	S	n.d	Immune response	n.d	WT	PE
20	Antibody 84A3	n.d	Immunoglobulin like ß sandwich	n.d	n.d	S	n.d	Immune response	n.d	WT	HYD
21	Antibody SN37.4	n.d	Immunoglobulin like ß sandwich	n.d	n.d	S	n.d	Immune response	+/++	WT	SO
22	Avidin (Av)	1VYO	Streptavidin-like	Homo tetramer	60	S	10.4	Biotin-binding	+++	WT	H, M
23	Binding domain of Rabenosyn (Rab4)	1YZM	Long α-hairpin	Monomer*	6	D	5.6	Membrane trafficking regulatory protein	n.d	+	H2O
24	Carbonic anhydrase II Bovine (CA)	1V9E	Carbonic anhydrase	Monomer	29	MS	6.4	CO_2 hydration	+	+	EO, H,PE
25	Carbonic Anhydrase II Human (hCAII)	1CA2	Carbonic anhydrase	Monomer	29	D, MS	6.9	CO_2 hydration	++	+++	TH, H, HF, EO, M,PE
26	Carboxypeptidase A	1M4L	Phosphorylase/ hydrolase-like	Monomer	34.4	D	6.3	Protease	+++	WT	H2O, HYD, O
27	Catabolite activator protein from *E. coli*	2CGP	DNA/RNA-binding 3-helical bundle	Homo dimer	47	D, Z	8.4	DNA binding, regulation of catabolite	+/++	+	PE
28	C-terminal domain of Calmodulin	2KZ2	EF Hand-like	Monomer	17	D	4.1	Messenger, Ca^{2+} binding protein	+/++	+	H2O
29	Cutinase	1CEX	α/ß hydrolase	Monomer	21	C	7.8	Cutin hydrolase	+	WT	H, M

Entry	Name	PDB-code	Protein Fold[a]	Oligomeric state[b]	M_w [kDa]	Anchoring Mode[c]	PI[d]	Native Function	Stability[e]	Mutants tested[f]	Reactions[g]
30	Cytochrome b_{562}	1QPU	Four-helical up-and-down bundle	Monomer	11	MS	7.9	Electron transport	++	+	H2
31	Cytochrome c_{552}	1DT1	Cyt c_8 family	Monomer	9	MS	9.6	Nitrite reduction	+++	M61A	H2
32	Cytochrome cb_{562}	2BC5	Four α-helix bundle	Monomer[h]	12	D, S	5.0	Oxidoreductase	+/++	+++	H2O
33	Cytochrome P450 (CYP119)	1IO7	Cytochrome P450	Monomer	43	S, D	6.1	Oxidoreductase	++/+++	+++	CH
34	Cytochrome P450-BM3	2IJ2	Cytochrome P450	Monomer	118	S	5.2	Oxidoreductase	+	+	CP
35	Due Ferro 1	1EC5	Designed four-helix bundle protein	Homo dimer	12	D	4.8	*De novo*-designed protein	+/++	+	PE
36	Ferredoxin (Fd)	1A70	ß-Grasp (ubiquitin-like)	Monomer	13	C, D	9.6	Electron transport	++	WT	H2
37	Ferritin (Fr)	1DAT	Ferritin-like	Homo 24-mer	480	D	5-5.7	Iron storage	+/++	+	PO, S
38	FhuA ΔCVF^{tev}	1BY3	Trans membrane ß-barrels	Monomer	64	C	n.d	Ferric hydroxamate uptake	+/++	+	DA, M
39	Flavodoxin (Fld)	1CZL	Flavodoxin fold	Monomer	19	MS	4.0	Electron transport	++	WT	H2
40	Glyoxalase II (Human)	1QH5	Metallo-hydrolase/oxido reductase	Homo dimer	58	D	6.9	Hydroxyacyl-glutathione hydrolase	+/++	+++	H2O

Entry	Name	PDB-code	Protein Fold[a]	Oligomeric state[b]	M_w [kDa]	Anchoring Mode[c]	PI[d]	Native Function	Stability[e]	Mutants tested[f]	Reactions[g]
41	$(gp27\text{-}gp5)_3$	1K28	Phage tail OB-fold	Hetero hexamer	>300	C	5.4	Needle of bacteriophage T4	++	WT	SO
42	$[(gp5ßf)_3]_2$	3A1M	OB-fold	Homo hexamer	88	C	4.8	Needle of bacteriophage T4	++++	+	ER, CL, CR
43	Heme Oxygenase (HO)	1IW0	Heme oxygenase-like	Monomer	24	S, D	5.5	Heme oxygenation	+/++	+	H2, OR
44	Hemoglobin	2DN1	Globin-like	Hetero tetramer	61.9	C	8.3	O2 transport	++	WT	O
45	Hen egg white Lysozyme (HEWL)	2VB1	Lysozyme-like	Monomer	14	D	11.4	Hydrolysis ß-(1-4)- peptidoglycan	+ +/+++	WT	DO, TH[i]
46	Horseradish Peroxidase (HRP)	1W4W	Heme-dependent peroxidases	Monomer	44	S	5.6	Peroxidase	++	WT	PE, PO
47	Human retinoid-X-receptor (hRXRα)	1RXR	Glucocorticoid receptor-like	Monomer	10	D	9.6	DNA binding	+/++	+++	L
48	HydA	3LX4	n.d	Monomer	49	D	5.9	Hydrogenase	+	WT	H2
49	Intestinal fatty acid binding protein (IFABP)	1ICM	Lipocalins	Monomer	15	C	6.9	lipid binding protein	n.d	+	HYD, TA
50	Laccase	1GYC	Cupredoxin-like	Monomer	53.6	MS	5.8	Oxidoreductase	++/+++	WT	DO
51	Lipase (*C. rugosa*)	1GZ7	α/ß hydrolase fold	Monomer	67	D	4.6	Lipase	+/++	WT	DO

Entry	Name	PDB-code	Protein Fold[a]	Oligomeric state[b]	M_w [kDa]	Anchoring Mode[c]	PI[d]	Native Function	Stability[e]	Mutants tested[f]	Reactions[g]
52	Lipase B from *C. antarctica* (CALB)	4K6G	α/ß hydrolases	Monomer	33	C	5.8	Hydrolysis of triglycerides	+++	WT	H, HK
53	Lipase from *G. thermocatenulatus* (GTL)	2W22	Rossmann fold	Monomer	43	C	6.4	Lipase	+++	+	DA
54	LmrR	4D	n.d	Homo dimer	13.5	C, S	6.6	Transcriptional repressor	n.d	+	DA, H2O, FC
55	Mouse adenosine deaminase	1A4L	TIM ß/α-barrel	Monomer	40	D	5.5	Adenosine deamination	++	+++	H2O
56	Myoglobin (Mb) (Horse heart) (Sperm whale)	2V1K (HH) 1MBI (SW)	Globin-like	Monomer	18	S, D, MS	7.4 (HH) 8.7 (SW)	Oxygen transport	+/++	+++	PE, SO, CH, H2, CP, DA, NO
57	Neocarzinostatin (Variant 3.24)	2CBM	Immunoglobulin -like ß - sandwich	Monomer	14	S	4.2	Enediyne binding	+	WT	SO, DA, TE
58	NikA	4I9D	Periplasmic binding protein-like II	Monomer	56	S	10.0	Nickel transport	+	WT	SO
59	Nitrobindin (Nb)	3EMM	Lipocalins	Monomer	19	C	8.7	NO transport	+/++	+	H2, DA, PO, EO, CH, M
60	Papain (PAP)	1PPP	Cysteine proteinases	Monomer	23	C	8.8	Protease	+/++	WT	TH, DA, H, EO,O
61	Photoactive Yellow Protein (PYP)	2PHY	Profilin-like	Monomer	14	C	4.8	Photoreceptor	+	WT	H, AAm
62	Photosystem I (PSI)	1JBO	Globin-like	Monomer	215	U	5.3	Photochemical energy conversion	+	WT	H2

Entry	Name	PDB-code	Protein Fold[a]	Oligomeric state[b]	M_w [kDa]	Anchoring Mode[c]	PI[d]	Native Function	Stability[e]	Mutants tested[f]	Reactions[g]
63	Phytase	1IHP	Phosphoglycerate mutase-like	Monomer	48.2	C, D	4.9	Phosphatase	+/++	+	SO, CP
64	Prolyl oligopeptidase (POP)	1QFS[n]	7-bladed beta-propeller	Monomer	80	C	5.5	Prolyl oligopeptidase	+++	+++	CP
65	Proteinase-K	5AVK	Subtilisin-like	Monomer	28.9	D	8.9	Protease	+/++	WT	DO
66	Ribonuclease S	2RNS	RNase A-like	Monomer	14	D	8.6	RNA cleavage	++	+	TH
67	Rubredoxin (Rd)	6RXN	Rubredoxin-like Zinc-ribbon fold	Monomer	5.5	MS	4.6	Electron transport	++	WT	H2
68	Serum Albumin Bovine (BSA)	4F5S	Serum albumin-like	Monomer	66.5	D, S	4.7	Plasma carrier, oncotic pressure regulator	+/++	WT	DO, DA, H, PO, SO
69	Serum albumin Chicken-egg (CSA)	1UHG	Serum albumin-like	Monomer	43	S	4.5	Plasma carrier, oncotic pressure regulator	+	WT	DA, SO
70	Serum albumin Porcine (PSA)	n.d	Serum albumin-like	Monomer	67	S	5.8	Plasma carrier, oncotic pressure regulator	+	WT	DA, SO
71	Serum albumin Rabbit (RSA)	3V09	Serum albumin-like	Monomer	66	S	5.7	Plasma carrier, oncotic pressure regulator	+	WT	DA, SO
72	Serum Albumin Human (HSA)	3JRY	Serum albumin-like	Monomer	65	S	4.7	Plasma carrier, oncotic pressure regulator	+/++	WT	SO, DA, HF
73	Serum albumin Sheep (SSA)	4LUF	Serum albumin-like	Monomer	66	S	5.6	Plasma carrier, oncotic pressure regulator	+	WT	DA, SO

Entry	Name	PDB-code	Protein Fold[a]	Oligomeric state[b]	M_w [kDa]	Anchoring Mode[c]	PI[d]	Native Function	Stability[e]	Mutants tested[f]	Reactions[g]
74	Small heat shock protein *(M. jannaschii)*	1SHS	HSP-20 like chaperones	Homo 24-mer	16.5	C	5.0	Thermotolerance	+++	+	M
75	Staphylococcus nuclease	2SNS	OB-fold	Monomer	16.8	C	9.6	DNA and RNA hydrolysis	+/++	WT	HYD (native)
76	Sterol Carrier Protein (SCP)	1IKT	SCP-like	Monomer	12.5	C	9.5	Sterol carrier	n.d	+	DA
77	Streptavidin (Sav)	2BC3	Streptavidin-like	Homo tetramer	64	S, S+D, U	6.4	Biotin-binding	++++	+++	H, TH, M, S, AA, CH, AO, SO, DO, MA
78	Thermosome (THS)	1A6D	GroEL equat.+ The "swivelling" ß/ß/α domains	Hetero 16-mer	117	C	5.9 (α) 5.1 (ß) domains	Chaperonin	+++	+	PO
79	tHisF	1THF	TIM ß/α- barrel	Homo dimer	28	C, D	5.2	imidazole glycerol phosphate synthase	+++	+	EO, CP, DA, Si-I
80	TRI peptide	3PBJ (structure analogue)	Three-helix bundles	Homo trimer	10	D	6.8	*De novo*-designed protein	n.d	+	H2O, NR
81	Trypsin	1S81	Trypsin-like serine proteases	Monomer	23.5	D	8.3	Protease	+++	+	PEP
82	Xylanase A (Xln)	1E0X	TIM ß/α-barrel	Monomer	51	S	6.2	Glycoside hydrolysis	+	WT	PE, SO, EO
83	Zif268 zinc-finger protein	1ZAA	ß-ß-α zinc fingers	Trimer	33	D, Z	10.1	DNA binding, mammalian transcription factor	n.d	+++	DNA binding

[a] based on *Structural Classification of Proteins* (SCOP). http://scop.mrc-lmb.cam.ac.uk
[b] based on PDBe classification.
[c] S = supramolecular, D = dative, C = covalent, MS = metal substitution, Z = non-natural aminoacid, U = undefined
[d] Theoretical PI calculated with ProtParam based on the amino acid sequence of the natural/*de novo*-designed protein.
[e] ++++ very high stability against chaotropic agents, +++ Tm >80°C, ++ Tm > 60°C , + Tm > 40°C, n.d no data available.
[f] +++ > 50 mutants tested, ++ > 10 mutants tested, WT: only wild-type tested
[g] AA = allylic alkylase, AAm = allylic aminase, ALD = aldolase, AO = alcohol oxidase, CH = C–H activase, CL = clickase, CO = catecohol oxidase, CP = cyclopropanase, CR = CO_2 reductase, DA = Diels-Alderase, DO = dihydroxylase, EO = epoxidase, ER = epoxide Ring Opening, FC = Friedel-Crafts alkylase, H = hydrogenase, H2 = dihydrogenase, HF = hydroformylase, HK = heckase, HYD = hydrolase, H2O = hydratase, L = ligase, M = metathase, MA = Michael addase, NR = nitrite reductase, NO = NO reductase, NU = nuclease, O = Oxidase, OR = oxygen reductase, PO = polymerase, PE = peroxidase, PEP = peptidase, PN = phenol nitratase, S = Suzukiase, Si-I = Si-H insertion, SO = sulfoxidase, TA = transaminase, TE = transesterase, TH = transfer hydrogenase.

[h] Tezcan *et al.* used a Zn(II)-mediated tetramer of cytochrome cb_{562} (with a mass of ~ 50kDa).
[l] Ueno *et al.* used as tetragonal and orthorhombic crystal.
[l] Kuhlman *et al.* used the dimer of the Rab4 binding domain of Rabenosyn (with a mass of ~12 kDa).
[m] Commercially available.
[n] POP from *Pyrococcus furiosus* (PDB : 5T88), submitted.

3. Historical Contributions

The aim of this section is to cover work on artificial metalloenzymes dating from the earliest studies on hybrid metal-protein catalysts to those completed around the year 2000. As noted in the introduction, around this date, modern tools of molecular biology began making a significant impact on ArM research. Presumably as a result of this, the five-year average number of publications on ArM research each year substantially increased substantially in the early 2000's (Chart 1). These early studies are presented in chronological order to highlight how different advances were made using different scaffolds and ArM formation strategies at the time of the original reports.

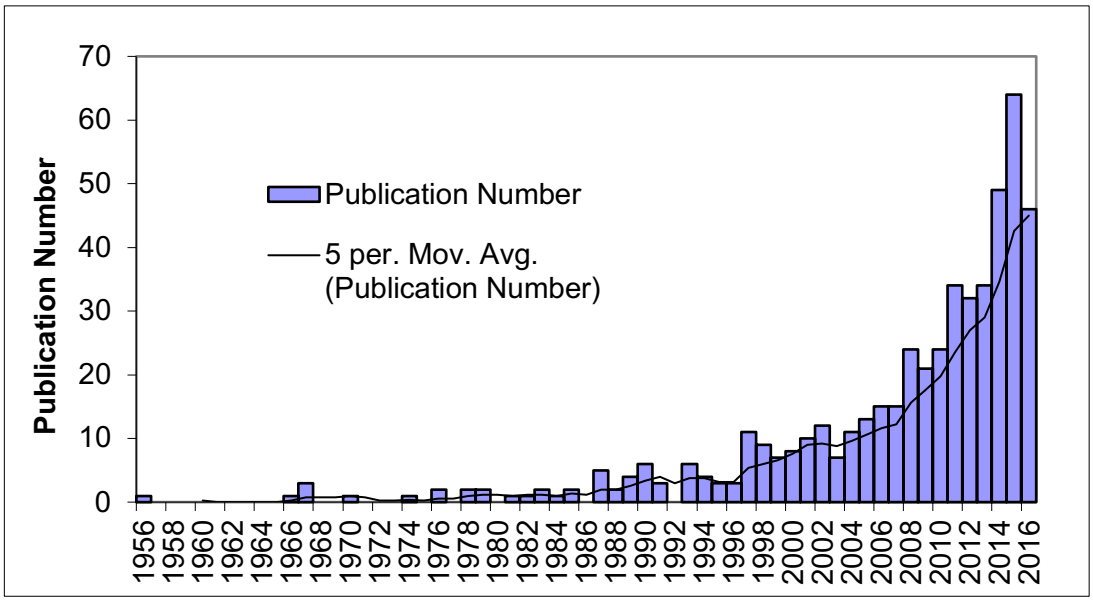

Chart 1. Number of publications and the five-year moving average of this number plotted versus publication year for publications cited in this review.

The first example of transition metal-catalyzed asymmetric synthesis, reported in 1956, also constitutes the first realization of a protein-modified transition metal catalyst.[101-102] S. Akabori et al. adsorbed palladium chloride on silk fibroin fibres and reduced the resulting material with hydrogen, likely resulting in the formation of Pd-nanoparticles embeded within an enantiopure protein environment.[103] The protein-immobilized palladium

catalyzed asymmetric hydrogenation of dehydroaminoacid derivatives **1**–**3** to provide products **4** and **5** with significant enantiomeric excess (Scheme 1). The reduction of α-benzildioxime, however, led to variable results, suggesting that the catalyst was poorly defined. Despite reproducibility issues,[101-102] this initial study has sparked research in biopolymer-immobilized Pd, sometimes termed Bio-palladium.[104] Pd-nanoparticles have recently also attracted attention for *in vivo* applications.[105-106]

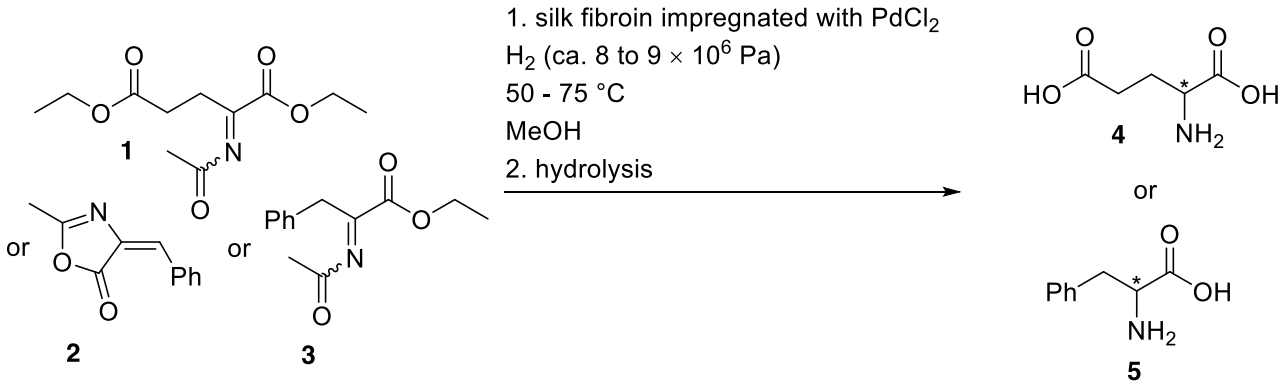

Scheme 1. Asymmetric hydrogenation of dehydroaminoacid derivatives with silk-fiber modified palladium reported in 1956.

Metal substitution has been used for the study of natural metalloenzymes since the late 1960s.[107-108] Metal-exchange studies often aimed at introducing spectroscopically observable metals as a means to elucidate structural details but did not focus on catalysis.[109-110] J. E. Coleman, however, observed that the CO_2 hydration activity of carbonic anhydrase remains roughly half when Zn(II) is exchanged for Co(II), whereas the esterase activity increased after metal exchange for carbonic anhydrase B.[108] In the same year (1967), P. Cuatrecasas et al. reported the replacement of Ca(II) for Sr(II) in a staphylococcal nuclease. Whereas the Ca(II)-dependent enzyme catalyzed both DNA and RNA cleavage, the Sr(II) exchanged nuclease cleaved DNA exclusively.[107]

Although not catalytic, the potential of metal-ion exchange to impact enzyme function was convincingly demonstrated in the activation of the zymogen trypsinogen by trypsin in 1970.[111] Trypsinogen contains two latent metal binding sites, the lower affinity of which is

located at the cleaved *N*-terminus.[112] Ca(II)-ions bound to this site led to a lowering of the K_m for the trypsin-trypsinogen interaction. Bound Nd(III) leads to a much more pronounced lowering of the K_m compared to Ca(II), even at a 100 fold lower concentration of metal ions.

Presumably the first example where alternative catalytic function was introduced through metal-exchange in a metalloprotein was reported by K. Yamamura and E. T. Kaiser in 1976.[1] Carboxypeptidase A was converted to an active oxidase by exchange of Zn(II) for Cu(II) (Scheme 2). Limiting k_{cat} and K_m values of k_{cat} = 6 min^{-1} and K_m = 0.24 mM where determined for the oxidation of ascorbic acid **6** to dehydroascorbic acid **7**.

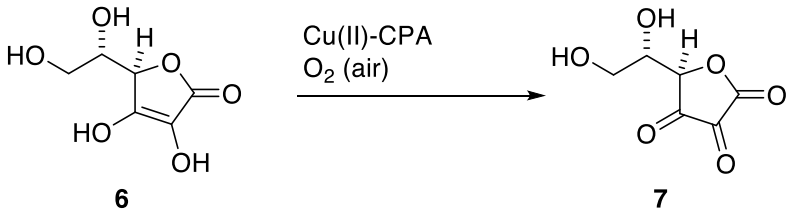

6 **7**

Scheme 2. Oxidation of ascorbic acid by carboxypeptidase A (CPA) after exchange of the active site metal ion Zn(II) for Cu(II).

M. E. Wilson and G. M. Whitesides were the first to realize the anchoring of a completely abiotic cofactor inside a protein cavity in a defined fashion.[2] Exploiting the remarkable affinity of the small molecule ligand biotin and some of its derivatives for avidin, a biotinylated Rh(I)-diphosphine precatalyst **9** was employed for the hydrogenation of α-acetamidoacrylic acid **8** in the presence of the host protein (Scheme 3). The system showed significant, albeit moderate, stereoinduction in aqueous phosphate buffer and, importantly, a definite increase in activity when compared to the protein-free cofactor. Avidin is a homotetrameric protein that can bind up to 4 equivalents of biotin. One equivalent of the biotinylated catalyst precursor vs. biotin binding sites led to a higher

enantiomeric excess than 0.5 equivalents indicating that the cofactors interact with each other when localized in adjacent binding sites. This study was reported in 1978.

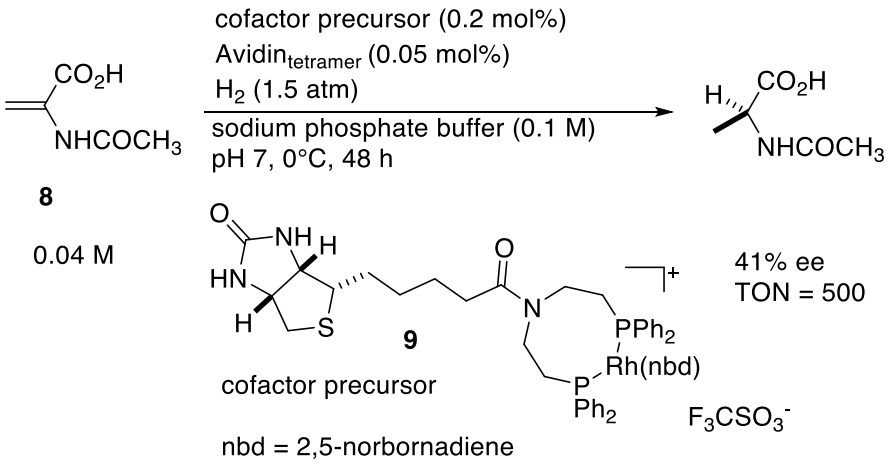

Scheme 3. Asymmetric hydrogenation of a dehydroamino acid derivative by a biotinylated Rh(I)-complex upon binding to avidin.

Catalytic enantioselective oxidation of sulfides by oxidants such as $NaIO_4$, *t*-BuOOH, or H_2O_2 in the presence of bovine serum albumine (BSA) was investigated by T. Sugimoto and T. Kokubo et al. in the late 70's and early 80's.[113-115] In one publication, the effect of stoichiometric metal additives, namely Cu(II), MoO_4^{2-}, or WO_4^{2-}, in combination with *t*-BuOOH was reported, though the results were less promising than other systems tested in terms of yield and selectivity.[113] Similarly, in 1983, T. Kokubo et al. investigated the asymmetric OsO_4-catalyzed dihydroxylation of alkenes with BSA as a chiral scaffold with remarkable success (Scheme 4).[116] An *ee* of 68 at a TON of 40 in the dihydroxylation of α-methylstyrene **10** with *t*-BuOOH as a stoichiometric oxidant was reported, clearly demonstrating the potential to exploit non-metalloproteins as ArM scaffolds.

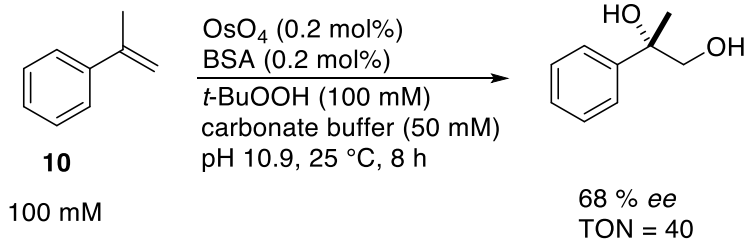

Scheme 4. Asymmetric dihydroxylation of α-methylstyrene with OsO_4/*t*-BuOOH in the presence of bovine serum albumin (BSA).

Cytochromes P450 have long attracted the attention of chemists. The ability of these enzymes to catalyze regio- and stereo-selective oxidative processes using molecular oxygen and reducing equivalents from NAD(P)H has so far been impossible to mimic reliably with purely synthetic methods. The sophisticated redox machinery required to transfer electrons from reduced nicotinamide cofactors to the heme center and generate an active iron-oxo species has contributed to the interest in these systems,[117] but it also hampers the application of P450 variants in synthetic processes.[118] Hemoglobin, another heme-containg metalloprotein, has been shown to catalyze P450-type oxidations when supported by an NADPH-cytochrome P450 reductase containing FAD and FMN cofactors.[119] T. Kokubo, S. Sassa, and E. T. Kaiser reported in 1987 on a catalytically competent 7-cyanoisoalloxazine-hemoglobin conjugate.[120] The flavin-substituted hemoglobin hybrid, named flavohemoglobin, catalyzed the para-hydroxylation of aniline **11** in the absence of NADPH-cytochrome P450 reductase with a higher rate than the reconstituted system and with a K_m value similar to that of the hemoglobin scaffold (Table 2, Scheme 5). The flavin derivative was attached to cysteine β-93 through a glycine-aminoethanthiol-linker. The X-ray structure (1988) of flavohemoglobin revealed that i) the flavin derivative is readily accessible to NADPH ii) the center of the isoalloxazine and the heme of the same subunit are 14 Å apart iii) the flavins of neighbouring subunits are in close contact, possibly enabling electron transfer between subunits.[121] Natural flavohemoglobins exist, for example in *E. coli*.[122]

Table 2. Comparison of catalytic paramters of flavohemoglobin with hemoglobin and reductase complemented hemoglobin.

Entry	Protein	k_{cat}^{app} (min^{-1})	K_m^{app} (mM)
1	flavohemoglobin	0.169	5.3

2	hemoglobin + P450-reductase	0.127	5.3
3	hemoglobin[a]	0.022	5.6

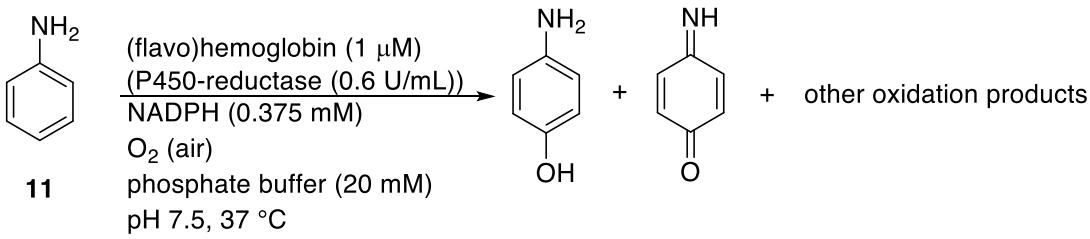

Scheme 5: Hydroxylation of aniline **11** catalyzed by flavohemoglobin, reductase-complemented hemoglobin or the non-modified parental protein.

Although enzymes are frequently highly substrate specific, this is by no means a general feature. The introduction of specificity to a natural metalloenzyme by complementation with a molecular recognition element was demonstrated by D. R. Corey and P. G. Schultz in 1987. Upon attachment of an oligonucleotide via a disulfide bridge, the relatively non-specific Ca(II)-dependent staphylococcal nuclease cleaved single stranded DNA in proximity to the attachment site. Only superstoichiometric conditions were reported.[123] In a similar manner, various oligonucleotide binding proteins or protein domains were converted to oligonucleotide cleaving proteins via covalent modification with EDTA or phenanthroline complexes of Fe(II) or Cu(II), respectively.[124-127] The combination of a reducing agent such as a thiol or ascorbic acid with molecular oxygen resulted in oxidative cleavage of the oligonucleotide backbone.[128] The systems were typically employed in superstoichiometric amounts relative to the oligonucleotide.

The ability to raise monoclonal antibodies against seemingly any hapten inspired ambitious research into the generation of antibody-based artificial metalloenzymes. It was envisioned that these could possess the ability to discriminate substrates and hence provide specificity toward selectable cleavage motifs.[129] B. L. Iverson and R. A. Lerner first reported in 1989 on a specific antibody-based ArM hydrolase for peptide substrates.[130] Monoclonal antibodies were raised against a peptide (trien)Co(III) complex

12 (trien = triethylentetramine). Substitution of the hapten for other metal(trien) complexes led to active peptidases that could distinguish between structurally related substrates **13** – **18** and cleaved a specific peptide bond in the small set of peptidic substrates investigated **17**, **18**; Scheme 6. The antibody ArM design was based on the prospective exchange of a coordinatively inert octahedral Co(III) complex used as the hapten against a kinetically more labile complex for catalysis. A simple TLC assay for the liberated terminal amino group enabled the fast evaluation of a range of constructs. One construct, antibody 28F11 in combination with Zn(II)trien, was investigated in more detail, and the authors concluded that all components, namely metal(trien), specific substrate, and antibody are required for the reaction. Various metal(trien) complexes could be employed, and a turnover number of 400 with a turnover frequency of 6×10^{-4} s^{-1} was reported.

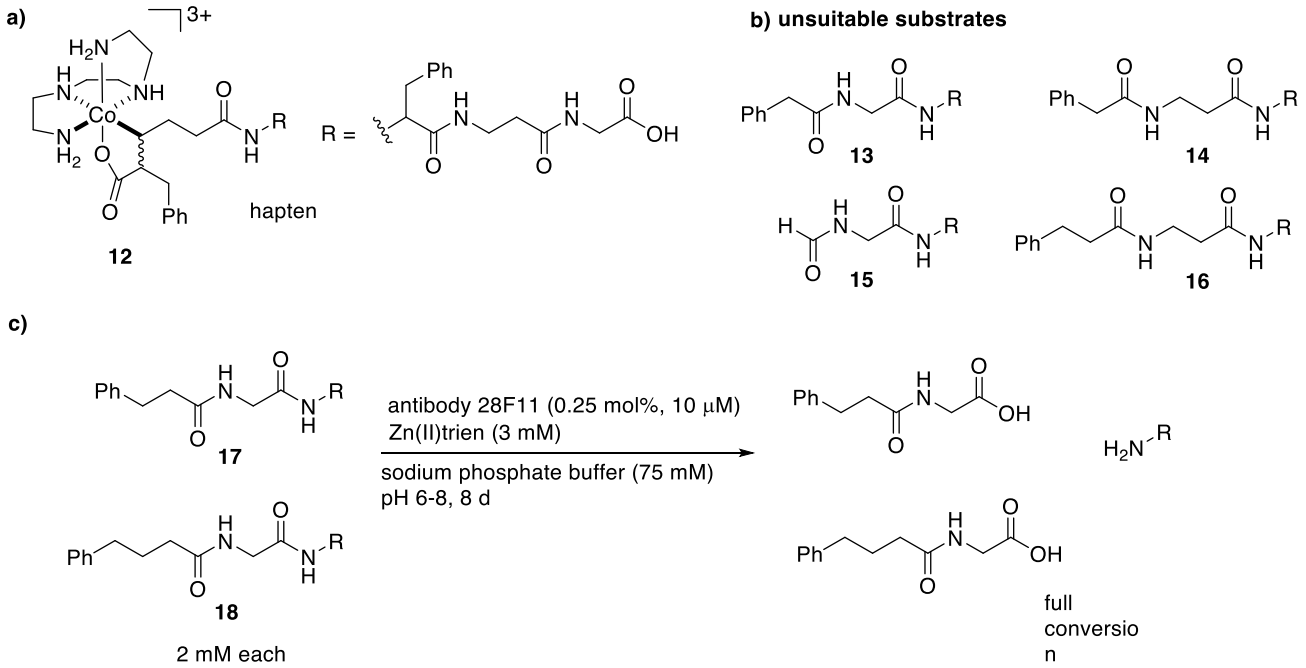

Scheme 6. Development of metal-dependent antibodies for specific cleavage of peptidic substrates. a) Kinetically inert cobalt(III) complex employed as hapten; b) peptidic structures not accepted as substrates; c) cleavage of peptidic substrates with antibody 28F11 in the presence of Zn(II)trien.

Following Kaiser's earlier work demonstrating that hemoglobin could be converted into a reductase-independent hydroxylase, T. Sasaki and E. T. Kaiser decorated Fe(III)

coproporphyrin with four identical fifteen-residue peptides.[131] In the presence of acetylflavin and NADPH, the resulting construct 'helichrome' was shown to hydroxylate aniline with k_{cat} and K_m values of 0.02 min^{-1} and K_m = 5.0 mM, respectively. The unmodified Fe(III) coproporphyrin showed only negligible hydroxylase activity under the same conditions. The study was published in 1989 and constitutes, to the best of our knowledge, the first report of a *de novo* 'heme'-enzyme.

A. G. Cochran and P. G. Schultz raised in 1990 monoclonal antibodies against *N*-methylmesoporphyrin IX **19** as a hapten (Figure 2).[132] *N*-methylporphyrins show out-of-plane distortion and can be considered as a transition state model for the metalation of the porphyrin, a reaction typically catalyzed by ferrochelatase in the conversion of protoporphyrin to heme. Three purified antibodies were specific for the hapten, and two of these catalyzed Zn(II)- and Cu(II)-porphyrin complex formation. The faster of these two showed rates for Zn(II) insertion comparable with those of ferrochelatase (80 h^{-1} vs 800 h^{-1}, respectively). Further studies revealed that the same antibody was effectively inhibited by iron(III) mesoporphyrin **20**. Intriguingly, the resulting construct catalyzed the oxidation of a range of typical chromogenic peroxidase substrates (using H_2O_2 as a stoichiometric oxidant) with significantly higher rates than iron(III) mesoporphyrin itself.[133] Notably, ABTS and pyrogallol red were converted by the construct, but not by iron(III) mesoporphyrin. In a closely related study, A. Harada and coworkers reported several years later that antigen binding fragments in combination with *meso*-tetrakis(4-carboxyphenyl)porphyrin (TCPP) complexes of Mn(III) and Fe(III) catalysed the oxidation of pyrogallol with H_2O_2 exclusively while other substrates tested by Cochran and Schulz such as hydroquinone, resorcinol, catechol and ABTS with a higher redox potential were not converted.[134]

In a conceptual paper published in 1990, E. Keinan et al. raised antibodies against the water soluble Sn(IV) porphyrin complex *meso*-tetrakis(4-carboxyvinylphenyl)porphinato tin(IV)dihydroxide (Sn(TCP)$(OH)_2$) **21** (Figure 2).[135] Antibody metallation with Mn(III)(TCP) cofactor **22** led to an ArM that catalyzed styrene epoxidation in the presence of iodosobenzene. The highest activity was observed under heterogeneous conditions in CH_2Cl_2, but no enantioinduction could be detected.

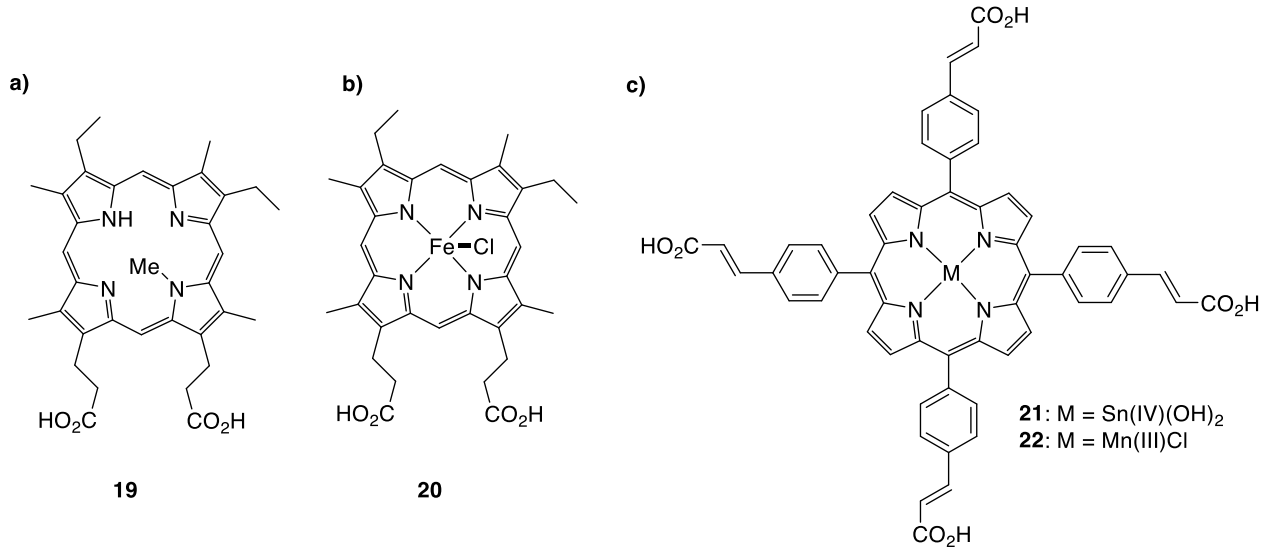

Figure 2. Haptens and cofactor precursors for monoclonal antibody-based, metalloporphyrin-dependent artificial metalloenzymes. a) *N*-methylated porphyrin as a transition state mimic for ferrochelatase afforded an antibody for Zn(II) and Cu(II) mesoporphyrin formation; b) the same antibody formed an active oxidase upon loading with Fe(III)mesoporphyrin; c) water soluble Sn(TCP)$(OH)_2$ used as a hapten to raise monoclonal antibodies that were subsequentely combined with Mn(TCP)Cl to yield an artificial epoxidase.

Despite the prevalence of non-covalent cofactor incorporation in early ArM efforts, work on covalent incorporation also continued. For example, J. P. Germanas and E. T. Kaiser (posthumously) communicated an artificial oxidase based on a covalently bound Cu(II)-bipyridine complex linked to the cysteine located in the active site of papain. The construct catalyzed the air-oxidation of ascorbic acid (compare Scheme 2) and more lipophilic derivatives at 15 – 26 fold higher rates compared to the free cofactor.[136] Although no catalysis was probed, in 1993, H. B. Gray, B. Imperiali, and coworkers demonstrated

photoinduced electron transfer between a covalently linked Ru-center and heme in a cytochrome c mutant. The heme-bearing mutant beared a $Ru(bipy)_2$-fragment coordinated to a bipyridyl-alanine bearing peptide constructed by semisynthesis.[137]

In 1993, R. A. Lerner, K. D. Janda, and coworkers disclosed a strategy to generate an antibody-based ArM hydrolase using a hapten that contained a methylpyridinium unit **23**, rather than a metal moiety (Scheme 7).[138] Based on the activation of picolinic acid esters by Lewis acids coordinated to the pyridine nitrogen atom, it was envisioned that the methylpyridinium-substituted hapten would select for antibodies that address to scaffold design criteria. First, the methyl group in the hapten would act as a placeholder for a metal ion. Second, the positive charge would elicit the expression of carboxylate residues to serve as additional ligands near the prospective metal binding site and thereby increase metal affinity. The ester moiety envisaged as a cleavage site, or more specifically, the expected tetrahedal intermediate, was simulated with a hydroxyl functional group. Upon metallation with Zn(II), the resulting antibody-based ArM showed a >10,000-fold rate acceleration against background and a > 1,000-fold rate acceleration against Zn(II) in equivalent concentration. The affinity of the antibody for Zn(II) and the substrate complexed to Zn(II) was weak, whereas the affinity for the substrate itself was substantially higher.

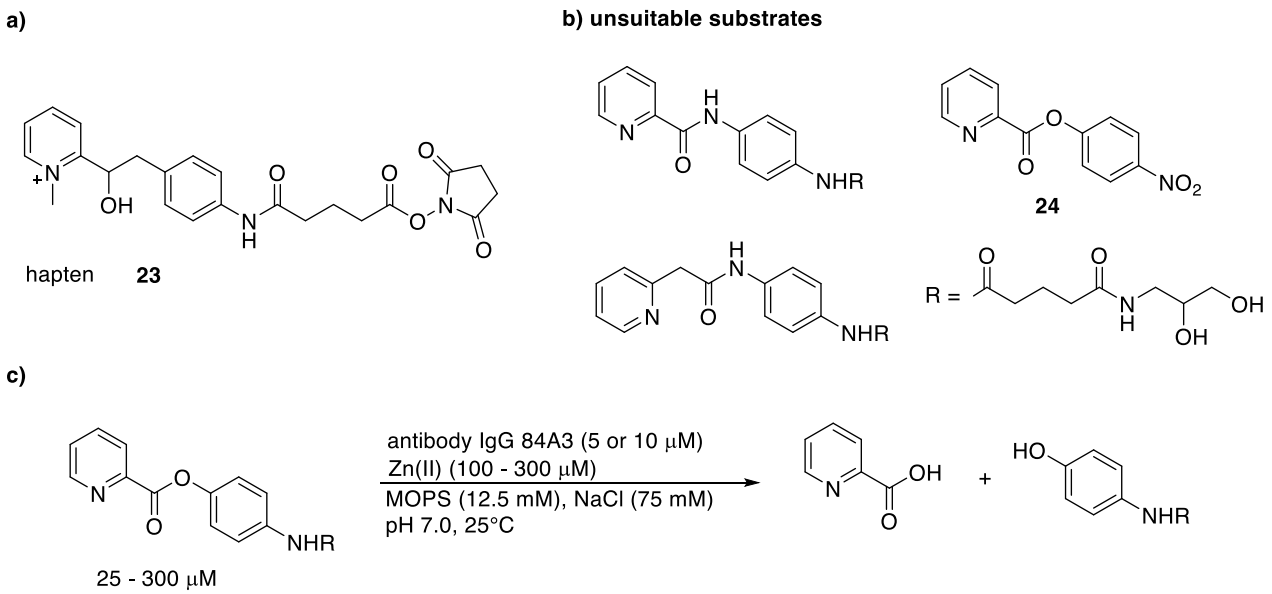

Scheme 7. Monoclonal antibodies catalyze the hydrolysis of a specific picolinic acid ester in the presence of Zn(II). a) *N*-methyl pyridinium employed as the hapten; b) substrates were not accepted by the antibody; c) hydrolysis of substrate by the antibody in the presence of Zn(II).

B. Imperiali and R. S. Roy reported in 1994 on an artificial transaminase generated by reassembly of the subtilisin-cleaved bovine ribonuclease A (RNase A) with a synthetic peptide fragment carrying a pyridoxal derivative (Figure 3). One reassembled construct displayed considerable rate acceleration (18 fold) for the conversion of L-alanine to pyruvate under single turnover conditions compared to the pyridoxal-derivative carrying the peptide fragment alone. Accelerating effects of metal ions observed with simple pyridoxal models had been studied previously and consequently their addition was probed in this complex system.[139] Cu(II)-ions had either beneficial or detrimental effects on the rate depending on the peptide fragment employed.[140] In a subsequent study, multiple turnovers could be realized in the conversion of pyruvate to alanine through the addition of L-phenylalanine accompanied by a moderate enantioselectivity.[141]

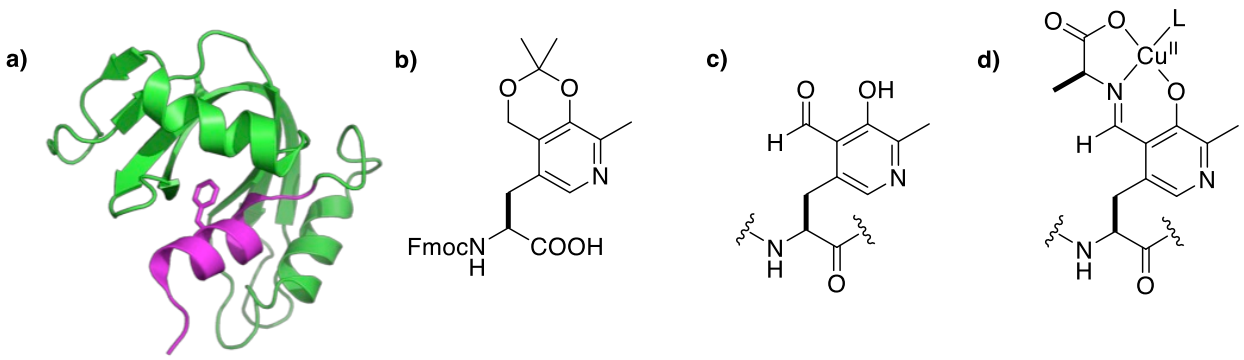

Figure 3. An artificial transaminase based on RNase A. RNase A is cleaved by subtilisin into fragments termed S-protein^{140} and S-peptide (magenta). Reassembly of S-protein with suitable synthetic S-peptides affords folded and functional supramolecular constructs. a) The side chain of 8-Phe targeted for cofactor introduction is displayed in stick mode (PDB ID 3DH5); b) unnatural amino acid used to introduce the pyridoxal mimic into the synthetic S-peptide; c) S-peptide bearing the pyridoxal mimic as a side chain resulting from deprotection and oxidation; d) postulated interaction of Cu(II)-ions with Schiff-base formed by condensation of side chain functionality with L-alanine.

C. S. Craik and coworkers successfully engineered a discrete metal binding site into trypsin in order to change its substrate specificity. A double mutation to introduce histidines in the S2' pocket (N143H-E151H) allowed selective cleavage of the peptide substrate AGPYAXSS, containing tyrosine at P1. Cleavage occured exclusively upon addition of either Zn(II) or Ni(II) and if the peptide contained a histidine at P2' (X = H; Figure 4). Surprisingly, wild type trypsin was also able to cleave this substrate in the presence of Zn(II) at 10-fold lower rate, although cleavage after tyrosine is highly disfavored in the absence of zinc. This unexpected result was rationalized by complexation of the substrate with the participation of glutamate 151. Indeed, exchange of glutamate for glutamine led to a mutant unable to cleave the peptide AGPYAHSS. The metal binding site was modeled based on the X-ray structure of a rat-trypsin mutant.

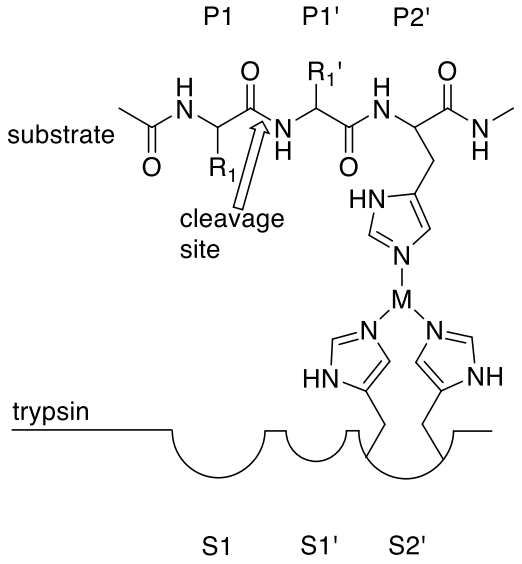

Figure 4. Modifying the substrate profile of trypsin through an engineered metal binding site for substrate coordination.

R. R. Davies and M. D. Distefano used covalent scaffold modification to anchor a catalytically active transition metal complex inside an existing protein cavity to exert control over the metal center. Their detailed study, published in 1997, described the reaction of iodoacetamido-1,10-phenanthroline with a unique cysteine residue inside the cavity (V = 600 $Å^3$) of adipocyte lipid binding protein (ALBP).[142] The X-ray structure confirmed the positioning of the phenanthroline unit inside the protein cavity (PDB ID 1A18).[143] Complexation with Cu(II) resulted in a construct (ALBP-Phen-Cu(II)) that accelerated the hydrolysis of the activated picolinic acid ester **24**, and, more importantly, a small set of racemic alanine, serine, and tyrosine esters. The L-enantiomer of the isopropyl ester of alanine **25** was converted significantly faster than the D-enantiomer resulting in an *ee* of 86% after 24 hours and around 1 turnover, whereas around 8 turnovers were realized with the methyl ester of tyrosine **26** (39% ee, Scheme 8). In a subsequent study, the position of the phenanthroline inside the protein cavity was varied by site directed mutagenesis to place the linking cysteine residue in different locations. The enantiomeric excess for the hydrolysis of the isopropyl ester of alanine could be

improved to 94%, although only relatively minor improvements resulted from altering the cofactor linkage site (Figure 5).[144] These remarkable studies mark the first examples of enantioselective catalysis involving small molecule substrates using ArMs generated via covalent scaffold modification.

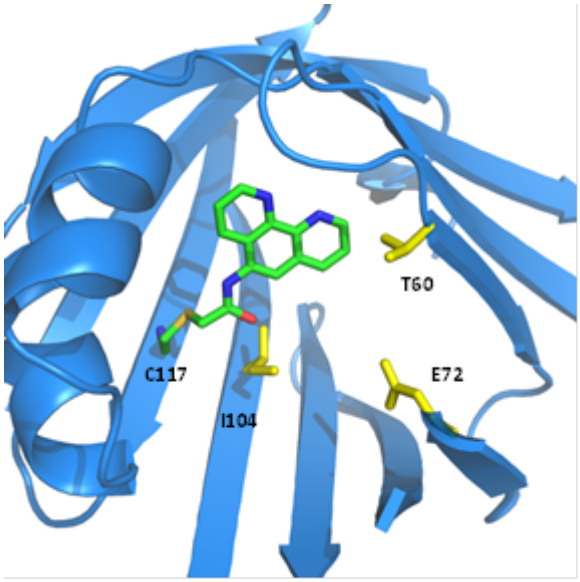

Figure 5. Cartoon representation of ALBP protein (PDB: 1A18) studied by Distefano.[142-144] Highlighted 1,10-phenanthroline (coloured in green C, blue N and red O) linked to Cys117. Side chains of aminoacids mutated to cysteine in additional constructs with alternative phenanthroline positions highlighted as yellow sticks.

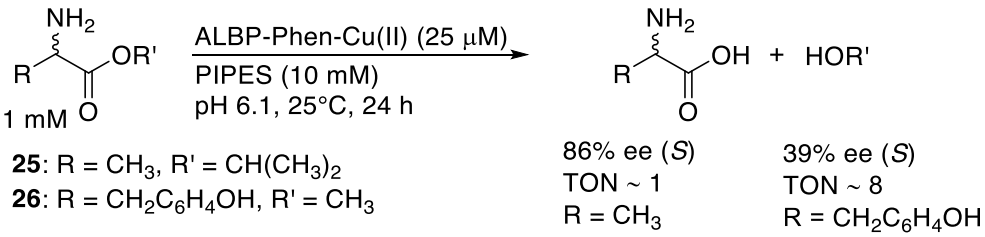

Scheme 8. Kinetic resolution of racemic amino acid esters catalyzed by a Cu(II)-phenanthroline complex anchored covalently to a cysteine residue in the cavity of ALBP.

M. D. Distefano and coworkers also investigated the immobilization of a pyridoxamine-derived cofactor in fatty acid binding proteins such as ALBP and the closely related intestinal fatty acid binding protein (IFABP) by cysteine linkage via disulfide bond formation.[145] One study scrutinized the effect of Cu(II), Ni(II), and Zn(II) on the catalytic performance of a range of constructs, including some where the location of the cysteine

in the protein cavity required for immobilization of the artificial cofactor had been altered by site directed mutagenesis.[146] Added metal ions were observed to result in rate acceleration but also erosion of enantioselectivity for the transamination of keto-carboxylic acids with phenylalanine as a sacrificial donor. Both a Cu(II)-Phen dependent hydrolase and a pyridoxal-derivative dependent transaminase were characterized by X-ray crystallography.[143]

Inspired by reported phytase inhibition by transition metal oxoanions and the structures of vanadium chloroperoxidases, R. Sheldon and coworkers doped phytase from *Aspergillus ficuum* with vanadate.[147] The resulting ArM oxidized thioanisole **27** in the presence of H_2O_2 at considerably increased rates relative to free vanadate and provided an *ee* of up to 66% (*S*)-**28** (Scheme 9). Unexpectedly, phytase even in the absence of vanadate also catalyzed the reaction, albeit at reduced rates and enantioselectivity. The original study was published in 1998 and was followed by further investigations communicated in 2000.[148-149] These later studies examined a range of protein hosts from various sources, e.g. acid phosphatase, apo-ferritin, aminoacylase, sulfatase etc. with vanadate, and phytase doped with alternative transition metal oxoanions, namely MoO_4^{2-}, ReO_4^-, and WO_4^{2-}. Although significant enantiomeric excess and rate acceleration was observed in the oxidation of thioanisole, none of the systems tested could improve on the original phytase-vanadate system.

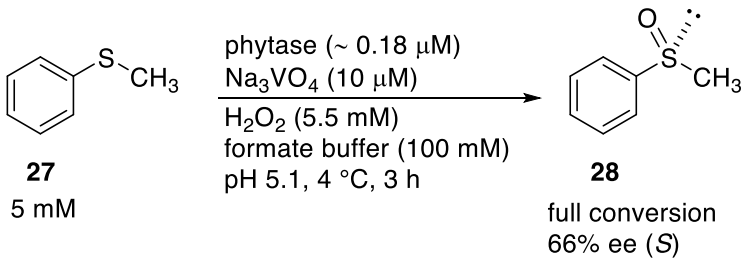

Scheme 9. Sulfoxidation of thioanisole with H_2O_2 catalyzed by vanadate-doped phytase.

M. G. Finn, R. A. Lerner, and C. F. Barbas, III, published in 1998 a study on the effect of metal ions on rate and enantioselectivity of antibody catalyzed aldol reactions.[150] The antibodies (33F12 and 38C2) were originally raised against a hapten able to form a covalent intermediate with a reactive lysine residue in the antibody active site via reactive immunization.[151-152] A wide range of metal ions was examined, but substantial effects were only observed for Pd(II) salts: rate enhancements of 2.3-2.6 fold with variable enantioselectivity. The authors concluded that a direct binding of Pd in the active site seemed unlikely given the moderate effect and favoured instead an allosteric interaction as explanation for their observations.

Following Whiteside's - at the time two-decade old - lead, A. S. C. Chan and coworkers published in 1999 a study in which more rigid and, importantly, enantiopure pyrphos ligand was biotinylated and the corresponding Rh(I)-complex **29** incorporated into avidin.[153] The authors studied the effect of hydrogen pressure, temperature and stereochemistry of the pyrphos moiety on the catalysis outcome in the hydrogenation of itaconic acid **30**, Scheme 10. Although stereoselectivity was improved in the presence of avidin and could even be inverted compared to the protein free cofactor, only moderate enantioselectivities were reported.

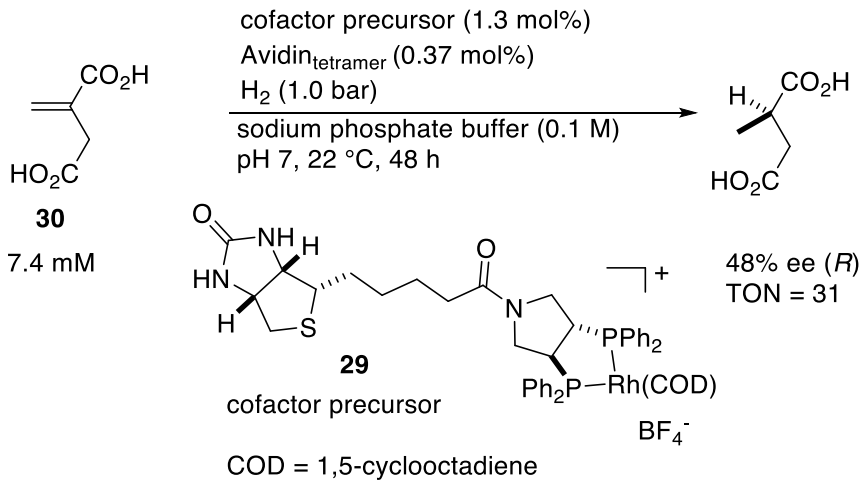

Scheme 10. Asymmetric hydrogenation of itaconic acid catalyzed by an enantiopure biotinylated Rh-diphosphine complex in the presence of avidin.

S. Nimri and E. Keinan reported in the same year on antibodies raised against a modified hapten compared to Keinan's previous design from 1990 (Figure 2 c).[154] Apart from a variation of the porphyrin scaffold (TCPP instead of TCP), the axial hydoxo-ligands of the tin center were exchanged for bulky α-naphthoxy-groups with the intention of creating a substrate binding site in the antibody scaffold. Antibody metallation with TCPP-Ru(II)-CO led to an active and enantioselective ArM sulfoxidase in the presence of iodosobenzene. A k_{cat} of 24 min^{-1}, a K_M of 10 mM, and an ee of 43% were obtained for the oxidation of thioanisole **27**, although only 75% of the cofactor was bound to the antibody even using ~13:1 antibody:cofactor ratio. A significantly higher k_{cat}-value (174 min^{-1}) was determined for the electron-rich substrate 4-methoxythioanisole, albeit at the expense of a diminished enantioselectivity (27% ee).

M. Marchetti and coworkers studied the biphasic rhodium-catalyzed hydroformylation of alkenes in the presence of a range of protein scaffolds. The initial study was published in 2000 and followed by a more detailed investigation in 2002.[155-156] Most successful system reported was generated by combining human serum albumin with [Rh(acac)$(CO)_2$]. A TON of 741,000 was observed at a TOF of 30,000 h^{-1}. At higher catalyst loadings (S : C = 10,400 : 1) good recyclability was demonstrated. 1,1-Diarylethenes were not viable ArM substrates despite their reactivity toward the common TPPTS-Rh(I) system (TPPTS = triphenylphosphine-3,3',3''-trisulfonic acid trisodium salt). A branched : linear-ratio of 90 : 10 was observed for styrene, whereas only a qualitative comment on stereoinduction (i.e. very low, but observable) was made. Stereoselectivity in biphasic hydroformylation reactions is generally considered to be problematic.[157]

In 2002, K. M. Nicholas, K. D. Jandas, and coworkers published an unexpected application of a monoclonal antibody for the generation of an artificial metalloenzyme.[158] Whereas previously antibodies were raised against metal complexes or ligands for the generation of ArMs, the authors employed an antibody selected for a completely unrelated activity, namely aldolase activity, as a protein host for a copper(II)-bis-imidazole complex. The antibody 38C2 discussed above contained a reactive lysine residue of low pK_a inside its binding pocket.[151-152] This lysine residue was modified with an electrophilic derivative of the copper(II)-bis-imidazole complex and the resulting construct successfully employed for the hydrolysis of picolinic ester **24** (k_{cat} = 2.3 min^{-1}, K_m = 2.2 mM), while it was inactive for benzylic hydroxylation with ascorbate/O_2 or *t*-BuOOH.

The advent of increasingly convenient site directed mutagenesis in the late 70's (Nobel prize in chemistry for M. Smith and K. B. Mullis in 1993) opened new opportunities to optimize natural enzymes enzymes for biocatalysis.[159-160] The possibilities for biocatalyst development were even further expanded by the development of directed evolution methods involving iterative round of random mutagenesis or gene shuffling followed by screening or selection.[161] These procedures involve large theoretical library sizes compared to site directed 'design'-protocols, but they enable identification of mutations that are not obvious from structural data. Moreover, the ability to simply iterate the mutagenesis and screening procedure eliminates the need to exhaustively (or even remotely) sample the full library diversity. A wide range of site-directed and random mutagenesis strategies are now commonly used to rapidly optimize biocatalyst activity.[162-163]

Despite these advances, the considerable effort required to express, purify, modify, and evaluate protein scaffolds for ArM catalysis posed and continues to pose a considerable

obstacle to optimizaing ArMs via mutagenesis. In 2002, M. T. Reetz proposed in conceptual articles the application of directed evolution protocols to hybrid catalyst development for non-biological reactions such as hydroformylation, olefin hydrogenation, metathesis, and allylic substitution.[164-165] In contrast, T. R. Ward and coworkers initially selected a chemo-genetic strategy to reduce the number of ArM components (protein scaffolds and cofactors) and simplify ArM optimization. This strategy involves the combination of a small set of protein mutants with a small set of cofactor variants to generate ArM diversity.[31]

Many exciting studies on systems related to ArMs but outside the scope of this review as outlined in the introduction were reported during the timeframe discussed in this section. These include active site redesign of natural metalloenzymes to elucidate structure-function relationships,[110] and early efforts on de-novo designed coiled-coil and helical bundle metallopeptides that would later be used for ArM catalysis.[166-168] Considering the widened opportunities for rational design guided by structural information and molecular modelling, standardized and new molecular biology protocols and kits, the renewed interest in water compatible transition metal catalysts and, a few years later, affordable gene synthesis, the ground was set for further research endeavors in the field of artificial metalloenzymes.

4. Reduction Chemistry

4.1 Hydrogenation

The discovery of homogeneous, phosphine-transition metal complexes capable of promoting the addition of molecular hydrogen to carbon-carbon double bonds ultimately precipitated the entire field of asymmetric transition metal catalysis.[101, 169] Factors contributing to the importance of this reaction for organic synthesis include its i) perfect atom economy, ii) high reaction rates, iii) high tunability via ligand design, and iv) ability to generate valuable, chiral products. Unsurprisingly, asymmetric hydrogenation has also been extensively explored as a benchmark reaction for artificial metalloenzymes.

As previously noted, Whitesides' seminal example of asymmetric hydrogenation using a biotinylated Rh(I)-bisphosphine complex embedded within avidin constituted not only the first example of ArM-catalyzed hydrogenation, but also the first example of asymmetric catalysis using an ArM and the first example of ArM formation via non-covalent cofactor anchoring. This work was first revisited by A. S. C. Chan and coworkers in 1999 (Scheme 10).[2, 153] M. T. Reetz later demonstrated that Cu-, Pd-, and Rh-complexes of maleimide-substituted dipyridine compounds (Figure 6) could readily alkylate the active site cysteine of papain, a cysteine protease. Only preliminary catalytic activity was reported for these ArMs, which were said to catalyze hydrogenation with low enantioselectivity.[164-165]

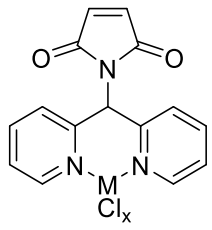

M = Cu, x = 2
M = Pd, x = 2
M = Rh, x = 3

Figure 6: Dipyridine complexes by Reetz.[164]

Initial efforts in the Ward group on building an artificial hydrogenase aimed at improving the original Whitesides system. Instead of avidin, the close homologue streptavidin (pI = 6.2) was used, based on the idea that the high pI of avidin (pI = 10.4) might significantly reduce the affinity of cationic complexes such as [Rh(COD)(**34**)]$^+$ for the host protein. Artificial hydrogenase [Rh(COD)(**34**)]$^+$ · WT Sav was used for the reduction of *N*-amidoacrylic acid to yield (*R*)-*N*-acetamidoalanine **31** with an ee of 92 % and quantitative conversion with 1 mol % catalyst loading. To obtain a structural model of the hydrogenation catalyst, docking studies were performed. Aminoacid S112 was found to be located in close proximity to the position of the rhodium moiety.[170] Thus, Sav variants bearing the remaining nineteen proteinogenic amino acids in position S112 were expressed and purified. In addition, a library of 22 biotinylated ligands was produced consisting of two different bisphosphine ligands (**34, 36**) and eleven spacer units.[44, 171-176] All 20 Sav isoforms were screened in the presence of the 22 biotinylated Rh-complexes and two *N*-protected dehydroamino acid substrates to yield **31** and **32**. The observed results (Scheme 11 and Table 3) and conclusions can be summarized as follows:

i) Generally, the “chemical” Rh-complex library contributed more to diversity than the “genetic” Sav-mutant library.

ii) The more flexible bisphosphine **34** scaffold afforded more active and selective ArMs than the rigid six-membered chelate formed with **36**.

iii) The flexible **34** is likely to adopt an enantioenriched conformation inside the scaffold protein reminiscent of the “induced lock-and-key” hypothesis.

iv) The two substrates displayed similar reactivity and selectivity profiles. This suggested a broad substrate scope of the artificial transfer hydrogenase, reminiscent of homogeneous catalysts.

v) Mutation at position S112X enabled an inversion of enantioselectivity (Table 3, entries 13 and 14)

vi) Good (*S*)-selectivity was obtained with complex **40** inside 'cationic' S112X Sav mutants (X = H, K, R; Table 3, entries 2-4).

vii) The (*S*)-selectivity could be further improved by introduction of (*R*)-proline as a spacer between the biotin anchor and the flexible **34** using either Avi or Sav as host protein.[174]

viii) Constrained spacers such as proline improved the stability of the ArM against organic solvents.[174]

ix) Both the free cofactor as well as the ArM display Michaelis-Menten kinetic behavior (k_{cat} = 3.1 min^{-1} vs. 12.3 min^{-1}; K_M = 7.38 vs. 4.36 mM for [Rh(COD)(**34**)]$^+$ and [Rh(COD)(**34**)]$^+$ · WT Sav, respectively).

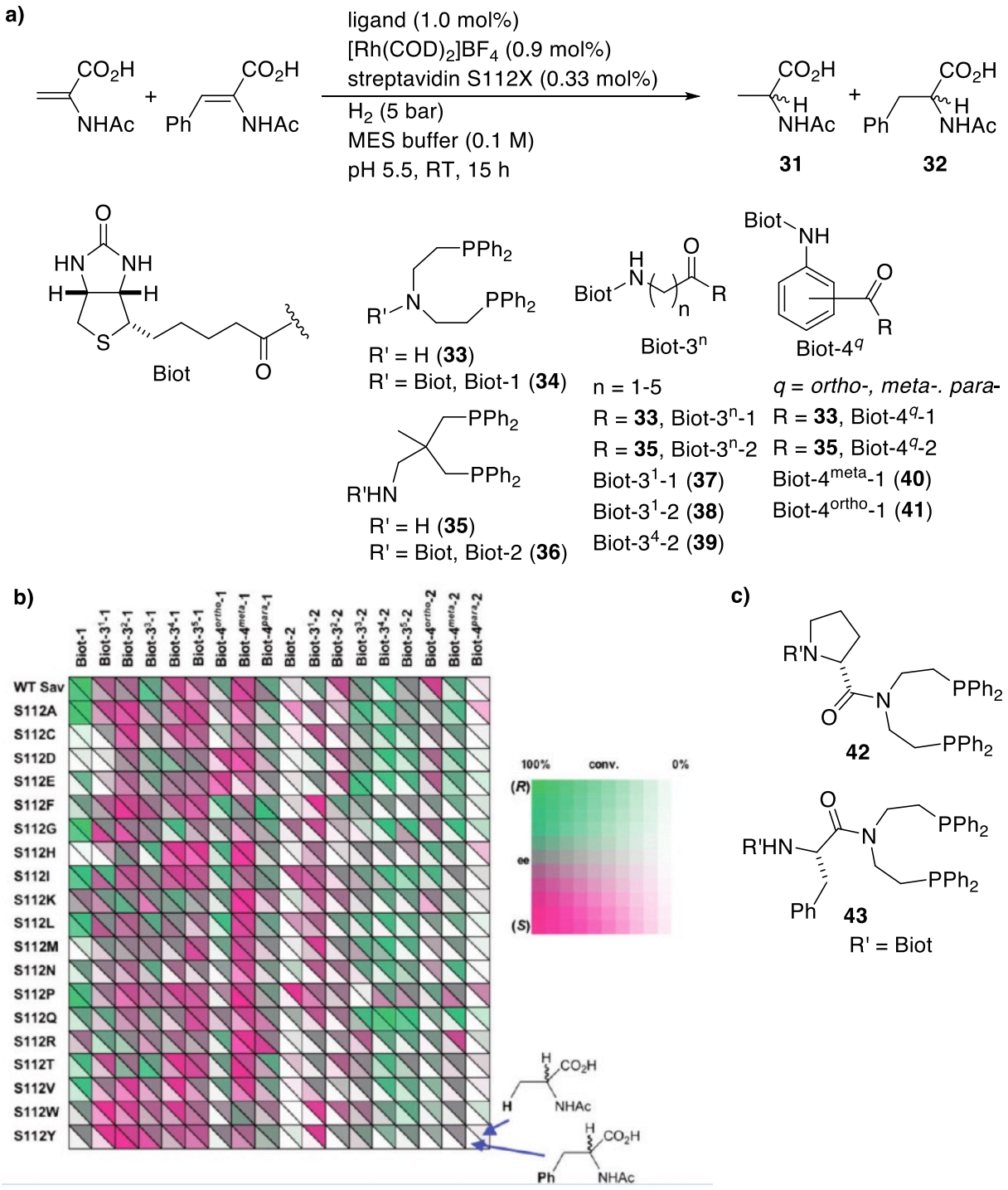

Scheme 11: Biotinylated rhodium diphosphine complexes anchored within Sav catalyze the asymmetric hydrogenation of dehydro aminoacid derivatives. To optimize the reaction, a library of biotinylated rhodium complexes with varying spacers and ligand head groups a) was combined with a Sav site-saturation mutagenesis library of position S112 . Both conversion and enantioselectivity for each protein-ligand combination are summarized in a fingerprint display b). Adapted with permission from ref. [175]. Copyright Wiley VCH 2005.

Table 3. Selected results for chemogenetic optimization of the artificial hydrogenase based on the biotin-(strept)avidin technology.

Entry	Ligand	Protein	**31** ee (%)	**31** Conv. (%)	**32** ee (%)	**32** Conv. (%)
1	**34**	WT Sav	94 (*R*)	quant.	93 (*R*)	84
2	**40**	S112H	58 (*S*)	quant.	81 (*S*)	88
3	**40**	S112K	63 (*S*)	quant.	88 (*S*)	89
4	**40**	S112R	63 (*S*)	quant.	86 (*S*)	71
5	**38**	S112W	59 (*S*)	96	33 (*S*)	8
6	**39**	S112Q	87 (*S*)	quant.	92 (*S*)	77
7	**42**	WT Avi	87 (*S*)	quant.	89 (*S*)	quant.
8	**42**	WT Sav	86 (*S*)	quant.	91 (*S*)	quant.
9	**42**	WT Sav[b]	87 (*S*)	quant.	86 (*S*)	94
10	**42**	WT Sav[c]	83 (*S*)	90	87 (*S*)	85
11	**42**	WT Sav[d]	76 (*S*)	76	89 (*S*)	36
12	**42**	S112W	95 (*S*)	quant.	95 (*S*)	quant.
13	**43**	S112H	87 (*S*)	quant.	78 (*S*)	65
14	**43**	S112M	73 (*R*)	quant.	87 (*R*)	quant.

[a] quant.: quantitative conversion; [b] Reaction carried out in 45% DMSO; [c] Biphasic with EtOAc; [d] Protein immobilization on biotin-sepharose.

In early studies, van Koten and Klein-Gebbink demonstrated that lipase inhibitors, such as nitrophenol phosphonate esters, can be used to selectively anchor metallopincers within Cutinase (**44**).[177-179] Cutinase from *Fusarium solani pisi* is a 21 kDa lipase containing a Ser_{120}-Asp_{175}-His_{188} catalytic triad that enables hydrolysis of fatty acids. Phosphonate esters function as transition-state analogues for this reaction and react irreversibly with Ser_{120}. A pincer–metal complex linked to a phosphonate moiety (**45** or **46**) may thus be suitable for covalent anchoring to cutinase. (Scheme 12). M. T. Reetz and coworkers discussed related studies with an esterase in 2002, but the resulting construct suffered from low hydrolytic stability. They suggested to improve hydrolytic stabilty by exchanging a nitrophenoxy-group at phosphorus for an ethoxygroup, a strategy later realized by van Koten and Klein-Gebink.[164]

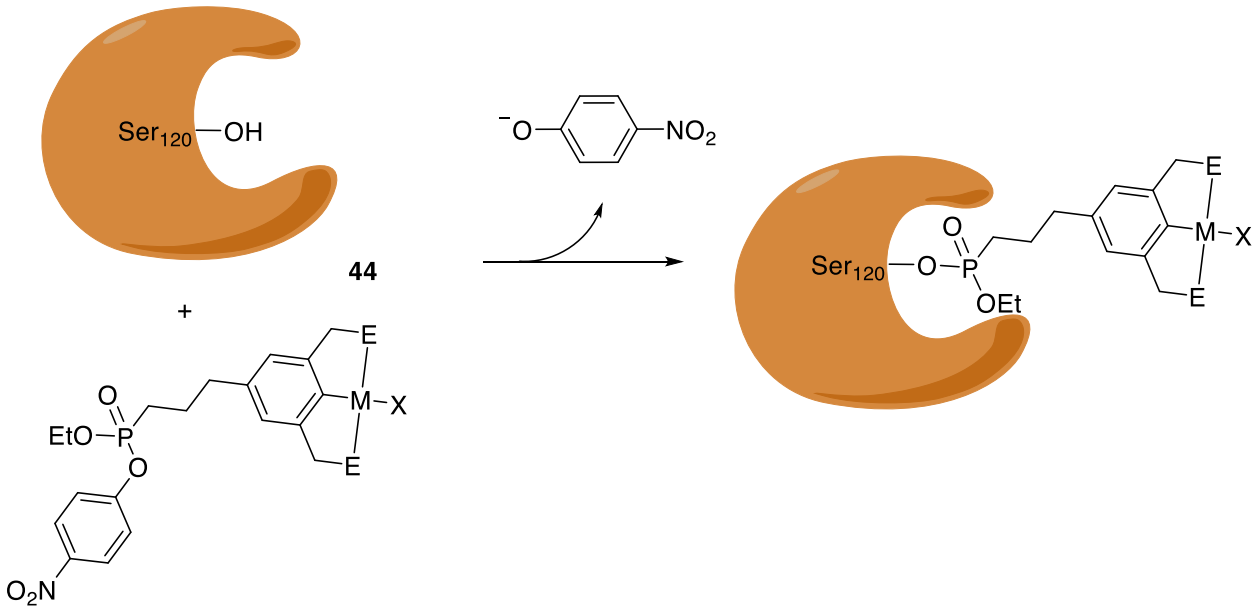

45: M = Pt, X = Cl, E = NMe_2
46: M = Pd, X= Br, E = SMe

Scheme 12. Covalent anchoring of pincer–metal complexes via nucleophilic substitution of an activated phosphonate ester Ser 120 in the active site of cutinase **44**. The anchoring is conveniently monitored by the release of *para*-nitrophenolate.

van Koten and Klein-Gebbink subsequently extended their proof-of-principle approach with Pd- and Pt-pincer complexes to Rh-based systems for the creation of artificial hydrogenases.[180] Building on the work of Kühn *et al.* concerning the hydrogenation of acetophenone in aqueous media with rhodium *N*-heterocyclic carbenes (NHCs),[181] Klein-Gebbink covalently linked the lipase inhibitor **47** within Cutinase **44** and CalB (33.5 kDa, lipase from *Candida antarctica)*, Scheme 13.[182]

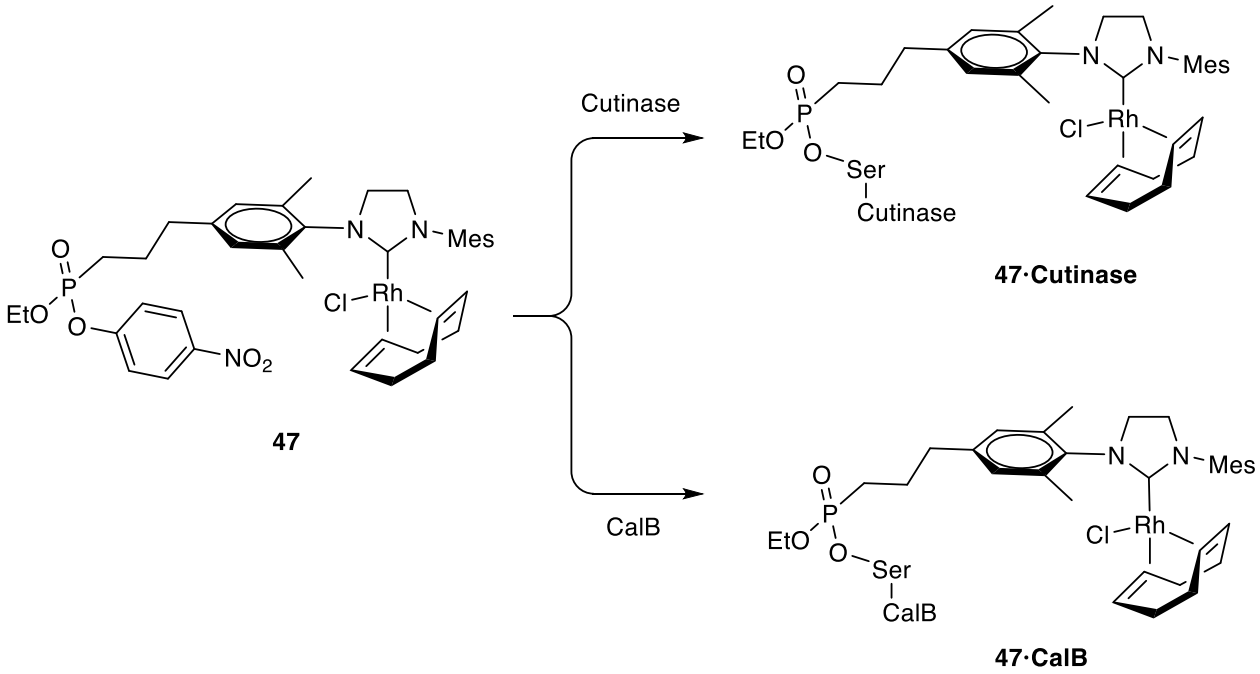

Scheme 13. Covalent anchoring of a Rh(NHC) in serine-hydrolases for the creation of artificial hydrogenases.

The resulting hybrids **47**·Cutinase and **47**·CalB (obtained using Cutinase and CalB respectively), were tested in the hydrogenation of acetophenone **48**, and methyl 2-acetamidoacrylate **49** (Scheme 14). Acetophenone was reduced in 90% yield (18 TON) with the free Rh-NHC catalyst (Table 4, entry 1), while the Rh-ArMs showed a reduced catalytic activity, yielding 1-phenylethanol **50** in 27% and 0% yield for Rh-cutinase **47**·Cutinase and **47**·CalB, respectively (Table 4, entries 2 and 3). For the hydrogenation of the olefinic substrate, both artificial hydrogenases afforded complete conversion to methyl-acetylalaninate **51**, (Table 4, entries 5 and 6), highlighting the preferred reduction of olefins over ketones.[183] Accordingly, **47**·CalB was fully chemoselective for the hydrogenation of olefin **49** (Table 4, entries 3 and 6), highlighting the benefit of the deep binding pocket provided by the active site in CalB to discriminate between both substrates. Similar results were observed for **47**·Cutinase at shorter reaction times (Table 4, entries 7-10). Unfortunately, no enantioselectivity was observed for any of the systems reported. These examples highlight the potential of second coordination sphere interactions provided by a host protein to discriminate between similarly reactive substrates.

Table 4. Selected results for the catalytic hydrogenation of acetophenone **48** and methyl 2-acetamidoacrylate **49** with **47**·Cutinase and **47**·CalB.

Entry	Protein	Sub.	T (h)	Ratio [Rh]/[Prot]	ee (%)	Conv. (%)	TON
1	–	**48**	20	-	*rac.*	90	18
2	cutinase	**48**	20	1	*rac.*	27	5.4
3	CalB	**48**	20	1	*rac.*	0	0
4	–	**49**	20	-	*rac.*	>99	20
5	cutinase	**49**	20	1	*rac.*	>99	20
6	CalB	**49**	20	1	*rac.*	>99	20
7	–	**48+49**	20	-	*rac.*	71, 93[a]	14, 19[b]
8	cutinase	**48+49**	20	1	*rac.*	15, 78[a]	3, 16[b]
9	–	**48+49**	0.66	-	*rac.*	15, 70[a]	3, 14[b]
10	cutinase	**48+49**	0.66	1	*rac.*	0, 63[a]	0, 13[b]

[a] Conversion for 1-phenylethanol **50** and methyl acetylalaninate **51**, respectively. [b] TON for 1-phenylethanol **50** and methyl acetylalaninate **51**, respectively.

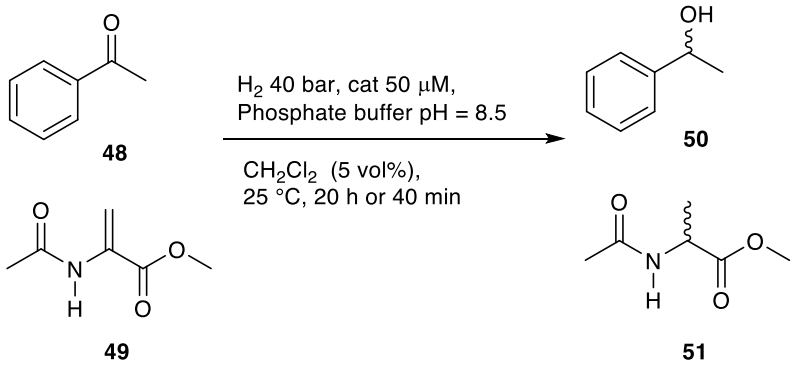

Scheme 14. Hydrogenation reaction catalalyzed by Cutinase and CalB.

Papain was used by J. G. de Vries and coworkers as a scaffold for covalent attachment of a monodentate phosphite ligand (Scheme 15) that was subsequently metallated by $[Rh(COD)]^+$ to generate an hydrogenase, but only very modest enantioselectivity was observed for the reduction of methyl-2-acetamidoacrylate.[184]

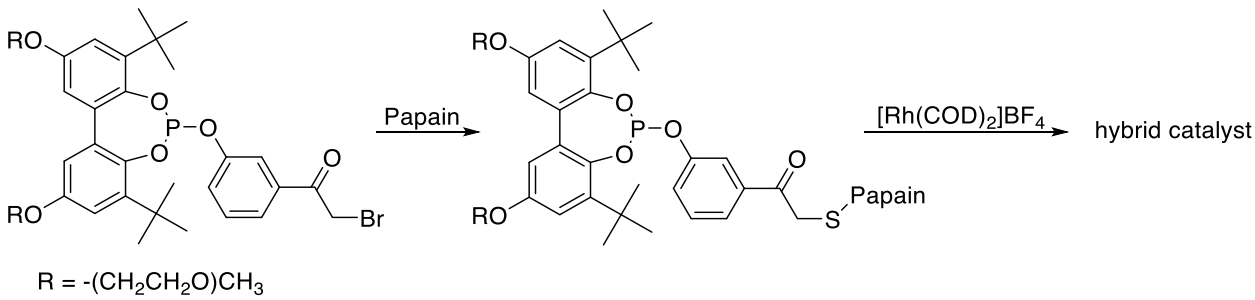

Scheme 15. Immobilization of a bulky phosphite ligand by thioether formation with the reactive site cysteine of papain and subsequent complexation to Rh(I).

Kamer demonstrated that a non-catalytic cysteine residue in apo-photoactive yellow protein (PYP) could be selectively acylated with a carboxylic imidazolide-substituted bisphosphine. This phosphine could also be metallated with $[Rh(cod)(MeCN)_2]BF_4$ (**52**) and subsequently reacted with PYP to generate an artificial hydrogenase, which catalyzed the reduction of dimethyl itaconate (**53**) with full conversion but low ee (Scheme 16). [185]

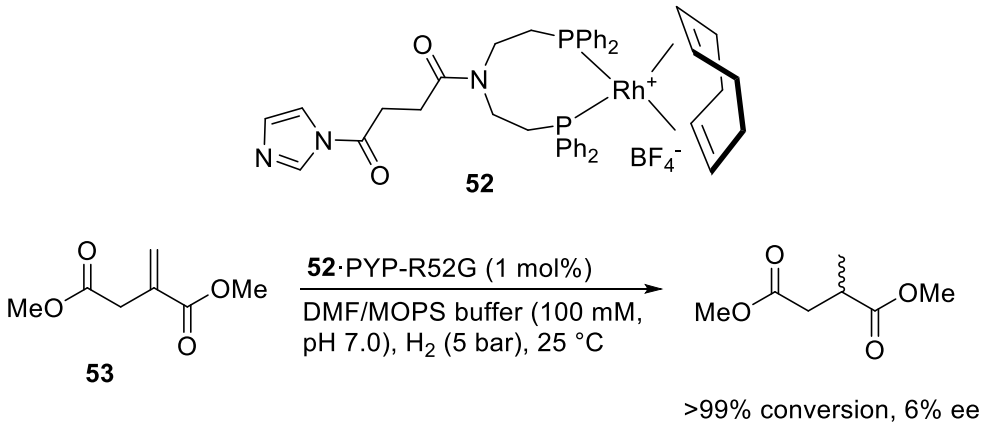

Scheme 16. Hydrogenation of itaconic acid methyl ester catalyzed by **52**.

A. Harada and coworkers elicited a monoclonal antibody 1G8 against an achiral rhodium complex **54**, Scheme 17.[186] In the hydrogenation of the 2-acetamidoacrylic acid **8**, the antibody 1G8 in combination with the hapten **54** afforded the reduction product with > 98% *ee* (*S*) and a TON of 854. In contrast, racemic product was obtained with either **54** or **54**·BSA (BSA = bovine serum albumin) accompanied by lower TONs, Table 5.

Table 5. Selected results for the hydrogenation of **8** catalyzed by an antibody loaded with hapten **54**.

Entry	Protein[a]	*ee* (%)	TON
1	No protein	0	409
2	Antibody 1G8	> 98 (*S*)	854
3	BSA	0	446

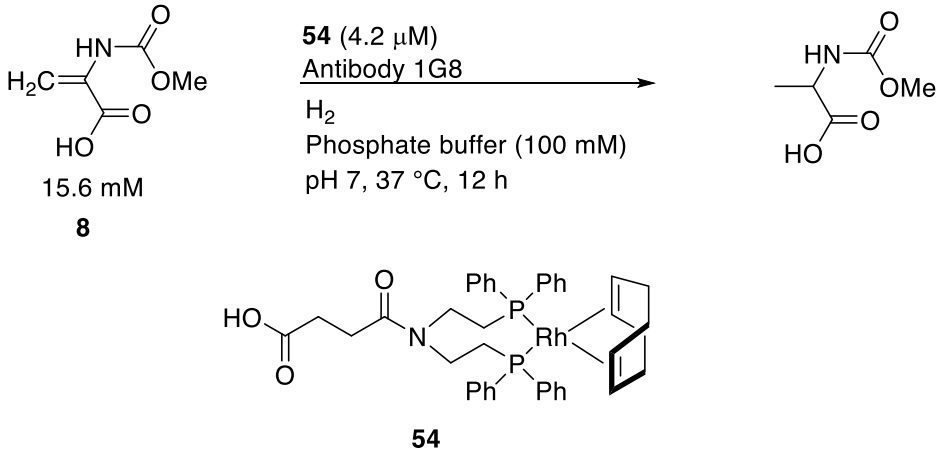

Scheme 17. Combination of hapten **54** with the antibody results in a highly selective and active hydrogenation catalyst.

A number of researchers have explored the formation of ArMs by substituting the catalytic Zn ion located in a His_3 binding site of carbonic anhydrase with different metals. For example, Kazlauskas created a *cis*-stilbene hydrogenase by metallation of apo-hCAII with $[Rh(cod)_2]BF_4$.[187] In addition to Rh incorporation in the CA active site, Rh also bound to the surface of the scaffold (Rh : hCAII = 6.5 by ICP-MS), leading to *cis/trans* isomerization (hydrogenation : isomerization = 6.3), Scheme 18. Site-directed mutagenesis was used to remove 9 histidine residues on the surface of hCAII that were believed to be involved in non-specific Rh-binding. The resulting ArM, 9*His-hCAII-[Rh], was found to have a reduced Rh : hCAII ratio of 1.8, provided an increased hydrogenation : isomerization ratio of 20.6, and displayed improved specificity for *cis*-stilbene over *trans*-stilbene, Table 6.

Table 6. Hydrogenation and *cis/trans* isomerization of *cis*-stilbene catalyzed by 9*hCAII-[Rh].

Entry	Catalyst	Rh / *h*CAII Ratio.	**55** / **56**
1	$[Rh(cod)_2]BF_4$	-	6.3
2	hCAII-[Rh]	6.5	3.5
3	9*His-hCAII-[Rh]	1.8	20.6

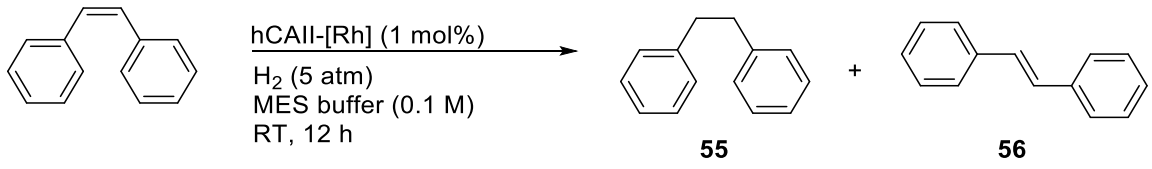

Scheme 18. Hydrogenation of styrene catalyzed by Rh-substituted hCAII.

Eppinger designed cofactors comprised of not only a catalytically active metal complex and a reactive group (epoxide) to covalently link the cofactor to protein scaffolds, but also a non-covalent amino acid recognition element to control cofactor orientation within the scaffold.[188] Half-sandwich ruthenium and rhodium cofactors were constructed in this manner and linked to cysteine proteases in the papain family to generate ArM hydrogenases. Ketone hydrogenation could be achieved with up to 64% ee for *p*-chloroacetophenone as substrate (Table 7 and Scheme 19).

Table 7. Hydrogenation of aromatic ketones catalyzed by protein affinity labels.

Entry	Catalyst	Substrate	H_2 (bar)	*t* (h)	Yield (%)	*ee* (%)
1	**57**	**60**	25	65	4	4 (*R*)
2	**57**·Papain	**60**	75	96	89	24 (*R*)
3	**58**·Papain	**60**	35	65	41	20 (*R*)
4	**59**·Papain	**60**	96	75	44	20 (*R*)
5	**57**·Papain	**61**	75	96	12	64 (*R*)

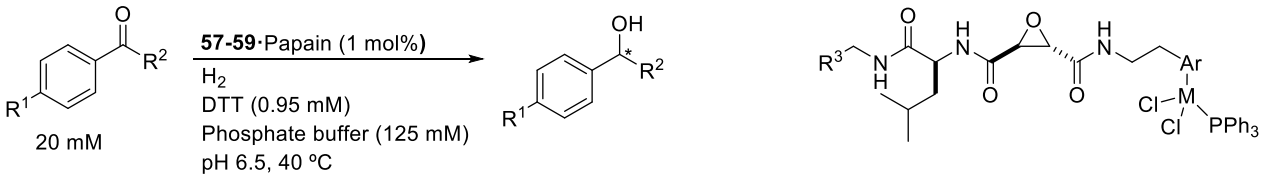

60: R^1 = H, R^2 = CF_3
61: R^1 = Cl, R^2 = CH_3

57: R^3 = Ph, Ar = $C_5(CH_3)_4$, M = Rh
58: R^3 = ^{i}Pr, Ar = $C_5(CH_3)_4$, M = Rh
59: R^3 = Ph, Ar = C_6H_5, M = Ru

Scheme 19. Hydrogenation of ketones catalyzed by Rh/Ru-substituted Papain.

Knölker-type [η^4-(cyclopentadienone)$Fe(CO)_3$] complexes catalyze the hydrogenation of polarized C-X double bonds (X = O, N).[189] Renaud, Ward and coworkers investigated the potential of biotinylated Knölker-type complexes (Figure 7) to catalyze the enantioselective hydrogenation of aromatic ketones and imines inside Sav.[190] A library of seven catalysts was synthesized with a biotin anchor tethered to the cyclopentadienone moiety via various linker groups. Hydrogenation of ketone α,α,α-trifluoro-acetophenone afforded the corresponding secondary alcohol with 20 TON but only 9 % ee. The best enantioselectivity (34 % ee (*R*)-product) was obtained in the conversion of *p*-methoxy-acetophenone albeit with only a single turnover.

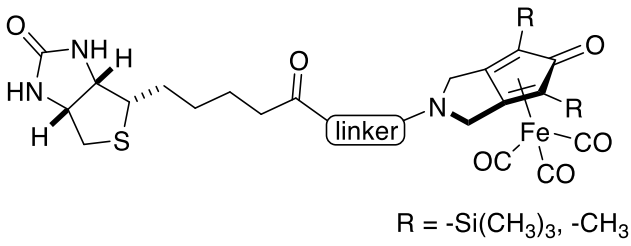

R = -Si(CH$_3$)$_3$, -CH$_3$

Figure 7. Biotinylated Knölker-type complexes.

4.2 Hydrogen Generation: Towards Artificial Hydrogenases

Today, scientists around the world face the challenge of finding a sustainable source of energy to support tomorrow's societal needs. In this context, valorization of solar energy is regarded by many as the "Holy Grail". However, efficient ways to convert solar energy directly to electricity or to a fuel, for storage and transportation, remains challenging. The development of artificial photosynthesis would allow conversion of sunlight into a fuel. Hydrogen (H_2) is one of the most explored potential fuel candidates.[60] Interestingly, its production from light and water has been observed in a living organism, and biocatalytic hydrogen production is catalyzed by hydrogenases. These are classified according to the nature of their active site, namely [FeFe]-, [NiFe]-, and [Fe]-hydrogenases. They catalyze the generation of H_2 from protons and electrons provided by the electron transport chain of photosynthesis under near thermodynamic equilibrium conditions (i.e. no overpotential required) with high catalytic rates (TOF up to 20 000 s^{-1}).[68] Interestingly, hydrogenases operate in both in the forward and reverse reaction and approach the efficiency of platinum.

The technological applications of natural hydrogenases are impaired by (i) their biosynthesis, which requires complex maturation machinery, (ii) their air sensitivity, and (iii) their high molecular weight, which limits the density of active sites that can be immobilized on an electrode.[58]

The former limitation has been recently addressed by Fontecave and coworkers with the [FeFe]-hydrogenase HydA. The natural formation of its di-iron catalytic site (H-cluster) requires a complete maturation machinery, involving at least HydE, HydG and HydF. HydE and HydG provides the iron-ligands (CO, CN^-, aza-propanedithiol), and HydF is the scaffold protein in which the di-iron complex is ultimately assembled. In the last step, the nearly-mature di-iron complex is transferred to apo-HydA. Fontecave and coworkers demonstrated that a hydrogenase could be maturated *in vitro*, without the need of the entire maturation machinery. By loading an inactive artificial di-iron cofactor into apo-HydF, they could transfer the synthetic complex into the apo form of the hydrogenase HydA, reconstituting a fully active HydA (Scheme 20, path a)).[191] This work unambiguously settled the controversy concerning the nature of the central atom of the bridging dithiolate ligand: catalytic activity was detected only in the presence of a nitrogen atom at this position (X in Scheme 20). Building on these results, Happe and Fontecave demonstrated that the use of HydF could even be avoided, that is, a direct loading of a synthetic complex into apo-HydA is possible (Scheme 20, path b).[192] Building upon this strategy, Hu and coworkers reported the direct reconstitution of an [Fe]-hydrogenase by loading its apo-form with a synthetic complex (Scheme 20, path c)).[193]

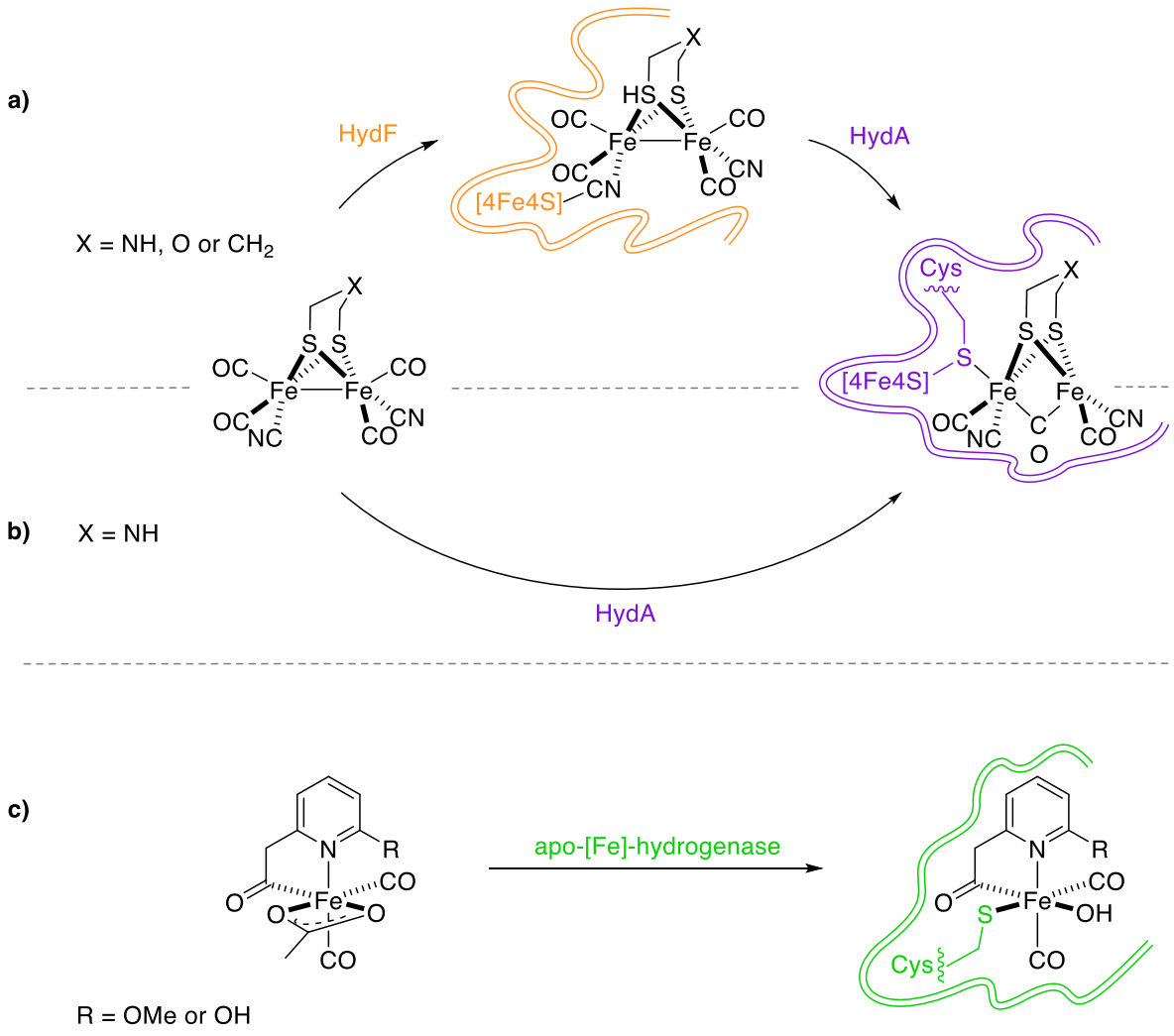

Scheme 20. Reconstitution of apo-hydrogenases with synthetic cofactors affords functional hydrogenases.

Besides shedding light on a long controversy concerning the key features of the cofactor, this methodology demonstrated that it is indeed possible to generate an active hydrogenase without the need of its complex maturation machinery. These results are of particular interest as: i) they allow the expression of the hydrogenase in a heterologous organism and ii) they open the possibility of introducing a fully synthetic cofactor within an apo-hydrogenase. The former feature should allow large screening campaigns of hydrogenases (e.g. homologous, directed evolution), to identify variants with higher activity and/or oxygen-resistance. As demonstrated by Hu and Lubitz, subtle variations of

the cofactor lead, in most cases, to inactive hydrogenases, thus allowing to establish structure-activity relationships for the cofactor.[194]

This strategy relies on a highly evolved scaffold, optimized for hydrogen production from its constituents (i.e. presence of proton- and electron-channels leading to and from the active site). The drawbacks of this strategy lie in the complexity and the size of the scaffold. For technological applications, one would favor a scaffold reduced to its minimum size and with a structure that is stable over a wide range of conditions. With large scale applications in mind, some groups explored the possibility of assembling synthetic complexes within various protein scaffolds to produce hydrogen. Only a limited number of catalysts and protein scaffolds have been used in this strategy. Alternatively, the metal-substitution strategy to repurpose natural metalloenzymes for hydrogenase activity has also been used. In this section, we summarize the reported studies fitting into either category, with a particular emphasis on the catalytic activity of the resulting artificial hydrogenases. Several recent papers have also reviewed other aspects of artificial hydrogenases.[57, 59, 61, 66, 68, 195]

Hayashi et al. inserted synthetic complexes that mimic the active site of [FeFe]-hydrogenases into various host proteins. They datively anchored a di-iron complex into the active site of apo-cytochrome *c*.[196] This protein naturally contains a Fe-protoporphyrin(IX) cofactor that is covalently attached to the protein via thioether linkage at a Cys-X_2-Cys motif. After removal of the heme, the Cys-X_2-Cys motif of the apo-cytochrome *c* could bind catalytically-inactive $[Fe_2(CO)_9]$ **62** (Scheme 21) to afford an active artificial hydrogenase containing a $[(\mu\text{-}S)_2Fe_2(CO)_6]$-moiety. When irradiated in the presence of the photosensitizer (PS hereafter) $[Ru(bpy)_3]^{2+}$ and ascorbate as sacrificial electron donor, in Tris·HCl at pH 4.7, the artificial metalloenzyme produced hydrogen (82

TON in 2h), with a maximum observed TOF of 0.035 s^{-1} (Table 8, entry 1). Notably, the electron transport from the PS to the active site is proposed to be the limiting factor in the reaction. Although the structure of this artificial hydrogenase is poorly defined, the protein environment provides robustness to the catalytic activity. When compared to **62** bound to a synthetic heptapeptide containing the Cys-X_2-Cys motif and a His residue to mimic the active site of cyt *c*, the entire protein scaffold performed better (i.e. ~4 fold higher TOF and ~8 fold higher TON), demonstrating a protective role of the protein environment.

Next, Hayashi et al. selected a more rigid scaffold to engineer an artificial hydrogenase. The di-iron cofactor [(μ-S)$_2$Fe$_2$(CO)$_6$]-moiety was anchored via a maleimide linker to the cysteine of apo-nitrobindin Q96C (Figure 8).[197] As suggested by the docked structure, the synthetic complex **62**, (Scheme 21) is embedded in the cavity formed by the β-barrel of nitrobindin, surrounded by a well-defined protein environment. Upon irradiation, the **63**·nitrobin generated hydrogen with a maximum TOF of 0.038 s^{-1} and up to 130 TON after 6 h of irradiation (120 after 2 h) (Table 8, entry 2). Under similar conditions, the free cofactor **63** performed c.a. 3 fold faster. This phenomenon is most likely due to a decreased accessibility of the complex inside the protein, decreasing the rate of electron transfer from the PS. Despite this decrease in rate, it is clear that the protein provides a stabilizing environment to **63** since its deactivation is slower than in solution. Compared to **62**·cytochrome *c*, the activity of **63**·nitrobin was less sensitive to the pH: raising the pH to 7.8 decreased the activity of the former by 93 % versus 72 % for the latter (Table 8, entry 3). In addition, due to the well-defined environment around the active site, improving catalytic activity by rationally mutating residues around at the β-barrel cavity can be envisioned.

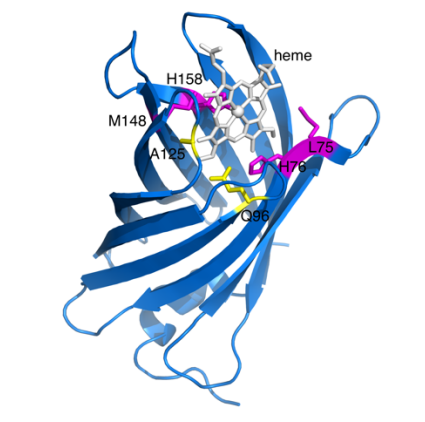

Figure 8. Nitrobindin (PDB code 3EMM) was employed to create ArMs for hydrogenation[197], ring-closing metathesis[198], phenylacetylene polymerization[199] and benzylic oxidation.[200] To afford ArMs, nitrobindin was produced in absence of the heme cofactor. Residues highlighted in yellow were mutated to cysteine residues to covalently attach a catalyst. Improved substrate accommodation was achieved by replacing bulky residues flanking the active site cavity (magenta) with smaller hydrophobic residues.

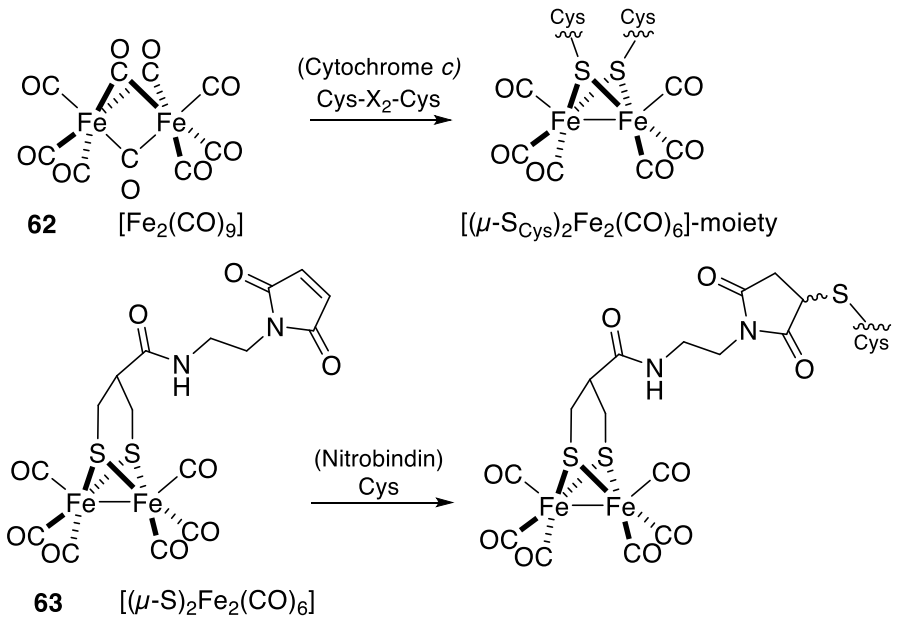

Scheme 21. Covalent anchoring of $[Fe_2(CO)_6]$ affords [FeFe]-hydrogenase mimics, upon irradiation in the presence of $[Ru(bpy)_3]^{2+}$ as photosensitizer.

Another example of an artificial hydrogenase containing a biomimetic-center was recently reported by the group of Shafaat. This work is reminiscent of the pioneering work from the groups of Moura and LeGall.[201-202] In this example, the aim was not to mimic the active site of the [FeFe]-hydrogenases, but those of [FeNi]-hydrogenases. For these systems, the nickel, coordinated by four cysteinate residues, is the redox-active metal operating

during the proton reduction. The first coordination sphere is reminiscent of rubredoxin. An iron to nickel substitution in the active site of rubredoxin yields an enzyme, termed NiRd, able to produce hydrogen, Scheme 22, a). When irradiated in presence of $[Ru(bpy)_3]^{2+}$ and ascorbate, in phosphate buffer at pH 6.5, NiRd generated hydrogen at a rate of 0.0083 s^{-1} and performedapproximately 70 TON over 8 h (Table 8, entry 4). Using Ti(III)-citrate as a light-independent electron source, NiRd performed up to 300 TON in 8 h, at 22 °C at pH 9.4 (Table 8, entry 5), suggesting that, with a strong electron source, NiRd can generate hydrogen at pH > 7. Importantly, most of the catalyst can be recycled, indicating that the inactivation is not due to protein degradation. However, this system requires a high overpotential (540 mV at pH 3-5). It is proposed that mutagenesis of residues close to the Ni-center may help to improve the catalytic properties of this artificial hydrogenase.

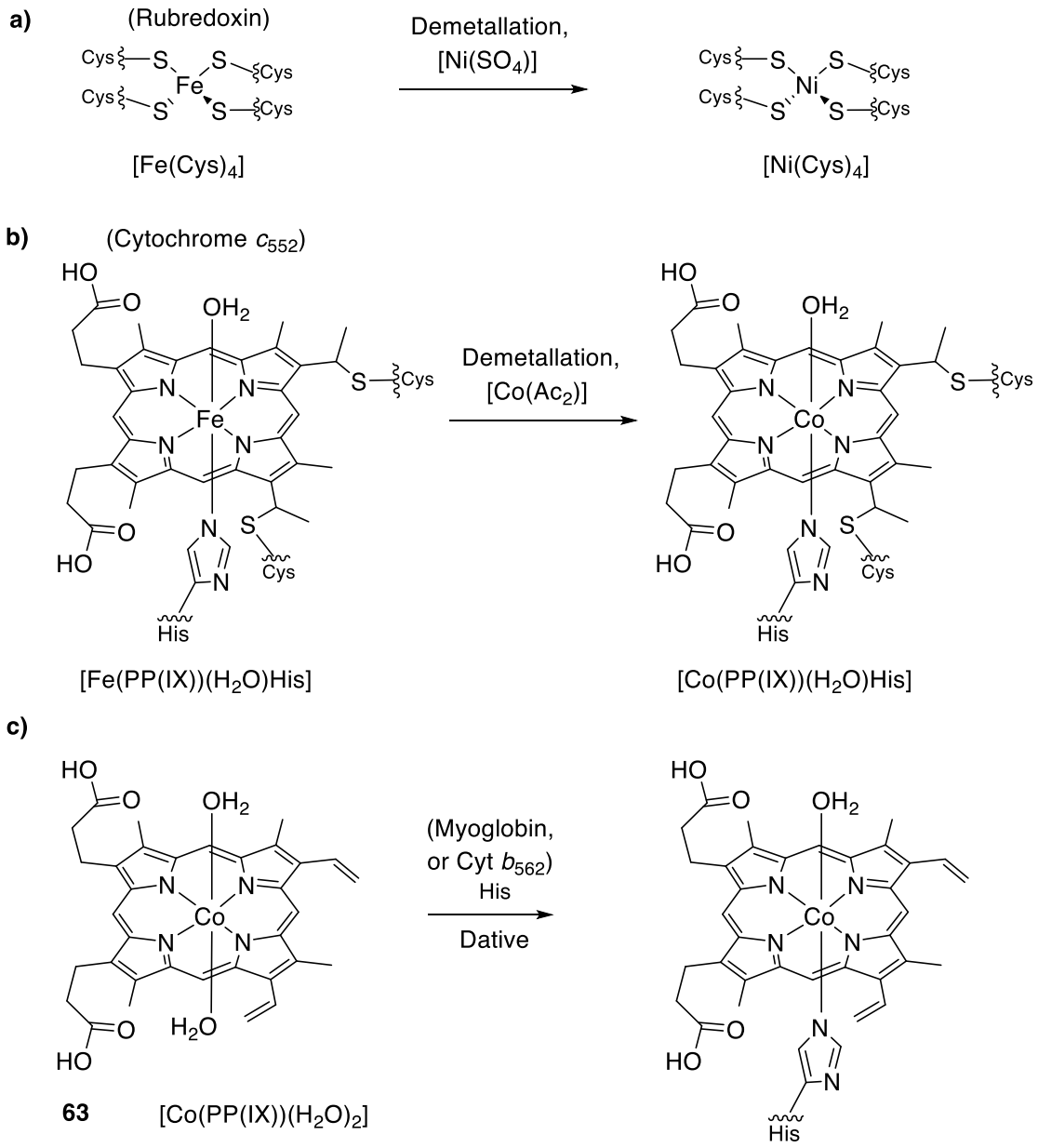

Scheme 22. Metal substitution in natural metalloenzymes yield artificial hydrogenases. The iron of rubredoxin can be replaced with nickel a). The iron in a heme protein can be substituted by cobalt either by demetallation followed by incubation with excess of $[Co(Ac)_2]$ b), or by removing the heme from the enzyme and inserting a [CoPP(IX)] complex c).

Following in Hayashi's footsteps, other groups have designed artificial hydrogenases based on heme-proteins. This family of proteins has been used extensively for their ability to bind heme moiety substituted by other metals as well as other planar complexes containing non-porphyrin ligands.[203] In addition, the potential of Co-porphyrins and cobaloximes for hydrogen production in aqueous solutions has been known since the

80's.[204-205] The latter usually require a smaller overpotential that the former, and both exhibit promising oxygen tolerance properties.

Bren and coworker demonstrated that substituting iron by cobalt in enzymes containing iron-protoporphyrin(IX) affords efficient artificial hydrogenases. The iron of the heme-protein cytochrome c_{552} from *Hydrogenobacter thermophilus* (*Ht c*-552) was substituted with cobalt, taking advantage of the thioethers linking the protoporphryin(IX) ligand and the cysteins of the protein that retains the porphyrin even under forcing conditions Scheme 22 b).[61] In this scaffold, the histidine residue acting as axial ligand was conserved. However, the distal methionine was mutated to alanine (M61A) to keep a free coordination site for proton reduction. Though no data was presented for photocatalysis, the electrocatalysis experiments showed remarkable stability for proton reduction: 11,000 TON after 6 h and up to 27,000 TON in 24 h at pH 7.0 (Table 8, entry 6). The major drawback of this system lies in the high overpotential that is required (i.e. 830 mV). On the other hand, comparing the performance of Co·*Ht c*-552 and CoMP11-Ac, an eleven aminoacid proteolytic fragment of the horse cytochrome c containing a cobalt-substituted heme, highlights the beneficial effect of a full protein environment (for a related structure of Fe-microperoxidase-8, see **217**).[206] CoMP11-Ac exhibits interesting proton reduction activity coupled with a remarkable oxygen tolerance. Although the cobalt ion possesses an identical first coordination sphere, it is exposed to the solvent in CoMP11-Ac but buried in the protein in Co·*Ht c*-552. The surrounding protein environment results in a longer catalyst lifetime (~24 h against ~4h), allowing to reach a ~10 fold higher TONs for the former. This clearly illustrates the protection provided by the second coordination sphere of the host protein. The presence of a defined protein environment however did not lead to a decrease of the overpotential required (830 vs 850 mV).

Ghirlanda and coworkers used a cobalt-substituted myoglobin termed **64**·Mb (i.e. dative anchoring via a His and no cysteine thioether linkages, Scheme 22 c).[207] Upon irradiation at pH 7.0 in the presence of ascorbate and a photosensitizer, **64**·Mb catalyzes the production of hydrogen in up to 518 TON in 12 h (Table 8, entry 7). This corresponds to a 4.3 fold increase of TON compared to the free cofactor **64**, highlighting the effect of the host protein. With this system, the maximum TON was observed at pH 7.0. Upon lowering the pH, the cofactor is released from **64**·Mb, and raising the pH decreases the proton concentration. In addition to the axial H93 ligation to the Co, second coordination sphere residues H64 and H97 form hydrogen bonds with the carboxylates of the cofactor **64**. Mutating these residues positively affects the catalytic activity. The corresponding TONs are 234 (**64**·Mb), 331 (**64**·Mb H64A) and 512 (**64**·Mb H64A-H97A) respectively, at pH 6.5. This increase may arise from a flexibilization of the protein structure in the proximity of the catalyst, facilitating interactions of the protein-bound cofactor with the photosensitizer (i.e. facilitating the electron transfer). (Figure 15 for Mb active site).

More recently, Ghirlanda and coworkers applied a similar strategy to anchor **64** within cytochrome b_{562}.[208] In this system, the metal of the heme is anchored via H102 and M7 (Figure 9). Mutation of the methionine-7 to an alanine (M7A) results in a 2.5 fold increase in photocatalytic activity (305 vs 125 TON), as it liberates one coordination site for catalysis. Continuous removal of hydrogen increased **64**·b_{562} M7A TON to 1450 (Table 8, entry 8). Even in the presence of air, **64**·b_{562} M7A afforded up to 400 TON. Upon catalyst stalling, addition of fresh photosensitizer ($[Ru(bpy)_3]^{2+}$) partially restored catalytic activity, while addition of fresh **64**·b_{562} M7A did not. This suggests that PS degradation is the primary limiting factor in this experiment rather than catalyst inactivation.

Next, **64**·b_{562} M7D and **64**·b_{562} M7E mutations were investigated. The authors speculated that the presence of a carboxylic acid in the vicinity of the catalytic center could enhance hydrogen production, similar to protonated amines.[209-210] Although better than the WT host, the activity of these carboxylate-bearing mutants however did not surpass that of the M7A mutant, suggesting that these residues do not behave as proton relays.

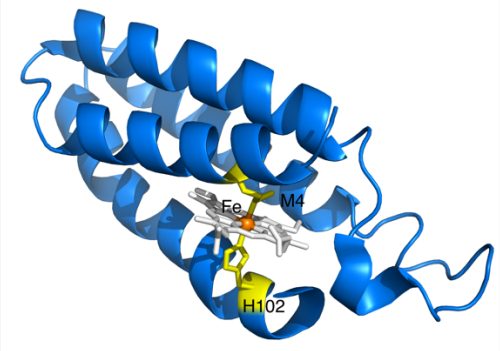

Figure 9 Cytochrome b562 (PDB code 1QPU) was mutated at position M4 to afford an artificial hydrogenase.[208]

Artero and coworkers explored a similar strategy using cobalt complexes with non-porphyrin ligands. Cobaloximes **65** and **66** (Scheme 23) were inserted into the apo-form of the sperm whale myoglobin.[203] The cobaloximes were shown to occupy the heme-site, where cobalt was coordinated by H93 and a water molecule. Modeling with **66** suggested that the coordinated water molecule could form a hydrogen bond with the distal histidine (H64). EPR parameters obtained for **65**·Mb suggest that the cobalt is exposed to a hydrophobic environment. This environment may account for the difference in redox potential (of the Co(I)/Co(II) couple) between **65**·Mb and **65**·imidazole. This observation suggests that the second coordination sphere from the protein indeed influences the redox-properties of a protein-bound synthetic complex. Both **65**·Mb and **66**·Mb catalyzed dihydrogen production under neutral aqueous solution with a low overpotential (~200 mV). **66**·Mb performed better than **65**·Mb, and at pH 7.0, **66**·Mb converted up to 65 % of the electron donor $[Eu(EGTA)]^{2+}$ to H_2, corresponding to 3.2 TON, within 5 min. For

comparison free cofactor **66** was deactivated after 2.5 TON, indicating that Mb provided modest catalyst protection.

Photochemical hydrogen production by cobaloxime·Mb ArMs was also performed using deazaflavin (DAF hereafter) and tris buffer as electron donor. At pH 7.0, **66**·Mb performed up to 5 TON in 15 min (Table 8, entry 9). In this case however, the free cofactor **66** outperformed the artificial hydrogenase, TON 8.3. Other heme-binding proteins were also investigated as scaffolds to generate ArM hydrogenases using either **65** or **66**. These included: rat heme oxygenase 1 (HO1 hereafter) and *Corynebacterium diphteriae* heme oxygenase (HmuO hereafter).[211] The resulting artificial hydrogenases **66**·HO1 and **66**·HmuO were more active than **66**·Mb both under thermal- and photochemical conditions. **66**·HO1 converted up to 82 % of the electron donor $[Eu(EGTA)]^{2+}$ into H_2 within 5 min, corresponding to 6.2 TON (Table 8, entry 10). Both TON and TOF were higher than that of **66** free in solution. However, these did not outperform the free catalyst **66** under photocatalytic conditions: at 10 μM concentration, **66** afforded 20 TON in 15 min, versus 6.3 and 15.3 for **66**·HO1 and **66**·HmuO respectively (Table 8, entries 11 and 12). Despite the low overpotential required and the shielding effect provided by the protein, these artificial hydrogenases suffered from a poor affinity of the host for the cofactor. This may be traced back to the absence of interaction with the propionate side-chains of the ligand, as well as significantly reduced hydrophobic interaction between the cobaloximes and the apo-heme proteins, compared to the natural cofactor-protein interaction.

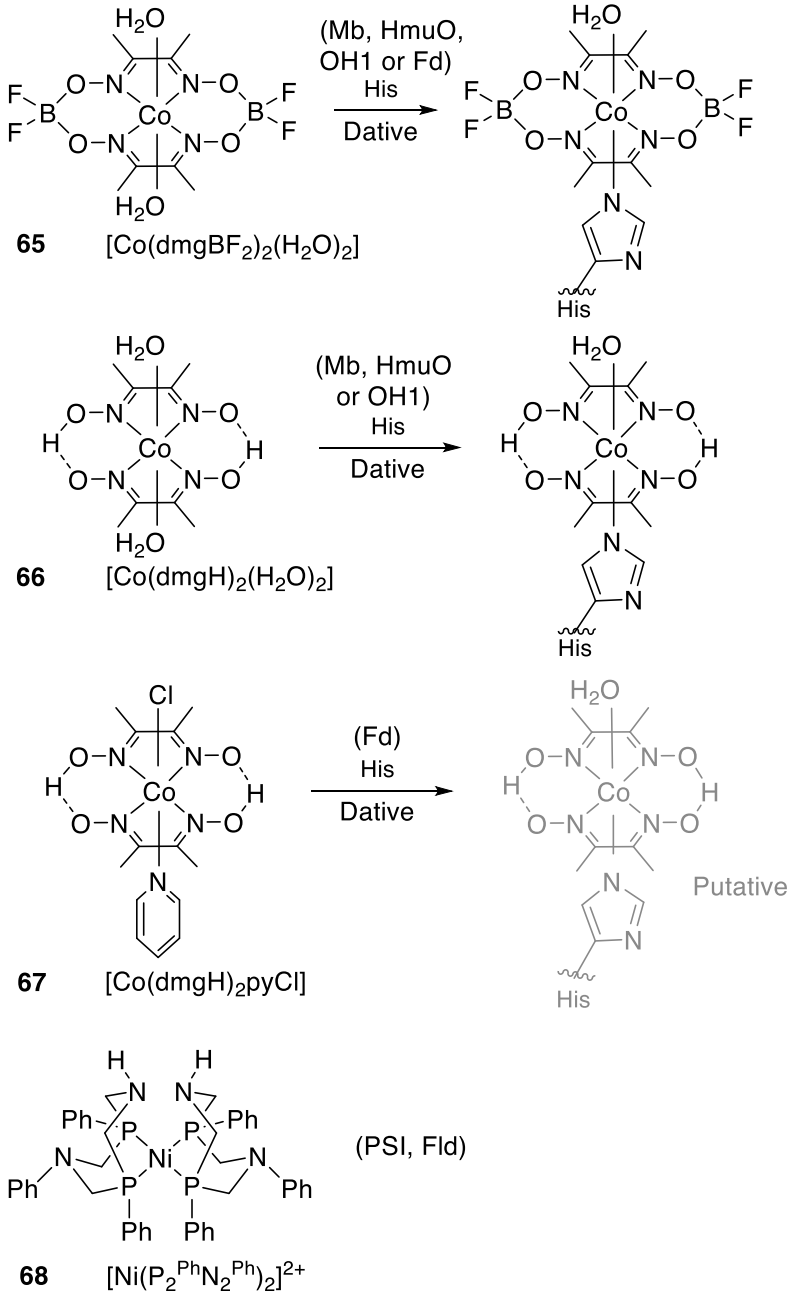

Scheme 23. Cobaloximes and nickel phosphines are synthetic complexes with high hydrogen production catalytic activity. Cobaloximes can be anchored via a histidine or a methionine residue of the apo-heme protein.

The artificial hydrogenases of Artero and coworkers proved to be better catalysts than the free cobaloximes at pH 7.0 in the case of thermal catalysis (using $[Eu(EGTA)]^{2+}$ as electron donor), while in photocatalysis, the free catalysts performed better. This could arise from the shielding effect of the protein, obstructing interaction between the PS and the anchored catalyst. In addition, the deactivation of the catalyst occurred rapidly. The

authors hypothesize that Co(III)–H intermediate may reduce the oxime ligand. A faster electron transfer to the catalyst could shorten the lifetime of this intermediate thereby avoiding ligand degradation, eventually leading to prolonged catalytic activity. One way to achieve this would be to maintain the PS and the catalyst in close vicinity, thus favouring fast electron transfer.

This issue has been directly addressed by Utschig and coworkers. In a first attempt, Utschig, Tiede and coworkers made use of the direct interaction between the synthetic complexes **67** and **68** with photosystem I (PSI hereafter).[212-213] This natural component of the photosynthetic electron transport chain possesses both a light-harvesting center and a series of electron relays, scaffolded within a large protein assembly. They demonstrated that **67** and **68** interact with PSI in a non-covalent manner. In contrast to other artificial hydrogenases described herein, the interaction between PSI and the two complexes were not unambiguously defined: the authors hypothesize that interaction may occur at the hydrophobic patches of PSI (and possibly at a histidine residue in the case of **67**). Following incubation of **67** with PSI, ascorbate (as sacrificial electron source) and cytochrome c_6 as electron transport (to reduce the oxidized PSI), afforded **67**·PSI. Upon irradiation, dihydrogen evolution could be detected. Relative to the cobalt content, this system performed 2080 TON in 1.5 h, with a maximum TOF of 1.13 s^{-1}, at pH 6.3 (Table 8, entry 13). Under similar conditions, **68**·PSI performed 1870 TON in 3 h (Table 8, entry 14). For both **67** and **68**, analysis of the catalytic mixture upon completion of the reaction revealed thatapproximately 90 % of the metal was lost. The poorly defined and weak interactions between PSI and those catalysts combined with possible catalyst degradation pathways may lead to leaching during catalysis. To overcome this limitation, the authors combined **68** with apo-flavodoxin (Fld), a protein known to interact via electrostatic interactions with the F_B cluster of PSI. The authors hypothesized that **68** could be inserted

is the FMN pocket of apo-flavodoxin. The metal content of the assembly was quantified, confirming this hypothesis. Irradiation of PSI in the presence of 30 equivalents of **68**·flavodoxin led to the rapid production of dihydrogen relative to PSI, improving the photon to hydrogen conversion. However, when converted to catalyst concentration (ie. 30 eq. vs. PSI), only 94 TON were obtained after 4 h (Table 8, entry 15). Despite its efficiency and elegant design, this biomimetic artificial hydrogenase is challenging to handle because of the membrane-bound nature of the proteins.

To reduce the complexity of the above system, Utschig and coworkers recently reported a simpler design, in which both the synthetic PS and the catalyst are anchored on a ferrodoxin protein, acting as scaffold naturally containing an electron relay.[214-215] This latter feature, as well as the defined and stable structure of the scaffold, differentiates their work with previous report from Hayashi and coworkers, in which a PS and a catalyst were attached on a peptide.[216] Ferredoxin is a small and soluble electron carrier protein containing a [2Fe−2S]-cluster. The cofactors **65** or **67** were datively anchored at H90 and the $[Ru(bpy)_3]^{2+}$-photosensitizer linked to C18 of ferredoxin. Only 40 % - 50% of the artificial hydrogenase included the covalently-bound PS, to afford **65**·ferredoxin·$[Ru(bpy)_3]$ and **67**·ferredoxin·$[Ru(bpy)_3]$ respectively. Both ArMs produced dihydrogen under irradiation and in the presence of ascorbate at pH 6.3. It is assumed that **65**·ferredoxin alone (i.e. lacking the PS), does not produce hydrogen under irradiation, even in the presence of other **65**·ferredoxin·$[Ru(bpy)_3]$. Thus, unlike the previous examples, the TON and TOF were estimated relative to the PS content. In 6 h, **65**·ferredoxin·$[Ru(bpy)_3]$ and **67**·ferredoxin·$[Ru(bpy)_3]$ yielded 210 and 650 TON respectively, with a maximum 0.047 s^{-1} TOF observed for the latter (Table 8, entries 16 and 17). Upon removal of the [2Fe−2S]-cluster from **65**·ferredoxin·$[Ru(bpy)_3]$, complete loss of photocatalytic activity resulted. Spectroscopic analysis suggested that electron

transfer from Ru(II)* to cobalt does not occur. The authors elegantly demonstrated that this could be traced back to the loss of the [2Fe−2S]-electron relay, substituting it by its redox inactive [2Ga−2S]-congener. The quaternary structure of **65**·ferredoxin was maintained but no photocatalytic dihydrogen evolution could be observed, suggesting that the extended distance between the cofactor and the PS prevents electron transfer in the absence of the electron relay station. The [2Fe−2S]-cluster is separated from the Ru PS and the cobalt cofactor by approximately 15 Å and 12.5 Å, respectively. Anchoring the PS and the cofactor to a rigid scaffold not only keeps them in close vicinity, but also maintains a suitable distance between them, thus avoiding fast charge recombination after the electron transfer. This increase of the lifetime of the charge-separated state, in which Co(I) is a key intermediate, empowers the proton reduction. For **65**·ferredoxin·[Ru(bpy)$_3$], the lifetime of this state was determined to be ~6 ms.

Finally, based on the observation that apo-flavodoxin can bind synthetic complexes, it was loaded with **65** and covalently modified by a [Ru(bpy)$_3$]$^{2+}$-moiety ~10 Å away from the FMN-binding site. This PS-catalyst distance is considerably shorter than within the ferredoxin host resulting in a faster direct electron transfer (~3000 times, based on distance alone), as well as a faster charge recombination. In contrast to the ferredoxin construct, **65**·flavodoxin·[Ru(bpy)$_3$] produced photocatalytically dihydrogen with a low productivity: only 85 TON were achieved in 6 h (Table 8, entry 18). This corresponds to 40 % of the activity of **65**·ferredoxin·[Ru(bpy)$_3$], highlighting the superiority of assemblies in which the PS and the catalyst are far enough to slow down back-donation (within milliseconds), but in which an electron relay favours the first electron transfer event within microseconds. Accordingly, the difference in activity of **65**·ferredoxin·[Ru(bpy)$_3$] and **65**·flavodoxin·[Ru(bpy)$_3$] correlates well with the lifetime of the charge-separated state

containing Co(I): for **65**·flavodoxin·[Ru(bpy)$_3$] and **65**·ferredoxin·[Ru(bpy)$_3$] the lifetimes are ~800 μs and ~6 ms respectively.

Table 8. Selected results for dihydrogen production by artificial hydrogenases.

Entry	Cof.	Protein[a]	PS[b]	Elec. donor	[Cof] (μM)	Ratio [PS]/[Cof]	t (h)	pH	T (° C)	TOF (s^{-1})	TON	Ref
1	**65**	cyt *c*	$[Ru(bpy)_3]^{2+}$	asc.[c]	14	10	2	4.7	25	0.035	82	196
2	**66**	NB	$[Ru(bpy)_3]^{2+}$	asc.[c]	7.8	18	6	4.7	25	0.038	130	197
3	**66**	NB	$[Ru(bpy)_3]^{2+}$	asc.[c]	7.8	18	6	7.8	25	nd	36.4	197
4	**Ni**	Rd	$[Ru(bpy)_3]^{2+}$	asc.[c]	2	500	8.3	6.5	4	0.008	70[l]	202
5	**Ni**	Rd	-	[Ti(citrate)][d]	2.5	-	8	9.4	22	nd	300	202
6	**Co**	*c*-552	-	-[e]	0.1	-	24	7.0	r.t.	nd	27000	61
7	**64**	Mb	$[Ru(bpy)_3]^{2+}$	asc.[c]	2.5	400	12	7.0	r.t.	0.025	518	207
8	**64**	*b*-562	$[Ru(bpy)_3]^{2+}$	asc.[c]	4	250	25	7.0	r.t.	0.025[h]	1450[g]	208
9	**66**	Mb	DAF	Tris	30	0.5	0.25	7.0	r.t.	0.015[i]	5	203
10	**63**	HO1	-	$[Eu(EGTA)]^{2-}$[f]	40	-	0.08	7.0	r.t.	0.067[j]	6.2	211
11	**66**	HO1	DAF	Tris	10	0.5	0.25	7.0	r.t.	0.015[k]	6.3	211
12	**66**	HmuO	DAF	Tris	10	0.5	0.25	7.0	r.t.	0.058[k]	15.3	211
13	**67**	PSI	PSI	asc.[c,g]	0.152	0.4	1.5	6.3	r.t.	1.13	2080[m]	212
14	**68**	PSI	PSI	asc.[c,g]	0.060	1	3	6.3	r.t.	0.73	1870[m]	213
15	**68**	Fld	PSI	asc.[c,g]	2	0.033	4	6.3	r.t.	0.042	94[m]	213
16	**65**	Fd	c-$[Ru(bpy)_3]^{2+}$[v]	asc.[c]	2	0.36	6	6.3	r.t.	0.014	210[n]	215
17	**67**	Fd	c-$[Ru(bpy)_3]^{2+}$[v]	asc.[c]	2	0.42	6	6.3	r.t.	0.047	650[n]	214
18	**65**	Fld	c-$[Ru(bpy)_3]^{2+}$[v]	asc.[c]	1.7	1	6	6.3	r.t.	0.008	85[n]	214

Entries highlighted in gray correspond to non-photocatalytic experiments. [a] apo-cytochrome *c* (cyt *c*); apo-nitrobindin (NB); rubredoxin (Rd); apo-*Ht* cytrochrome c_{552} M61A (*c*-552); myoglobin (Mb); apo-cytochrome b_{562} M7A (*b*-562) ; apo-rat heme oxygenase 1 (HO1); apo-*Corynebacterium diphteriae* heme oxygenase (HmuO); photosystem I (PSI) ; apo-flavodoxin (Fld) ; ferredoxin (Fd). [b] deazaflavin (DAF); $[Ru(bpy)_3]^{2+}$ free in solution ($[Ru(bpy)_3]^{2+}$) or covalently attached to the protein scaffold (c-$[Ru(bpy)_3]^{2+}$). [c] ascorbate 100mM (asc.); [d] [Ti(III)citrate], 39 mM ([Ti(citrate)]). [e] Electocatalysis. [f] 600 μM. [g] Cyt c_6 (4-20 μM) was added as an electron carrier. [h] Derived from Fig. 5 of ref [208]. [i] Minimal value, estimated from Fig. 11 of ref [203]. [j] Minimal value, estimated their Fig. 7 of ref [211]. [k] Minimal value, estimated from Fig. S7 of ref [211]. [l] The 40 TON observed in the absence of catalyst were substracted from the 110 TON for NiRd, depicted in Fig.3.[202] [m] Re-calculated relative to the metal cofactor. [n] Calculated relative to the PS, considering the metal cofactors embedded in a scaffold not containing a PS have no catalytic activity, based on the fact that solution of PS and cat at 1 μM did not yield the photocatalytic production of H_2.

In summary, the artificial hydrogenases reported to date show that anchoring a catalytically competent proton-reduction catalyst within a protein scaffold can impart compatibility with aqueous media at neutral pH and increase both TOF and TON. In some cases however, the artificial hydrogenases are less efficient than the cofactor alone. This is especially valid for photocatalytic systems whereby the PS catalyst interactions are hampered, eventually leading to slow catalytic rates or catalyst degradation. The recent studies from Utschig and coworkers offer promising avenues to overcome this issue.

Some advantageous aspects of artificial hydrogenases remain to be systematically explored. For example, very few reports on random mutagenesis or directed evolution

schemes have been published, although such avenues are often suggested in the outlook of these publications. Only a handful of modifications in the direct environment of the metal have been tested either by mutating residues or by testing different scaffolds from a same family (e.g. heme-binding proteins). None of these examples led to a dramatic improvement of catalytic activity however. In contrast, directed evolution could be used to tune the protein environment, rather than the PS or the catalyst.[217] Finally, in a biomimetic spirit, artificial hydrogenases could be improved by engineering facilitated pathway for proton/electron delivery/removal at the metal center, and gas release pathways, reminiscent of the channels and electron relays present in natural hydrogenases.

4.3 Transfer Hydrogenation

Background. Catalytic asymmetric transfer hydrogenation (ATH) provides a powerful means for reducing unsaturated substrates including ketones, imines, nitro compounds, nitriles, oximes, α,β-unsaturated carbonyl compounds, heterocycles, alkenes, and alkynes.[218-226] It requires neither hazardous hydrogen gas nor pressure vessels. Instead, a number of cheap, non-toxic, and easy to handle reductants, including formic acid, formate salts or isopropanol, have been used as hydrogen donors. Recent advances and trends in ATH using homogeneous, heterogeneous, organo- and transition-metal catalysts were recently reviewed.[227]

A major breakthrough in ATH was reported by Noyori and coworkers in 1995: enantiopure TsDPEN-Ru(II)-based complexes (TsDPEN = N-(*p*-toluenesulfonyl)-1,2-diphenylethylenediamine) were found to be outstanding homogeneous catalysts for the asymmetric reduction of a variety of substrates.[228-230] Building upon this finding, some of the most effective catalysts reported to date are d^6-pianostool complexes of rhodium,

iridium and ruthenium. As amply demonstrated by Xiao and coworkers, closely related homogenous catalysts are efficient for the asymmetric reduction of prochiral ketones and cyclic imines in water.[231-233] This is obviously an important feature in the context of ArMs.

In nature, NAD(P)H-dependent enzymes including ketoreductases, imine reductases (IRED), and ene reductases can be used for the asymmetric reduction of C=O, C=N and activated C=C bonds respectively. While both keto-[234] and ene-reductases[235] are well known and widely used on industrial scale,[162] IREDs were only recently discovered by Nagasawa in 2011.[236] These have been further exploited by, among others, the Turner and Hauer groups.[237,238]

In this section, we summarize the progress in artificial transfer hydrogenases (ATHases) for the asymmetric reduction of prochiral ketones, enones, imines as well as $NAD(P)^+$ and its analogs. For several groups, ATHase has provided a fertile playground to benchmark various challenging concepts including: catalyst immobilization, directed evolution, enzyme cascades, allosteric regulation etc. These are presented at the end of this section.

Transfer Hydrogenation of Ketones. To assemble an artificial metalloenzyme for the asymmetric transfer hydrogenation of prochiral ketones, the Ward group set out to adapt Noyori's homogeneous d^6-pianostool complexes bearing a Ts-DPEN-ligand.[229] Several Ir(III), Rh(III) and Ru(II) d^6-pianostool complexes were prepared by complexation of a achiral biotinylated *N*-arylsulfonamide-1,2-ethylenediamine ligands (**69**, *q* = *ortho*, *meta*, *para*) to either $[\eta^5\text{-Cp*IrCl}(H_2O)_2]^+$, $[\eta^5\text{-Cp*IrCl}(H_2O)_2]^+$, or $[(\eta^6\text{-arene})\text{RuCl}(H_2O)_2]^+$. The resulting pianostool complexes $[(\eta^n\text{-arene})\text{M}(\mathbf{69})\text{Cl}]^+$ were combined with an Sav site-saturation mutagenesis library Sav S112X as well as selected single- and double point mutants (Scheme 24).[18, 239] The aminoacid positions subjected to mutagenesis were selected based on their estimated proximity to the catalytic metal. Instead of screening

the whole chemo-genetic diversity matrix, Ward and coworkers first screened all cofactors [(η^n-arene)M(**69**)Cl]$^+$ with a subset of Sav isoforms. Only the best biotinylated catalysts were subsequently screened with the entire set of proteins. The best catalyst·protein combinations were evaluated toward various substrates. Selected results are summarized in Table 9.

Noteworthy features for the ATHases included (Scheme 24 and Table 9):

i) Complexes bearing a *para*-substituted spacer (**70**) outperform those with *ortho*- and *meta*-spacers.

ii) Exchange of the capping arene ligand from benzene to *p*-cymene led to stereoinversion; this is most pronounced with mutants Sav S112K ((*S*)-selective) and Sav S112A ((*R*)-selective), respectively (Table 9, entries 6 vs. 3).

iii) Aryl alcohols **71-73** yielded good to very good (i.e. ee > 90%) whereas reduction of dialkyl ketones resulted in only modest ees. This is in line with findings for homogeneous pianostool catalysts: the key enantiodiscriminating interaction is between the η^n-bound arene moiety and the aryl moiety of the prochiral substrate.

iv) Sav S112X mutants bearing a potentially coordinating aminoacid side-chain have an inhibitory effect on catalysis, resulting in modest conversions.

An X-crystal structure of the most (*S*)-selective artificial transfer hydrogenase (ATHase hereafter) [η^6-(benzene)Ru(**70**)Cl]·Sav S112K was determined (PDB 2QCB, Figure 10).[240] The following features are apparent:

i) The Ru-center is located in the biotin-binding vestibule in close proximity to residues $S112K_A$, $L124_A$, $S112K_B$, $K121_B$ (subscripts A and B refer to Sav monomers). This observation highlights the importance of scrutinizing

mutagenesis libraries Sav S112X, K121X and L124X for the genetic optimization of the ATHase.

ii) A (*S*)-Ru-Cl absolute configuration was determined for [η^6-(benzene)Ru(**70**)Cl]·Sav S112K. This configuration is reminiscent of the homogeneous catalytic system as both ArM and homogeneous catalyst, (*S*)-reduction products are formed preferentially in the presence of an (*S*)-Ru-Cl moiety. This suggests that both catalysts rely on a similar enantioselection mechanism.

iii) The short $Ru_A \cdots\cdots Ru_B$ distance (4.44 Å) suggests that it is unlikely that two neighboring cofactors can fit within a biotin-binding vestibule (which contains two biotin binding sites): the maximum activity and selectivity is achieved in the presence of two cofactors occupying one Sav tetramer.

iv) Substitution of the benzene cap with *p*-cymene would result in steric clashes between the cofactor and the protein. Therefore, the corresponding *p*-cymene complex is expected to adopt a different orientation within the biotin-binding vestibule.

v) The overall Sav structure in the complex-bound Sav vs. apo-Sav is virtually identical (RMSD = 0.276 Å).

From the crystal structure, it was concluded that site-saturation mutagenesis libraries in position K121 and L124 may allow to further fine-tune the catalytic performance of the ATHase. Thus, the following libraries K121X, L124X, S112A-K121X, S112K-K121X, S112A-L124X and S112K-L124X were produced to afford eighty double mutants and forty single mutants. This Sav library was combined with both (*S*)- and (*R*)-selective cofactors [η^6-(benzene)Ru(**70**)Cl] and [η^6-(*p*-cymene)Ru(**70**)Cl] respectively. The resulting ATHase were screened for the reduction of aryl-alkyl and dialkylketones **71-**

75, Scheme 24. To speed-up the screening effort, the Sav mutants were tested in catalysis in semi-purified form. First, mutants were expressed and the cells were lysed. Next, the lysates were centrifuged and biotin-sepharose beads were added to the supernatant. The sepharose-bound mutants were screened and the best hits were validated using purified and solubilized Sav isoforms. With this procedure, ATHases could be obtained that produced up to 97 % ee (*R*) and 92 % (*S*) for aryl-alkylketones **71**, **72** and **73** (Table 9, entries 15-18) and up to ee 90 % (*R*) for dialkylketone **74** and **75** (Table 9, entries 19-21).

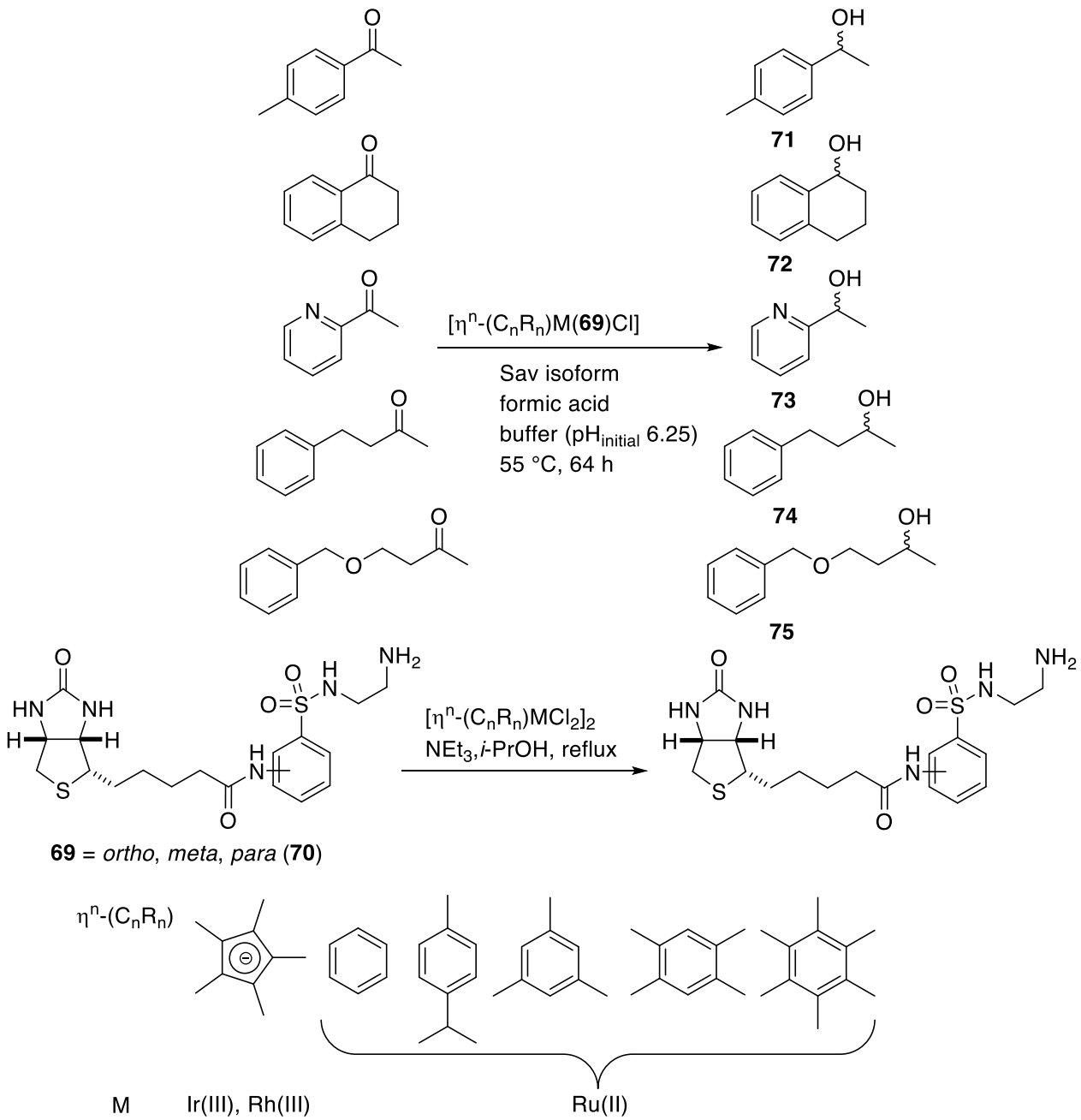

Scheme 24: An artificial transfer hydrogenase based on biotinylated Noyori-type d^6-pianostool complexes anchored within Sav catalyzes the asymmetric reduction of ketones. Adapted with permission from ref.[239] Copyright 2006 American Chemical Society.

Table 9. Summary of the catalytic performance of ATHase for the reduction of prochiral ketones.[a]

Entry	Complex	Protein	Product	ee	Conv.
1	[η⁶-(*p*-cymene)Ru(**70**)Cl]	WT Sav	**71**	89 (*R*)	95
2	[η⁶-(benzene)Ru(**70**)Cl]	WT Sav	**71**	29 (*R*)	38
3	[η⁶-(*p*-cymene)Ru(**70**)Cl]	S112A	**71**	91 (*R*)	98
4	[η⁶-(benzene)Ru(**70**)Cl]	S112A	**71**	41 (*R*)	74
5	[η⁶-(*p*-cymene)Ru(**70**)Cl]	S112K	**71**	10 (*S*)	34
6	[η⁶-(benzene)Ru(**70**)Cl]	S112K	**71**	63 (*S*)	24
7	[η⁶-(*p*-cymene)Ru(**70**)Cl]	P64G	**71**	94 (*R*)	92
8	[η⁶-(benzene)Ru(**70**)Cl]	P64G	**71**	44 (*S*)	44
9	[η⁶-(*p*-cymene)Ru(**70**)Cl]	S112Y	**72**	97 (*R*)	79
10	[η⁶-(benzene)Ru(**70**)Cl]	S112A	**72**	51 (*S*)	44

11	[η⁶-(benzene)Ru(**70**)Cl]	S112R	**73**	70 (*S*)	95
12	[η⁶-(*p*-cymene)Ru(**70**)Cl]	S112F	**73**	76 (*R*)	95
13	[η⁶-(*p*-cymene)Ru(**70**)Cl]	S112A	**74**	48 (*R*)	98
14	[η⁶-(*p*-cymene)Ru(**70**)Cl]	S112A	**75**	69 (*R*)	97
15	[η⁶-(*p*-cymene)Ru(**70**)Cl]	L124V	**71**	96 (*R*)	97
16	[η⁶-(*p*-cymene)Ru(**70**)Cl]	L124V	**72**	87 (*R*)	20
17	[η⁶-(benzene)Ru(**70**)Cl]	S112A-K121N	**72**	92 (*S*)	54
18	[η⁶-(benzene)Ru(**70**)Cl]	S112A-K121N	**73**	92 (*S*)	quant.
19	[η⁶-(*p*-cymene)Ru(**70**)Cl]	S112A-K121T	**74**	88 (*R*)	quant.
20	[η⁶-(*p*-cymene)Ru(**70**)Cl]	S112A-K121W	**74**	84 (*R*)	quant.
21	[η⁶-(benzene)Ru(**70**)Cl]	S112A-K121T	**75**	90 (*R*)	quant.

[a] The catalytic runs were performed at 55 °C for 64 h using the mixed buffer HCO_2Na (0.48 M) + $B(OH)_3$ (0.41 M) + MOPS (0.16 M) at $pH_{initial}$ = 6.25. Ru/substrate/formate ratio 1:100:4000 (i.e., 100 equiv. substrate vs. Ru).

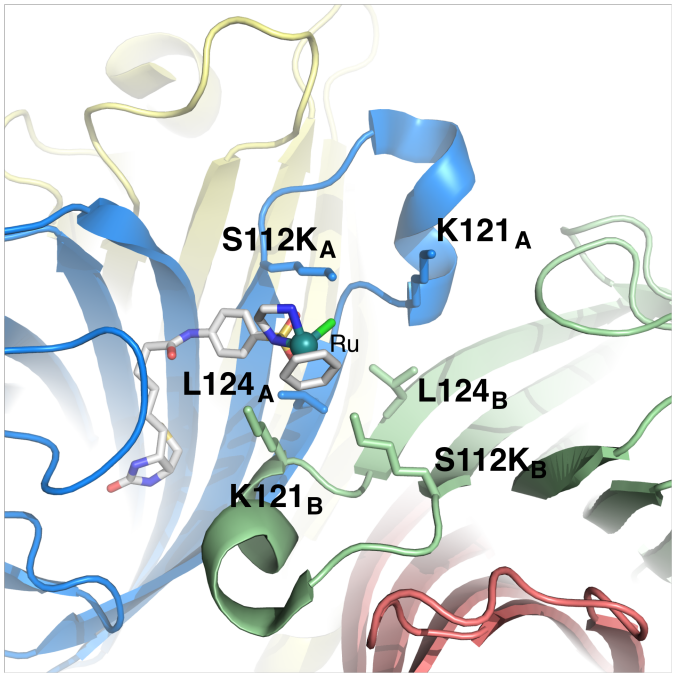

Figure 10: The X-ray crystal structure of [η⁶-(benzene)Ru(**70**)Cl]·Sav-S112K tetramer (PDB code 2QCB) reveals the ruthenium location in the biotin-binding vestibule. Optimization of the artificial transfer hydrogenase is achieved by mutagenesis of residues S112 and K121 and L124 located in proximity of the metal in the Sav monomer (blue)-monomer (yellow) interface. For simplicity the cofactor in Sav monomer B was removed.

The asymmetric reduction of trifluoroacetophenone **60** was evaluated by Salmain and coworkers. Previously, they demonstrated that the active site of papain (PAP) could be used to anchor organometallic cofactors via a covalent linkage to the Cys25.[241-242] They applied this strategy to anchor d⁶-pianostool complexes (Ru(II) and Rh(III)) via a maleimide moiety. Upon covalent anchoring of either **77** or **78** in PAP (Scheme 25), respectively 99 and 82 TON were obtained after 60 h. Unfortunately, low enantioselectivity

was observed (15 % for (*R*)- **76** at best),[243] which was proposed to stem from the high conformational flexibility of the cofactor within the protein-cavity. Attempts to address this challenge by shortening the linker led to test cofactors **79** and **80**. The ArM **80**·PAP performed best, with 48 TON in 24 h and 9 % *ee* in favor of (*S*)- **76**. The free **80** afforded 100 TON in 1.25 h.

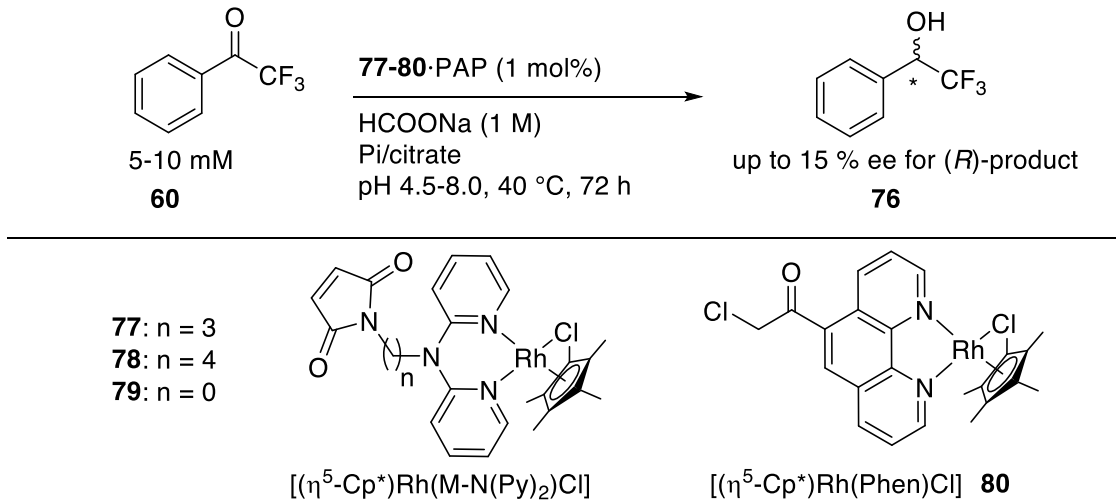

Scheme 25. Covalent anchoring of **77-80** in PAP affords ArMs that catalyze the transfer hydrogenation of trifluoroacetophenone **60**.

Moving away from ArMs based on covalent anchoring, Salmain and coworkers designed ATHases based on the "Trojan horse" strategy relying on bovine β-lactoglobulin (β-LG hereafter). This β-barrel protein binds long fatty acids with submicromolar affinity, with the carboxylate group pointing towards the solvent. The authors coupled different fatty acids to the dipyridylamine of the [(η^5-Cp*Rh(N(Py)$_2$)Cl)-moiety, resulting in **81-83**, Scheme 26.[244-245] The resulting ArMs catalyzed the transfer hydrogenation of trifluoroacetophenone **60**. The ATHase **81**·β-LG, led to full substrate conversion (i.e. 25-50 TONs), but only 7 % *ee* in favor of (*R*)- **76**. **83**·β-LG(A) was the most enantioselective ArM based on the lactoglobulin scaffold achieving 32 % ee for (*R*)- **76**.

Although the authors identified the EF loop of β-LG and L39 as a position to mutate, no attempt to genetically improve the catalytic performance of the artificial transfer hydrogenase was reported.[246]

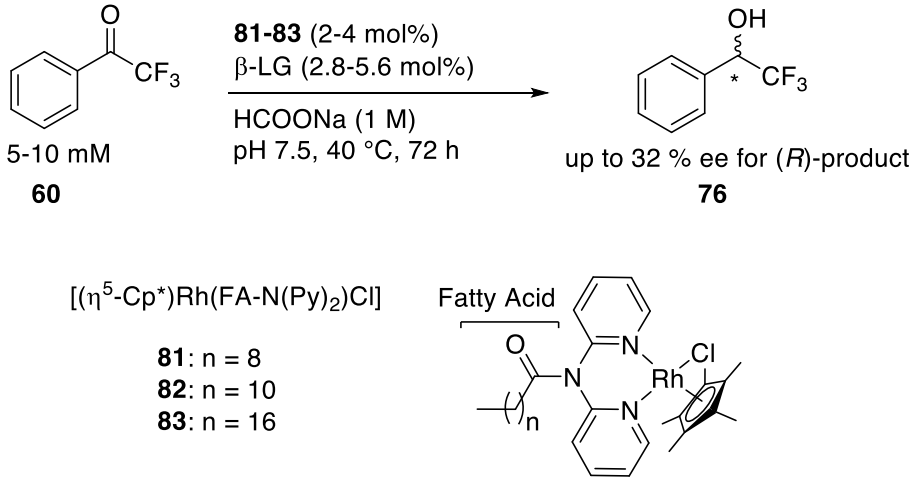

Scheme 26. Supramolecular anchoring of **81-83** into β-LG affords ArMs that catalyze the transfer hydrogenation of trifluoroacetophenone.

Protein Crystals. The asymmetric transfer hydrogenation of acetophenone derivatives was also investigated by Ueno and Kitagawa *et al.* in 2014.[247] In this study, a pianostool catalyst precursor was soaked into a protein scaffold crystal to generate a heterogeneous ArM. A tetragonal crystal and an orthorhombic crystal of the hen egg white lysozyme (HEWL, hereafter) were used for ArM formation. After treatment of the crystals with glutaraldehyde to cross-link the monomers, the resulting protein crystals were soaked with a solution of $[Ru(benzene)Cl_2]_2$ **86**, Scheme 27. For the transfer hydrogenation of isobutyrophenone **84** using sodium formate as a hydride source, **86**·HEWL (tetragonal) and **86**·HEWL (orthorhombic) afforded the corresponding alcohol in 23 % *ee* (*R*)-**85**· and 36 % *ee* (*S*)-**85**· respectively, Table 10. When using dissolved HEWL and **86**, the ATHase conversion decreased to 7% (0.3 TON) compared to 38% (3.3 TON) and 46% (4.0 TON) conversions obtained using either **86**·HEWL (tetragonal) and **86**·HEWL (orthorhombic) respectively. Based on Sadler's report,[248] it seems reasonable to speculate that the Ru-

pianostool complex is coordinated to H15 of HEWL. These results suggest that the formation of catalytic compartments upon incorporation of Ru(II) complexes favour the ATH and affords different enantiomers depending on the crystal form used (tetragonal vs. orthorhombic).

Table 10. Selected results for transfer hydrogenation of isobutyrophenone **84** catalyzed by a ruthenium complex immobilized within and hen egg white lysozyme (HEWL) protein crystal.[247]

Entry	Cofactor	Protein	Sub.	pH	T (°C)	[Ru] (mM)	ee (%)	TON
1	**86**	HEWL_solution	**84**	7.5	35	2.6	24(*R*)	0.3
2	**86**	HEWL_tetragonal	**84**	7.5	35	1.3	23(*R*)	3.3
3	**86**	HEWL_orthorhombic	**84**	7.5	35	1.3	36(*S*)	4.0

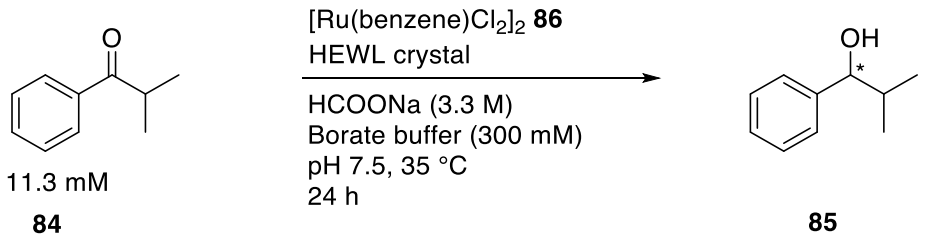

Scheme 27. Cross-Linked Egg Hen White Lysozyme crystals catalyze the ATH of isobutyrophenone in the presence of $[Ru(benzene)Cl_2]_2$.

Transfer Hydrogenation of Imines. Besides the ATH of ketones, the Ward group developed ATHases for the reduction of cyclic imines. In an initial screening, the complex [η^5-(Cp*)Ir(**70**)Cl] outperformed complexes [η^6-(arene)Ru(**70**)Cl] (which were most active in the asymmetric transfer hydrogenation of ketones) and [η^5-(Cp*)Rh(**70**)Cl].[249] For the reduction of the salsolidine precursor **88**, 57 % ee in favor of (*R*)-amine **87** was obtained with [η^5-(Cp*)Ir(**70**)Cl] · WT Sav. Genetic optimization of the ArM was achieved by screening the site-saturation mutagenesis libraries in position S112X and K121X as well as double mutants of the corresponding sites. The following trends and observations resulted from the screening (Scheme 28):

i) Artificial transfer hydrogenase [η^5-(Cp*)Ir(**70**)Cl]·Sav S112A yielded 91 % ee

for (*R*)-**87** with > 100 TON at pH 6.5, 5 °C in 24 h.

ii) The opposite enantiomer (*S*)-**87** was obtained with ee 78 % at 5 °C and pH 7.5 in the presence of the cationic mutant [η^5-(Cp*)Ir(**70**)Cl]·Sav S112K.

iii) The double mutant [η^5-(Cp*)Ir(**70**)Cl]·Sav S112A-K121A displayed a 7.6-fold improved catalytic efficiency compared to WT Sav for substrate **89**.[250]

iv) Reducing the ArM concentration to 17 μM for the reduction of **88** resulted in TON > 4'000.

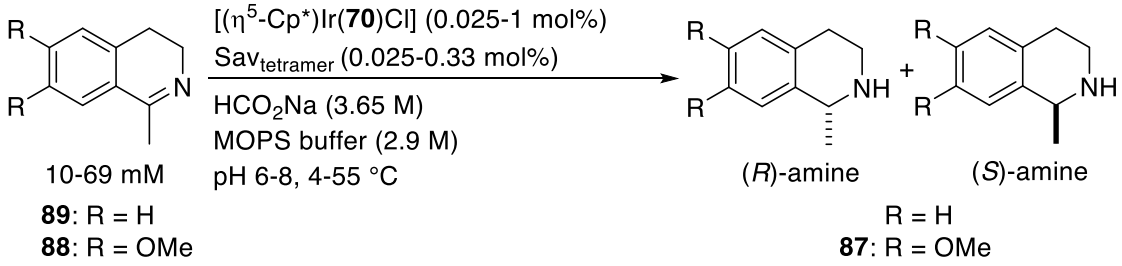

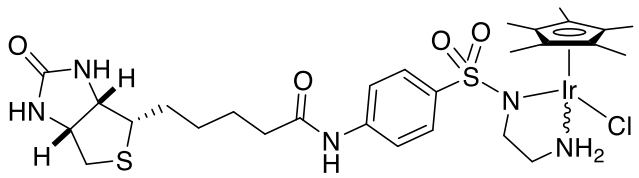

[(η^5-Cp*)Ir(**70**)Cl]

Sav	S	pH	T (°C)	[cat] (μM)	t (h)	ratio [Ir]/[Sav$_{tetr}$]	k_{cat}/K_M ($min^{-1}M^{-1}$)	ee (%)	TON
-	**88**	7.3	25	690	5	-	-	*rac.*	>100
WT	**88**	7.3	55	690	2	3	-	57 (*R*)	>100
S112A	**88**	7.3	55	690	2	3	-	79 (*R*)	>100
S112A	**88**	6.5	5	690	24	3	-	91 (*R*)	>100
S112A	**88**	6.5	5	17	96	1	217	96 (*R*)	>4000
S112K	**88**	7.5	5	690	48	3	-	78 (*S*)	>100
S112K	**88**	7.5	24	25	0.75	1	7	70 (*S*)	-
WT	**89**	7.8	37	93	18	1.5	189	60 (*R*)	>92
S112A-K112A	**89**	7.8	37	23	18	1.5	1591	47 (*R*)	>435

Scheme 28: Artificial transfer hydrogenases for the reduction of cyclic imines result from incorporation of an iridium d^6-pianostool complex within Sav isoforms.

To identify the transition state for the reduction of isoquinoline **88** in the presence of either [η^5-(Cp*)Ir(**70**)Cl]·Sav S112A/K, Ward, Maréchal and coworkers relied on a custom tailored QM/MM strategy.[251] The computed results nicely corroborated the catalysis

results:

i) In the transition state for [η^5-(Cp*)Ir(**70**)Cl] · Sav S112A, the imine cofactor is located in the biotin-binding site opposite to the position of the biotinylated cofactor (see below).

ii) Residue K121^B forms a cation-π with the electron-rich arene moiety of the substrate **88**.

iii) The computed difference in transition-state free energy (1.21 kcal · mol^{-1}) is in line with the enantioselectivity observed at room temperature.

Varying the Cofactor : Protein Ratio Streptavidin is a homotetrameric protein but is best viewed as a dimer of dimers. The biotin-binding vestibule is made up of two close-lying biotin-binding sites. Upon addition of four cofactors per Sav tetramer, each cofactor is forced into the proximity of its neighboring cofactor. The metal-metal distance between a pair of *cis*-related cofactors is typically 4-5 Å. In order to investigate the influence of adjacent cofactors, Ward and Maréchal analyzed the ATHase structure, reaction rates and resulting enantioselectivites as a function of Ir : Sav ratios for both [η^5-(Cp*)Ir(**70**)Cl] · Sav S112A and [η^5-(Cp*)Ir(**70**)Cl] · Sav S112K.[252] For [η^5-(Cp*)Ir(**70**)Cl] · Sav S112A, increasing the Ir-cofactor: Sav tetramer ratio from 1:1 to 4:1 caused an erosion in ee for the formation of (*R*)-amine **87** from 96 to 45 % in the transfer hydrogenation of **88**. This erosion was accompanied by a twentyfold decrease in catalytic efficiency (k_{cat}/K_M = 0.22 min^{-1}mM^{-1} to 0.011 min^{-1} · mM^{-1}). This can be traced back to a sixfold increase in K_M, which emphasizes the role of an empty *cis*-biotin site required for substrate recognition. In contrast, the catalytic efficiency of the (*S*)-selective ATHase [η^5-(Cp*)Ir(**70**)Cl] · Sav S112K decreased only 1.5-fold. The ee increased from 70 % (*S*)- **87** to 78 % (*S*)- **87** at Sav tetramer saturation. Analysis of the X-ray structure of [η^5-(Cp*)Ir(**70**)Cl] · Sav S112K revealed two equally populated metal cofactor positions, allowing to fit up to four cofactors without leading to significant steric clash. Importantly, the absolute configuration at the

metal was found to be opposite that found for the [η^5-(Cp*)Ir(**70**)Cl] · Sav S112A. Docking experiments were used to rationalize the variation in rates and enantioselectivity for both ATHases. The authors concluded that the position of the cofactor within the biotin-binding vestibule determines the absolute configuration at the metal, which in-turn, determines the absolute configuration of the product, Figure **TH12**.

As mentioned above, enantiopure 1,2-aminosulfonamides, such as TsDPEN combined with d^6-pianostool moieties are priviledged catalysts for asymmetric transfer hydrogenation.[230] Building upon this, Gandolfi-Rimoldi and coworkers investigated the properties of Ru complexes chelated with chiral 1,3-aminosulfonamides for the ATH of prochiral ketone in water.[253] Inspired by the work of Ward and coworkers based on 1,2-aminosulfonamides,[38] Pellioni and Rimoldi extended this work to biotinylated substituted 1,3-aminosulfonamides for the reduction of prochiral imines. Both enantiopure and achiral bidentate ligands were evaluated, Figure 11.[254]

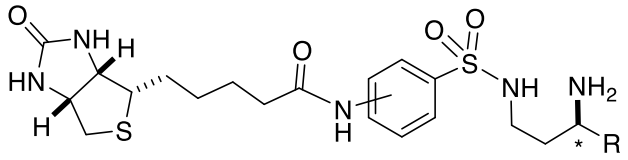

90: *p*-(*R*)-*Biot,* R = Ph
91: *p*-(*S*)-*Biot,* R = Ph
92: *m*-(*R*)-*Biot,* R = Ph
93: *m*-(*S*)-*Biot,* R = Ph
94: *o*-(*R*)-*Biot,* R = Ph
95: *o*-(*S*)-*Biot,* R = Ph
70a: *p*-*Biot,* R = H
96: *m*-*Biot,* R = H
97: *o*-*Biot,* R = H

Figure 11. Biotinylated 1,3 aminosulfonamides. All six diastereoisomers **90-95** as well as the achiral ligands **70a, 96, 97** were used for the preparation of d^6 Ir piano-stool complexes. ArMs formed after supramolecular interaction with streptavidin were tested in the ATHase of salsolidine precursor **88**.

Biotinylated 1,3-aminosulfonamides **70a, 90-97** were used as ligands for the preparation of d^6 Ir-pianostool complexes and tested for their ATHase properties for the reduction of the salsoline precursor **88**, Scheme 29. The free cofactor **90** (Table 11, entry 1) displayed

high activity and very low enantioselectivity (6% ee (*S*)-**87**), highlighting the poor asymmetric induction imposed by the flexible six-membered chelate ring. Upon incorporation within WT Sav, the cofactors **90-95** led to nearly racemic **87**, with a very modest preference for the (*R*)-**87** (up to 18 % (*R*)-**87**, Table 11, entries 2-7). Inspired by an X-ray structure and the previous computational studies on Sav/biotinylated iridium(III) ATHase with achiral 1,2-aminosulfonamides ligands (Scheme 28), residue Sav S112 was selected for mutagenesis studies. Various Sav S112-mutants were tested and led to a drastic improvement in enantioselectivity.[239-240, 249] The highest enantioselectivity observed was with [η^5-Cp*Ir(**91**)Cl]·Sav S112C (65% ee (*R*)-**87**, 60% yield) and [η^5-Cp*Ir(**92**)Cl]·Sav S112Y (47% ee (*S*)-**87**, 72% yield) (Table 11, entries 9 and 11). Mutant Sav S112C was also tested with the achiral 1,3-aminosulfonamide ligands **70a, 96** and **97** (Table 11, entries 14-16). Interestingly, the *para*-biotinylated catalyst [η^5-Cp*Ir(**70a**)Cl] showed the highest enantioselectivity at the cost of a reduced activity (83% ee (*R*)-**87**, 25% yield, Table 11, entry 9 vs 14).

It is interesting to note that [η^5-(Cp*)Ir(**70**)Cl]·Sav S112C affords (*R*)-**87** in 75% yield and 25% ee at 55°C (Scheme 28).[249] In contrast, no catalytic activity was detected for the [η^6-(arene)Ru(**70**)Cl]-based ArMs in the presence of S112C for the ATHase of ketones, suggesting that the nucleophilic cysteine poisons the latter precious metal (Scheme 24).[239]

Table 11. Selected results for the asymmetric transfer hydrogenation of prochiral imine **88** in MOPS buffer using sodium formate as a hydride source.

Entry	Protein	Ligand	Sub (mM)	[Ir] (μM)	ee[a](%)	Conv(%)	TON
1	-	**90**	**28**	280	- 6	>99	100
2	SavWT	**90**	**28**	280	5	58	58
3	SavWT	**91**	**28**	280	18	83	83
4	SavWT	**92**	**28**	280	5	99	99
5	SavWT	**93**	**35**	350	8	76	76
6	SavWT	**94**	**28**	280	*rac.*	>99	100
7	SavWT	**95**	**35**	350	*rac.*	>99	100
8	S112R	**90**	**28**	280	- 12	43	43
9	S112C	**91**	**28**	280	65	60	60
10	S112C	**93**	**35**	350	40	26	26
11	S112Y	**92**	**28**	280	- 47	72	72

12	S112M	**94**	**28**	280	9	95	95
13	S112E	**95**	**28**	280	18	73	73
14	S112C	**70a**	**10**	140	83	25	18
15	S112C	**96**	**10**	140	52	15	11
16	S112C	**97**	**10**	140	56	15	11

[a]positive and negative *ee* values correspond to the (*R*)- and (*S*)-enantiomers respectively.

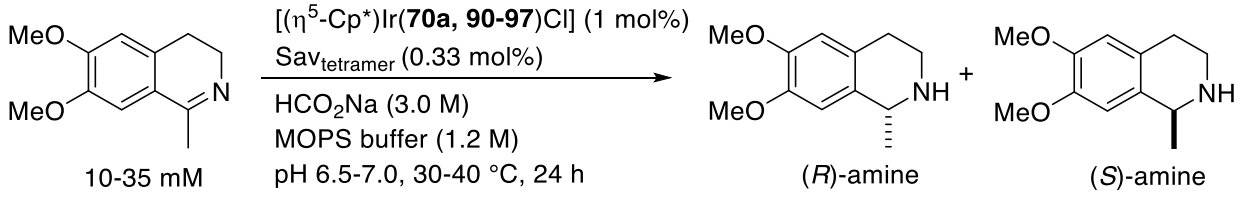

88 **87**

Scheme 29. ATHase of imine **88** based on six-membered ring aminosulfonamide chelating ligands.

To rationalize these results, a docking study was carried out with S112C and S112Y mutants in combination with [η5-Cp*Ir(**91**)Cl] and [η5-Cp*Ir(**92**)Cl] catalysts respectively. As for previous studies by Maréchal and coworkers,[252] the host protein dictates the absolute configuration at iridium, which in turn determines the preferred approach of one prochiral face of the substrate **88**. Ward and Maréchal coined this chiral relay mechanism "induced lock-and-key" as the host protein favours one metal absolute configuration upon incorporation within Sav. With the diastereopure cofactor in place, the approach of the prochiral substrate is dictated by the Sav host.

A Dual Anchoring Strategy for ATHAse Based on the Biotin-Streptavidin Technology. Although incorporation of ArMs in Sav is best achieved via a biotin anchor, additional dative interactions between the metal cofactor and engineered amino acid side chains can be envisaged. This strategy may contribute to firmly localize the metal within the shallow biotin-binding vestibule. To evaluate the potential of this strategy, Ward designed a biotinylated Cp* ligand, thus ensuring localization of a d^6-pianostool moiety but leaving the remaining three coordination sites available for coordination to amino acid residues and for catalysis. Accordingly, Ward and coworkers designed cofactor [(**98**)$MCl_2(H_2O)$] (M = Rh(III), Ir(III)) inspired by structure-based modeling.[255] The presence

of the ethyl spacer projects the metal in proximity to both Sav S112 and Sav K121 positions. The authors hypothesized that the imidazole side chains of mutations S112H and K121H may coordinate thereby influencing the ArMs activity and selectivity. As a model reaction, the asymmetric transfer hydrogenation of salsolidine precursor **88** was selected. The reaction's stereoselectivity was very similar for complexes [(**98**)$IrCl_2(H_2O)$] and [(**98**)$RhCl_2(H_2O)$] in the presence and absence of WT Sav (*rac*-**87** and 6 % (*S*)-**87**, respectively). When [(**98**)$RhCl_2(H_2O)$] · Sav S112H was tested, (*S*)-**87** was produced with 55 % ee and > 100 TON at 55 °C and pH 5, Scheme30 a). As suggested by docking, [(**98**)$RhCl_2(H_2O)$]·Sav K121H leads to stereoinversion; (*R*)-**87** is obtained with 79 % ee and > 100 TON under identical conditions. Decreasing the temperature leads to erosion in ee and TON. At 4 °C ATHase [(**98**)$RhCl_2(H_2O)$]·Sav K121H produces only 50 % (*R*)-**87** with 12 TON. X-ray crystal structures were solved for both [(**98**)$RhCl_2(H_2O)$]·Sav S112H and [(**98**)$RhCl_2(H_2O)$]·Sav K121H (Scheme 30 b) and c). The pseudo-mirror image environments around the Rh-complexes found in the two mutants confirmed that the dual anchoring may indeed be at the origin of observed activity and selectivity of the corresponding ATHases.

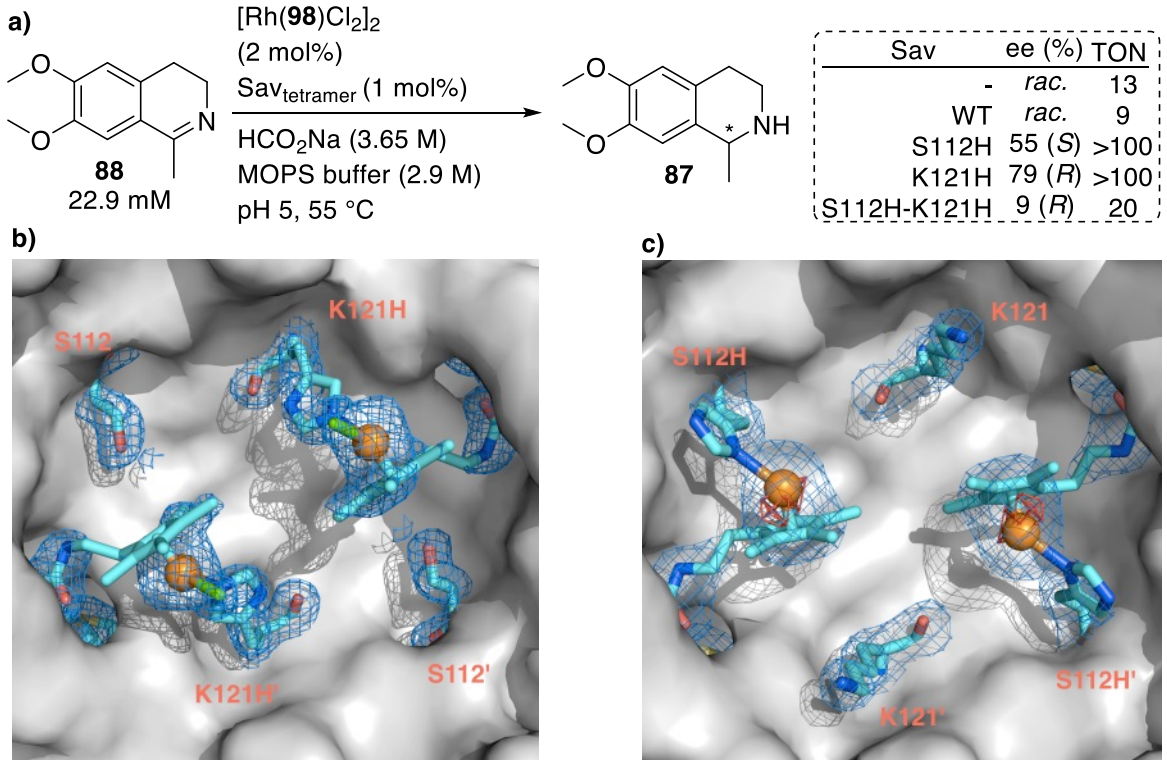

Scheme 30: A dual-anchoring strategy allows to localize and activate the biotinylated cofactor [(**98**)$MCl_2(H_2O)$] within Sav. a) The imine reductase is activated by introduction of a coordinating His-residue either at position Sav S112 or Sav K121; b/c) as highlighted by a crystal structure, the position of the pianostool complex imposed by either S112H- or K121H-coordination to Rh(III) leads to an inversion of the ATHase's enantioselectivity. Adapted with permission from ref.[38] Copyright 2016 American Chemical Society.

Transfer Hydrogenation of Imines, Bidentate Ligand Screening. Iridium pianostool complexes bearing a biotinylated arene cap allow for the screening of a bidentate ligand library within the Sav scaffold. This easily accessible chemical diversity component may lead to a rapid identification of ATHases with improved activity and selectivity. To test this hypothesis, Ward and coworkers preincubated complexes [(**98**)M_2Cl_2)]$_2$ (M = Rh, Ir) in the presence of eight bidentate ligands (diamines, amino acids and amino amides) at room temperature followed by addition of WT Sav.[256] The reaction was initiated by addition of the substrate 1-phenyl-3,4-dihydroisoquinoline and 1.5 M sodium formate in a MOPS-buffered solution (pH 7.8). All Rh-based ATHases displayed very limited activity and yielded virtually racemic product. The bidentate ligand glycineamide in conjunction with [(**98**)$IrCl_2(H_2O)$] · WT Sav was most active (372 TON) and most selective albeit yielding

the corresponding imine in 43 % (*S*)-ee. Encouraged by the promising result obtained with glycineamide, the amide derivatives of all 20 natural amino acids were screened in the presence [(**98**)$IrCl_2(H_2O)$]·WT Sav. The amides of L-proline (67 % ee), L-valine (63 % ee), L-leucine (63 % ee), L-arginine (61 % ee), L-isoleucine (65 % ee) and L-threonine (63 % ee) displayed improved selectivity for (*S*)-product. Further genetic fine-tuning with a focused Sav mutant library did not further contribute to improve the ee significantly. The authors hypothesize that the three legs of pianostool moiety are projected towards the aqueous solution, offering limited means to optimize the performance by mutagenesis of the Sav scaffold.[256]

Transfer Hydrogenation of Imines, ATHase Immobilized on Silica Nanoparticles. Silica nanoparticles are used in biocatalysis to immobilize enzymes, to protect these against denaturation and to improve the reaction rates. Ward and coworkers tethered the ATHase [η^5-(Cp*)Ir(**70**)Cl]·Sav S112A, Sav S112K and Sav S112A-K121A via imine formation to an aldehyde group at the surface of a silica nanoparticle (SNP). The protein-functionalized SNP surface was further treated with a protective silica layer.[257] The immobilized ATHase [η^5-(Cp*)Ir(**70**)Cl]·Sav S112A had a 4-fold increased TON vs. the free enzyme (TON: 4294 vs. 1154) in the asymmetric transfer hydrogenation of cyclic imine **88**. Upon lowering the catalyst loading to 0.0013 mol% 16990 TON were achieved. The selectivity of complex [η^5-(Cp*)Ir(**70**)Cl]·Sav S112A for (*R*)-**87** increased from 79 % ee to 90 % ee upon immobilization. The opposite effect was observed with (*S*)-selective mutant S112K where the ee decreased from 66 % ee to 56 % ee upon immobilization. The most active mutant tested was S112A-K121A which afforded up to 46'747 TON (in 24 hours) at a catalyst loading of 0.0075 mol%.

Neutralizing Cellular Glutathione for ATHases. Natural evolution of function relies on

mutagenesis and selection. In contrast to homogenous catalysts, artificial metalloenzymes bear the potential to be genetically optimized by mutagenesis. Directed evolution relies on the efficient high-throughput screening of genetic diversity to identify and characterize functionally evolved mutants. Parallel *in vivo* expression of Sav in *E. coli* (e.g. in 96-well plates) followed by cofactor addition could in principle allow directed evolution of the corresponding ArMs. A challenge in the development of HTS methods for ArMs optimization is the presence of glutathione (GSH) in millimolar concentration in aerobic *E. coli* cells.[258] The soft acid character of the precious metals in ArMs favors their coordination to GSH. One way to decrease the cellular GSH content is to treat cell lysates with GSH scavengers such as electrophiles or oxidants. Ward and coworkers evaluated the potency of various GSH scavengers to recover artificial transfer hydrogenase activity in cellular media.[259] Experiments were carried out in the presence of (*R*)- and (*S*)-selective ATHases [η^5-(Cp*)Ir(**70**)Cl]·Sav S112A and [η^5-(Cp*)Ir(**70**)Cl]·Sav S112K. Upon addition of 2.5 mM GSH, the reduction of salsolidine precursor **88** in the presence of both mutants S112A and S112K completely stalled, Scheme 31. In contrast, oxidized glutathione (GSSG) had a significantly less pronounced detrimental effect. From all the GSH scavengers tested, diamide **99**, phenylvinylsulfone **100** and 2-bromoacetophenone **101** led to the best recovery of activity. However, overnight incubation was essential to recover maximum activity. Up to 90 % initial activity and similar ee were obtained with [η^5-(Cp*)Ir(**70**)Cl]·Sav S112A for substrate **88** after incubation with **99**. For ATHase [η^5-(Cp*)Ir(**70**)Cl]·Sav S112K, less activity was recovered. In the presence of cell free extracts, **99** outperformed all other scavengers. With 10 mM **99** and only 2 h preincubation time, > 50 % of the pure protein's activity and very similar ee's were obtained. When cell lysates were used, very good results could be obtained with [η^5-(Cp*)Ir(**70**)Cl]·Sav S112K (64 % pure protein activity, - 68 % ee) whereas the corresponding ArM with mutant Sav S112A

yielded reduced ee and TON.

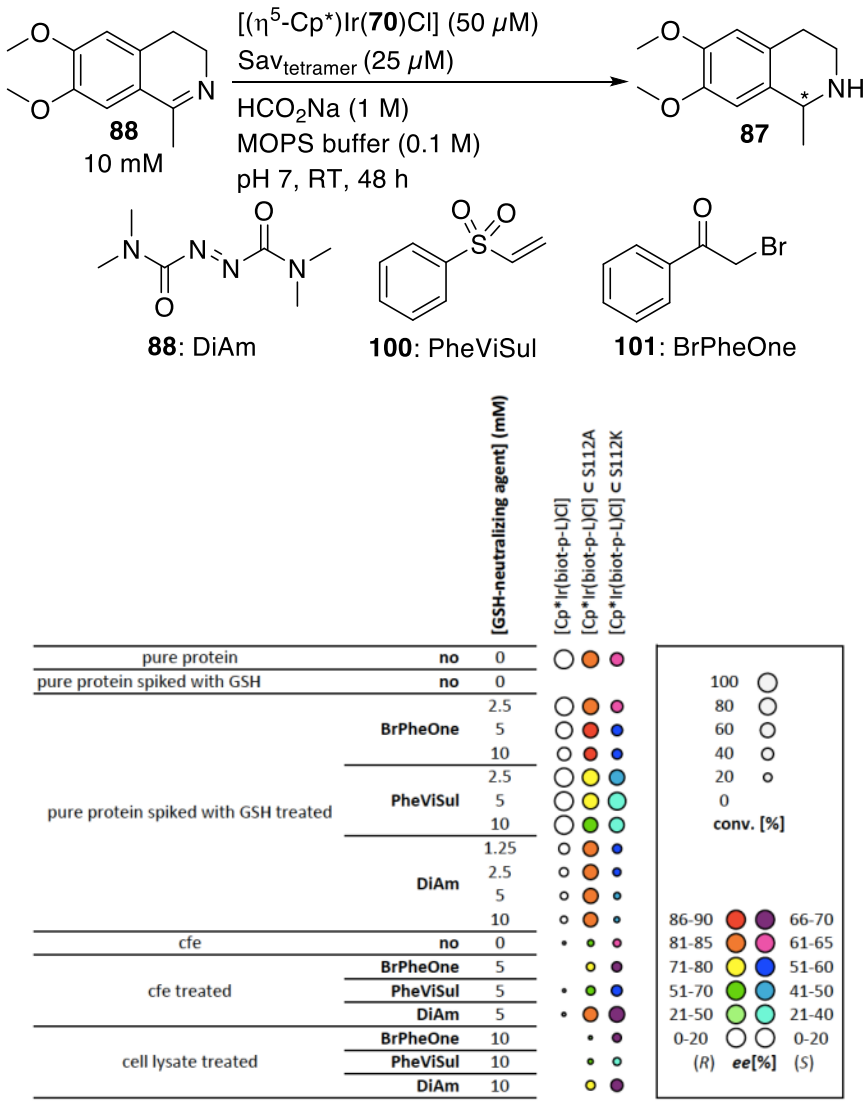

Scheme 31. Biotinylated Ir-pianostool complexes anchored within Sav are inactivated by physiological concentrations (~1 mM) of glutathione. Electrophiles and oxidizing agents react with glutathione and restore ATHase activity. Adapted with permission from ref.[38] Copyright 2016 American Chemical Society.

Transfer Hydrogenation of Imines, High-Throughput Screening. Ward and coworkers extended the glutathione scavenger strategy to implement a high-throughput genetic screening of artificial transfer hydrogenases. For this purpose, they selected diamide **99** as GSH neutralizing agent.[260] To parallelize Sav mutant expression, a 24-well deep well plate format was introduced. In six milliliter medium, sufficient Sav (~0.5 mg) can be produced to run 1-2 catalytic reactions. Accordingly, twenty eight amino acids within a 15

Å distance to the metal were selected for mutagenesis. Instead of introducing all 20 amino acids at each position, the effort was reduced to 12 amino acids: A, V, L, D, E, Q, K, H, M, Y, S, P as representatives of the different types of amino acids (acidic, basic, polar, hydrophobic). The autoinduction medium Zyp-5052 was used to express all Sav isoforms, Scheme 32. After 24 h expression, cell free extracts of the mutants were prepared and biotin-4-fluorescein titration was applied to determine the number of free biotin-binding sites per well. To the cell-free extracts, **99** was added to neutralize GSH. After incubation, the catalyst, the substrate and the reductant were added. The reaction was followed by UPLC. The procedure allows the screening of 335 Sav mutants within 20 days (including mutagenesis, expression and activity screening).

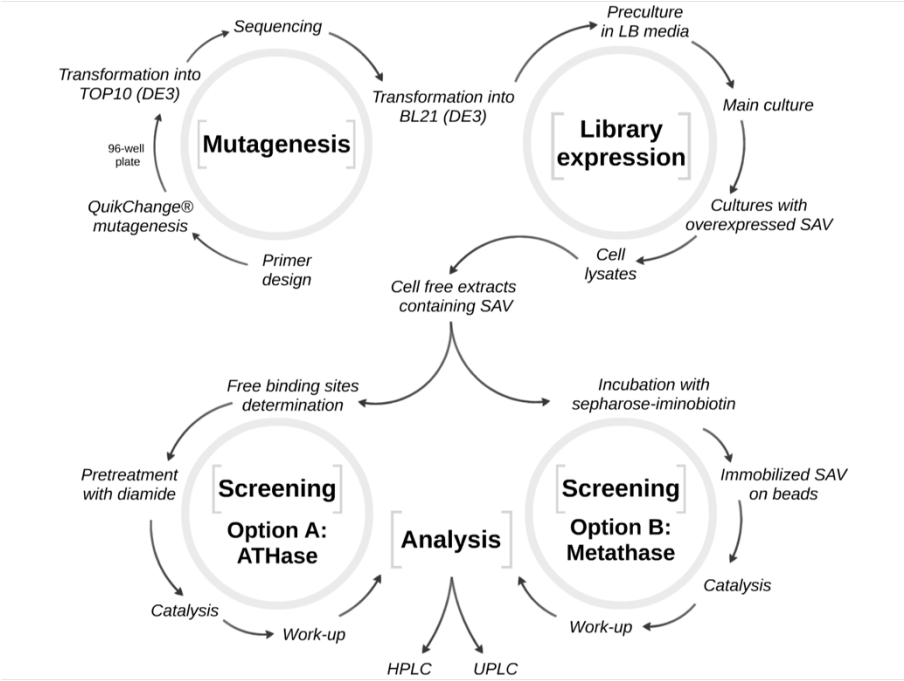

Scheme 32. a) Streamlined Sav library production, isolation and screening for ATHase activity in cell-free extracts relying on diamide treatment; b) metathesis activity in cell free extracts using a reversible imminobiotin-sepharose immobilization. Adapted with permission from ref.[260] Copyright MacMillan 2016.

Transfer Hydrogenation of Imines, Cascade with Amine Oxidase. In the Ward group, initial efforts towards the creation of cascade reactions aimed at combining an artificial

transfer hydrogenase with a natural amine oxidase. ATHase [η^5-(Cp*)Ir(**70**)Cl] · Sav S112T is moderately (*R*)-selective (59 % ee) for imine **89**.[261] The ATHase was combined with monoaminooxidase MAO-N which has very high selectivity for the oxidation of (*S*)-amine **102,** Scheme 33. Unfortunately, shortly after the reaction had started, the ATHase was inhibited by the hydrogen peroxide produced by the MAO upon oxidation of the amine substrate. Addition of catalase restored activitiy and allowed the dynamic kinetic resolution to afford (*R*)-**102** in > 99 % ee. The same strategy was applied for the one pot dynamic kinetic resolution of pyrrolidines **103** and **105** which were obtained in essentially enantiopure (*R*)-form thanks to the exquisite (*S*)-selectivity of MAO-N. Similarly, tertiary imine **104** was reduced to the corresponding (*R*)-amine **105** with >99 % ee and 65 TON. Cyclic imine **104** is in equilibrium with the ring-open keto form **106** at pH 7.5. Interestingly, the nature of the Sav mutant determines which substrate is preferentially reduced: [η^5-(Cp*)Ir(**70**)Cl]·Sav S112A-K121T produces preferentially the imine **104** (76 : 11). In contrast, [η^5-(Cp*)Ir(**70**)Cl]·Sav S112G favors the reduction of the keto form of **104,** yielding the corresponding alcohol **107** (3 : 79).

Transfer Hydrogenation of Enone and Nicotinamide Regeneration. Many enzyme-driven reactions utilize NAD(P)H as cofactor which increases the production costs of biocatalytic transformations. Several enzymatic NAD(P)H regeneration systems are known. Additionally, regeneration systems based on organometallic catalysts exist. However only few of them actually work in cascade reactions in the presence of NAD(P)H-dependent enzymes. Ward and coworkers applied the ATHase [η^5-(Cp*)Ir(**70**)Cl] · WT Sav to recycle NADH in a cascade with NADH-dependent hydroxybiphenyl monooxygenase (HbpA, Scheme 34).[261] In this reaction, hydroxybiphenyl **108** was converted to the corresponding catechol **109** with TON > 99 in the presence of O_2 as oxidant. No catalase was required since the reaction's byproduct is water.

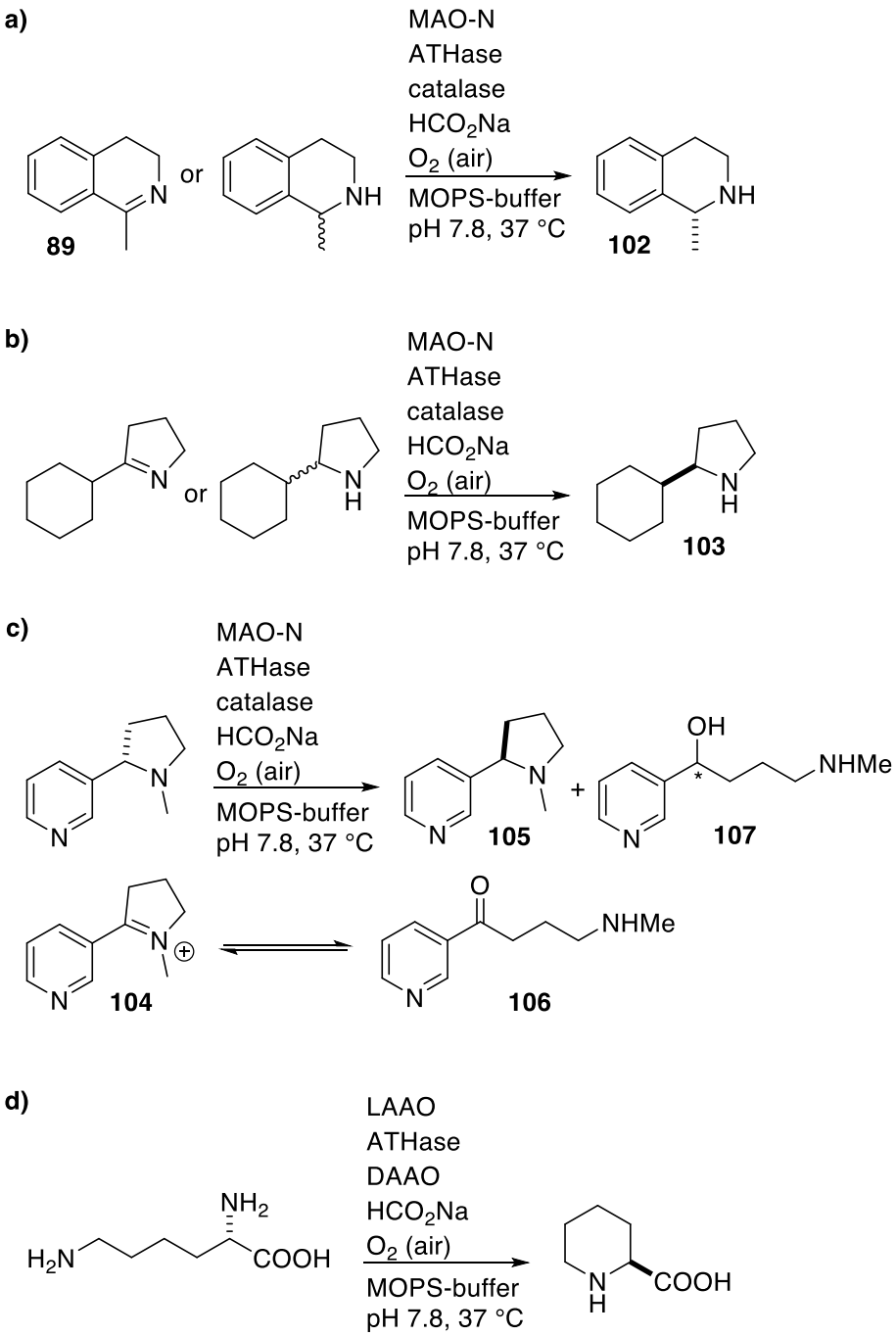

Scheme 33. Enzyme cascades combining an ATHase and an amine oxidase afford enantiopure amines. This can be applied for the synthesis of a/b) isoquinolines and pyrrolidines, c) nicotine, and d) pipecolic acid. Addition of either horseradish peroxidase or catalase prevents the oxidation of the iridium cofactor by hydrogen peroxide resulting from MAO activity. Adapted with permission from ref.[261] Copyright MacMillan 2013.

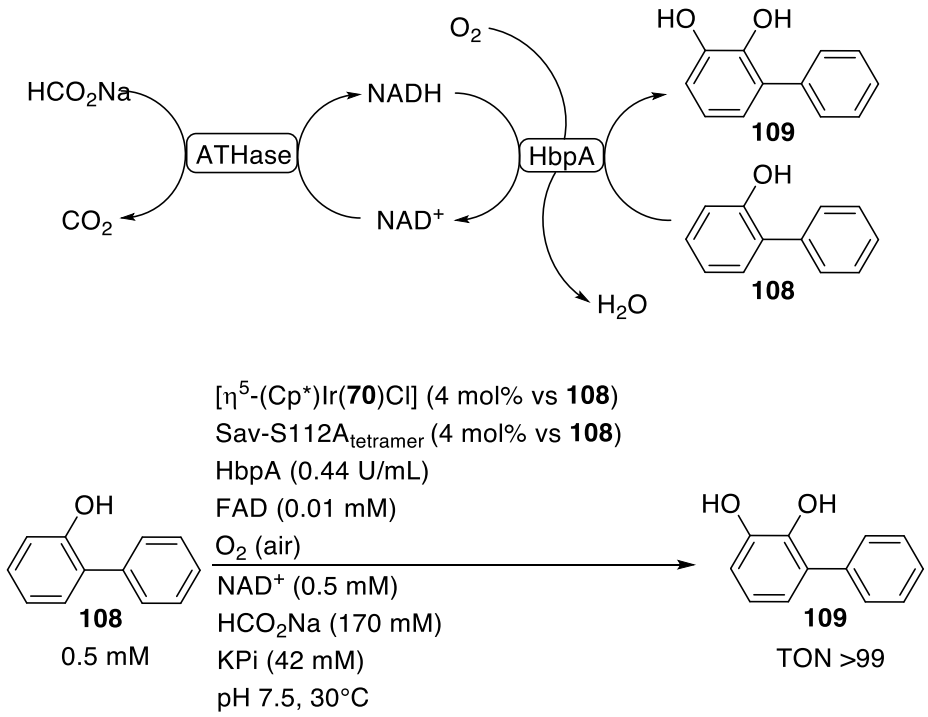

Scheme 34. ATHases can be used to recycle NADH using formate as reductant. The NADH-recycling ATHase can be applied in a cascade with HbpA monooxygenase to produce dihydroxy biphenyl. Adapted with permission form ref.[261] Copyright MacMillan 2013.

The NADH regeneration employing ArMs and sodium formate as hydride source (Scheme 35) was also investigated by Salmain and coworkers. The Papain scaffold was used to host the precious metal d^6-pianostool complexes using a covalent anchoring strategy via a maleimide moiety.[241-242] They evaluated the catalytic transfer hydrogenation performance for the reduction of NAD^+ **111** into NADH **110**. The bispyridine-rhodium complex **77** proved most active upon anchoring in PAP.[262] The authors showed that **77**·PAP has comparable catalytic activity to the benchmark complex $[(\eta^5\text{-Cp*})Rh(bpy)H_2O]^{2+}$. The artificial transfer hydrogenase **VLC16**·PAP had comparable activity to the free cofactor **77**. Disappointingly, no attempt was reported by the coauthors to couple this NADH regeneration ArM with natural NADH-consuming enzymes.

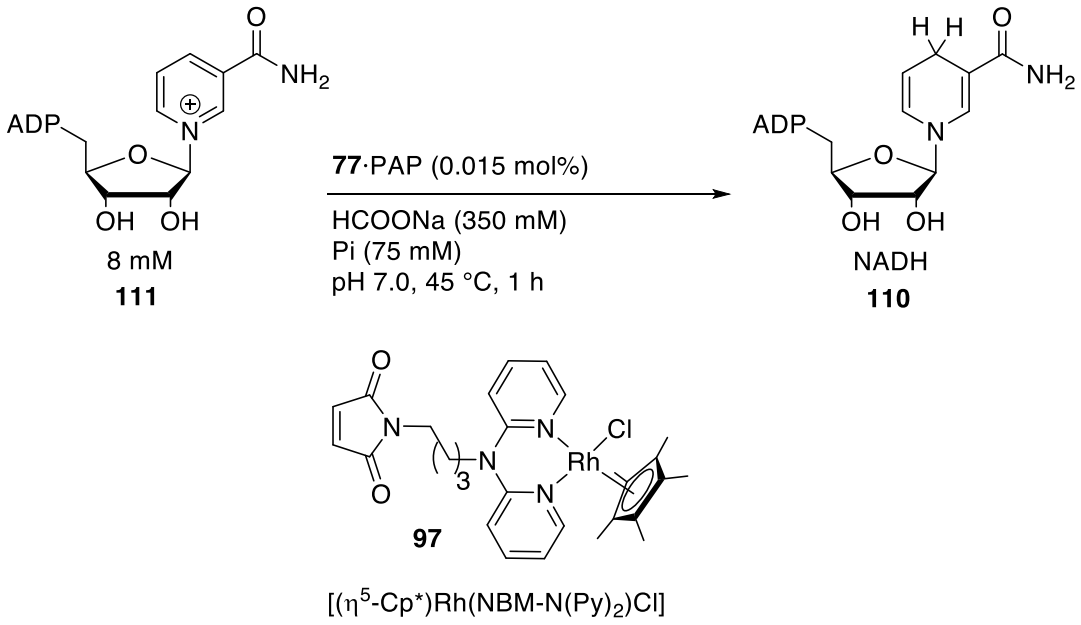

Scheme 35. Covalent anchoring of **77** in PAP yields an ArM that catalyzes the reduction of NAD^+ to NADH using formate as hydride source.

Transfer Hydrogenation of Enones, Regeneration of NADH Mimics. Mimics of NAD(P)H are attractive in biocatalysis as the natural NAD(P)H cofactors are costly. Non-enzymatic regeneration systems based on organometallic catalysts are only moderately active when applied in cascades as they are typically inhibited by enzymes. Based on a previous finding that ATHase [η^5-(Cp*)Ir(**70**)Cl]·Sav S112A regenerates NADH using sodium formate as hydride source, Ward and coworkers set out to investigate whether NADH mimics could be regenerated. The ATHases were applied in a cascade with ene-reductase *Ts*OYE of the old yellow enzyme family which was previously shown to accept NADH mimics as reducing equivalents.[263] Various ATHase isoforms with point mutations at positions Sav S112, K121 and L124 were tested towards the reduction of five NAD^+ mimics ($mNAD^+$ hereafter). The model substrate *N*-ethyl-2-methylmaleimide **113** was converted by *Ts*OYE to the corresponding enantiopure unsaturated imide **114,** Scheme 36. Only the ketone-bearing $mNAD^+$ **112** afforded high turnover numbers (100 – 1000 TON) and enantioselectivity (~90 % ee for (*R*)-product). Sav-mutant S112K showed the highest conversion (~100 %). The protein matrix prevents the inactivation of the

organometallic cofactor by TsOYE. The (*R*)-selectivity of the cascade could be increased to 98 % ee when the Ir-catalyst concentration was reduced to 5 μM and the substrate was added slowly. This strategy helps to minimize the reduction of the substrate by the ATHase, which leads to an erosion of ee. The maximum TON achieved was > 1980. Other substrates tested included ketoisophorone **115** and 2-methylcyclohexenone **116** which were converted into the corresponding products with up to 86 % ee ((*R*)-product) and 94 % ee ((*R*)-product), respectively, and TONs ranging between 550 and 1655.

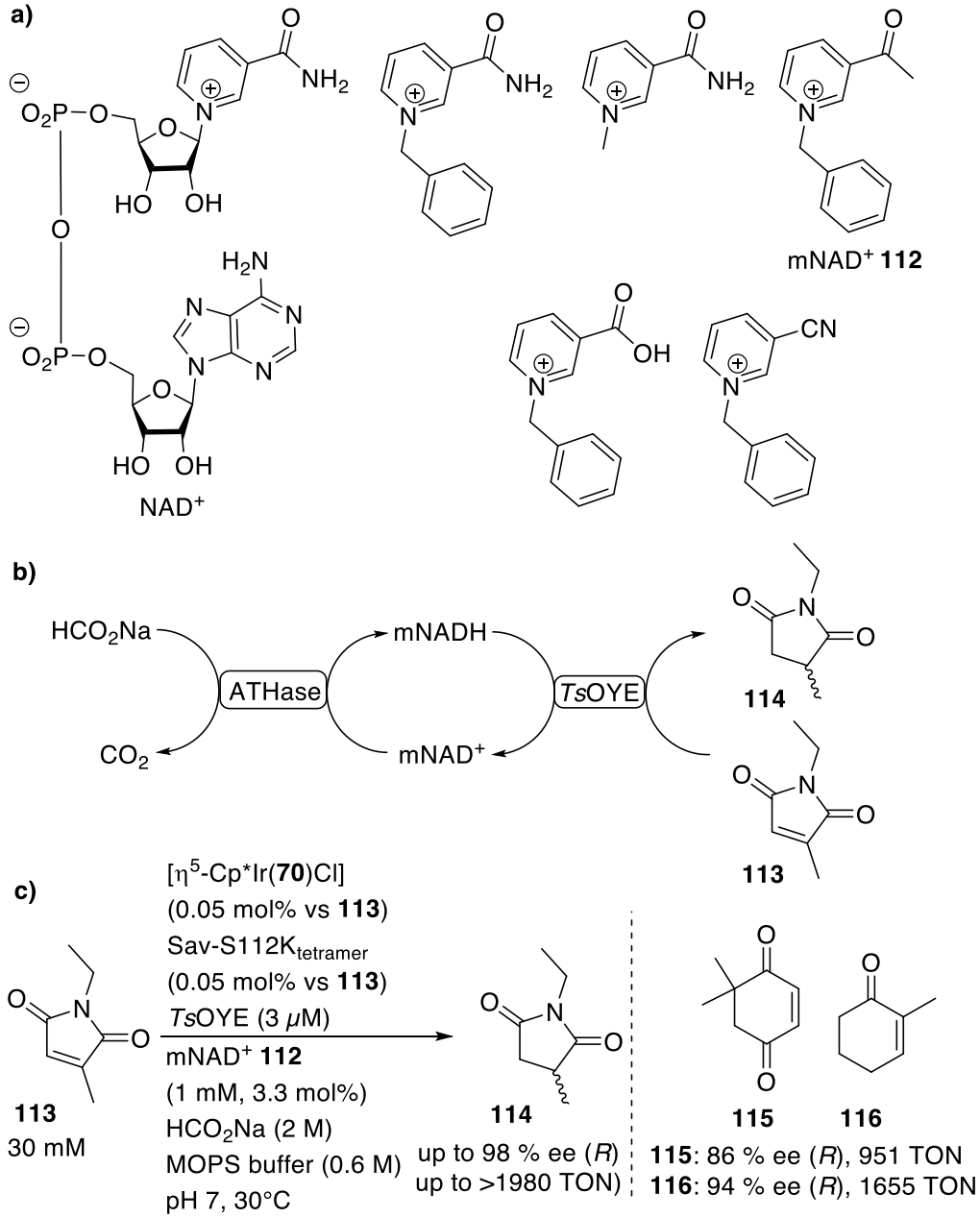

Scheme 36. An ATHase for the recycling of NADH-mimics in the presence of an ene reductase. a) Structure of NAD^+ and $mNAD^+$; b/c) the ATHase can be applied in an enzyme cascade in the presence of ene-reductase TsOYE to afford highly enantioenriched α,β-saturated ketones from the corresponding enones.

Ward and coworkers demonstrated that ATHase [η^5-(Cp*)Ir(**70**)Cl]·Sav can be applied in the diasteroselective transfer hydrogenation of NAD^+ with sodium formate.[264] In phosphate buffer (pH 7.5) and in the absence of Sav, the reduction of NAD^+ by DCO_2Na proceeded with a diastereomeric excess for de = 38 %. For [η^5-(Cp*)Ir(**70**)Cl] · Sav S112A and [η^5-(Cp*)Ir(**70**)Cl] · Sav S112K, the de increased to 87 % and 90 % respectively. In stark contrast to the reduction of either ketones or imines, both ATHases yielded the same enantiomer as determined by ^{1}H-NMR

Transfer Hydrogenation of Imines, NADH-dependent ATHase. Living organisms rely widely on NAD(P)H as redox cofactor to modulate redox reactions. The artificial transfer hydrogenases developed in the Ward group utilize formate as hydride source. To integrate an ATHase into an *in vivo* cascade, it would be desirable to use NAD(P)H as hydride source. To address this challenge, Ward and coworkers screened a number of bis-imino Ir-Cp* complexes for the reduction of 1-methyl-dehydroisoquinoline **89** using NADH as hydride source.[265] The most active ligand identified was 4,7-dihydroxy-1,10-phenantroline (**117**). Complex [(**98**)Ir(**117**)Cl]$^+$ afforded ~200 TON in 20 h. Next, to recycle the spent NADPH, glucose dehydrogenase (GDH) was added to the cascade for the reduction of imine **89**. By screening various Sav isoforms, [(**98**)Ir(**117**)Cl]·Sav K112R yielded the highest conversion in 14 hours (up to 961 TON). Unfortunately, amine **102** was produced in low ee (13 % ((*R*)-**102**), Scheme 37. To upgrade the ee via a dynamic kinetic resolution, monoamine oxidase (MAO-N) and catalase were added to the ATHase-GDH cascade. The four-enzyme cascade yielded amine (*R*)-**102** with >99 % ee and >99 TON, Scheme 37.

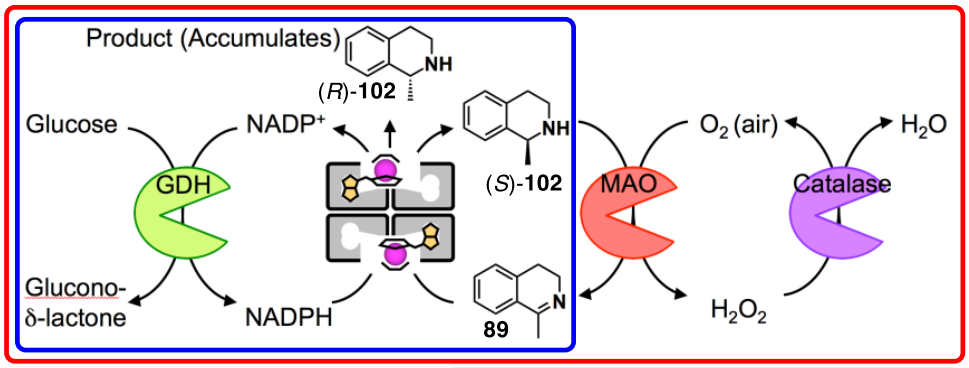

Catalyst:

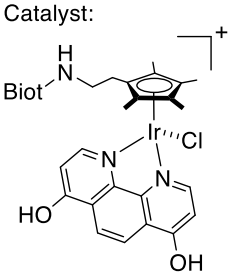

[(**98**)Ir(**117**)Cl]$^+$

Sav	Hydride source	TON_{Ir}	ee (%)
no Sav	NAD+/glucose	75	1 (*R*)
WT	NAD+/glucose	202	17 (*S*)
K121R	NAD+/glucose	679	13 (*S*)
K121R	NADP+/glucose	961	13 (*S*)

50 μM [(**98**)Ir(**117**)Cl]-Sav (0.1 mol%), 0.1 mg/mL GDH, 1 mM $NAD(P)^+$ (2 mol%), 50 mM substrate **89**, 60 mM glucose, 0.3 M MOPS (pH 7.9), 37 °C

Sav	MAO-N (mg/mL)	Time (h)	Conv. (%)	ee (%)
no Sav	0.2	12	6	>99 (*R*)
K121R	0.2	12	89	75 (*R*)
K121R	0.2	24	>99	>99 (*R*)
K121R	-	24	>99	13 (*R*)

100 μM [(**98**)Ir(**117**)Cl]-Sav (0.2 mol%), 0.1 mg/mL GDH, 0.2 mg/mL MAO, 500 U catalase, 1 mM $NADP^+$ (2 mol%), 50 mM substrate **89**, 100 mM glucose, 0.3 M MOPS (pH 7.9), 37 °C

Scheme 37: A biotinylated [(**98**)Ir(**117**)Cl]$^+$ cofactor anchored within Sav can rely on NADPH as reducing agent for the asymmetric transfer hydrogenation of imines.[265] This ATHase was integrated in a four-enzyme cascade to produce enantioenriched **102**, relying on glucose as hydride source (blue frame) and MAO-N to upgrade the enantioselectivity of the ATHase (red frame).

Transfer Hydrogenation of Imines, Allosteric regulation. In living organisms, enzymatic activity is typically (cross)-regulated via weak molecular interactions. Molecular or physical (e.g. optical, magnetic, temperature etc.) tools with the ability to control artificial metalloenzyme's activity would be highly desirable to regulate enzyme cascade *in vivo*. Ward and coworkers developed a latent artificial transfer hydrogenase that is activated by a protease, Scheme 38.[266] As cofactor, a biotinylated Ir-Cp* complex [(**98**)$IrCl_2(H_2O)$] was selected. As demonstrated previously, activation by an additional ligand is required to ensure ATHase activity. Inspired by the work on Hilvert and coworkers[267] they screened and identified a Ser-Gly-Phe tripeptide (SGF) that leads to significant enhancement of the catalytic activity upon coordination to [(**98**)$IrCl_2(H_2O)$].[267] Fused to the *C*-terminus of Sav and flanked by a protease-recognition sequence, the tripeptide becomes available to activate the cofactor upon digestion of the *C*-terminus by protease Factor Xa. While [(**98**)$IrCl_2(H_2O)$]·WT Sav was only moderately active for the reduction of

pentafluoroacetophenone with **118** (29 TON), addition of SGF led to a fiftyfold increase in activity (1431 TON). Next, the SGF peptide was fused to the C-terminus of Sav preceeded by the Factor Xa protease cleavage site. Incubation of the ATHase with Factor Xa prior to addition of formate and the ketone **118** led to significantly improved TONs (compare 23 for the undigested to 1778 TON, Scheme 38). Such irreversible activation is widespread amongst enzymes and is commonly referred to zymogens.

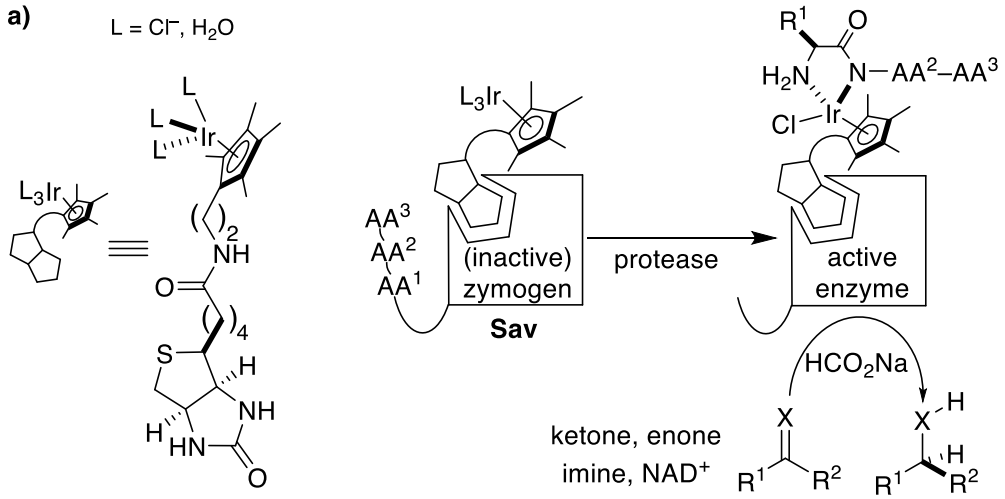

Sav-mutant	FactorXa	TON	ee (%)
K121A-SGF	-	23	-
K121A-SGF	+	1778	39 (*R*)
no protein	-	8	-

Scheme 38: An artificial transfer hydrogenase is upregulated by a protease. A zymogen is formed upon incorporation of [(**98**)$IrCl_2(H_2O)$] into Sav K121A bearing an SGF tripeptide at its *C*-terminus. Incubation of the zymogen with the protease Factor Xa releases the SGF ligand to afford [(**98**)Ir(SGF)Cl]·Sav K121A which displays significant ATHase activity b).[266]

Transfer Hydrogenation of Imines using Ribonuclease S as host protein. Ribonuclease A digestion by subtilisin affords a clove-shaped S-protein as well as an α-helical S-peptide. The S-protein and the S-peptide bind to each other with nanomolar

affinity to form a functional RNase S enzyme. Sträter, Ward and coworkers set out to engineer RNase S into an artificial metalloenzyme.[268] S-peptide variants with metal binding capacity including non-natural amino acids can be readily obtained by solid-phase synthesis. Incubation of metallated S-peptides with S-protein may allow to engineer RNase S isoforms displaying new-to-nature activities. Tuning of reaction activity and selectivity may be possible via second coordination sphere interactions stemming mainly from the S-protein. This concept was tested with the asymmetric transfer hydrogenation of the cyclic imine **88**. The authors speculated that two histidine residues provided by the host protein may activate the cofactor. The RNase S crystal structure allowed to identify two residues (K7 and Q11) in the proximity of the α-helical S-peptide. Thus RNase S K7H-R10Q-Q11H isoform was synthesized and incubated with $[\eta^5\text{-}(Cp^*)IrCl_2]_2$, $[\eta^5\text{-}(Cp^*)RhCl_2]_2$ or $[\eta^6\text{-}(p\text{-cymene})RuCl_2]_2$ prior to complexation with the S-protein. The iridium RNase S K7H-R10Q-Q11H complex was most active affording 28 TON. The corresponding WT RNase S however yielded 70 TON under the same conditions, suggesting that the metal does not bind to the two-histidines introduced in the S-peptide. The enantioselectivity was very low (4-8% ee (*S*)-**87**) for both S-peptide triple mutant and WT. When the WT S-peptide Ir complex was used in the absence of S-protein, the ee increased minimally to 22 % (*S*)-**87** at the cost of a lower activity (10 TON), suggesting a modest protein acceleration. The best ee obtained with the RNase S system was 39 % (*S*)-amine **87** obtained with RNase S mutant H12A in which the only histidine within the WT S-peptide was replaced by an alanine.

Transfer Hydrogenation of Imines, hCAII as host protein. Most artificial metalloenzymes developed in the Ward group are based on the (strept)avidin-biotin technology to anchor a transition metal complex within a protein environment. Human carbonic anhydrase II (hCAII) is another attractive scaffold for ArM design. It is a

monomeric protein which binds with sub-nanomolar affinity numerous arylaminosulfonamide derivatives.[269] The crystal structure of many of the hCAII-ligand complexes are deposited in the protein data bank (PDB) and provide insight for rational ArM design. Moreover, hCAII can be expressed in large amounts in *E. coli.* In an initial effort to build an ArM from hCAII, Ward and coworkers tethered pianostool complex [η^6-(C_6Me_6)Ru(bispyridine)Cl]$^+$ to a benzene sulfonamide anchor.[270] The Ru-cofactor did not afford any transfer hydrogenation activity but bound to hCAII with nanomolar affinity. A second arylsulfonamide cofactor was based on iridium complexes [η^5-(Cp*)Ir(pico)Cl] (**119-120**).[271] In the asymmetric transfer hydrogenation of cyclic imine **88** inside WT hCAII, this ArM afforded 9 TON and up to 70 ee for (*S*)-salsolidine **87**, Scheme 39. A crystal structure of complex [η^5-(Cp*)Ir(**pico**)Cl] **119**·WT hCAII was solved which served as a model for a computational enzyme redesign. In a collaboration with the Baker group, Ward and coworkers relied on the Rosetta design algorithm to identify mutants that may stabilize the Ir-cofactor within hCAII.[272] The hypothesis was that cofactor stabilization and localization might increase the relative concentration of the active catalytic species vs. unproductive conformations of the ATHase. Rosetta predicted four hCAII constructs containing up to 8 mutations (**d1 – d4**) that were predicted to display increased affinity. Binding assays of the mutated hCAII revealed that indeed the designs had on average a ~50-fold increased affinity vs. WT hCAII (K_d = ~0.33-0.46 nM vs. 21 nM). Gratifyingly, the imine reduction activity was also positively affected: up to 98 TON with 74 % ee (*S*)-**87** with the hCA II **d1** construct. The best enantioselectivity was obtained with the design hCAII **d4** and afforded 92 % ee (*S*)-**87** and 78 TON. Substituting a single methyl- by a propyl group on the Cp* cap in the hybrid [η^5-(Cp^{propyl})Ir(**pico**)Cl] **120** · hCAII **d4** further increased the ee to 96 % (*S*)-**87** and 59 TON at 4°C, Scheme 39.

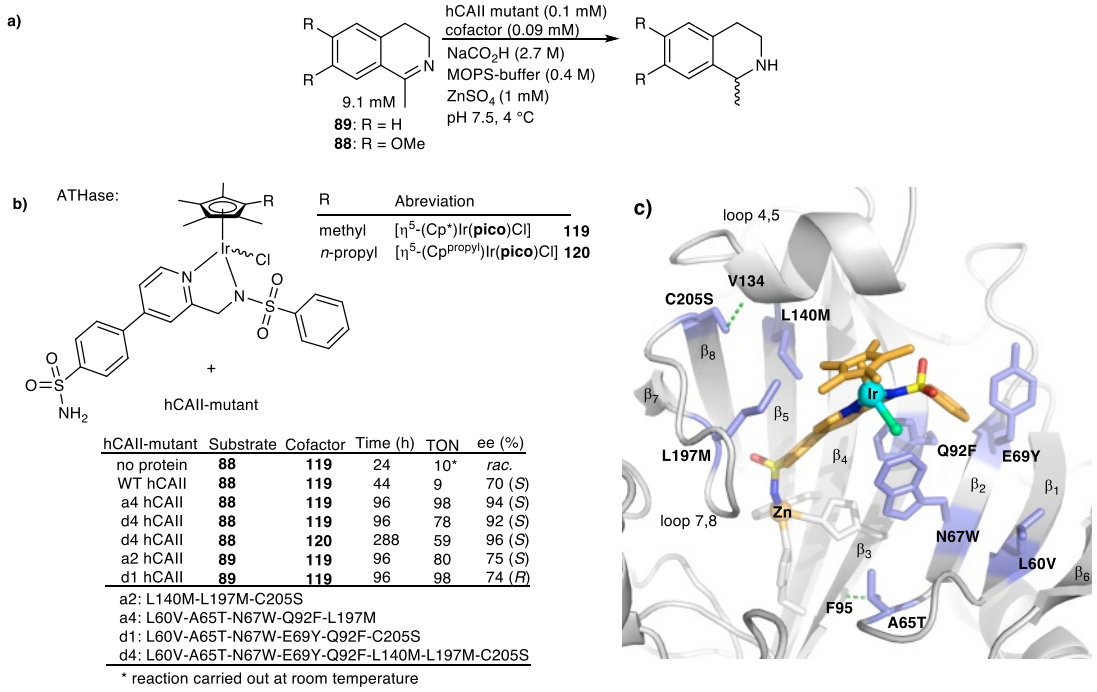

Scheme 39, Rosetta-optimization of an ATHase based on human carbonic anhydrase II. a) Reaction conditions; b) structure of the pianostool complex and computationally-designed mutants predicted to increase the affinity of [η^5-Cp*Ir(**pico**)Cl] for hCA II and c) X-ray crystal structure of the WT ATHase crystal structure (PDB 3zp9) used as template for computational mutagenesis with the Rosetta design algorithm (complex stabilizing residues displayed in purple). Adapted from ref.[272] Copyright 2015 American Chemical Society.

Transfer Hydrogenation of Enones. Noyori-type pianostool complexes have been widely applied in the asymmetric reduction of enones.[273] To test whether ATHase [η^5-(Cp*)Ir(**70**)Cl]·WT Sav chemoselectively reduces enones to the corresponding ketones, Ward and coworkers designed the profluorescent enone **121**. Upon Michael addition of a hydride, a spontaneous E1cB elimination leads to the release of fluorescent umbelliferone, Scheme 40 a).[274] As little as 1 μM of [η^5-(Cp*)Ir(**70**)Cl]·WT Sav sufficed to observe the appearance of the fluorescent product. Screening purified Sav mutants in positions S112X and K121X led to the identification of [η^5-(Cp*)Ir(**70**)Cl] · Sav K121F with a significantly improved activity (initial rate: TOF 147 AU · min^{-1} vs. 7.5 AU · min^{-1} for the WT ATHase).

With *in vivo*-applications in mind, Ward and coworkers encapsulated the best ATHase [η^5-(Cp*)Ir(**70**)Cl]·Sav K121F within a polymersome. The polymersome consisted of block-co-

polymers poly(2-methyloxazoline)-β-poly(dimethylsiloxane)-β-poly(2-methyloxazoline) (PMOXA-PDMS-PMOXA) developed by Meier and coworkers Scheme 40 b).[275] Upon incorporation inside the capsule, the ATHase activity was reduced however. Activity could be improved upon incorporation of the bacterial outer membrane protein ompF into the polymersome which assists small molecule trafficking across the membrane.

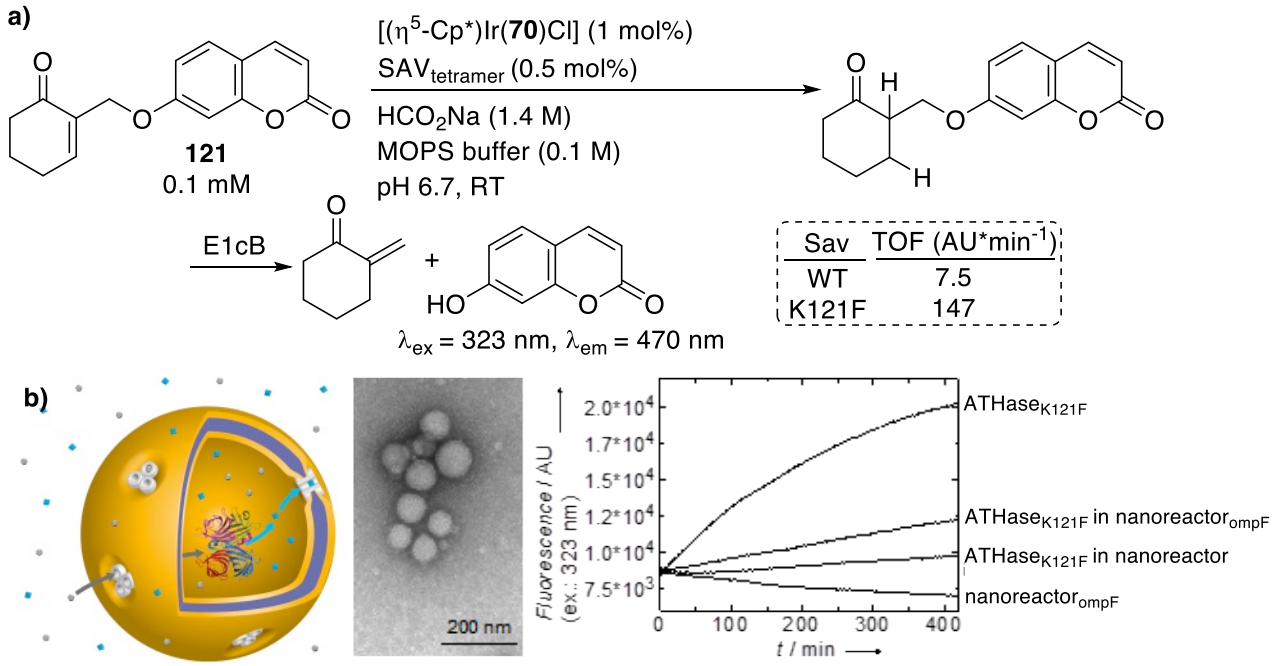

Scheme 40. An artificial transfer hydrogenase consisting of Sav and [(η5-Cp*)Ir(**70**)Cl] reduces enones. a) The reduced ketone spontaneously undergoes an E1cB elimination to release umbelliferone, thus allowing high-throughput genetic optimization of ATHase activity; b) the best ATHase-K121F is active inside a polymersome equipped with bacterial pore protein ompF. Adapted with permission from ref.[38] Copyright 2016 American Chemical Society.

4.4 Hydroformylation

Hydroformylation of olefins is widely used to synthesize aldehydes in both commodity and fine chemicals due to its perfect atom economy[276] and the availability of olefins and syngas. Both linear and branched aldehydes can be accessed, in the latter case leading to a stereogenic center α to the aldehyde, presenting the opportunity for catalyst control over both regio- and enantiooselectivity.[277] As noted in section 3, early studies by Marchetti established that ArMs generated via metallation of HSA with $Rh(acac)(CO)_2$ catalyze

styrene hydroformylation with a branched-to-linear ratio of ~90:10.[156] Building on extensive work showing that the active site Zn of carbonic anhydrase could be substituted with different metals,[278] Kazlauskas replaced the active site Zn of hCAII with [Rh(acac)$(CO)_2$] to generate a hydroformylase.[279] The branched aldehyde product of styrene hydroformylation was favored by the free cofactor and ArMs generated using wt hCAII, Scheme 41. Analysis of this ArM using ICP-MS indicated that it possessed a Rh/scaffold ratio of 5.4, which was believed to result from non-specific Rh-binding sites on the scaffold surface. Targeted mutagenesis and chemical modification of surface histidine residues was therefore carried out, and ArMs generated from the resulting hCAII variants had Rh : scaffold ratios of 1.2 and 1.4. The hydroformylation of styrene catalyzed by the modified ArMs reversed its regioselectivity to favor the linear product (linear/branched ratio up to 8.4, Scheme 41).

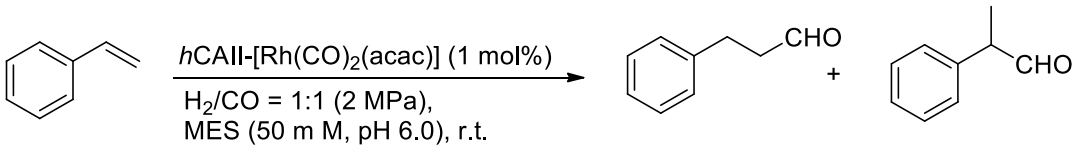

Catalyst	Rh/hCAII Ratio	Conversion%	Linear/Branched
$Rh(CO)_2(acac)$	-	39	0.21
*h*CAII-[$Rh(CO)_2(acac)$]	5.4	50	0.39
9*His-*h*CAII-[$Rh(CO)_2(acac)$]	1.2	50	3.0
DEPC-H4/10R-H17F-[$Rh(CO)_2(acac)$]	1.4	74	8.4

Scheme 41. Hydroformylation of styrene catalyzed by a Rh-substituted hCAII.

More recently, Hartwig reported detailed characterization of rhodium- and iridium-substituted hCAII ArMs.[280] Metallation of apo hCAII was monitored using a colorimetric assay, which indicated that metallation was significantly impacted by the ligands on the metal precursors used but suggested that surface histidine residues had only a minor impact. [$Rh(nbd)_2$]BF_4 and [$Rh(acac)(CO)_2$] (nbd = norbornadiene and acac =

acetylacetonate) afforded 71% and > 90% metallation, and the Rh/scaffold ratio was approximately 1:1 even with surface histidine present. A elegant series of HSQC NMR experiments, which had been previously used to study the catalytic mechanism of hCAII,[281] indicated that Rh was only coordinated by two of the three His residues in the active site. Multiple ligand substitution reactions of hCAII-[Rh(nbd)$_2$] were also examined.

4.5 Small Molecule Reductases

Natural enzymes performing reductions of small molecules are located in the super-group of the oxidoreductases (Enzyme Commission number: EC 1) and act on nitrite, nitric oxide, nitrous oxide, elemental nitrogen, sulfite, elemental sulfur as well as dioxygen, chlorate and perchlorate. Enzymes involved in these transformations are amongst others flavodiiron proteins[282], heme proteins[283-284] and enzymes depending on copper[285], molybdenum[286-288] and vanadium.[289] Beside the large variety of natural small molecule reductases, researchers have engineered artificial metalloenzymes for the reduction of nitrite, nitric oxide, dioxygen and carbon dioxide.

Inspired by the structural homology of heme copper oxidases (HCOs) and nitric oxide reductases (NORs), Lu designed and engineered a copper binding site in sperm whale myoglobin (Mb) by introducing two histidine residues (L29H, F43H) into the distal heme pocket. Metal binding in the resulting scaffold (Cu$_B$Mb) was supported by UV-Vis and EPR, and increased O_2 affinity was observed when Ag(I) (as a Cu(I) mimic) bound.[290] NO reduction(Equation 1) was catalyzed by Cu$_B$Mb-Cu(I), with a turnover number close to a native enzyme (~ 2 mol NO · mol Cu$_B$Mb^{-1} · min^{-1}).[291] Lu later designed a heme/non-heme Fe$_B$ binding site in Mb by incorporating L29H, F43H, and an additional glutamate residue (V68E) into this scaffold.[292] The binding of Fe(II) in the new artificial enzyme (Fe$_B$Mb) was

supported by the crystal structure of Fe(II)-Fe$_B$Mb, in which the non-heme iron was coordinated with three histidines, one O atom of glutamate and one water molecule. Thirty percent conversion was observed for NO reduction catalyzed by Fe(II)-Fe$_B$Mb. The catalytic activity was further enhanced (~100% increase) by introducing a second glutamate to the second coordination sphere of Fe$_B$ binding site (I107E), which was believed to facilitate proton delivery via a hydrogen binding network. The same group reported an alternate binding pocket (Fe$_B$Mb(-His)) for Cu, Fe and Zn ions, consisted of two histidines and one glutamate (L29E, F43H, H64). Both Fe$_B$Mb(-His)-Cu and Fe$_B$Mb(-His)-Fe catalyzed the reduction of NO, while the former ArM had better activities (32% vs 6% conversion after 20 h).[293]

$$2NO + 2e^- + 2H^+ \longrightarrow N_2O + H_2O \qquad \textbf{(Equation 1)}$$

In 2006, Watanabe and coworkers studied the electron transfer between an artificial metalloenzyme and a natural enzyme. For this purpose, they incorporated a Fe-salophen **(122** or **123)** into heme oxygenase (HO). This enzyme converts heme to biliverdin using electrons provided by NADPH/cytochrome P450 reductase (CPR, Scheme 42).[294] The crystal structure of **123**·HO highlighted the presence of a hydrogen bond between the propionic acid carboxyl group and R177 of HO. Accordingly, the electron transfer rate from CPR$_{red}$ to **123**·HO is 3.5-fold faster than that of **122**·HO, although the redox potential of **123**·HO is lower than that of **122**·HO (Table 12).

Table 12. Catalytic NADPH and O_2 consumption by HOs reconstituted with Fe-salophen complexes.[a]

Entry	Cofactor	Protein	[Cof] (μM)	-d[NADPH]/dt (μM / min)	-d[O_2]/dt (μM / min)	-d[NADPH]/d[O_2]	Ref
1	**122**	No Protein	2	24	4.8	0.20	294
2	**123**	No Protein	2	31	12	0.39	294
3	**122**	HO	2	21	21	1.0	294
4	**123**	HO	2	5.5	5.1	0.93	294

[a] Reactions conditions: see **Scheme 42**.

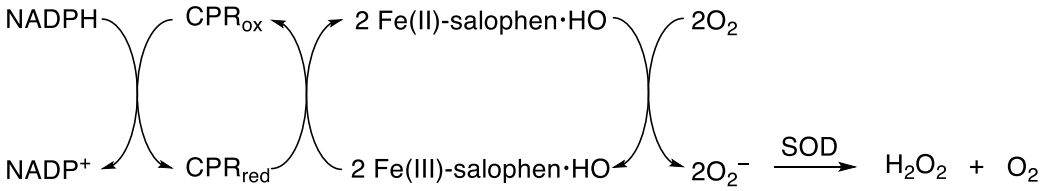

Fe-salophen·HO (2 μM), CPR (1 μM), Superoxide dismutase (SOD) (100 units)
NADPH (100 μM), Tris-HCl (10 mM), pH 7.4, 15 °C

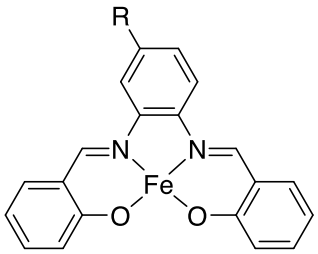

[Fe-salophen]

122: R = H

123: R = CH_2CH_2COOH

Scheme 42. Dioxygen reduction catalyzed by HO reconstituted with Fe-salophen coupled with cytochrome P450 reductase (CPR).

An artificial CO_2 reductase, based on two covalently-anchored metal complexes within $[(gp5\beta f)_3]_2$ (sections 5.8 and 7.4), was designed by Ueno *et al.* in 2011.[295] A maleimide-Re(bpy)$(CO)_3$Cl complex **124** and a succinimide-Ru$(bpy)_3$ complex **125** were conjugated to a cysteine and a lysine residue respectively (Scheme 43 and Figure 12). In the presence of 1-benzyl-1,4-nicotinamide as a sacrificial reductant, the electron transfer reaction from the photo-reduced Ru-moiety to the Re-moiety for the reduction of CO_2 to CO was investigated. The reaction efficiency depends on the distance between the Ru-moiety and Re-moiety: The turnover frequency of **124**-**125**·$[(gp5\beta f)_3]_2$ was 3.3 times higher than a mixture consisting of **124**·$[(gp5\beta f)_3]_2$ and Ru$(bpy)_3$-COOH **126** (Table 13).

Table 13. Selected results for the photocatalytic reduction of CO_2 by Ru and Re complexes covalently anchored to $[(gp5\beta f)_3]_2$.[a]

Entry	Cof1	Cof2	Protein	[Cof1] (μM)	[Cof2] (μM)	[1-benzyl-1,4-nicotinamide] (mM)	TOF (s^{-1})	Ref
1	**124**	**125**	$[(gp5\beta f)_3]_2$ (K41C)	70	20	100	2.8	[295]
2	**124**	**125**	$[(gp5\beta f)_3]_2$ (N57C)	72	20	100	1.2	[295]
3	**124**	**125**	$[(gp5\beta f)_3]_2$ (D69C)	80	20	100	1.5	[295]
4	**124**	**126**	$[(gp5\beta f)_3]_2$	70	20	100	0.8	[295]

(K41C)

[a] Reactions were carried out in a solution of 1 : 1 DMF/MOPS (40 mM, pH 7.0) at 25°C.

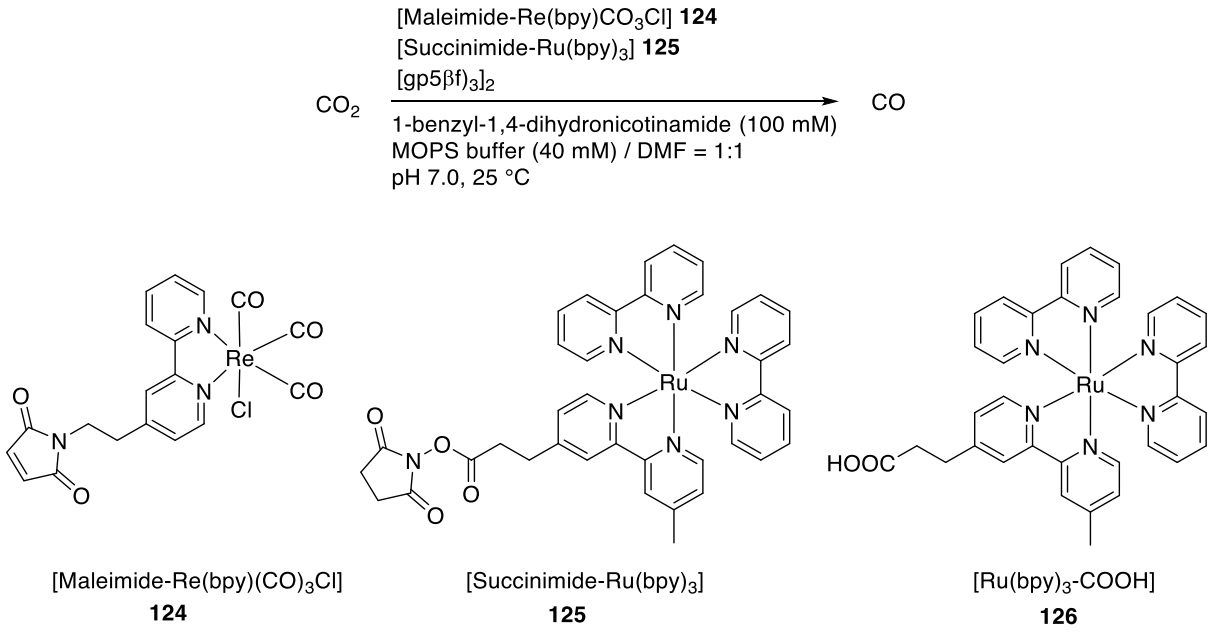

Scheme 43. Photocatalytic reduction of CO_2 catalyzed by Ru and Re complexes anchored to $[(gp5\beta f)_3]_2$ with 1-benzyl-1,4-dihydronicotinamide as the stoichiometric reductant.

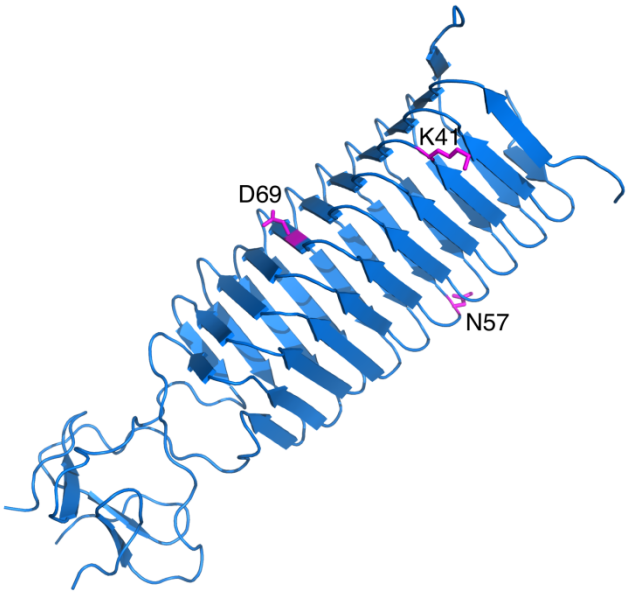

Figure 12. Bionanotube $[(gp5\beta f)_3]_2$ (PDB code 3A1M) was covalently functionalized at selected positions (magenta) with a Sc(bpy) complex to afford clickase[296], epoxide ring forming[297] and CO_2 reductase.[295]

One year later, Pecoraro *et al.* engineered an artificial nitrite reductase based on a previously designed α-helical coiled-coil motif (section 7.1).[298] The construct $(TRIL23H)_3$

is able to bind Cu(I) and Cu(II) with picomolar and nano/micromolar affinities respectively. Binding occurs via coordination to three histidine residues (mutation L23H). The nature of the active site, a structural analogue of copper nitrite reductase, was characterized by spectroscopy. The designed artificial metalloenzyme Cu(I/II)(TRIL23H)$_3^{+/2+}$ catalyzes the reduction of nitrite to nitric oxide with ascorbate as electron donor, Equation 2. Kinetic investigations revealed similar rates for the oxidation of ascorbate by Cu(II)(TRIL23H)$_3^{2+}$ and for the oxidation of Cu(I)(TRIL23H)$_3^{+}$ by nitrite ($k_{ascorbate}$ = 4.6 · 10^{-4} s^{-1} and k_{Cu} = 5.2 · 10^{-4} s^{-1} at pH 5.8). This suggests that the electron transfer from Cu(I)(TRIL23H)$_3^{+}$ to nitrite with simultaneous formation of Cu(II)(TRIL23H)$_3^{2+}$ is the rate-limiting step of the catalytic cycle. Under optimized conditions, the artificial nitrite reductase exceeded 5 turnovers and formed predominantly NO as product (i.e. almost no formation of N_2O).

$$NO_2^- + e^- + 2H^+ \longrightarrow NO + H_2O \qquad \textbf{(Equation 2)}$$

5. C–C Bond Formation

5.1 Allylic Alkylation

Allylic alkylation is a C–C bond forming reaction catalyzed by a range of transition metal complexes, though Pd-phosphine complexes are most commonly used for synthetic applications.[299] These catalysts activate heteroatom-substituted allyl compounds to attack by a soft nucleophiles via a metal-allyl intermediates. Though no natural enzyme has been reported to catalyze this reaction, terpene synthases rely on allyl cation intermediates that react in a similar fashion with an intramolecular carbon nucleophile to create a C-C bond.[300] Researchers have demonstrated that Ru-catalyzed allylic substitution proceeds even inside of cells, making this reaction particularly attractive for *in vivo* applications.[301-303] Encapsulating the transition metal within a protein scaffold could help to protect the metal in a biological environment, induce substrate specificity, and enable selective cell or even organelle targeting.

Toward this end, Ward and coworkers generated a panel of ArMs by incorporating biotinylated Pd-bisphosphine complexes into different Sav variants and investigated their activity toward asymmetric allylic alkylation of 1,3-diphenylallylacetate using malonate as a nucleophile.[304] In total, fourteen Pd complexes were screened against 20 Sav isoforms bearing mutations at S112X and two additional positions (Scheme 44 and Table 14). Didodecyldimethlyammonium bromide (DMB) was added to suppress 1,3-diphenylallylacetate hydrolysis (Scheme 44). With this modification, ArMs containing ligands **37** (which yielded *rac*-product), **41** (mostly (*R*)-selective), and **42** (mostly (*S*)-selective) were identified. The sterically constrained spacers in these ligands were believed to project bound Pd centers into a protein environment more suitable for alkylation rather than hydrolysis in bulk solvent. Replacement of DMB by DMSO was

possible in case of ligand **41** and led to increased enantioselectivity and conversion (i.e. 95 % ee, TON 45, Table 14, entry 3). The (*S*)-selectivity was increased to 82 % ee upon combining mutants S112G and V47G mutations.

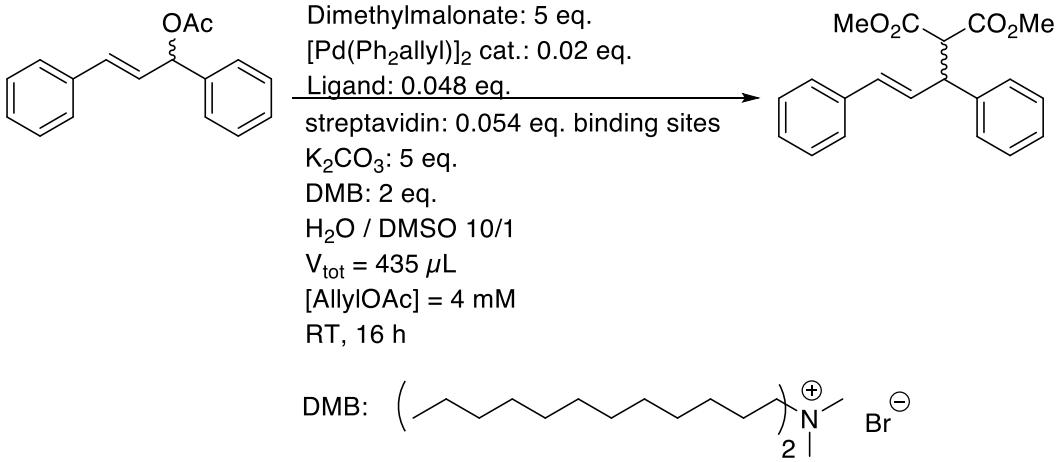

Scheme 44. A biotinylated bisphosphine palladium complex anchored within streptavidin affords an artificial allylic alkylase. Adapted with permission from ref.[304] Copyright Wiley VCH 2008.

Table 14. Selected results of the catalytic performance of the allylic alkylase based on the biotin-streptavidin technology.

Entry	Ligand[a]	Protein	ee	Conv.
1	**41**	S112A	90 (*R*)	95
2	**41**	S112A[b]	93 (*R*)	20
3	**41**	S112A[c]	95 (*R*)	90
4	**41**	S112Q	31 (*S*)	96
5	**42**	S112Y	80 (*R*)	87
6	**42**	S112G	54 (*S*)	96
7	**42**	S112G-V47G	82 (*S*)	92

[a] See Scheme 11 for the structure of the ligands. [b]No DMB added. [c]No DMB added, reaction carried out in 45% DMSO.

5.2 Suzuki Cross-Coupling

Carbon-carbon cross-coupling reactions offer a highly versatile means to assemble functional molecules. The palladium-catalyzed Suzuki-Miyaura cross-coupling reaction of aromatic halides and aryl boronic acids to afford biaryls is particularly notable in this regard.[305] The importance of biaryls to the agrochemical, pharmaceutical, and polymer industries, coupled with the bioorthogonality of the Suzuki-Miyaura cross-coupling in general have led to extensive development of catalysts for this reaction. Researchers

have also started to apply this and closely-related reactions for chemical biology applications,[306-309] although these efforts are limited by the high catalyst loadings required, presumably due to catalyst inactivation under biologically relvant conditions[306]. Anchoring Pd-catalysts within a protein scaffold could potentially i) protect the Pd-catalyst from inactivation in a biological reaction medium and ii) control the stereochemistry of the cross-coupling reaction.

To date, three studies have been reported on ArM Suzukiases. The first of these, reported by Ueno, Watanabe, and coworkers, was generated by loading $[Pd(allyl)Cl]_2$ **127** into apo-ferritin (Scheme 45).[310] Ferritin is an iron storage protein consisting of 24 self-assembled four helix-bundle subunits. The crystal structure of **127**·apo-ferrtin reveals two dinuclear Pd complexes located at the so-called accumulation center and threefold channel, respectively (Figure 13). Localization of the Pd centers is ensured via coordination to cysteine, histidine, and glutamic acid residues. The resulting ArMs catalyzed the Suzuki–Miyaura cross-coupling between 4-iodoaniline **128** and phenylboronic acid **129** with up to TOF = 3500/hour (Scheme 45 and Table 15, entry 1).

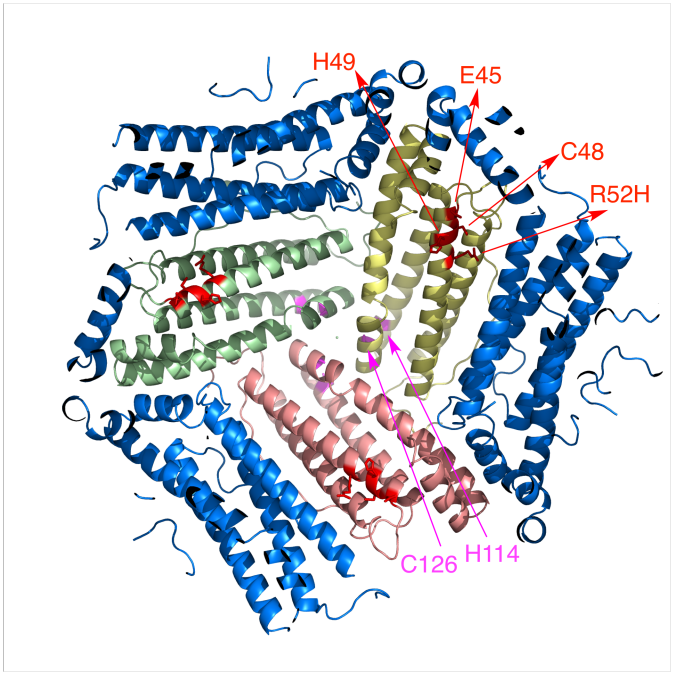

Figure 13. Ferritin (PDB code 1DAT) was engineered to carry out Suzuki-Miyaura cross-coupling[310] and phenylacetylene polymerization reactions.[311] Crystal structure analysis of Pd- and Rh-bound ferritin indicated metal binding to amino acid side chains in the "threefold channel" (magenta) and the "accumulation center" (red). Only a fraction of ferritin is displayed for clarity.

Several mutations were introduced around the Pd binding site in **127** ·apo-ferrtin to decipher the role of the coordination geometry on the catalytic activity (Figure 13).[312] Among the mutants, the ferritin E45C-R52H variant gave the highest TOF = 4300/hour (Table 15, entry 7).

Table 15. Suzuki-Miyaura coupling reaction catalyzed by a Pd(allyl) · ferritin ArM.

Entry	Cofactor	Protein	NaOH (mM)	T (°C)	[Pd] /Fr determined by ICP	TOF per Pd(allyl) · Fr (h^{-1})	Ref
1	**127**	Fr (WT)	4.5	50	103	3500	310
2	**127**	Fr (H49A)	4.5	50	99	3400	310
3	**127**	Fr (C48A-H49A)	4.5	50	54	1900	310
4	**127**	Fr (H114A)	4.5	50	78	900	310
5	**127**	Fr (C126A)	4.5	50	37	830	310
6	**127**	Fr (E45C-C48A)	4.5	50	98	4200	312
7	**127**	Fr (E45C-R52H)	4.5	50	154	4300	312
8	**127**	Fr (E45C-H49A/R52H)	4.5	50	154	4200	312

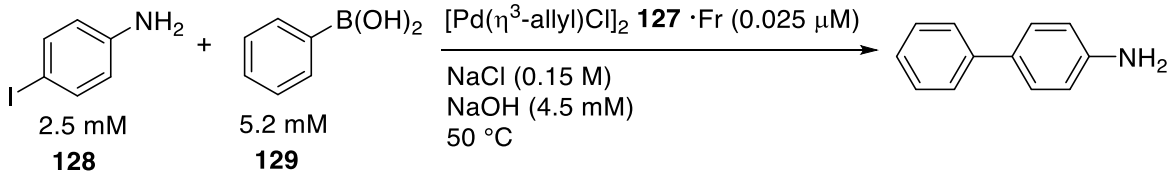

Scheme 45. Suzuki-Miyaura coupling reaction catalyzed by a $[Pd(allyl)Cl]_2$-loaded ferritin.

Based on the promising results obtained with the asymmetric allylic alkylases outlined above, Ward and coworkers screened a number of biotinylated NHC- and monophosphine ligands in the presence of $[Pd(\eta^3\text{-cinnamyl})Cl]_2$ for Suzuki cross-coupling to afford enantioenriched binaphtyls (Scheme 46).[313] Anchored within WT Sav, the monophosphine complexes $[Pd(\eta^3\text{-cinnamyl})Cl(\text{Biot-Et-P}(t\text{-Bu})_2)]$ **131** and $[Pd(\eta^3\text{-cinnamyl})Cl(\text{Biot-Pr-P}(t\text{-Bu})_2)]$ **132** yielded binaphtyl **135** with 78 and 73 TON,

respectively. The NHC-complex [Pd(η^3-cinnamyl)Cl(Biot-L)] **130** was less active (45 TON) and afforded *rac*-**135**. For the *tert*-butyl phosphine complexes, the ethyl and propyl spacers yielded opposite product enantiomers in 58 % ee ((*R*)-**135**) and 10 % ee ((*S*)-**135**), respectively. Screening a panel of ArMs generated by combining different Sav variants with [Pd(η^3-cinnamyl)Cl(Biot-Et-P(*t*-Bu)$_2$)] **131** led to the identification of Sav S112Y-K121E, which produced (*R*)-**135** with 90 % ee and 50 TON at 4 °C. Mutant K121A yielded the (*S*)-**135** with 47 % ee and 32 TON.

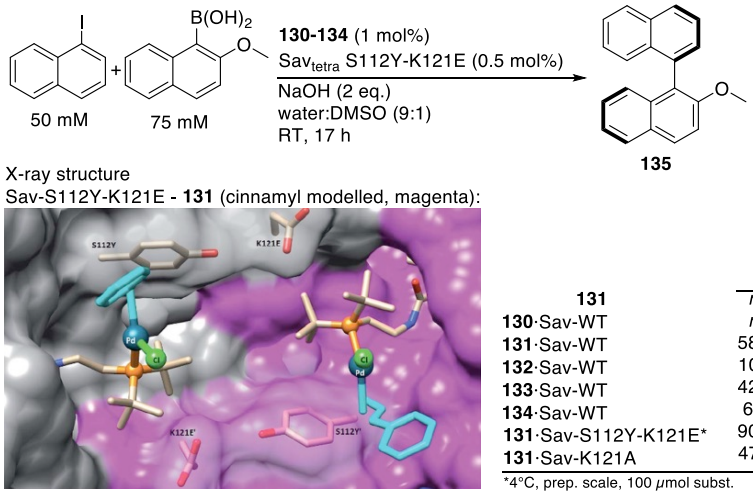

	ee	TON
131	*rac.*	20
130·Sav-WT	*rac.*	45
131·Sav-WT	58 (*R*)	78
132·Sav-WT	10 (*S*)	73
133·Sav-WT	42 (*R*)	45
134·Sav-WT	6 (*R*)	8
131·Sav-S112Y-K121E*	90 (*R*)	50
131·Sav-K121A	47 (*S*)	32

*4°C, prep. scale, 100 μmol subst.

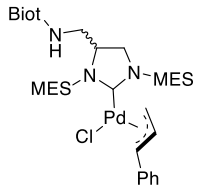

[Pd(η^3-cinnamyl)Cl(**Biot-L**)] **130**

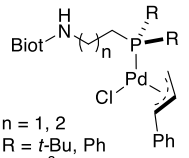

n = 1, 2
R = *t*-Bu, Ph

[Pd(η^3-cinnamyl)Cl(**Biot-Et-P(*t*-Bu)$_2$**)] **131**
[Pd(η^3-cinnamyl)Cl(**Biot-Pr-P(*t*-Bu)$_2$**)] **132**
[Pd(η^3-cinnamyl)Cl(**Biot-Et-PPh$_2$**)] **133**
[Pd(η^3-cinnamyl)Cl(**Biot-Pr-PPh$_2$**)] **134**

Scheme 46. An artificial Suzukiase for the synthesis of enantioenriched binaphtyls based on the biotin-streptavidin technology. Insert: X-ray crystal structure of [Pd(η^3-cinnamyl)Cl(Biot-Et-P(*t*-Bu)$_2$)] **131**·Sav S112Y K121E.

5.3 Heck Reaction

The Heck reaction is an extremely powerful means of forging C-C bonds between widely available aryl hailides and olefins. Moreover, substituted olefins can give rise to regio- and enatiomeric products, which necessitates the development of catalysts that can impart selectivity to these transformations. Filice and Palomo therefore took on the challenge of developing an ArM Heckase.[314] Covalent modification of a variety of lipases, including CAL-B, was achieved using phosphonate-substituted Pd-pincer complex **136** (Figure 14 a) in analogy to the previous work of Gebbink and van Koten (Scheme 12).[180, 182]

Optimization of reaction conditions and immmobilization methods led to the finding that **136**·CAL-B immobilized on aldehyde-activated Sephabeads (**136**·CAL-B-CHO-SP) catalyzed a model Heck reaction with high efficiency (Figure 14 b). This system was compatible wth remarkably high temperatures (70-120 °C) and organic solvent concentrations (75-100% DMF). Further optimization of the SP surface using different alkyl amine capping agents (methyl, octyl, etc.) led to the development of **136**·SP-CAL-B-C_8, which had higher activity toward the model Heck reaction than **136**·CAL-B-CHO-SP. Even more remarkably, this catalyst provided high enantioselectivity (96.6 % ee) in the Heck coupling of 2,3-dihydrofuran **137** with phenyl iodide at 120 °C in 75% DMF, though no conversion was observed at 70 °C or with phenyl bromide (Figure 14 c). Beyond highlighting the potential for ArMs to catalyze selective Heck reactions, this study provides compelling support for further exploration of immobilized ArMs.

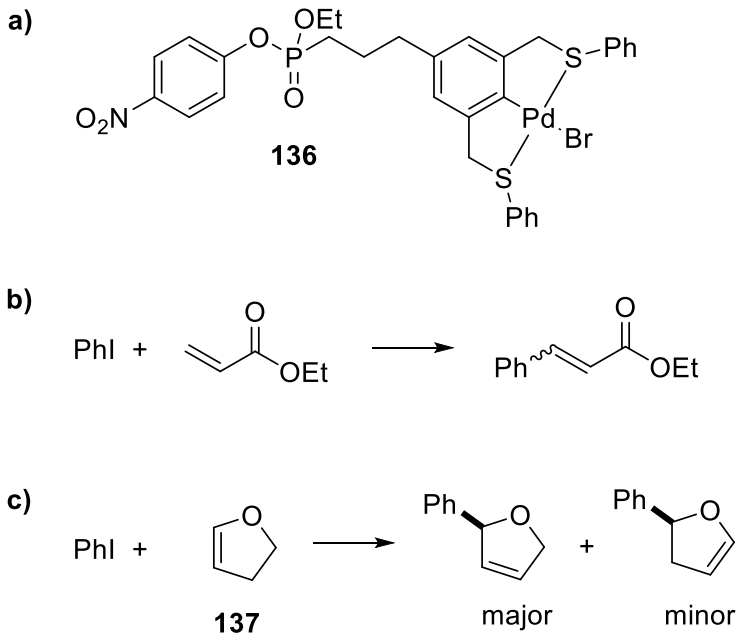

Figure 14. Structure of phosphonate-substituted Pd-pincer complex used to generate ArM Heckase a). Model Heck reaction used to optimize immobilized ArM Heckases b). ArM-catalyzed asymmetric Heck reaction between 2,3-dihydrofuran and iodobenzene c).[314]

5.4 C–H Activation

Carbon-carbon bond formation via carbon-hydrogen (C-H) bond functionalization remains a highly attractive yet equally challenging transformation in organic synthesis.[315] By eliminating the need for prefunctionalized starting materials, these reactions can enable new disconnection strategies, reduce synthetic manipulations, and decrease waste. All of these benefits, however, require a catalyst to activate a single C-H bond in the presence of many other, often similarly reactive, C-H bonds, and functionalize the resulting metallated position with the desired regio- and enatioselectivity. The impressive levels of selectivity exhibited by a number of natural enzymes that catalyze C-H bond functionalization clearly demonstrates the potential for protein scaffolds to control these transformations.[316] A number of researchers have therefore explored the possibility of using ArMs to control the selectivity of synthetic C-H functionalization catalysts.

Rovis and Ward, for example, hypothesized that incorporating a biotinylated Rh-complex [(**98**)$RhCl_2(H_2O)$] into Sav could provide a chiral environment for enantioselective hydroarylation reactions[317-318] catalyzed by $[\eta^5\text{-}(Cp^*)RhCl_2]_2$.[319] One such reaction, involving hydroarylation of methyl acrylate with pivaloyl-protected benzhydroxymic acid **138** and subsequent cyclization (i.e. benzanulation), provides regioisomeric isoquinolones **139** and **140** (Scheme 47 a)). While this reaction proceeded poorly using the free cofactor in water, addition of acetate buffer increased TON from 5 to 80 and provided **139** and **140** in a 4:1 ratio. This was hypothesized to result from acetate participation in a rate limiting concerted metallation-deprotonation step (CMD) of the overall C-H functionalization process (Scheme 47 b)). Incorporating [(**98**)$RhCl_2(H_2O)$] into WT Sav decreased TON to 40, but the regioisomeric ratio (rr) and ee values increased to 9:1 and 50% (favoring *R*-**139**), respectively. Sav variants bearing a carboxylate residue in the proximity of the Rh

cofactor (i.e. S112D/E or K121D/E) were then examined to determine if these could replace acetate and allow to carry out the desired reaction at neutral pH. Indeed, Sav K121D provided an ArM that catalyzed benzanulation of **138** with improved TON and rr (up to 89 and 15:1, respectively), but the ee remained virtually identical to WT Sav. Promising single point mutations were then combined to generate Sav variants N118K-K121E and S112Y-K121E, which, upon metallation, provided (*R*)-**139** with 50 TON, 64% ee, 15:1 rr and 47 TON, 82% ee, and 19:1 rr, respectively.

The role of glutamate K121E as general base in the rate limiting *ortho*-C_{aryl}-H deprotonation step was investigated. A kinetic isotope effect (KIE) of 4.8 was observed for substrate **138** with [(**98**)$RhCl_2(H_2O)$]·Sav S112Y-K121E. The KIE of the corresponding WT Sav ArM was only 2.8. To highlight the rate accelerating effect of the Sav, the protein: cofactor ratio was varied and the enantioselectivity was determined using substrate **138**. Strikingly, the artificial benzannulase [(**98**)$RhCl_2(H_2O)$]·Sav S112Y-K121E retained a high ee even in the presence of a large excess of cofactor; a rate acceleration of ~100-fold was determined.

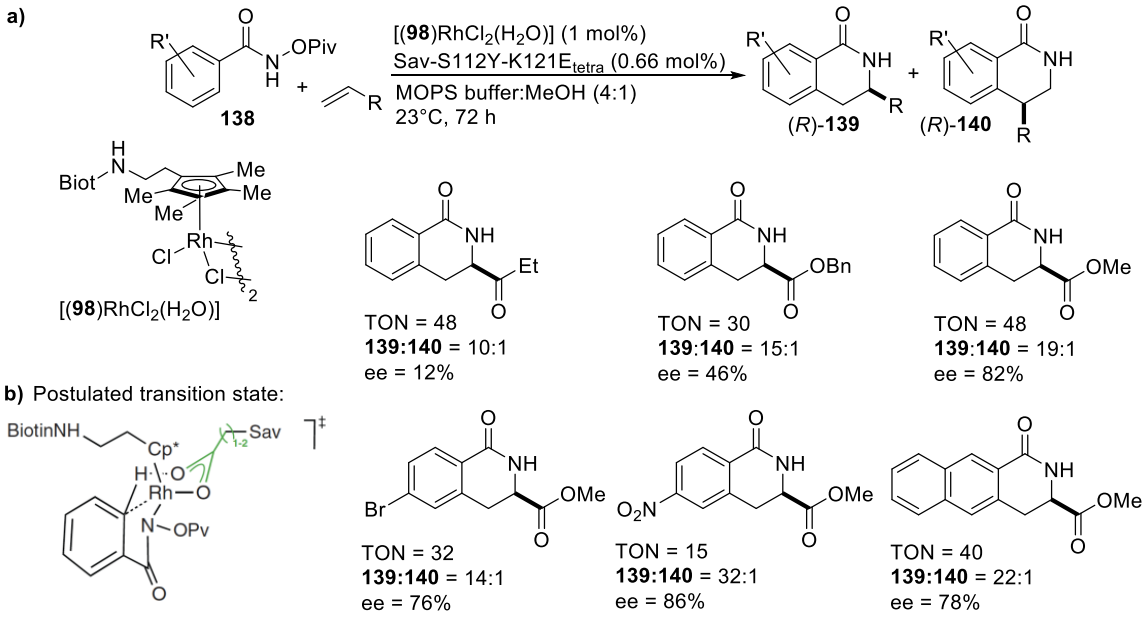

Scheme 47. An artificial benzannulase for the synthesis of enantioenriched dihydroisoquinolones based on the biotin-streptavidin technology. Reaction conditions

and substrate scope and postulated transition state of the CMD step are displayed in a) and b), respectively. Adapted with permission from ref.[38] Copyright ACS Publications 2016.

Metal porphyrin complexes catalyze a range of C-H insertion reactions via generation of highly reactive metal-oxo, -peroxy, -carbene, and -nitrene intermediates upon reaction with suitable precursors for these species.[320] While oxo insertion reactions catalyzed by heme-dependent oxygenases and peroxygenases have been extensively studied,[321] reactions of these enzymes with carbene and nitrene precursors has only recently been explored in detail.[322] As discussed in the review by Fasan and coworkers elsewhere in this issue, this has been exploited to enable carbene insertion into olefins (cyclopropanation)[12] and nitrene insertion into C-H bonds using cytochromes P450, myoglobin, and other heme enzymes.[323-324] To obtain systems with further expanded function, a number of researchers have incorporated unnatural porphyrins and other heme-like cofactors into heme proteins and enzymes to generate ArMs.[55] These efforts take advantage of well-formed active sites that evolved to accommodate a planar (heme) cofactors and small molecule substrates. While this approach has also been extensively explored for oxo insertion reactions (section 6.1), significantly less has been done for carbene and nitrene insertion reactions.

Despite the ability of heme enzymes to catalyze carbene insertions into olefins, analogous insertions into C-H bonds using these enzymes have not been reported. Hartwig and Clark therefore investigated the activity of ArMs generated by metallating eight different apo-myoglobin variants containing a different mutation at the axial ligand position (H93X) with protoporphyrin IX (PPIX) cofactors containing different noble metals. Of these, an ArM generated from (PPIX)Ir(Me) catalyzed both cyclopropanation (*vide infra*) and intramolecular carbene insertion using diazo carbene precursors.[325] In the later case, reaction of diazoester **141** to form the corresponding chiral dihydrobenzofuran, which has

not been reported for natural heme enzymes, was examined. Stepwise targeted mutagenesis of the myoglobin active site led to ArMs with good enantioselectivity reactions of multiple substrates (86% ee for C-H insertion, Figure_15). Variants were identified that catalyzed intramolecular carbene insertion in one particular substrate to provide either product enantiomer with up to 84% and 50% ee (Scheme 48 a)).

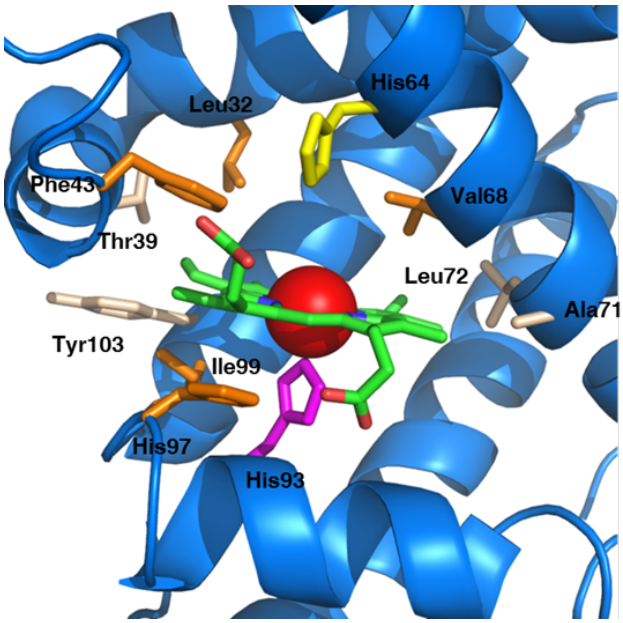

Figure_15. Cartoon representation of Myoglobin's active site with its natural cofactor (PDB: 1MBI). Highlighted in magenta and yellow are the axial (H93) and distal (H64) histidines, respectively. Highlighted in orange are additional amino acids modified to evolve the ArMs as C-H activase, cyclopropanase[325] and dihydrogenase.[207] Highlighted in beige are amino acids mutated to modify the affinity or the orientation of the artificial cofactors for the evolution of sulfoxidase[326 327-328] and peroxidase.[329-331] Heme displayed in green (C), red (O) and blue (N).

The same group also reported that a thermostable cytochrome P450 from *Sulfolobus solfataricus* (CYP119) could be reconstituted with (PPIX)Ir(Me) to generate a thermostable ArM (T_m = 69 °C).[332] Intramolecular carbene insertion using diazoester **141** was again selected as a model reaction (Scheme 48 b)). A catalytic efficiency (k_{cat}/K_M) of 0.071 $min^{-1}·mM^{-1}$ was observed for the single mutant C317G, which was improved by introducing hydrophobic and uncharged residues into the ArM active site (Figure 16). The quadruple mutant (L69V-T213G-V254L-C317G) showed a more than 4000-fold higher

catalytic efficiency (k_{cat}/K_M = 269 $min^{-1} \cdot mM^{-1}$) than the initial wild type construct, accompanied by an initial turnover frequency of 43 min^{-1} and a high enantioselectivity (94% ee).

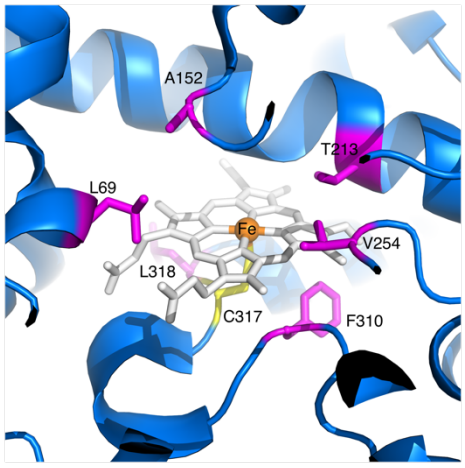

Figure 16. Cytochrome P450 Cyp119 (PDB code 1IO8) catalyzes carbene insertion into C-H bonds.[332] Residues in proximity to the heme cofactor that were subjected to mutagenesis are highlighted in magenta and yellow.

ArMs optimized for this model reaction also catalyzed the intramolecular carbene insertion into a variety of activated primary, secondary and sterically hindered C-H bonds with high turnover numbers and enantioselectivities, Scheme 48 b). Intramolecular carbene insertion into an unactivated primary C-H bond, (Scheme 48 c) and intermolecular reaction between phthalan **143** and ethyl diazoacetate **142** to provide **144** was also observed (Scheme 48 d). The latter is particularly challenging since diazo coupling **145** or formal insertion of the carbene into the O-H bond of water to form alcohol **146** can occur. Diazoester **141** was transformed into the corresponding dihydrobenzofuran on a preparative scale (1.0 g substrate, 55% isolated yield, 93% ee), whereby the ArM exceeded 3200 turnovers. On a smaller scale (10 mg substrate) a TON > 35,000 was achieved. Supported on sepharose beads, the ArMs could be recycled at least 4 times without erosion of enantioselectivity and retaining 64% of its initial activity.

a)

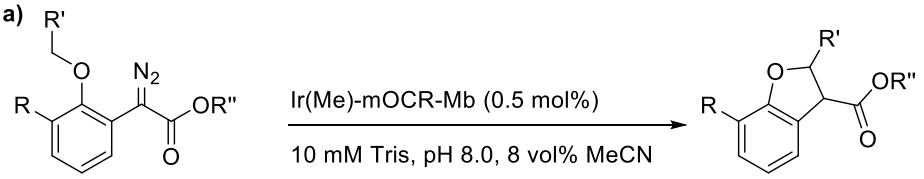

141: R=H, R'=H, R''=Me

Substrate	Mutant	ee%	TON
R=H, R'=Me, R''=Me	H93G-H64L-F43L-I99F	84	92
R=OMe, R'=H, R''=Me	H93G-H64L-V68A-L32F-H97Y	-77	144
R=OMe, R'=H, R''=Me	H93A-H64A-F43W-V68G	68	7260*

b)

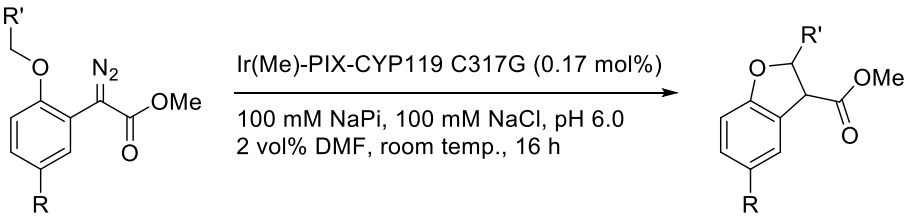

141: R=H, R'=H

Substrate	Mutant	ee%	de%	TON	
R=H, R'=H	L69V-T213G-V254L	94		582	activated, primary C-H
R=H, R'=H	L69W-T213G-F310G	-93		120	
R=OMe, R'=H	L69Y-T213G-A152W	-98		582	
R=OMe, R'=H	T213A-V254L	87		204	
R=Cl, R'=H	L69Y-T213G-A152W	94		276	
R=H, R'=Me	L69W-T213G-L318G	73	>92	414	activated, secondary C-H
R=H, R'=Me	L69F-T213G-V254L	-77	>92	402	
R=H, R'=Ph	T213G-V254L	-61	-92	107	sterically hindered C-H
R=H, R'=Ph	L69W-T213G	90	-85	582	

c)

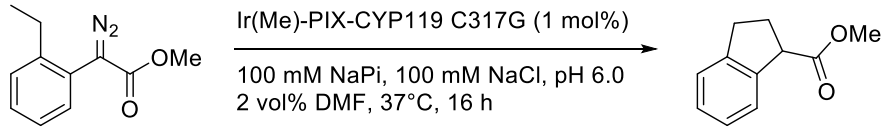

Mutant	ee%	TON
L69V-T213G-V254L	90	31

d)

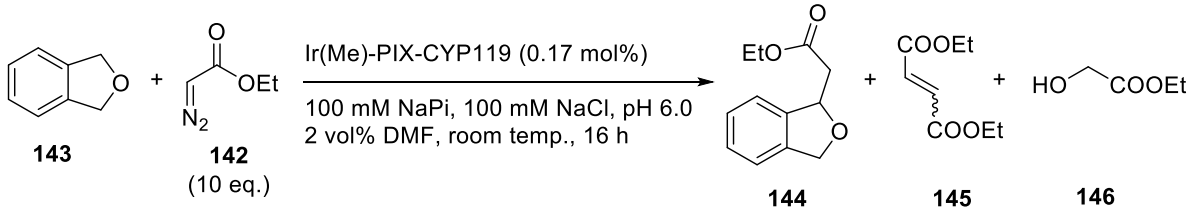

143 **142** (10 eq.) **144** **145** **146**

Mutant	ee%	yield%	ratio 144:145
L69V-T213A-V254L-A152W	68	55	120:1

Scheme 48. C-H insertion reactions catalyzed by heme-substituted ArMs. Intramolecular insertion into activated C-H bonds catalyzed by a) myoglobin variants and b) P450-CYP119 variants; c) intramolecular insertion into unactivated C-H bonds by a P450-CYP119 variant; d) intermolecular insertion into activated C-H bonds by a P450-CYP119 variant. TON: turnover number, e.r.: enantiomeric ratio, d.r.: diastereomeric ratio (trans : cis), * with 0.0025 mol% catalyst.

5.5 Olefin Metathesis

Transition metal catalyzed olefin metathesis has become a highly versatile tool for C–C bond formation.[333] The development of *Z*- and *E*-selective cross metathesis catalysts has enabled construction of a wide range of molecule containing a double bond. Moreover, the bioorthogonality of many olefin metathesis reactions has led to their use in chemical biology,[334-336] particularly for selective functionalization of biopolymers.[337-338] More recently, olefin metathesis has been considered as a means to expand the chemical toolkit of biochemistry given that it is thus far unknown to living organisms. A number of ArM metathases have been developed toward this end.

The first ArM metathases were introduced in 2011 by Ward *et al.* and Hilvert *et al.*[339-340] The former employed (strept)avidin as a host for biotinylated cofactors based on a Grubbs-Hoveyda 2nd generation catalyst (GH-type catalyst). In fact, all the artificial metathase published to date use this type of cofactor. This is most probably due to its high stability toward air and water. Two such cofactors **148** and **149** with different linkers were synthesized and anchored within either avidin or streptavidin via a supramolecular interactions. Diallyl tosylamide **147** served as a model substrate for ring closing metathesis (Scheme 49).

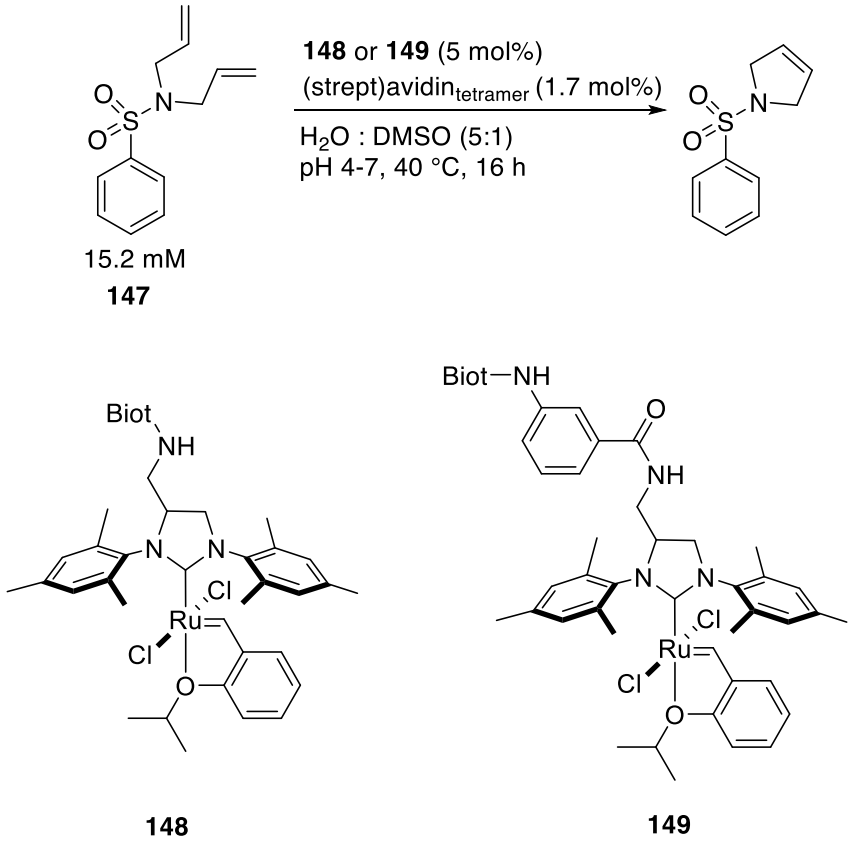

Scheme 49. Artificial metathase based on the biotin-(strept)avidin technology.

Different reaction conditions were explored, and the best yields were obtained at low pH with high concentrations of $MgCl_2$ (Table 16). Similarly, Matsuo *et al.* investigated the effect of added chloride ions in aqueous metathesis and found that catalyst stability is significantly enhanced by the addition of KCl.[341] They proposed that the replacement of the chloride ligands by hydroxy ions may lead to decomposition of the catalyst. This could explain why the addition of chloride salts and lowering of the pH has a beneficial effect. In a subsequent article, Ward and coworkers tested a large number of biotinylated catalysts where the biotin anchor was placed not at the backbone but on one of the mesityl units of the NHC ligand.[342]

Table 16. Summary of the results obtained for the artificial metathase system based on the biotin-(strept)avidin technology for substrate **147**.

Entry	Catalyst	Protein	pH[a]	$MgCl_2$ [M]	Yield (%)	TON

1	**148**	-	7	-	74	15
2	**148**	Sav	7	-	<1	0
3	**149**	Sav	7	-	8	2
4	**149**	Sav	7	0.5	33	7
5	**149**	Sav	4	-	41	8
6	**149**	Sav	4	0.5	71	14
7	**148**	Avi	7	-	17	3
8	**149**	Avi	7	-	6	1
9	**149**	Avi	7	0.5	54	11
10	**148**	Avi	4	-	79	16
11	**148**	Avi	4	0.5	95	19
12	**148**	-	4	0.5	95	19

[a] pH 7: no buffer; pH 4: acetate (0.1 M)

The construct of Hilvert *et al.*, on the other hand, was generated via covalent modification of a small heat-shock protein from *Methanocaldococcus jannaschii* (MjHSP).[340] This protein assembles into a spherical substructure with large pores, which allow for the diffusion of small molecules. Similar to streptavidin, the protein displays a remarkable stability towards high temperatures and low pH. GH-type catalyst **150** substituted with a α-bromoacetyl group was reacted with the thiol of a surface cysteine in the G41C mutant of MjHSP to yield the artificial metathase **151** (Scheme 50).

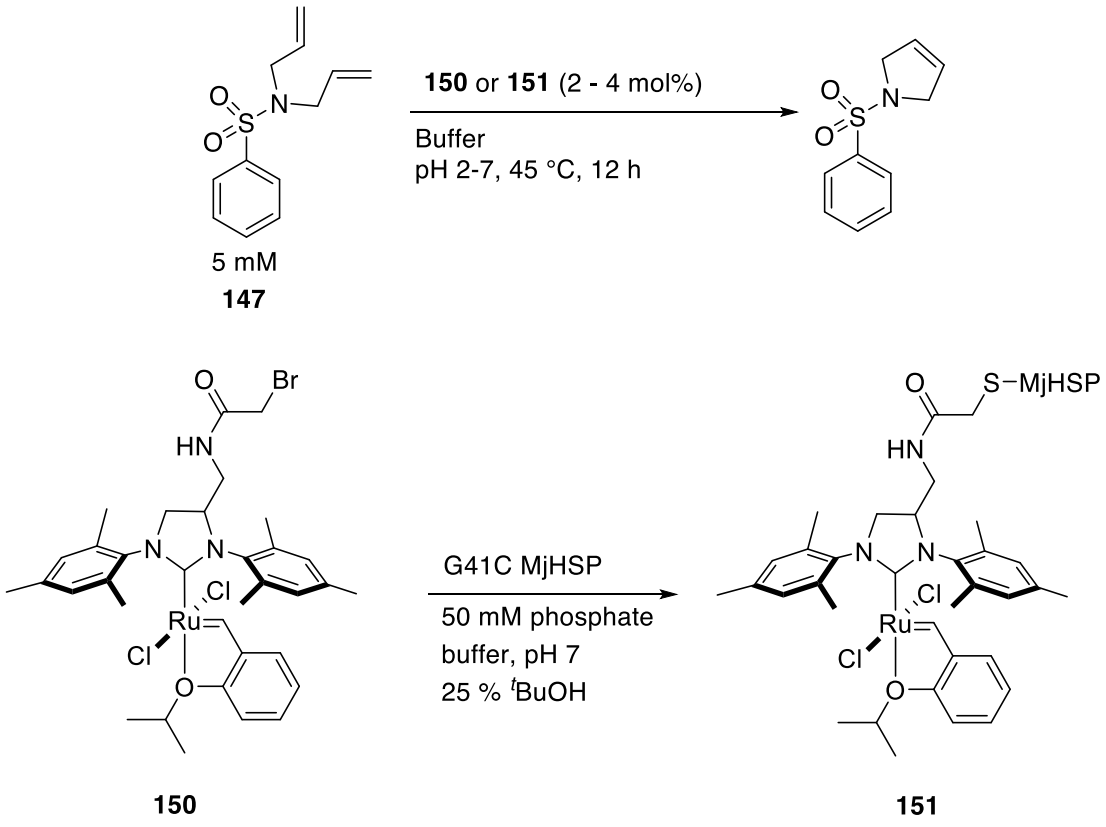

Scheme 50. Covalent anchoring strategy to produce a metathase by Hilvert *et al.*[340]

The same trend observed for the metathase of Ward *et al.* was also apparent for this system: the lower the pH, the better the performance of the metathase. A total turnover number of 25 could be achieved for ArM **151** at pH 2, but the free catalyst **150** gave slightly better results (Table 17, compare entries 1-3 with entries 4-6).

Table 17. Selected results for the metathase with substrate **147** based on the heat-shock protein MjHSP by Hilvert *et al.*[340]

Entry	Catalyst	pH[a]	Catalyst loading (mol %)	TON
1	**150**	7.0	2	2
2	**150**	3.9	2	16
3	**150**	2.0	2	33
4	**151**	7.0	4	3
5	**151**	3.9	4	12
6	**151**	2.0	4	25

[a] pH 7.0: 50 mM phosphate; pH 3.9: 50 mM MES; pH 2.0: 10 mM HCl.

An covalent anchoring strategy was also used by Matsuo et al. to generate an ArM metathase.[343] GH cofactor **152**, which contains an L-phenylalanine moiety bearing an α-chloroketone, was used to both covalently anchor the cofactor to α-chymotrypsin and selectively interact with the S1 site of α-chymotrypsin via hydrophobic contacts. Nucleophilic attack of the imidazole of H57 on the chloroketone resulted in a covalent link between the cofactor and α-chymotrypsin to provide **153**. Interestingly, the authors showed that the enantiomer of **152** with inverted stereochemistry did not react with the protein. This provided convincing evidence that the functionalization indeed occured inside the active site of α-chymotrypsin which is known to only recognizes L-phenylalanine. The authors tested three different substrates for metathesis and reported good turnover numbers when using the glycosylated diene **154**. In contrast, they observed only low TONs for the cationic substrate **155** and the lipophylic diallyl tosylate **147** (Table 18, entries 1-6 and Scheme 51).

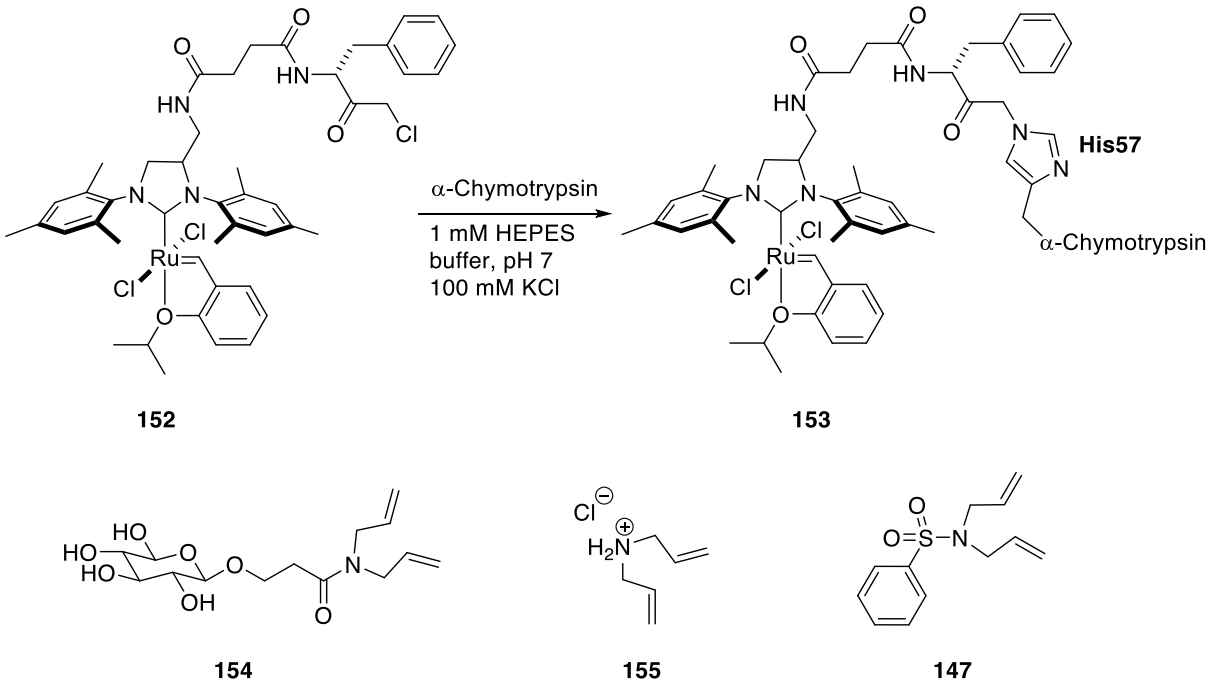

152 **153**

154 **155** **147**

Scheme 51. Conversion of α-Chymotrypsin into a metathase via covalent anchoring.

Table 18. Selected results for RCM using the metathase based on α-chymotrypsin.

Entry	Catalyst	Sub.	TON (after 2 h)
1[a]	**153**	**154**	20
2[a,b]	**152**	**154**	14
3[c]	**153**	**155**	N.D.
4[c,d]	**152**	**155**	<2
5[b,e]	**153**	**147**	4
6[b,e]	**152**	**147**	12

[KCl] = 100 mM; [a] [**154**] = 8 mM; [cat] = 50 μM; [b] contains 10 % DMSO (v/v); [c] [**155**] = 8 mM, [cat] = 0.2 mM; [d] contains 10 % MeOH (v/v); [e] [**147**] = 1 mM, [cat] = 25 μM.

Yet another anchoring strategy was used by Gebbink et al.[344] to link a GH-type catalyst substituted with a phosphonated alkyl chain to cutinase. The cofactor underwent irreversible transesterification with S120 in the cutinase active site to form an ArM. The authors first explored a catalyst with a short alkyl chain **156**, but this had no metathesis activity. When the chain length was increased (**157**), the resulting ArM catalyzed both ring closing metathesis of diallyl tosylamide **147** and cross-metathesis of allylbenzene **158**. To our knowledge this was the first example of cross-metathesis using an ArM (Table 19).

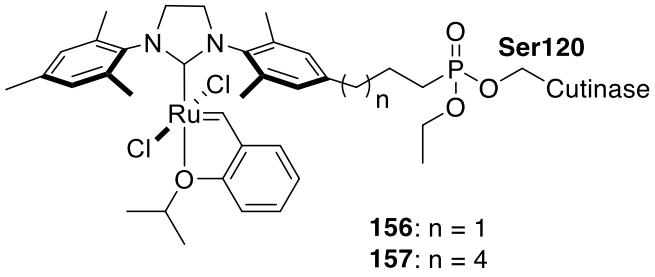

Figure RR1: Artificial metathase using cutinase as a host.

Table 19. Selected results for an artificial metathase with a cutinase host.

Entry	Catalyst	Sub.	Buffer	TON
1	**156**	**147**	tris-HCl pH 8.5	-
2	**156**	**147**	HCl 0.01M	-
3	**156**	**147**	acetate pH 5	<1
4	**Grubbs-Hoveyda II**	**147**	acetate pH 5 plus cutinase	18
5	**157**	**147**	tris-HCl pH 8.5	-
6	**157**	**147**	acetate pH 5	17
7	**156**	**158**	acetate pH 5	<1
8	**157**	**158**	Acetate pH 5	20

[a] conditions: Catalyst (5 mol%), $MgCl_2$(10 eq.), Buffer, CH_2Cl_2 5 %(v/v), 25 °C, 20h.

An artificial metathase based on on human carbonic anhydrase II (hCA II) was reported by Ward *et al.*[345] The hCA II protein has a strong affinity (typically nM - pM) toward arylsulfonamides due to sulfonamide coordination to an active site zinc ion. Three different sulfonamide-substituted catalysts were prepared (**159-161**), and their activity toward ring closing metathesis of substrate **147** was evaluated. Catalyst **160**, bearing *ortho*-isopropoxy groups at the NHC aryl groups, performed best. The ArM had similar activity to the free cofactor, but moderate turnover was observed even at pH 7.0, which may be relevant for *in vivo* applications (Table 20 and Scheme 52).

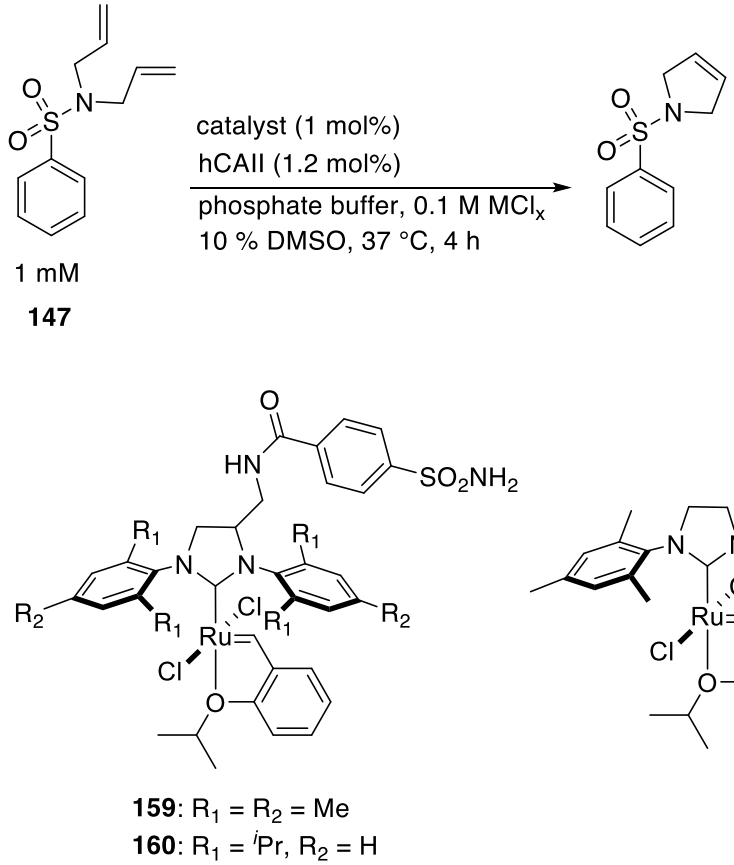

Scheme 52. Human carbonic anhydrase as host for an artificial metathase.

Table 20. Selected results for RCM with an artificial metathase based on hCA II.

Entry	Cat	hCAII	pH	MCl_x mol/l	TON	Entry	Cat	hCAII	pH	MCl_x mol/l	TON
1	**159**	-	6.0	$MgCl_2$ 0.1	20	15	**160**	WT	8.0	-	21
2	**160**	-	6.0	$MgCl_2$ 0.1	48	16	**160**	-	7.0	NaCl 1.5	32
3	**161**	-	6.0	$MgCl_2$ 0.1	25	17	**160**	WT	7.0	NaCl 1.5	21
4	**159**	WT	6.0	$MgCl_2$ 0.1	13	18	**160**	WT	7.0	NaCl 0.5	32
5	**160**	WT	6.0	$MgCl_2$ 0.1	45	19	**160**	WT	7.0	NaCl 1.0	29
6	**161**	WT	6.0	$MgCl_2$ 0.1	16	20	**160**	I91A	7.0	-	18
7	**160**	WT	6.0	NaCl 0.2	40	21	**160**	F131A	7.0	-	16
8	**160**	WT	7.0	NaCl 0.2	28	22	**160**	L198F	7.0	-	18
9	**160**	-	7.0	-	23	23	**160**	L198H	7.0	-	22
10	**160**	WT	7.0	-	14	24	**160**	L198H	7.0	NaCl 0.15	28
11[a]	**160**	WT	7.0	-	20	25	**160**	L198A	7.0	-	15
12	**160**	-	5.0	$MgCl_2$ 0.5	85	26	**160**	L198Q	7.0	-	14
13	**160**	WT	5.0	$MgCl_2$ 0.5	78	27	**160**	K170A	7.0	-	15
14	**160**	WT	6.0	-	23						

[a] [substrate] = 5 mM, [catalyst] = 50 μM, [hCAII] = 60 μM;

Okuda and Schwanenberg reported the first artificial metathase for ring opening metathesis polymerization (ROMP). In their original publication, the authors described a strategy to engineer the β-barrel protein FhuA via modification of an internal cysteine mutant (K545C) of the protein (Figure 17).[346] Two additional positions (N548V and E501F)

were also mutated to ensure cysteine accessibility and improve catalyst performance. Both maleimide- and α-bromoacetyl-functionalized GH-type catalysts reacted with the internal cysteine residue in the FhuA triple mutant to generate ArM metathases. Of the metathases evaluated, **166**·FhuA, generated from maleimide functionalized GH-catalyst **166**, provided the highest activity for polymerization of 7-oxanorbornene **162**, but higher activity was observed for the free catalyst. In a subsequent publication, the authors performed chemical optimization of the linker length.[347] Gratifyingly, shortening the linker increased the efficiency of the metathase, and modest selectivity towards *cis*-double bonds was observed in the polymer product (Table 21, entries 1-8 and Scheme 53).

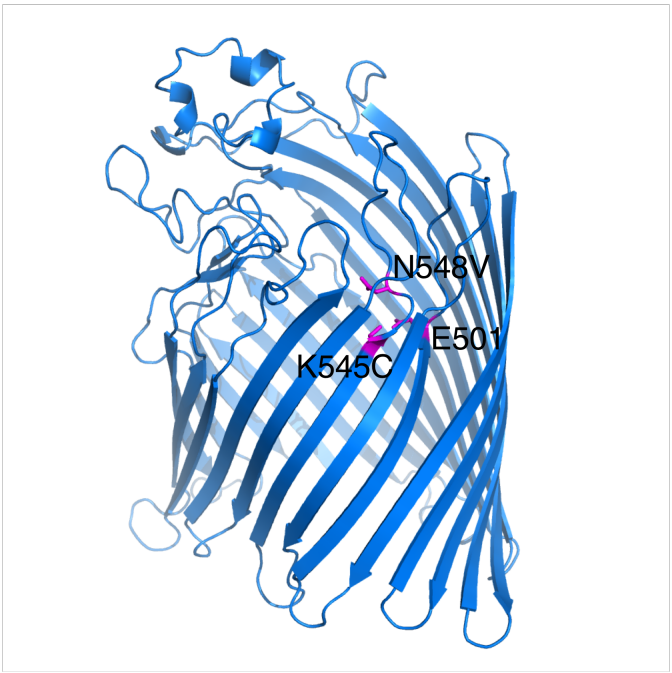

Figure 17. An artificial metathase[347] and a Diels-Alderase[348] were generated based on the FhuA scaffold (PDB code 1BY3). Metal catalysts were covalently tethered to the protein scaffold via mutation K545C.

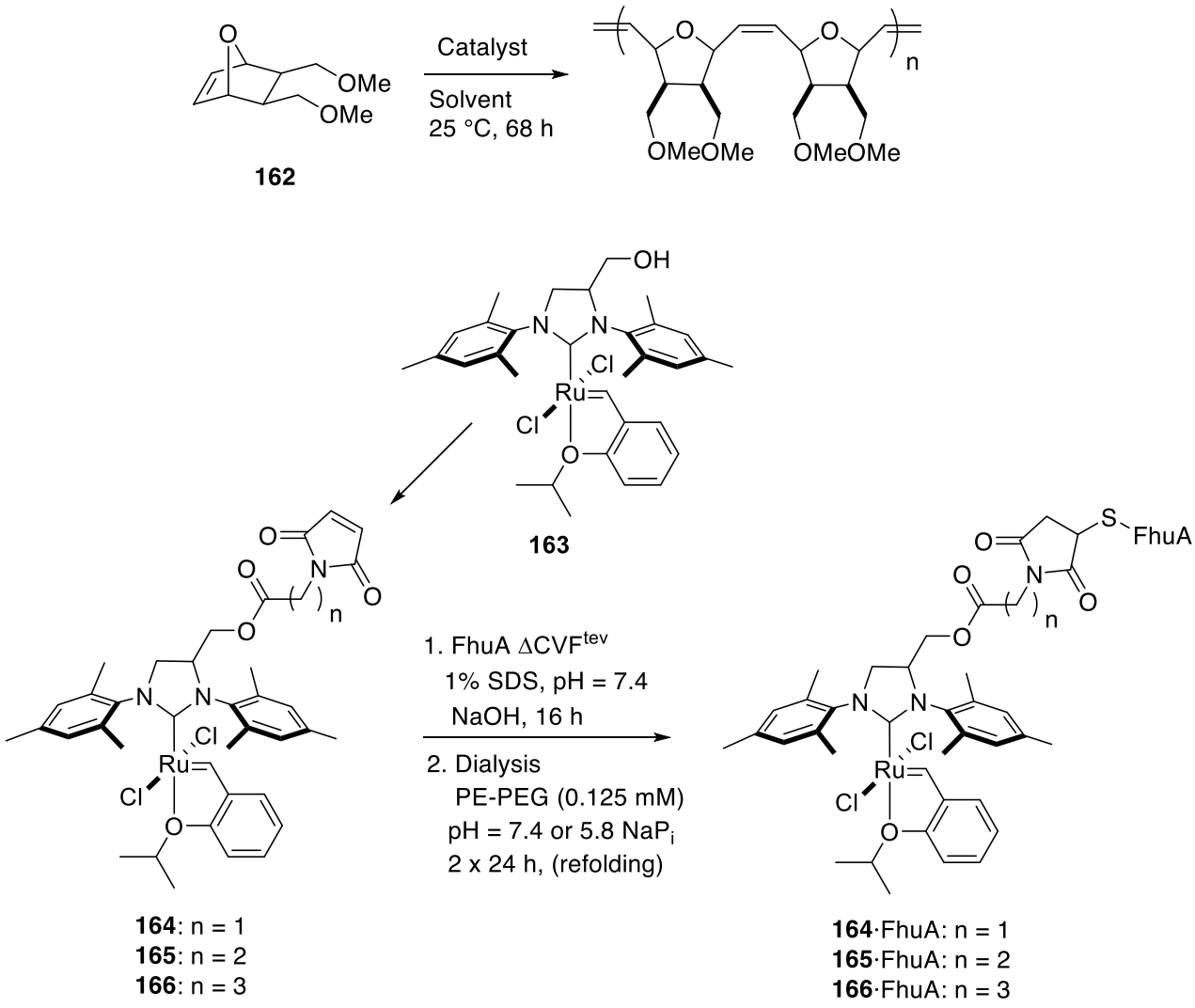

Scheme 53. Artificial metathase based on the FhuA barrel protein.

The same authors then examined a cysteine mutant of nitrobindin as a protein scaffold for their second generation metathases.[198] Low bioconjugation yields were observed presumably due to the small size of the barrel interior relative to the sterically demanding GH-type catalysts. A cofactor bearing a longer linker **166**, on the other hand, reacted to form the desired ArM **166**·Nb1. Enlarging the cavity of the nitrobindin 1 scaffold led to higher bioconjugation yields. This mutant (nitrobindin 2) enabled formation of multiple metathases **164**·Nb2, **165**·Nb2 and **166**·Nb2. The ArM generated using the cofactor bearing the longest linker **166**·Nb2 again proved to be most active. The metathase also catalyzed ring closing metathesis with 2,2-diallyl-1,3-propanediol **167**, but no protein acceleration was observed for this reaction (Table 21, entries 9-17 and Scheme 54).

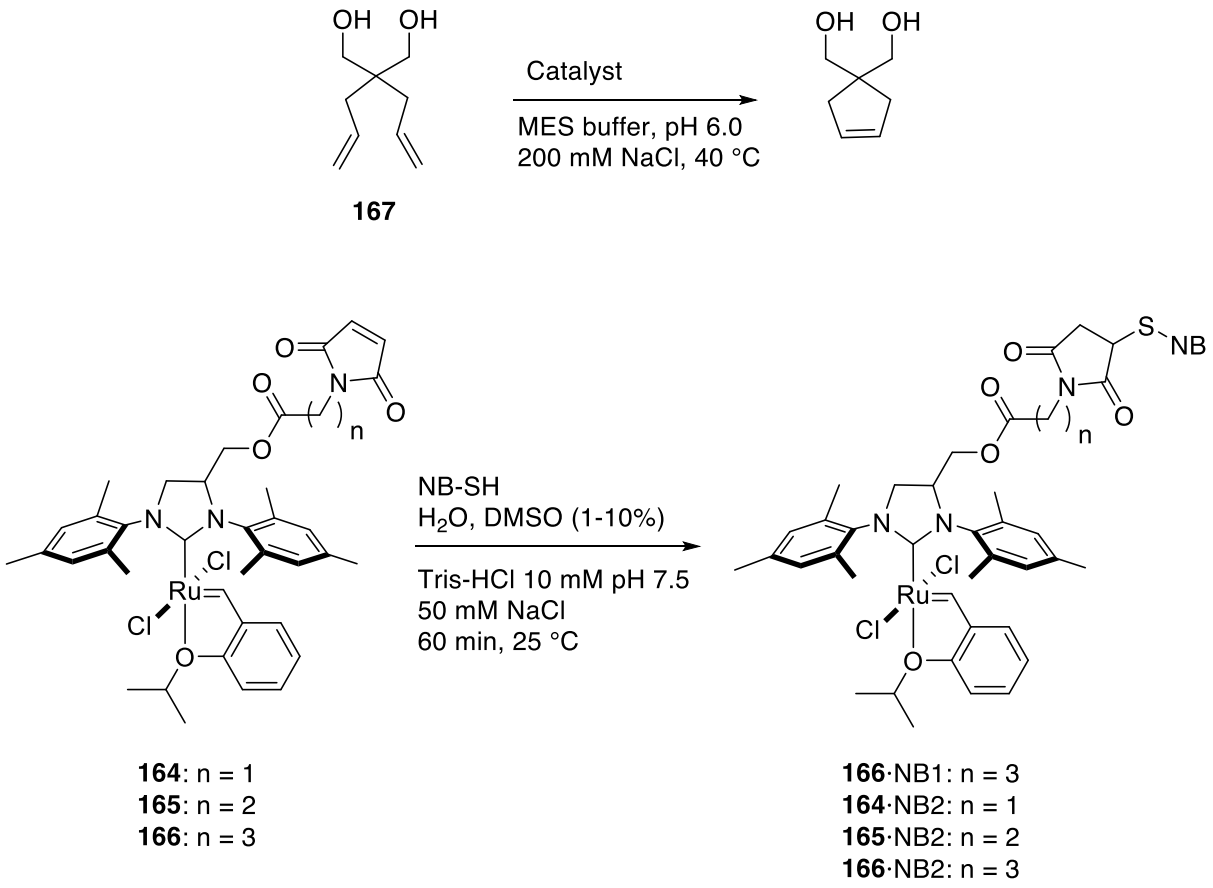

Scheme 54. Second generation metathase based on a nitrobindin scaffold.

Table 21. Selected results for the artificial metathase based on FhuA and Nitrobindin with substrates **162** and **167**.

Entry	Catalyst	Sub.	Conversion (%)	*cis*/*trans*	TON	Ref	Entry	Catalyst	Sub.	Conversion	TON	Ref
1[a]	**163**	**162**	70	48/52	530	346	14[c,e,f]	**163**	**167**	>99	100	198
2[a]	**163** + FhuA	**162**	0	n.d.	n.d	346	15[d,e,f]	**165**·Nb2	**167**	89	89	198
3[a]	**166**·FhuA	**162**	37	56/44	365	346	16[d,e,f]	**166**·Nb2	**167**	>99	100	198
4[b]	**163**	**162**	99	50/50	990	347	17[d,e,g]	**166**·Nb2	**167**	57	178	198
5[b]	**164**·FhuA	**162**	41	58/42	555	347						
6[b]	**165**·FhuA	**162**	24	56/44	325	347						
7[c]	**163**	**162**	41	70/30	4100	198						
8[d]	**163**	**162**	<5	n.d.	n.d	198						
9[d]	**166**·Nb1	**162**	10	40/60	1100	198						
10[d]	**164**·Nb2	**162**	<5	n.d.	n.d.	198						
11[d]	**165**·NB2	**162**	19	42/58	2100	198						
12[d]	**166**·NB2	**162**	78	43/57	9700	198						
13[d,e]	**166**·NB2	**162**	80	48/52	9900	198						

[a] phosphate buffer pH 7.4, 10% THF, 0.125 mM PE-PEG; [b] phosphate buffer pH 5.8, 10% THF, 0.125 mM PE-PEG; [c] in THF, 12 h, 0.01 mol% catalyst; [d] 0.008 mol% catalyst, MES buffer pH 6.0, 0.2 M NaCl, 25 °C, 12h; [e] performed at 40 °C; [f] [Sub] = 125 mM; [cat] = 1.25 mM; [g] 0.3 mol% catalyst.

A breakthrough in the field of artificial metalloenzymes and metathases in particular was achieved in the groups of Ward and Panke.[349] Relying on the biotin-streptavidin couple,

researchers in these groups selectively assembled an ArM metathase within the periplasm of *Escherichia coli*. The secretion of streptavidin into the periplasm was achieved by fusing Sav with the signal peptide OmpA. The *E. coli* strain combined a biotinylated GH-type catalyst **171** and periplasmic streptavidin as the protein host. This approach offers several important benefits. First, the metathase is not exposed to metabolites that could potentially interfere with the reaction or poison the catalyst. Glutathione, for example, is known to inhibit many precious metal catalysts,[259] but in the periplasm, this metabolite is only present in low concentrations and primarily in its oxidized form. The latter was shown to be significantly less harmful to d^6-metal complexes. Second, conducting metathesis reactions *in vivo* substantially sped up genetic optimization of the ArM metathases. A screening protocol was designed using microtiter plates and substrate **168**, which yielded fluorescent umbelliferone **169** upon RCM. Saturation mutagenesis libraries for twenty different amino acid positions were generated and over 3000 clones were screened. A quintuple mutant (47A-49K-114Q-119G-121R) with a cell-specific activity 5.4 times higher than the wild type metathase was identified. The activity of the purified ArM was also evaluated on two additional water soluble RCM substrates. The evolved metathase had increased activity over free catalyst as well as two benchmark, commercial catalysts toward uncharged diol substrate **167**. When the positively-charged diallylsulfonamide derivative **170** was tested with the quintuple mutant, however, a lower activity than the wild type was observed. The authors hypothesized that this may be due to electrostatic repulsion of the quarternary ammonium ion and the positively charged guanidinium group of arginine K121R. Consequently, a new round of saturation mutagenesis was performed at this position and a new clone (47A-49K/114Q-119G-121L) was found with leucine as an apolar residue at the 121 position. Upon removing this charge, the new mutant brought

a significant improvement for the positively charged substrate **170** (Table 22 and Scheme 55).

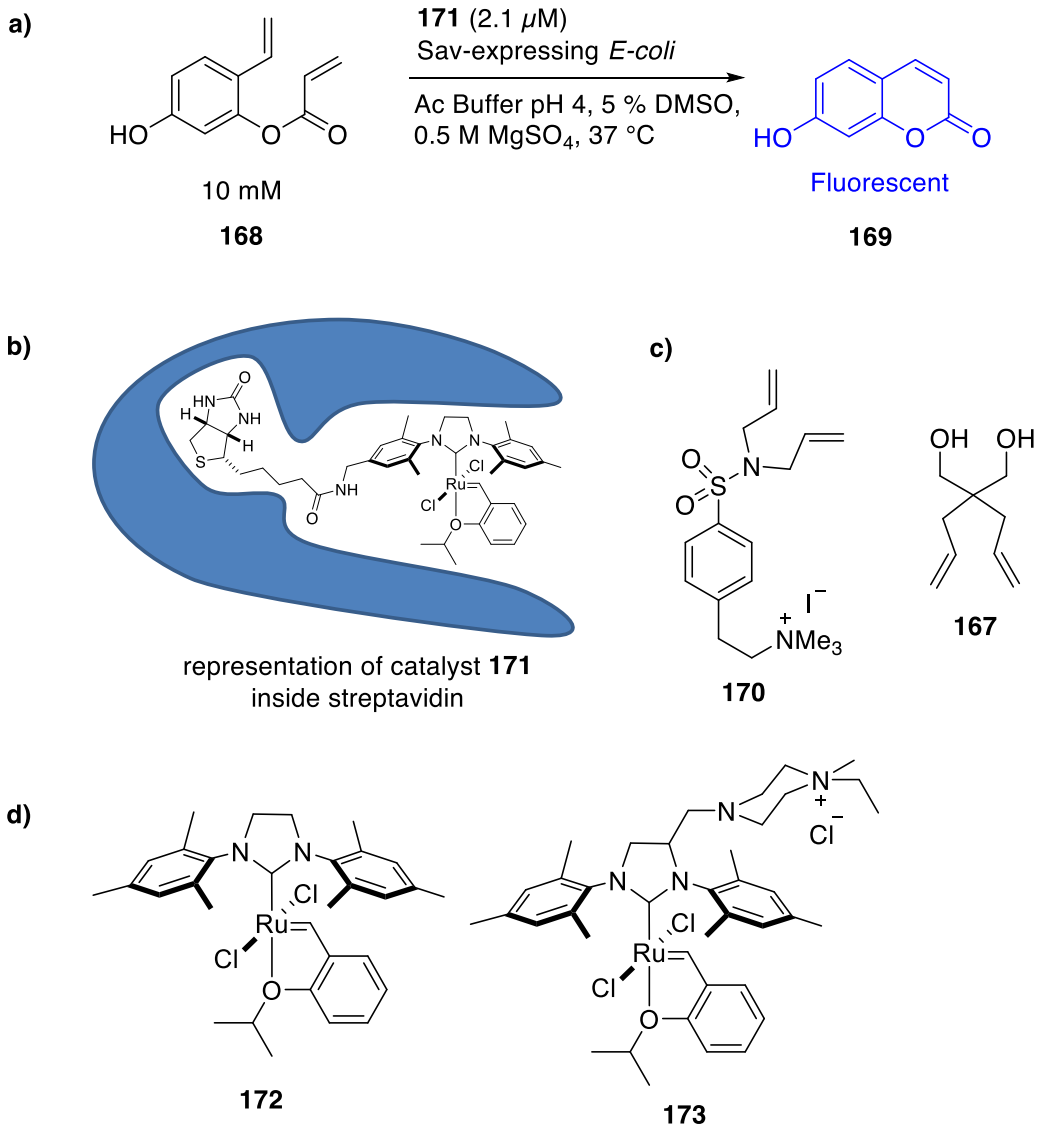

Scheme 55. *In vivo* directed evolution of an artificial metathase based on the biotin-streptavidin technology.

Table 22. *In vitro* performance of artificial metathases obtained by directed evolution.

Entry	Cat	SAV mutant	Sub	TON
1[a]	**172**	-	**167**	230
2[a]	**173**	-	**167**	340
3[a]	**171**	-	**167**	155
4[a]	**171**	Wild Type	**167**	445
5[a]	**171**	(47A/49K/114Q/119G/121R)	**167**	645
6[a]	**171**	(47A/49K/114Q/119G/121L)	**167**	455
7[b]	**172**	-	**170**	18
8[b]	**173**	-	**170**	30
9[b]	**171**	-	**170**	32

10[b]	**171**	Wild Type	**170**	53
11[b]	**171**	(47A/49K/114Q/119G/121R)	**170**	46
12[b]	**171**	(47A/49K/114Q/119G/121L)	**170**	89

[a] conditions: deuterated acetate buffer pH 4, 1.5 % DMSO-d6, [cat] = 50 μM, [sub] = 50 mM; [b]conditions: acetate buffer pH 4, 1.5 % DMSO, [cat] = 50 μM, [sub] = 10 mM.

In conclusion, it has been shown that metathesis is a versatile tool for the construction of artificial metalloenzymes, performing non-natural reactions. Within the past five years, the efficiency of metathases rose from a TON of 20 to hundreds of turnovers. Furthermore, all of the common metathesis reactions including cross-metathesis, ring closing metathesis, as well as ring opening metathesis polymerization have been achieved by artificial metathases. It has also been shown that such metathases under certain conditions can also work inside cells, which raises fascinating perspectives for their potential use *in vivo*. Yet, some major hurdles have to be overcome for such hybrid catalysts to be applicable as real alternatives to their organometallic counterparts. Since these systems rely on GH-type cofactors, they remain fragile toward reactive cell metabolites, especially thiols including GSH. This problem could be solved by either chemical engineering of more stable metathesis catalysts or by biological engineering of highly shielded active sites. The second challenge is the modest reactivity, compared to established commercial catalysts. However, taking into account the powerful tools offered by enzyme engineering, it is only a matter of time until highly efficient metathases can be developed for *in vivo* applications.

5.6 Cyclopropanation

As noted in section 5.4, several heme enzymes have been reported to catalyze olefin cyclopropanation via carbene insertion into olefin substrates. Metal substituted heme proteins also catalyze this reaction. Indeed, (PPIX)Ir(Me)-substituted myoglobin (see active site in Figure_15) catalyzed cyclopropanation reactions of an internal alkene **174**

and an unactivated aliphatic olefin **175**, neither of which has been reported for natural heme enzymes (Scheme 56 a), b). To facilitate *in vivo* generation of ArMs containing heme cofactors, Brustad and Snow recently reported an orthogonal P450-Fe-DPIX pair and demonstrated that the resulting ArMs could catalyze carbene insertion into olefins to generate cyclopropanes (Scheme 56 c), Figure 18).[350]

a)

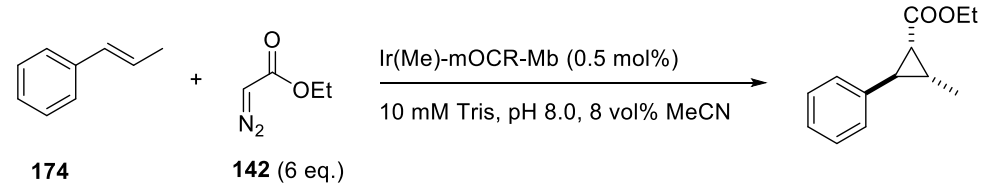

174 **142** (6 eq.)

Mutant	**ee%**	**de%**	**TON**
H93A-H64V-F43Y-V68V-H97F	40	94	20

b)

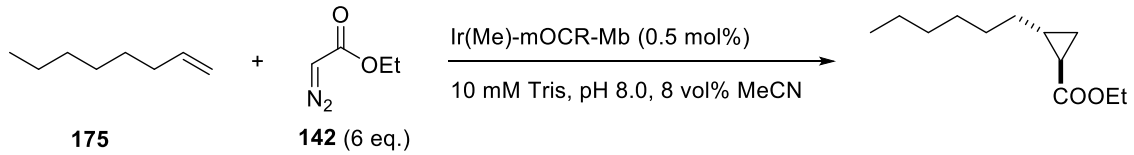

175 **142** (6 eq.)

Mutant	**ee%**	**de%**	**TON**
H93A-H64A-V68F	82	95	40

c)

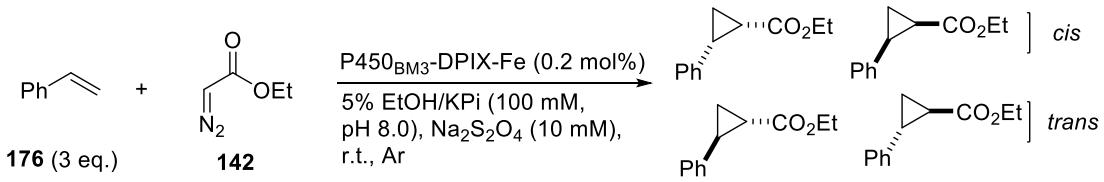

176 (3 eq.) **142**

Mutant	**ee%**	**de%**	**TON**
G265F-T269V-L272W-L322I-F405M-T268A	-51(cis) -46 (trans)	76	221

Scheme 56. Cyclopropanation reactions catalyzed by heme-substituted ArMs: a) aromatic olefins and b) aliphatic olefins catalyzed by myoglobin variants; c) styrene cyclopropanation catalyzed by P450BM3 variants.

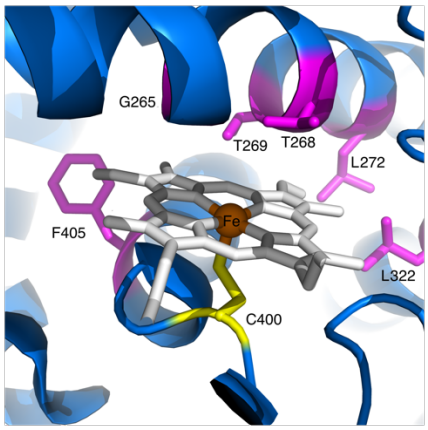

Figure 18. Cytochrome P450BM3 (PDB code 2IJ2) was evolved (mutant P450BM3 G265F-T269V-L272W-L322I-F405M-T268A) to preferentially bind a synthetic heme derivative, DPIX-Fe, which bears two methyl groups instead of the bulkier vinyl groups.[350] The ArM is a cyclopropanation catalyst.

Prior to any reported studies on carbene insertion chemistry using metal-substituted heme enzymes, Lewis reported that ArMs containing a dirhodium cofactor could catalyze cyclopropanation of 4-methoxystyrene and insertion into the Si-H bond of diphenylmethylsilane using diazoacetate carbene precursors (Scheme 57). The dirhodium ArMs were constructed by genetically encoding a *p*-azidophenylalanine residue at different sites within tHisF and phytase scaffolds, followed by strain-promoted azide-alkyne cycloaddition (SPAAC) of bicyclononyne (BCN)-substituted dirhodium cofactor (**177**).[10] Neither of the carbene insertion reactions investigated proceeded with significant enantioselectivity, likely as a result of the dirhodium center projecting out of the scaffolds investigated. Significant levels of formal carbene insertion into the O-H bond of water were also observed, but these ArMs accepted donor acceptor carbenes, which has not yet been reported using heme protein scaffolds.

To determine if a protein scaffold could be used to correct the chemo- and enantioselectivity problems encountered by initial dirhodium ArM constructs, bioconjugation of **177** to several additional scaffolds was pursued. Gratifyingly, incorporating **177** into a prolyl oligopeptidase (POP)[351] scaffold from *Pyrococcus furiosus*,

which has a large active site capable of completely encapsulating the bulky dirhodium cofactor, led to modest enantioselectivity for styrene cyclopropanation (38% ee).[352] Targeted mutagenesis of residues in the POP active site led to dirhodium ArMs that catalyzed styrene cyclopropanation with up to 92% ee and improved selectivity for cyclopropanation over competing formal insertion into the O-H bond of water (Scheme 57 b)). Key residues introduced into the POP scaffold included a histidine (H328), believed to coordinate to one of the Rh centers in **177**, and two phenylalanines (F99, F594) across the active site relative to the coordinating histidine (Figure 19).

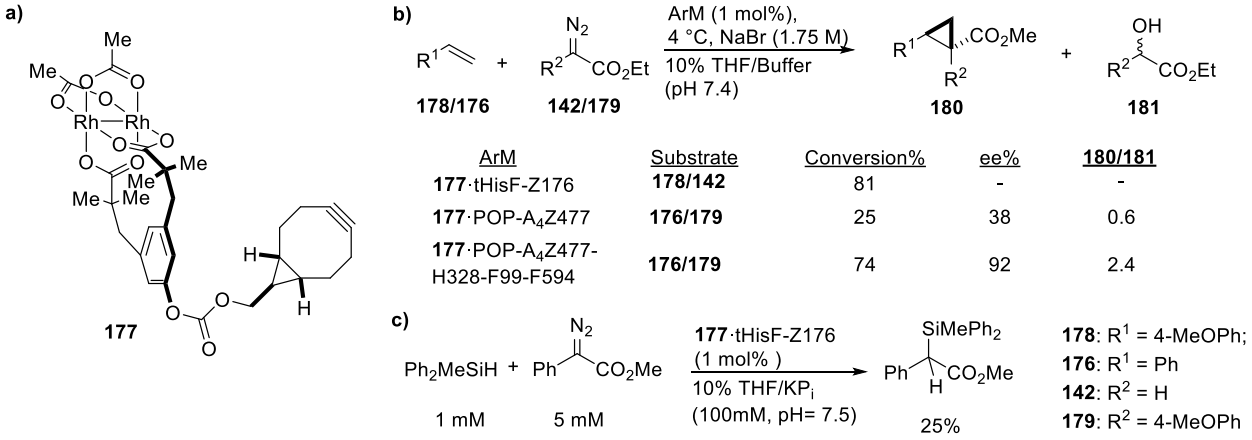

Scheme 57. Bicyclononyne-substituted dirhodium cofactor a). Dirhodium ArMs catalyzed cyclopropanation b) and Si-H insertion reactions c).

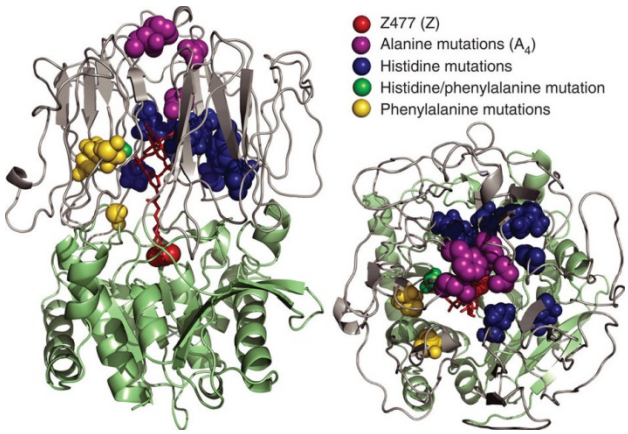

Figure 19. Homology model of Pfu POP.[353] The hydrolase domain is shown in green, the propeller domain is shown in grey and cofactor **177** linked at Z477 is shown in red. In magenta are highlighted alanine mutations introduced to widen the pore and thereby enable access of the cofactor to the active site. Additional mutations introduced into Pfu

POP are shown as coloured spheres. Adapted with permission from ref.[352] Copyright 2015, Rights Managed by Nature Publishing Group.

5.7 Polymerization (non-ROMP)

The stereochemistry, molecular weight (M_w), and polydispersity (M_w/M_n) of polymers are critical factors that can be influenced by the secondary coordination sphere of metal catalysts. Researchers have also explored the potential to control polymer properties using interactions provided by either a protein scaffold or a protein assembly. The well-defined interiors of these systems could provide a hydrophobic environment to favor polymerization, orient substrates, and influence polymer size and polydispersity. ArM polymerases that lead to the formation of C–C bonds via a variety of mechanisms, including ATRP, acetylene polymerization, and ROMP have been developed. The latter metathesis-type polymerization is presented in section 5.5.

In 2009, Ueno and Watanabe *et al*. introduced $[Rh(nbd)Cl]_2$ (nbd = norbornadiene) **184** into apo-ferritin and evaluated Rh-loaded capsule as catalyst for the polymerization of phenylacetylene **182** (Scheme 58).[311] The crystal structure of **184**·apo-ferrtin revealed one rhodium ion at the threefold channel and two rhodium ions in the accumulation center (Figure 13) via coordination of histidine and cysteine residues. The polyphenylacetylene **183** produced by **184**·apo-ferrtin displayed an average molecular weight (M_w) = 13.1 ± 1.5 · 103 g/mol and a polydispersity (M_w/M_n) = 2.6 ± 0.3. For comparison, the polymer produced by free $[Rh(nbd)Cl]_2$ **184** had M_w = 63.7 ±4 · 103 g/mol and M_w/M_n = 21.4 ± 0.4 (Table 23, entries 1 and 2).

Hayashi and coworkers covalently linked a maleimide-substituted Cp*Rh(cod) complex (**185**) to the interior of apo-nitrobindin (Nb) to perform the polymerization of phenyl acetylene **182** (Scheme 58).[199] Nb contains an Fe-protoporphyrin IX **222** cofactor in a

cavity formed by eight β-strands. In order to covalently anchor the pianostool cofactor, Q96, located at the entrance of the cavity, was mutated to a cysteine. The resulting artificial metalloenzyme was tested for alkyne polymerization. The free cofactor, **185**, yielded the thermodynamically preferred *cis*-poly(phenylacetylene) **183** with *trans* : *cis* = 7 : 93. In contrast, **185**·Nb(Q96C) afforded **183** with *trans* : *cis* = 53 : 47 (Table 23, entries 3 and 4).

Next, they genetically optimized the artificial polymerase to improve the *trans*-selectivity (Scheme 58). They selected aminoacid residues within 6 Å from the computed position of the Rh center. Gratifyingly, **185**·Nb(H76L-Q96C-H158L) produced **183** with *trans* : *cis* = 82 : 18 (Table 23, entry 5).[354] Molecular dynamic simulations of **185**·Nb variants suggested that mutations which lock the orientation of the Rh-moiety and guide the access of the monomer enhance *trans*-stereoselectivity.

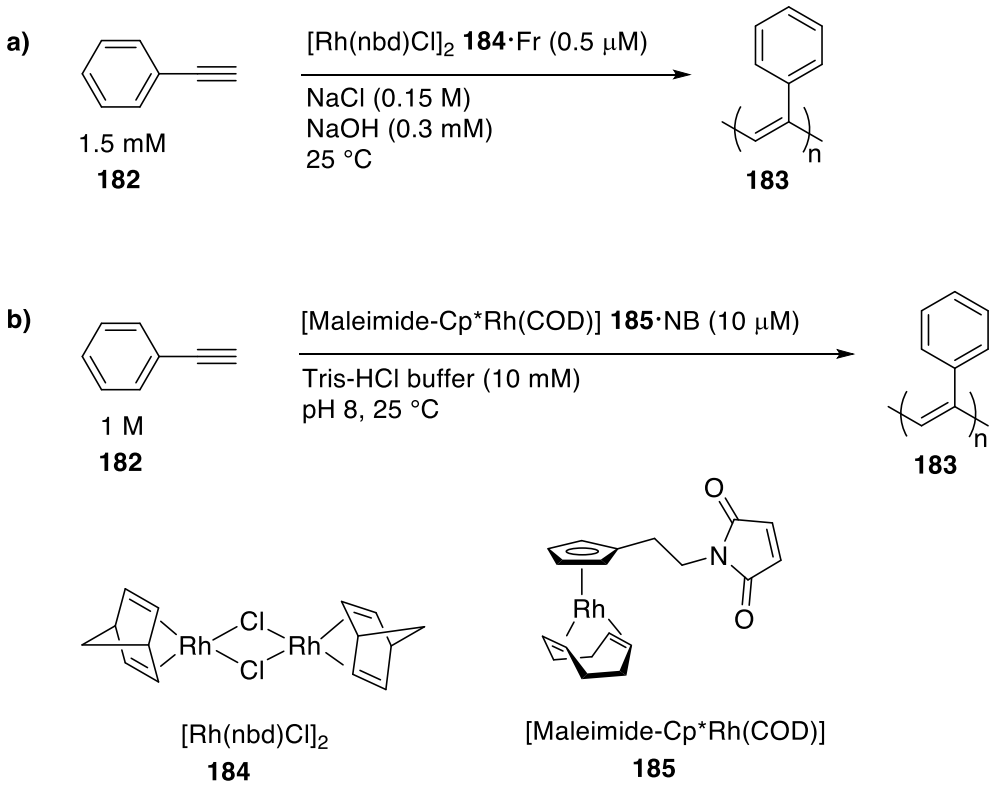

Scheme 58. Polymerization of phenylacetylene catalyzed by Rh(I)-modified proteins.

In 2011, Bruns and coworkers reported that horseradish peroxidase (HRP) was able to catalyze atom transfer radical polymerization (ATRP) using *N*-isopropyl acrylamide (NIPAAm, **187**) as the monomer and alkylbromide (**186**) as initiator (Table 23, entry 6).[355]

In 2014, Bruns and coworkers constructed an ArM ATRPase comprised of copper complex **189** and the group II chaperonin thermosome (THS) from the archaea *Thermoplasma acidophilum* as a protein scaffold.[356] THS is a hexadecameric protein complex and can switch between an open and a closed state by consumption of ATP. In its closed state, the protein possesses two cavities of 130 nm^2 each that can host a polymerization event. In its open state, the pores are large enough allow the polymer to exit the capsule. The ATRPase, **189**·THS C363A-K316C-C364A catalyzed the polymerization of **187** under ATRP conditions (Scheme 59). This ATRPase yielded Poly-NIPAAm (PNIPAAm, **188**) with a lower M_w/M_n and M_n compared to the catalyst bound on the surface of bovine serum albumin, a globular protein (BSA-**189**). These results indicate that the protein cage not only improves the polymerization process, but also limits the diffusion of monomers into the active site of the polymerase (Table 23, entries 7 and 8).

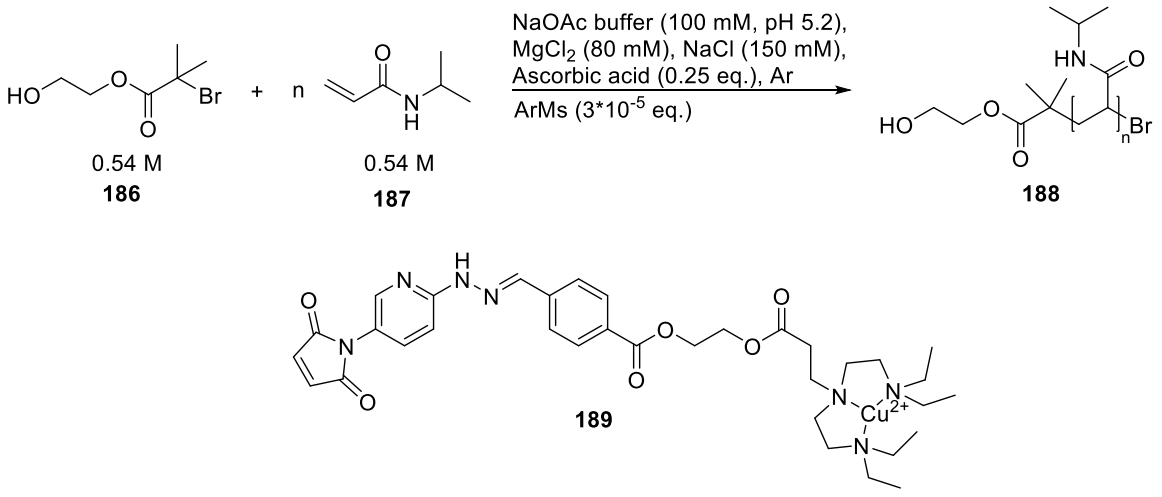

Scheme 59. N-isopropyl acrylamide (NIPAAm) atom transfer radical polymerization (ATRP) catalyzed by **189** ArMs.

Table 23. Selected results for the ATRP polymerization catalyzed by artificial polymerases.

Entry	Cofactor	Sub	Protein	T (°C)	t (h)	[Metal] (μM)	M_n (g/mol)	M_w/M_n	*trans* : *cis*	Ref
1	**184**	**182**	No Protein	25	3	30.0	63700	21.4	–	[311]
2	**184**	**182**	Fr (WT)	25	3	28.8	13100	2.6	–	[311]
3	**185**	**182**	No Protein	25	24	10.0	22900	2.6	7 : 93	[199]
4	**185**	**182**	Nb (Q96C)	25	24	10.0	42600	2.2	53 : 47	[199]
5	**185**	**182**	Nb (H76L-Q96C-H158L)	25	24	10.0	38900	2.4	82 : 18	[354]
6	**222**	**187**	HRP	r.t	2.5	16.2	99900	1.44	–	[355]
7	**189**	**187**	THS	r.t.	20	16.2	1500	1.11	–	[356]
8	**189**	**187**	BSA	r.t.	20	16.2	42600	1.94	–	[356]

5.8 Diels-Alder Reaction

Diels-Alder reactions are widely used for the construction of six-membered rings due the predictable regio- and stereospecificity of these reactions.[357] Copper(II)-catalyzed Diels-Alder reactions of azachalcones with cyclopentadiene (Scheme 60 a)) have been extensively employed in fundamental studies on the design of a wide range of catalysts,[358] including ArMs. An early example, particularly notable for its high enantioselectivity, was reported by Reetz. ArM Diels-Alderases were constructed via non-covalent binding of a Cu(II) phthalocyanine complex (Figure 21, **190**) to various serum albumins. Up to 91% conversion, 91:9 endo/exo ratio, and 98% ee could be obtained using this system (Table 24, entry 1-6), although the rate of the ArM-catalyzed reaction was slower than that catalyzed by cofactor alone. In a separate effort, Reetz also demonstrated that a His_2Asp Cu(II) binding site could be introduced into tHisF, the thermostable synthase subunit of the glutaminase synthase enzyme complex from *Thermotoga maritima*, to generate an ArM Diels-Alderase.[359] EPR spectroscopy was used to confirm Cu(II) binding in the designed site, and eliminating potential metal-binding cysteine and histidine residues from the scaffold surface improved the enantioselectivity of this system (up to 46% ee, Table 24, entry 7 and Figure 20.

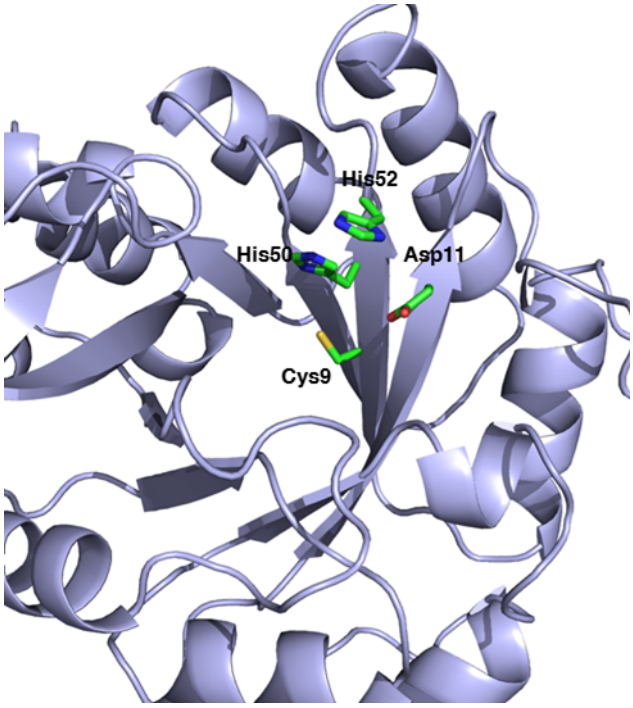

Figure 20. Designed putative metal binding site in the thermostable protein tHisF for the evolution of Diels-Alderase at the top of the TIM barrel (based on the crystal structure PDB: 1THF). Highlighted are the existing aspartate residue in tHisF and the two histidines introduced to create the 2-His-1-carboxylate motif. The cysteine residue in the middle of the TIM barrel was replaced with alanine to prevent metal binding.

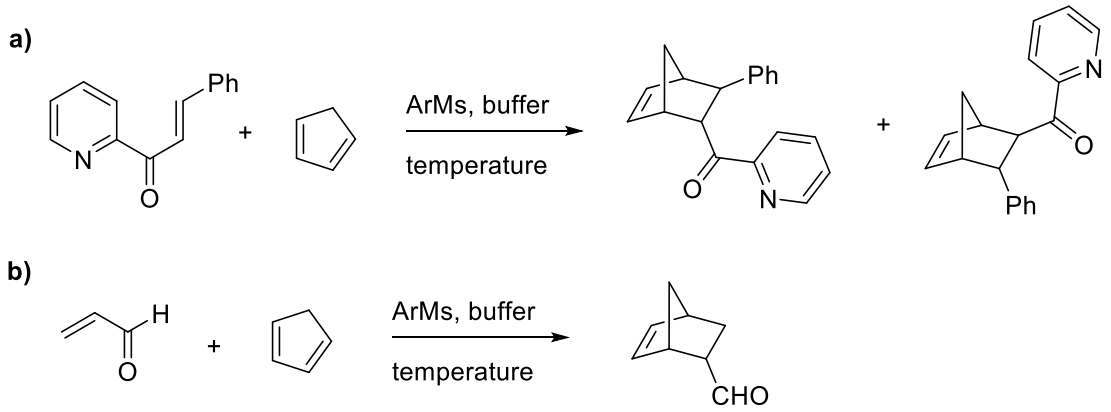

Scheme 60. Model Diels-Alder reactions catalyzed by ArMs.

Scaffold-specific interactions have also been used to anchor catalysts into protein scaffolds to generate ArMs that catalyze the Diels-Alder reaction displayed in Scheme 60 a). For example, Niemeyer reconstituted apo myoglobin using a heme cofactor substituted with both ssDNA and a Cu(II)-bipy complex (**Figure 21**, **191**).[360] The resulting ArM catalyzed the Diels-Alder reaction with improved enantioselectivity relative to the heme-ssDNA cofactor alone (18% ee for endo product and 10% for exo, Table 24, entry 8). More

recently, Mahy and Ricoux demonstrated that a testosterone-substituted Cu(II)-phenanthrene complex (Figure 21, **192**) could be incorporated into a neocarzinostatin variant engineered to bind testosterone with improved affinity relative to the WT enzyme.[361] The scaffold exhibited tighter binding affinity to the Cu(II)-phenanthroline-testerone cofactor (K_d = 3 μM) than toward testosterone (K_d = 13 μM), and docking experiments suggested that the added phenanthroline ligand enhanced the complementarity of the cofactor to the protein. The resulting ArM catalyzed the reaction displayed in Scheme 60 a) with an increased *endo* : *exo* ratio compared to cofactor alone, but with lower conversion and no enantioselectivity (Table 24, entry 9).

Several approaches to generate ArM Diels-Alderases via covalent modification of scaffold proteins have also been reported. For example, Salmain constructed a Diels-Alderase by covalently linking a chloroacetamide-substituted [(η^6-arene)ruthenium(II)]-complex to papain via cysteine alkylation (Figure21, **193**).[362] The TOF of the Diels-Alder reaction between cyclopentadiene and acrolein (a rare example not involving aza-chalcones, Scheme 60 b)) was increased more than threefold with the ArM relative to the free cofactor. Kamer[351] and later Okuda and Hayashi[363] have demonstrated that bidentate and tridentate nitrogen ligands (Figure 22, **194-202**) can be introduced into protein scaffolds to generate ArM Diels-Alderases for the reaction shown in Scheme 60 a) following metallation with Cu(II). Modest enantioselectivity was observed in the former case (Table 24, entries 10-11)[351] while improved conversion relative to free cofactor was observed in the latter(Table 24, entry 12)[363]. A similar tridentate ligand **196** was used to generate an improved ArM Diels-Alderase via bioconjugation to an engineered variant of the transmembrane protein ferric hydroxamate uptake component A (FhuA).[348] The *endo*-selectivity was improved to 98% by the **196**·FhuA compared to 54% and 66% obtained for the free copper ion and **196** respectively (Table 24, entry 13).

Filice showed that a similar approach could be used to generate immobilized ArM Diels-Alderases. A lipase from *G. thermocatenulatus* (GTL) containing cysteine mutation in a cleft distal to the active site was immobilized on hydrophobic sepharose. A Cu(II) cofactor derived from ligand **200** was used to alkylate the distal cysteine in GTL to generate an ArM, which catalyzed the reaction shown in Scheme 60 a) with up to 92% ee (Table 24, entries 14-15). Both the support agent and immobilizing orientation had a large impact on the selectivity of the reaction, and the native activity of the lipase was still remained after cofactor incorporation in the distal site.[364]

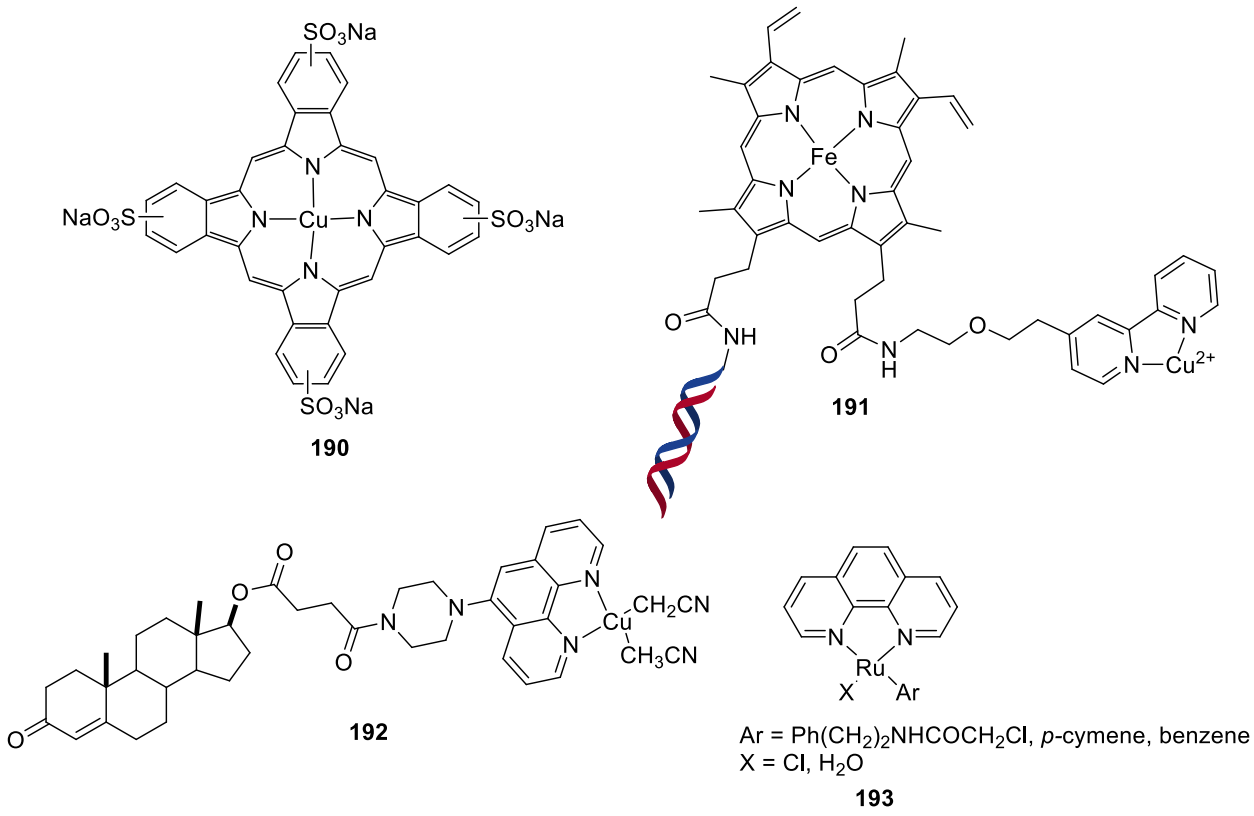

Figure 21. Cofactors used to construct an artificial Diels-Alderase.

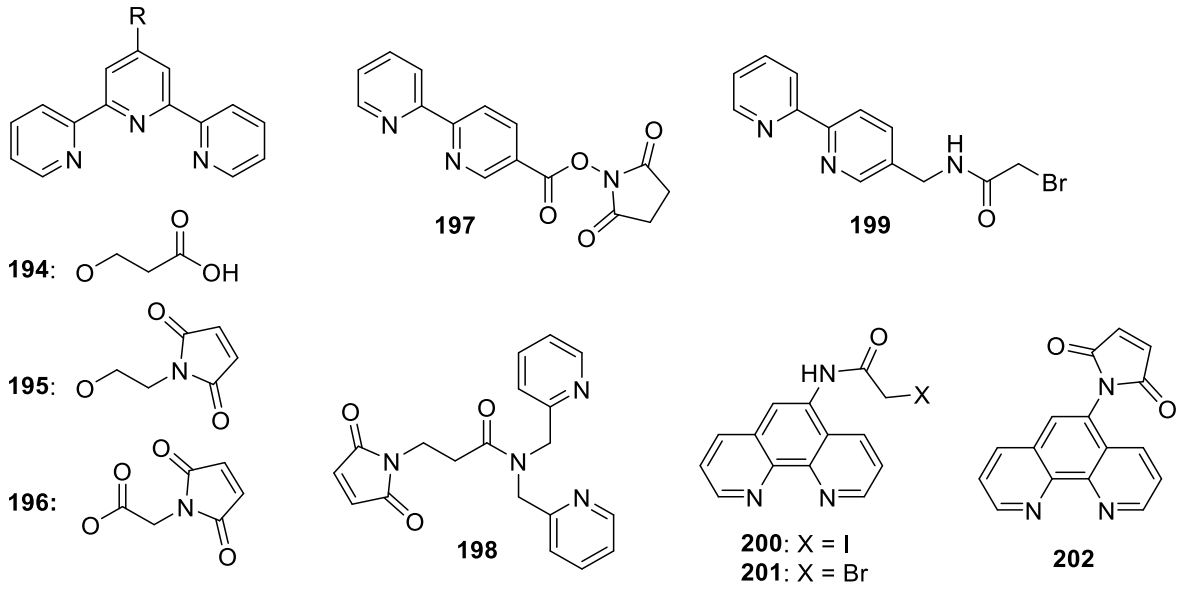

Figure 22. Bidentate and tridentate nitrogen cofactors used to form ArM Diels-Alderases.

Concurrent with much of this work, Roelfes conducted a number of studies on the development of Cu(II)-bipyridine and related ArMs that catalyze the Diels-Alder reaction and other Lewis Acid catalyzed processes. Initial studies showed that the lactococcal multidrug resistance regulator (LmrR), a dimeric transcription repressor, could be alkylated with an haloacetamide-substituted bipyridine (**199**) and phenanthroline ligands **201** at the dimer interface to generate ArM Diels-Alderases following metallation with Cu(II).[365] High conversion and enantiomeric excess (both >90%) were observed for the reaction displayed in Scheme 60 a) (Table 24, entry 16). Point mutants of this ArM also catalyzed enantioselective hydration of azachalcones with a slightly lower conversion and enantiomeric excess (up to 84% ee) as discussed in chapter 7 (Scheme 93).[366]

Table 24. Selected results for the Diels-Alderase.

Entry	Protein	pH	T (°C)	[Cof] (μM)	t (day)	[Cof]/[Prot]	Endo/Exo	ee (%)[b]	Ref
1	BSA	4.0	5	0.4	3	1:1.2	96:4	93	[367]
2	HSA	4.0	5	0.4	3	1:1.2	91:9	85	[367]
3	PSA	4.0	5	0.4	3	1:1.2	89:11	68	[367]
4	RSA	4.0	5	0.4	3	1:1.2	88:12	7	[367]
5	SSA	4.0	5	0.4	3	1:1.2	87:13	75	[367]
6	CSA	4.0	5	0.4	3	1:1.2	78:22	1	[367]
7	tHisF-HHD-4xAla	7.5	12	115	4	1:1.3	93:7	46	[359]

8	apo-Mb	7.4	4	100	3	1:1	90:10	18, 10[a]	360
9	NCS-3.24	7.5	4	114	3	1.1:1	81:19	-	361
10	SCP-2LV83C	6.0	4	56	3	1:1.1	88:12	25	351
11	SCP-2LA100C	6.0	4	56	3	1:1.1	92:8	-	351
12	Nb-Q96C/M75L/M148L/H76L/H158L	7.0	4	100	3	1:1.1	90:10	-	363
13	FhuA	7.4[c]	25	10	3	1:1	98:2	-	348
14	GTL-S114C	6.0	4	2.4	3	1:1	99:1	18	364
15	GTL-S196C	6.0	4	2.4	3	1:1	94:6	92	364
16	LmrR-M89C	7.0	4	30	3	1:1.1	95:5	97	365

[a] For both endo and exo; [b] Positive and negative ee values correspond to the (*R*)- and (*S*)-enantiomers respectively; [c] Buffer contains 0.125 mM polyethylene polyethylene glycol and 20%(v/v) THF.

5.9 Huisgen [3+2] Cycloaddition

Ueno and coworkers have explored the use of self-assembled protein scaffolds for ArM catalysis.[368] For example, the tubular structure formed by the triple-stranded α-helical assembly of three subunits of gene product 5, $(gp5)_3$, from bacteriophage T4, was used to generate an ArM that catalyzes a Huisgen [3+2] cycloaddition.[296] A protease resistant fragment from the *C*-terminal region of $(gp5)_3$, termed $(gp5\beta)_3$, was fused to a foldon (f) domain that promotes trimerization of bacteriophage T4 fibritin to generate a stable tubular scaffold. A succinimide moiety conjugated with flavin **204** was introduced at lysines located on the outer-surface of the $[(gp5\beta f)_3]_2$ (Scheme 61 and Figure12). Upon addition of copper ions, the artificial metalloenzyme catalyzed the azide-alkyne [3 + 2] cycloaddition. The hybrid catalyst **204**·$[(gp5\beta f)_3]_2$ catalyzed the "click reaction" reaction faster than **205** or of a mixture of **205** and $[(gp5\beta f)_3]_2$ (Table 25).

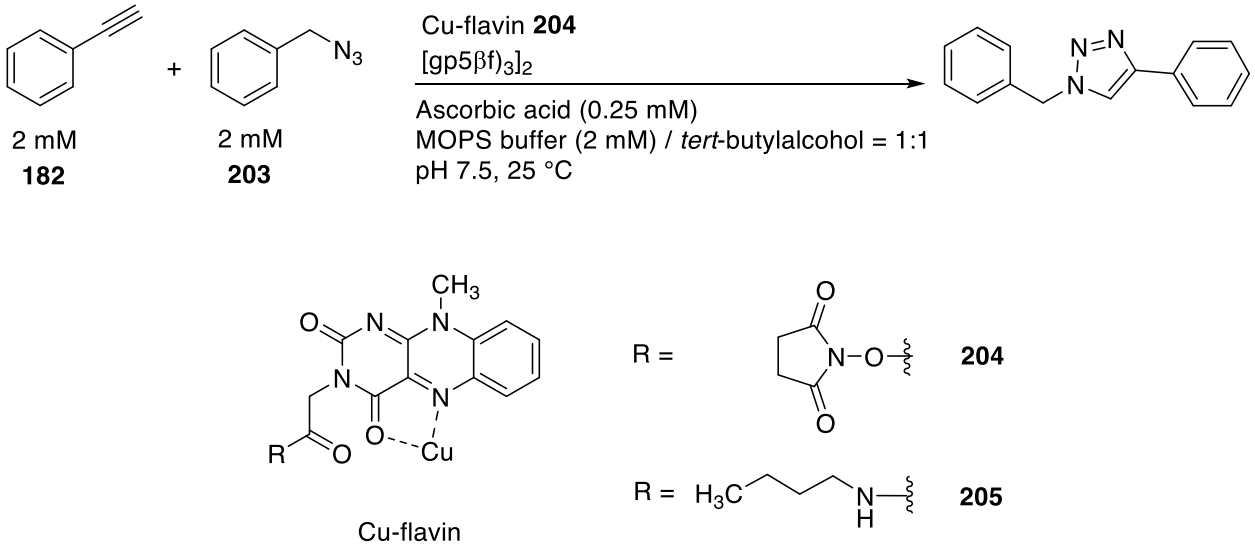

Scheme 61. Cu(I)-catalyzed cycloaddition catalyzed by the copper-flavin complex conjugated to $[(gp5\beta f)_3]_2$.

Table 25. Selected results for the Cu(I)-catalyzed cycloaddition of substrate **182** and **203** in the presence of $[(gp5\beta f)_3]_2$.[a]

Entry	Cofactor	Protein[a]	t (h)	[Cof] (μM)	[Ascorbic acid] (mM)	TON	Ref
1	**204**	$[(gp5\beta f)_3]_2$	5	250	0.25	5.86	[296]
2	**205**	$[(gp5\beta f)_3]_2$	5	250	0.25	0.14	[296]
3	**205**	No Protein	5	250	0.25	0.62	[296]

[a] Reactions were carried out in a solution of 1 : 1 tert-butylalcohol/MOPS (2mM, pH 7.5) at 5°C.

5.10 Friedel-Crafts Reaction

Although the Friedel-Crafts reaction was introduced more than 130 years ago, it still represents an attractive tool to alkylate aromatic compounds.[369] Initially, it required ≥ 1.0 equivalent of Lewis acid, and alkyl halides. Today however, alkyl alcohols, ethers, tosylamides, or styrenes can be used instead of alkyl halides, and catalytic asymmetric Friedel-Crafts reactions have been developed.[369-371]

Artificial metalloenzymes that catalyze the Friedel-Crafts reaction have been developed by Roelfes et al. A BpyAla residue was genetically encoded into LmrR to eliminate the need for covalent modification of the scaffold.[372] Metallation with Cu(II) provided an ArM that catalyzed the Friedel-Crafts alkylation of a variety of indoles (Scheme 62) with

conversions as high as 94% and high enantioselectivity (up to 83% ee, Table 26, entries 2-7). Interestingly, when the ligand was placed outside of the hydrophobic pocket, the opposite product enantiomer was formed (Table 26, entry 3). More recently, Roelfes demonstrated that the hydrophobic cavity of dimeric LmrR was capable of binding an unsubstituted Cu(II) phenanthroline cofactor directly to form ArMs through supramolecular assembly.[373] The binding affinity of the cofactor was measured by tryptophan fluorescence quenching, which showed the dissociation constant (K_d) was much higher when an interfacial tryptophan residue (W96A) was removed (45 μM compared to 2.6 μM). Fluorescence decay also showed decreased lifetime when the scaffold was saturated with Cu(II), suggesting cofactor binding at the hydrophobic pore. The enantioselectivity of these ArMs toward Friedel-Crafts alkylations was significantly higher (up to 94% ee) (Table 26, entries 8-11) than the covalently linked systems noted above. These studies constitute one of the few cases in which covalent scaffold modification, metal binding to a scaffold residue (albeit an unnatural amino acid), and non-covalent scaffold binding have all be used to generate ArM catalysts, all of which provided high enantioselectivity.

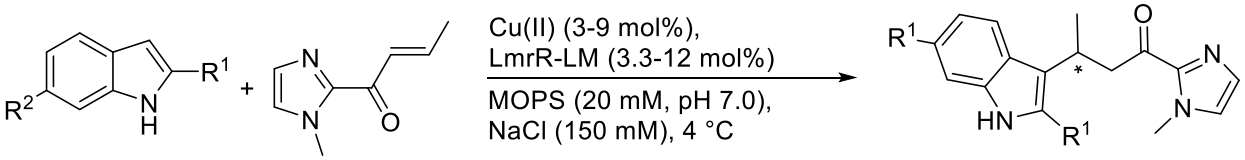

206: R^1 = H, R^2 = OMe
207: R^1 = H, R^2 = H
208: R^1 = H, R^2 = Cl
209: R^1 = Me, R^2 = H

Scheme 62. Friedel-Crafts reaction catalyzed by LmrR-Cu ArMs.

Table 26. Selected results for the asymmetric Friedel-Crafts reaction based on Cu(phen) ArMs

Entry	Protein	Sub.	t (h)	Ratio [Cof]/[Prot]	Conversion (%)	ee (%)	Ref
1[a]	-	**206**	72	-	98	0	[372]
2	LmrR_LM (M89X)	**206**	72	1/1.25	27	49 (*S*)	[372]

3	LmrR_LM (F93X)	**206**	72	1/1.25	36	22 (*R*)	[372]
4	LmrR_LM (M89XE107A)	**206**	72	1/1.25	22	66 (*S*)	[372]
5	LmrR_LM (M89XF93W)	**207**	72	1/1.25	16	55 (*S*)	[372]
6	LmrR_LM (M89XF93W)	**208**	72	1/1.25	3	50 (*S*)	[372]
7	LmrR_LM (M89XF93W)	**209**	72	1/1.25	94	83 (*S*)	[372]
8[b]	LmrR_LM	**206**	16	1/1.33	90	84 (*S*)	[373]
9[b]	LmrR_LM	**207**	64	1/1.33	Full	94 (*S*)	[373]
10[b]	LmrR_LM	**208**	64	1/1.33	19	64 (*S*)	[373]
11[b]	LmrR_LM	**207**	64	1/1.33	Full	93 (*S*)	[373]
12[b]	LmrR_LM	**206**	16	1/1.33	53	<5 (*S*)	[373]

[a] $Cu(NO_3)_2$ only; [b] None covalent binding with Cu(phen).

6. Oxygen Insertion Chemistry

6.1 Peroxidation or Oxygenation

Dioxygen is widely used as a terminal oxidant in biological processes. Although the reaction of organic compounds with dioxygen is generally thermodynamically favorable, kinetic barriers slow the oxidation of most organic compounds. This can be traced back to spin considerations: organic compounds exist mostly as spin-paired species whereas dioxygen has a triplet ground-state, thus rendering the reaction spin-forbidded.[374] To overcome the high energetic barrier, nature typically generates metal–O_2 species in the active site of metalloenzyme including: such as cytochrome P450, methane monooxygenase and tyrosinase etc. Inspired by these metalloenzymes relying on dioxygen for oxygenation and oxidation reactions, heme analogues or copper complexes have been exploited as a cofactors to create numerous artificial oxidases. This section summarizes oxidation reactions catalyzed by artificial oxidase using peroxides and molecular oxygen as oxidant. Oxygen-atom insertion reactions are described in the following sections.

Shortly after the initial reports of catalytic antibodies, Schultz and Cochran described a class of metallo-catalytic antibodies which they coined “hemoabzymes”.[133, 375] Shortly thereafter, Imanaka and Mahy joined these efforts.[376-377] This term "hemoabzyme" stems from their composition: a porphyrin (“hemo-“), inserted into an anti-body (“-ab-”) that has been elicited in mice against a protein-conjugated heme hapten. Progress achieved relying on this strategy has been reviewed recently.[62-63]

In 1990, Schultz and coworkers used *N*-methyl-mesoporphyrin IX (**19**) as the hapten. This molecule was selected as a transition-state analogue for porphyrin metalation. The metallation of the mesoporphyrin IX was accelerated by monoclonal anti-**19** to afford the

hemoabzyme **20**·Ab-7G12. Peroxidase degradation catalyzed by this metallo-antibody was quantified using *o*-dianisidine oxidation (**210**) (Scheme 63).[133, 375] The hemoabzyme **20**·Ab-7G12 displayed saturation kinetics and was > 4 times more efficient than the [Fe(MPIX)] **20** (Table 27, entries 1 and 2).

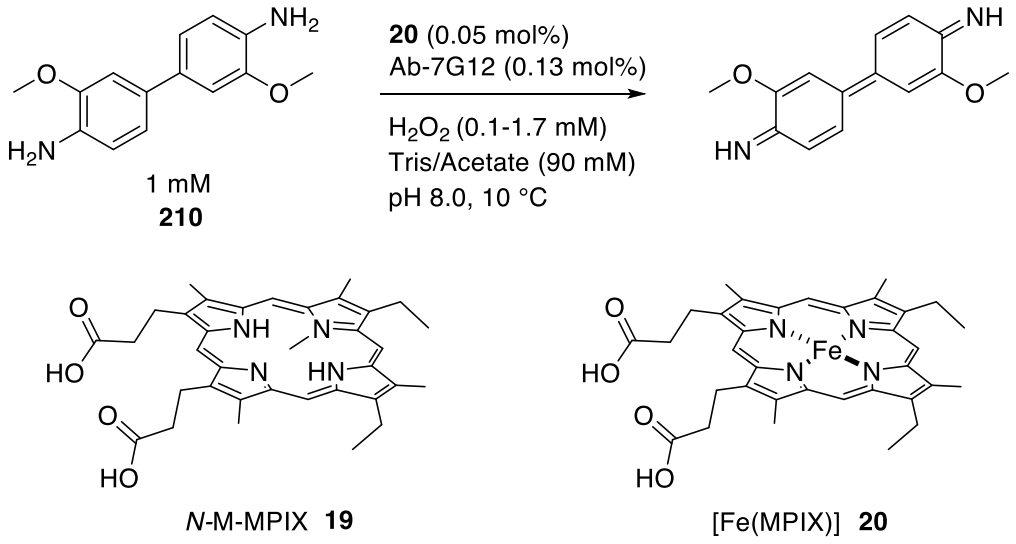

Scheme 63. Antibodies raised against **19** catalyze the oxidation of *o*-dianisidine **210** upon loading with cofactor **20.**

In 1999, Kawamura-Konishi and coworkers also utilized the same set of hapten **19** and catalyst **20** to generate an ArM peroxidase.[378] The affinity between **20** and the isolated antibody 2B4 was K_D = 0.064 μM. In the presence of hydrogen peroxide, oxidation of ABTS **211**, *o*-dianisidine **210**, and pyrogallol **212** was investigated (Scheme 64). The ArM exhibited higher peroxidase activity for *o*-dianisidine **210** and ABTS **211** than the ferric mesoporphyrin itself, while such enhancement was not observed for pyrogallol **212** (Table 27, entries 3 and 4). The authors hypothesize that the antibody imposed a certain degree of substrate preference to the cofactor.

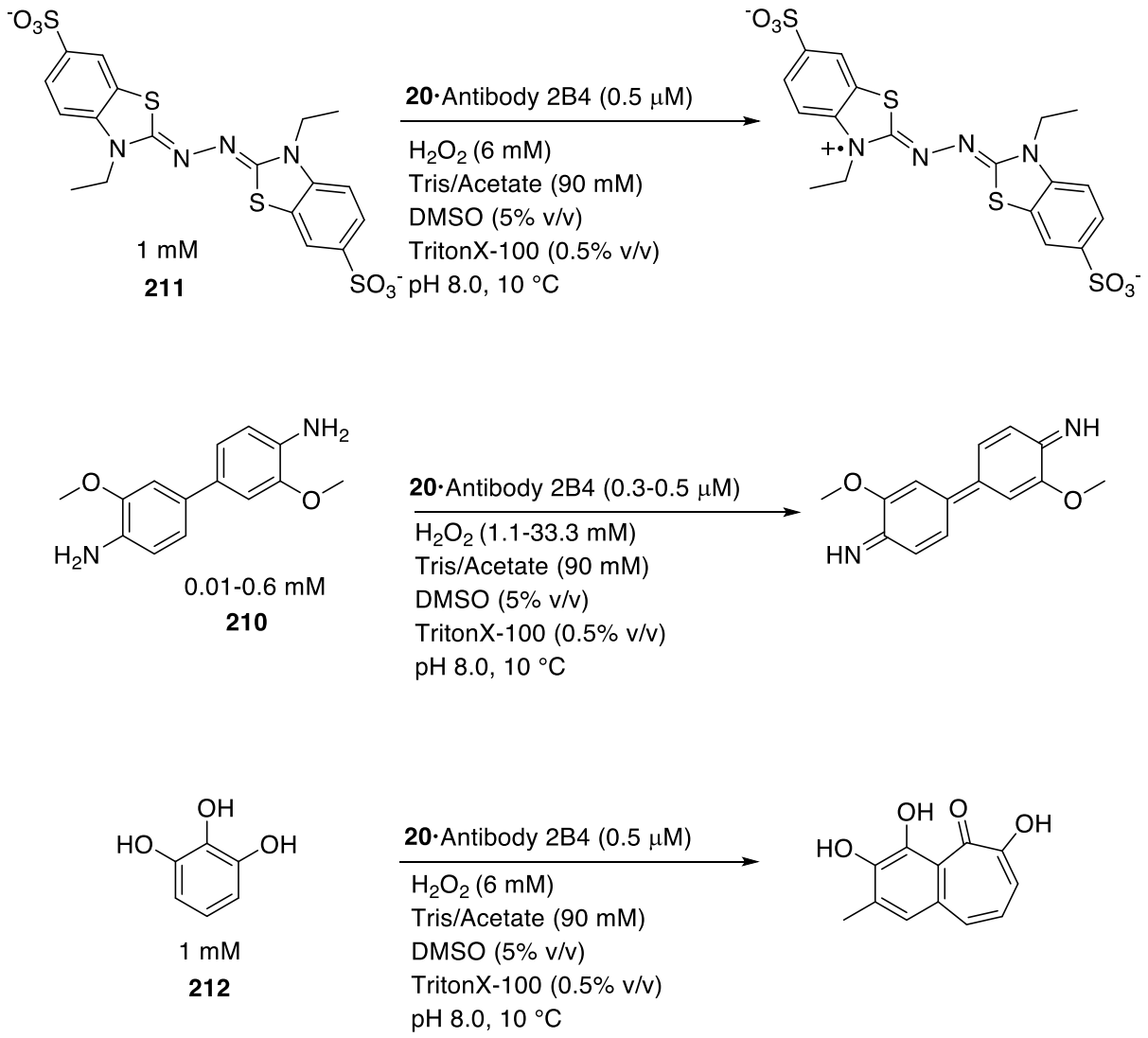

Scheme 64. Peroxidase activity of iron porphyrin derivatives in the presence of an antibody elicited against *N*-methylmesoporphyrin **19**. For structures **19** and **20** refer to Scheme 63.

In 1995, the group of Imanaka immunized mice using T*p*CPP as a hapten (Scheme 65).[376] Both monoclonal antibodies as well as the light chain (L) of one of these antibodies (L-Ab-13-1) were isolated. Incorporating **213** into L-Ab-13-1 afforded an ArM that was more thermostable and displayed a higher peroxidase activity than the complex of **213** with the complete antibody. The peroxidase activity of **213**·L-Ab-13-1 was significantly higher than other hemoabzymes, and remains among the highest reported to date (Table 27, entry 5).

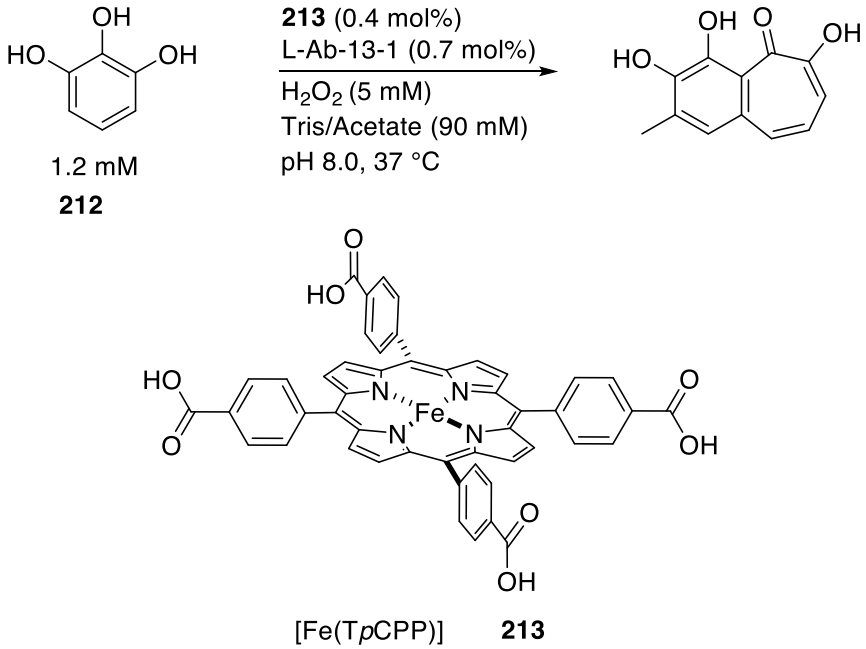

Scheme 65. Antibodies raised against T*p*CPP bind **213** to afford hemoabzymes with peroxidase activity.

In 1996, Mahy and coworkers selected the tetra-aryl porphyrin **214** as a hapten (Scheme 66).[377] Two IgG_1 monoclonal antibodies, Ab-14H7 and Ab-13G10, bind **214** with a dissociation $K_D = 5.5 \times 10^{-9}$ M and $K_D = 2.9 \times 10^{-9}$ M respectively.[377] These are the highest affinity values reported for porphyrin/Ab-antiporphyrin interactions.[379] The protein pocket provided a beneficial effect on the peroxidase activity of **214**. Indeed, both **214**·Ab-14H7 and **214**·Ab-13G10 showed ~5 times higher k_{cat}/K_M than **214** alone at pH 5.0 (Table 27, entries 6-8). **214**·Ab-13G10 showed even higher activity at pH 4.6 (Table 27, entry 9).

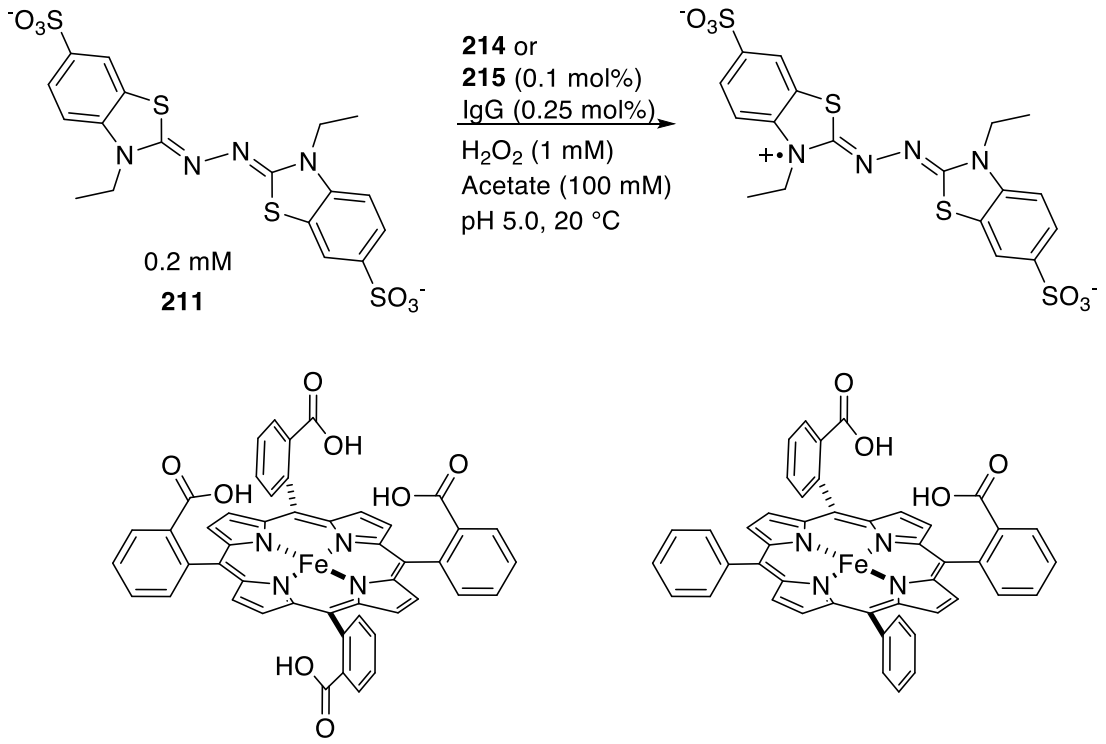

Scheme 66. Supplementation of a synthetic *o*-carboxyphenyl-porphyrin **214** or **215** with their cognate antibodies affords artificial peroxidases.

Harada and coworkers elicited monoclonal antibodies 03-1 and 12E11G against the anionic porphyrin **213** and the cationic porphyrin **216**, respectively (Scheme 67).[134, 380] The dissociation constant between the antibody 03-1 and Fe-*meso*-tetrakis(4-carboxyphenyl)porphyrin (TCPP) **213** was 1.5×10^{-7} M and the antibody 12E11G bound to Fe-*meso*-tetrakis(4-*N*-methylpyridyl)porphyrin (TMPyP) **216** with K_d of 2.6×10^{-7} M. In the presence of hydrogen peroxide, the resulting ArMs catalyzed the oxidation of pyrogallol **212** with higher catalytic performance than the free cofactor (Table 27, entries 10-13).

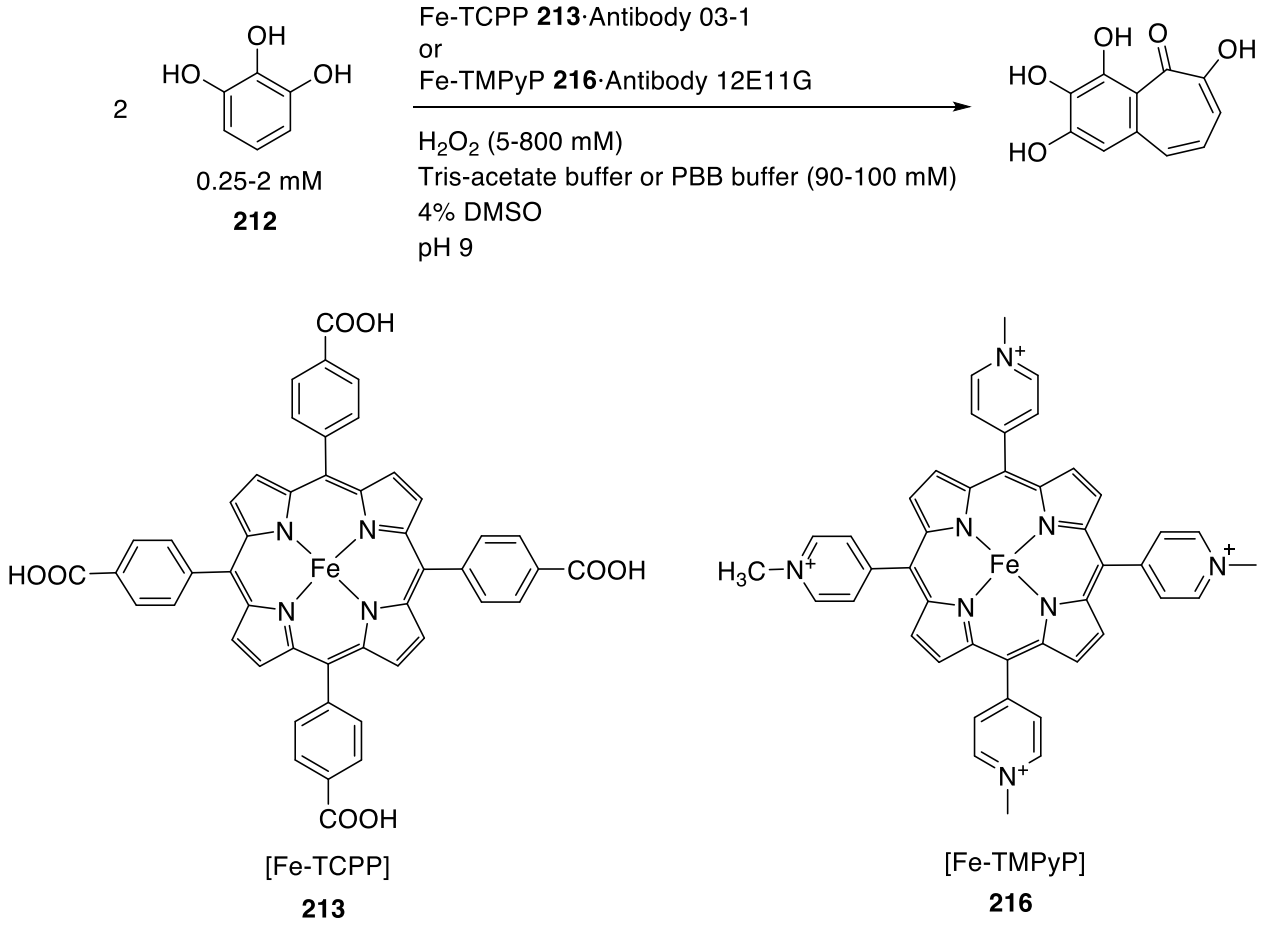

Scheme 67. Oxidation of pyrogallol catalyzed by iron porphyrin derivatives in the presence of an antibody.

In 2002, Mahy and coworkers investigated the impact of added imidazole on the peroxidase activity of their hemoabzyme to mimic the histidine ligation found in natural peroxidases.[381] The effect was deleterious in the case of hindered porphyrins: the peroxidase activity of **214**·Ab-13G10 decreased by fifty percent upon addition of 50 mM imidazole. (Scheme 66) However, for **215**·Ab-13G10, addition of 50 mM imidazole increased the k_{cat}/K_M by a factor ~15 (Table 27, entries 14 and 5). Under these conditions, **215**·Ab-13G10 displayed higher k_{cat} and k_{cat}/K_M than **214**·Ab-13G10 (Table 27, entries 8, 9 and 15).

To further improve catalytic activity, microperoxidase 8 (MP8, **217**), which contains an intramolecular imidazole-moiety, was also examined as a catalyst.[382] MP8 is a digestion product of the horse cytochrome *c* and consists of a heme [Fe(PPIX)] linked to an

octapeptide via two thioether linkages and provides a histidine ligated to iron. The IgG_1 monoclonal antibody Ab-3A3 binds **217** with a dissociation constant $K_D \sim 10^{-7}$ M. **217** alone catalyzes peroxide degradation as well as monooxygenation reactions; however, its performance is limited by dimerization and by its oxidative degradation during catalysis. Upon integration within the antibody, the authors hoped to alleviate these challenges and to improve catalytic efficiency by providing a well-defined second coordination sphere environment for enantioselective monooxygenation. They investigated **217**·Ab-3A3 for peroxidase activity toward both *o*-dianisidine (**210**) and ABTS (**211**) (Scheme 68). The **217**·Ab-3A3 showed a $k_{cat}/K_M \sim 3.3 \times 10^4$ $M^{-1}.s^{-1}$ with **210** as substrate. This corresponds to the highest catalytic efficiency reported to date for an hemoabzyme (Table 27, entry 17). This represents a ~50 % improvement over the free cofactor **217** (Table 27, entry 16).

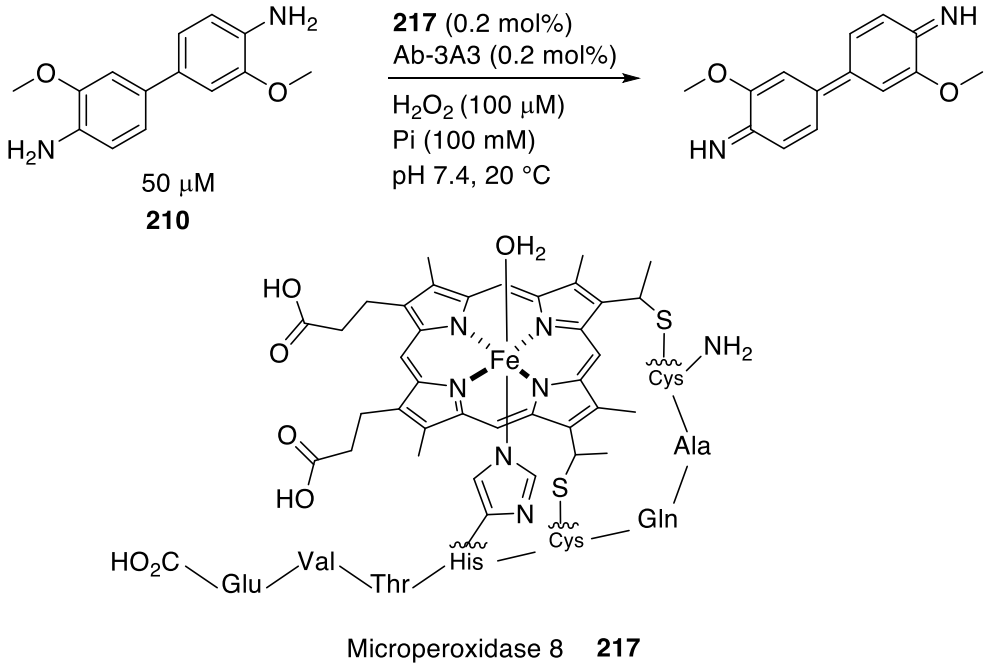

Microperoxidase 8 **217**

Scheme 68. Peroxidase activity of **217** is enhanced upon binding to Ab-3A3.

In the presence of hydrogen peroxide and a nitrite anion, **217**·Ab-3A3 also catalyzes the nitration of phenol **218** to yield in *para*-nitrophenol ***p*-219** and *ortho*-nitrophenol ***o*-219** with an 11 : 8 regioselectivity (Scheme 69).[383] Upon incorporation into the antibody Ab-3A3,

both the activity (36 TON vs. 19 TON) and the selectivity increased: the ***o*-219** was favored by a factor two over ***p*-219**.

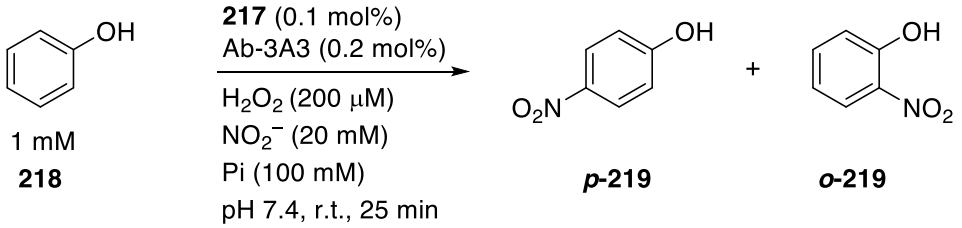

Scheme 69. Supramolecular assembly of **217** with Ab-3A3 yields an ArM for the nitration of phenol. (The catalyst loading is reported vs. the hydrogen peroxide concentration)

In 2004, Mahy and coworkers reported a "Trojan Horse" strategy to construct ArMs. In the previous hemoabzymes, antibodies were raised against a molecule that is directly involved in the reaction (e.g. the catalyst, a structural analog of a reaction intermediate or transition state). In the "Trojan Horse" strategy, an anchor moiety was used as hapten. This constitutes a versatile means to elicit an host-anchor couple for assembling ArMs, alleviating the requirement of natural protein-cofactor specific interactions. As proof of principle, they tethered a porphyrin to estradiol (**220**, Scheme 70) and incorporated this cofactor into Ab-7A3, an antibody raised against estradiol.[384-386] The resulting antibody·porphyrin conjugate **220**·Ab-7A3 had an affinity K_D = 4 x 10^{-7} M and displayed peroxidase activity twofold improved compared to the free cofactor **220**. [385]

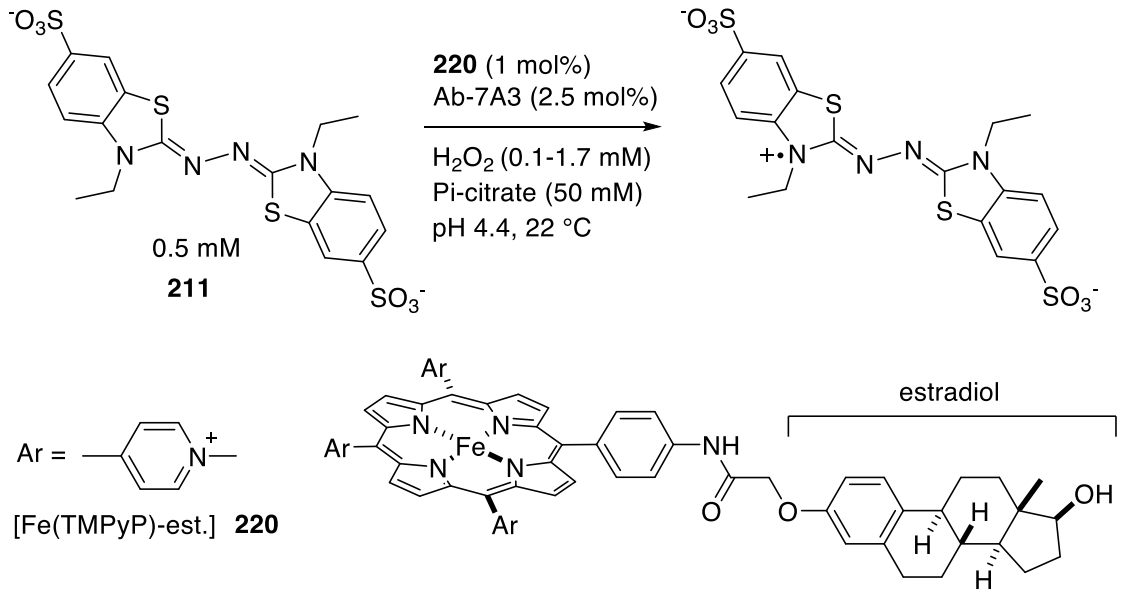

Scheme 70. A Trojan Horse anchoring strategy affords an "Hemoabzyme" with peroxidase activity.

Table 27. Selected results for the peroxidase activity of “hemoabzymes”.

Entry	Cof.	Protein	Sub.	pH	T (°C)	[Cof] (μM)	[H2O2] (mM)	KM (mM -1)	*k*cat (s -1)	*k*cat/KM (s-1M-1)	Ref
1	**20**	–	**210**	8.0	10	0.5	5	43	2.77	64	[133]
2	**20**	Ab-7G12	**210**	8.0	10	0.5	5	24	6.57	274	[133]
3	**20**	No Protein	**210** (0.3 mM)	8.0	10	0.3	0.0103-0.613	43	5.5	128	[378]
4	**20**	Antibody 2B4	**210** (0.3 mM)	8.0	10	0.3	0.0103-0.613	25	1.3	51	[378]
5	**213**	L-Ab-13-1	**212**	8.0	37	0.5	5	2.3	11.12	4833	[376]
6	**214**	–	**211**	5.0	20	0.2	1	42	0.85	21	[377]
7	**214**	Ab-14H7	**211**	5.0	20	0.2	1	9	1.05	119	[377]
8	**214**	Ab-13G10	**211**	5.0	20	0.2	1	16	1.67	105	[377]
9	**214**	Ab-13G10	**211**	4.6	20	0.2	0.7	16	9.33	222	[387]
10	**213**	No Protein	**212**	9.0	–	0.5	5	–	0.15	–	[134]
11	**213**	Antibody 03-1	**212**	9.0	–	0.5	5	4.0	0.83	208	[134]
12	**216**	No Protein	**212**	9.0	r.t.	0.5	50	–	1.38	–	[380]
13	**216**	Antibody 12E11G	**212**	9.0	r.t.	0.5	50	8.6	11.3	1318	[380]
14	**215**	Ab-13G10	**211**	5.0	19	0.3	0.7	34	0.53	15.7	[381]
15	**215**	Ab-13G10	**211**	5.0	19	0.3	0.7	10a	2.53a	253a	[381]
16	**217**	–	**210**	7.4	20	0.1	0.1	0.4	9.83	24580	[382]
17	**217**	Ab-3A3	**210**	7.4	20	0.1	0.1	0.45	14.75	32780	[382]

[a] 50 mM imidazole added.

Many hemoproteins, including myoglobin, cytochrome b5, horseradish peroxidase, and cytochromes P450 possess a Fe-protoporphyrin IX cofactor (FePPIX). Since FePPIX is

bound in the pocket of hemeproteins via only non-covalent and dative interactions, it can readily be removed under acidic conditions. The resulting apo-hemoprotein can be reconstituted with synthetic FePPIX analogues to generate ArMs. [52]

Hayashi and coworkers varied the propionate side chain of PPIX, hypothesizing that this could affect substrate-binding.[329] A double-winged Fe-PPIX derivative (**223**) that possessed two aromatic rings and eight carboxylates (Figure 23) was synthesized and used to reconstitute apo-Mb. Compared to **222**·Mb, **223**·Mb displayed a higher k_{cat} and a lower K_M for the oxidation of guaiacol (**221**) with hydrogen peroxide (Table 28, entries 1 and 2 and Scheme 71), suggesting that the dendridic wedges act as substrate-binding moieties. Further improvements to catalytic activity were realized using the Mb H64D variant.[330] Reconstituting this scaffold with **222** and **223** led to ArMs that oxidized **221** with k_{cat}/K_M 96- and 434-fold higher than the ArMs generated using the wt Mb scaffold(Figure 23, Table 28, entries 3-6).

While reconstituting Mb with double-winged Fe-PPIX cofactors led to ArMs with reduced K_M, the improvement for k_{cat} was modest (Table 28, entries 3-6). Since the chemical modification of both propionates of **222** decreased the reactivity of the corresponding oxoferryl intermediate, the single-winged Fe-PPIX cofactor **224** was also prepared (Figure 23).[388] When bound to Mb, **224** can form hydrogen bonds between its unmodified propionate and Mb R45 to lock the orientation of the cofactor. Accordingly, **224**·Mb (H64D) showed 20-fold higher k_{cat} and 3.7-fold higher k_{cat}/K_M for guaiacol **221** oxidation compared with **223**·Mb (H64D) (Table 28, entries 6 and 7).

Hayashi and coworkers also reconstituted Mb with Fe-porphycene **225**, a constitutional isomer of Fe-PPIX (Figure 23).[331] Fe-porphycene **225** binds to myoglobin (Mb) more tightly than Fe-PPIX due to a stronger interaction between the porphycene Fe center and

with His93. This strong electron σ-donation also increases the peroxidase activity of the ArM. In the presence of hydrogen peroxide, the rate of guaiacol oxidation catalyzed by **225**·Mb is eleven-fold higher than that observed with native Mb (**222**·Mb) (Table 28, entries 8 and 9). (see active site in Figure_15). The same group also reconstituted HRP with Fe-porphycene **225** since the active species responsible for the peroxidase activity has a longer lifetime in HRP compared to Mb (Figure 23).[389] In the presence of hydrogen peroxide, **225**·HRP oxidized the guaiacol **221** with a comparable rate to native HRP (**222**·HRP). (Table 28, entries 10 and 11).

Finally, Fe-corrole **226** was also used to reconstitute both Mb and HRP. Hayashi and coworkers hypothesized that the high-valent oxidation states of this cofactor might be better stabilized due to the trianionic character of the corrole (Figure 23). The resulting Mb- and HRP-based ArMs were used to catalyze guaiacol oxidation in the presence of hydrogen peroxide. The catalytic activity decreased in the following order: **222**·HRP > **226**·HRP >**226**·Mb >> **222**·Mb (Table 28, entries 12-15).[390]

Table 28. Selected results for the peroxidase activity by reconstituted hemoproteins with iron porphyrin derivatives.

Entry	Cof.	Protein[a]	Sub.	pH	T (°C)	[Cof] (μM)	[H_2O_2] (mM)	K_M (mM^{-1})	k_{cat} (s^{-1})	k_{cat}/K_M (s^{-1}M^{-1})	TOF (s^{-1})	Ref
1	**222**	Mb (WT)	**221**	7.0	20	1	9.7	32	0.36	11	–	329
2	**223**	Mb (WT)	**221**	7.0	20	1	9.7	7.4	1.1	149	–	329
3	**222**	Mb (WT)	**221**	6.0	25	2	100	54	2.8	53	–	330
4	**223**	Mb (WT)	**221**	6.0	25	2	100	3.4	6.2	1800	–	330
5	**222**	Mb (H64D)	**221**	6.0	25	2	15	1.8	9.0	5100	–	330
6	**223**	Mb (H64D)	**221**	6.0	25	2	15	0.052	1.2	23000	–	330
7	**224**	Mb (H64D)	**221**	6.0	25	4	100	0.29	24	85000	–	388
8	**222**	Mb (WT)	**221**	7.0	20	1	20	–	–	–	0.021	331
9	**225**	Mb (WT)	**221**	7.0	20	1	20	–	–	–	0.230	331
10	**222**	HRP (WT)	**221**	7.0	25	0.1	4	–	–	–	40	389
11	**225**	HRP (WT)	**221**	7.0	25	0.1	4	–	–	–	38	389
12	**222**	Mb (WT)	**221**	7.0	20	2	5	–	–	–	~0	390
13	**226**	Mb (WT)	**221**	7.0	20	2	5	–	–	–	0.43	390
14	**222**	HRP (WT)	**221**	7.0	20	2	5	–	–	–	11	390
15	**226**	HRP (WT)	**221**	7.0	20	2	5	–	–	–	1.6	390

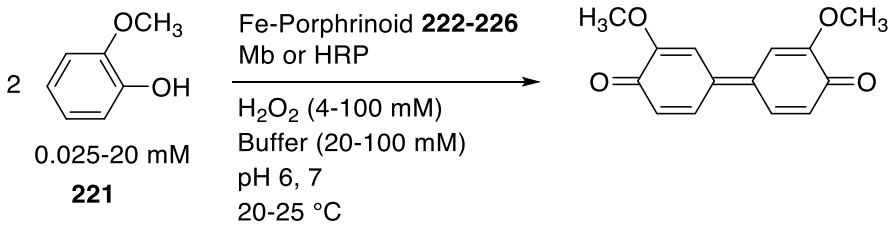

Scheme 71. Oxidation of guaiacol performed by myoglobin and horseradish peroxidae.

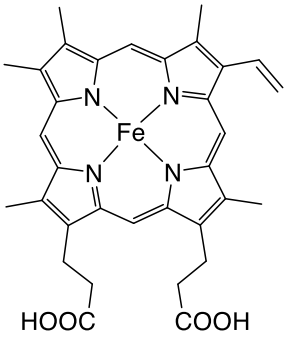

[Fe-protoporphyrin IX]

222

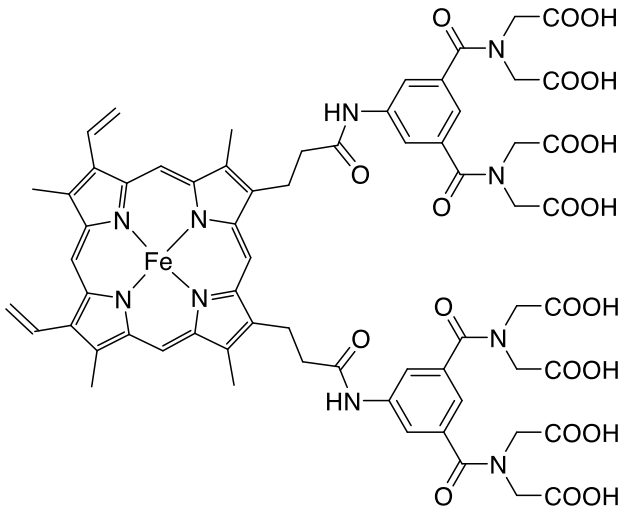

[Fe-double winged protoporphyrin IX]

223

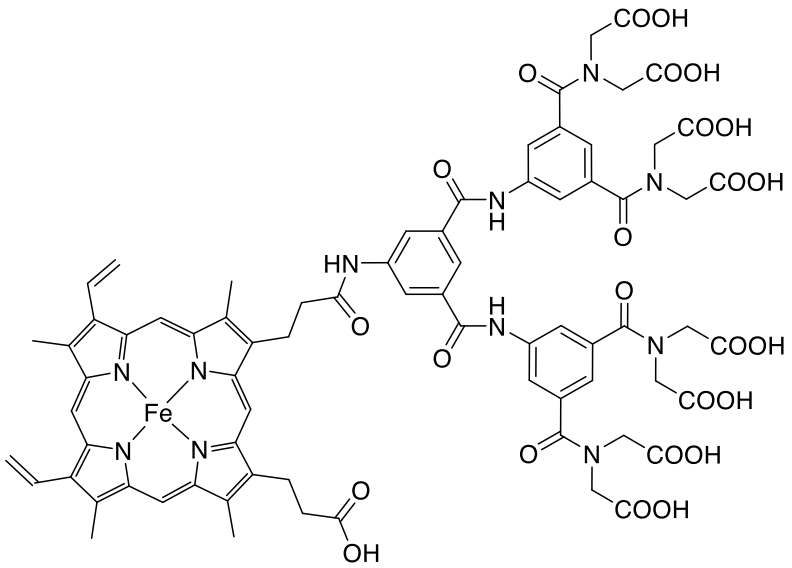

[Fe-single winged protoporphyrin IX]

224

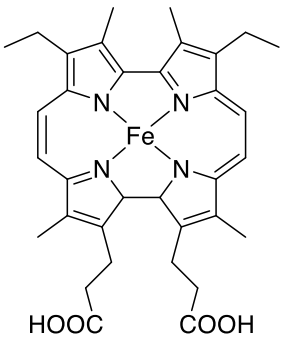

[Fe-porphycene]

225

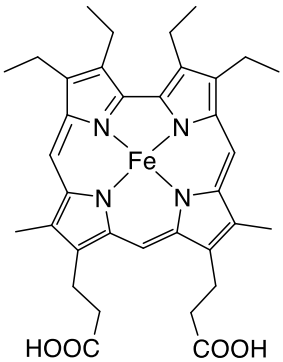

[Fe-corrole]

226

Figure 23. Cofactors used for the oxidation of guaiacol and thioanisole in the presence of apo heme proteins.

De *novo* designed proteins have also been used as scaffolds to generate ArM oxidases and oxygenases via metallation with both metal ions and metal porphyrin complexes. DeGrado and Kaplan, for example, designed a phenol oxidase based on DF_{tet}, a four-chain heterotetrameric helix bundle from the family of the dueferri (DF) proteins.[391] The *de novo*-designed metalloenzyme contains two Fe-ions in its active site and its catalytic activity depends on the presence of dioxygen. Phenol oxidase activity occurs via formation of an oxo-bridged di-Fe(III) species (Scheme 72). Combinations of different monomeric units and introduction of mutations in the active site (i.e. increasing the size of cavity in the active site) led to highly active variants. The engineered metalloenzymes catalyze the oxidation of 4-aminophenol (**227**) to the corresponding benzoquinone monoimine (**228**). Catalytic efficiencies (k_{cat}/K_M) of up to 1540 $M^{-1} \cdot min^{-1}$ along with a ~1000-fold rate enhancement relative to the background reaction were achieved, and the best variant (G_4-DF_{tet}) provided over 100 turnovers.

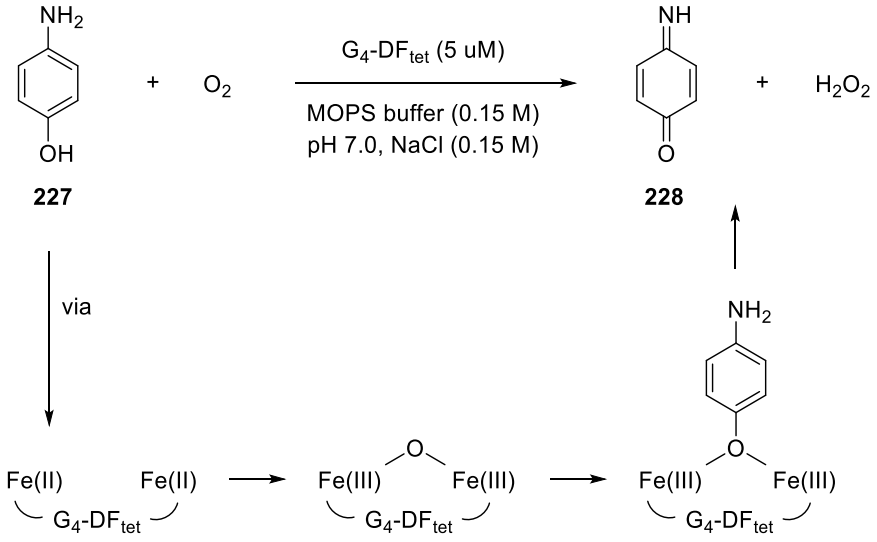

Scheme 72. Oxidation of 4-aminophenol (**227**) using an engineered di-iron metalloenzyme G_4-DF_{tet}.

Lombardi *et al.* also engineered an ArM oxidase using the DF1 scaffold (PDB entry 1EC5), a well-characterized metalloprotein of the dueferri protein family.[392] DF1 is a dimeric

protein in which each monomer adopts an helix-loop-helix structure.[393] The active site consists of two Fe-ions coordinated by two glutamates and one histidine each (Figure 24). Introducing mutations beneficial for the catalytic activity of the G_4-DF_{tet} analogue led to a destabilization of the protein fold, but this issue was solved by mutating the interhelical turn. An NMR structure of the new DF3 variant was determined (PDB entry 2KIK), and the designed artificial metalloenzyme displayed oxidase activities towards various substrates (Table 29).

Table 29. Oxidase activity of *de novo*-designed artificial di-iron oxo-proteins.

Entry	Protein	Substrate	K_M (mM)	k_{cat} (min^{-1})	k_{cat}/K_M ($M^{-1} \cdot min^{-1}$)	TON	Ref
1	DF3	3,5-di-*tert*-butylcatechol	2.09 ± 0.31	13.2 ± 1.2	6315		392
2	DF3	**227**	1.97 ± 0.27	2.72 ± 0.19	1380	>50	392
3	DF3	*p*-phenylenediamine	8.87 ± 2.58	0.73 ± 0.03	83		392
4	G_4-DF_{tet}	**227**	0.83 ± 0.06	1.30 ± 0.10	1540	>100	391

Reaction conditions: HEPES buffer (100 mM, pH 7.0), 100 mM NaCl.

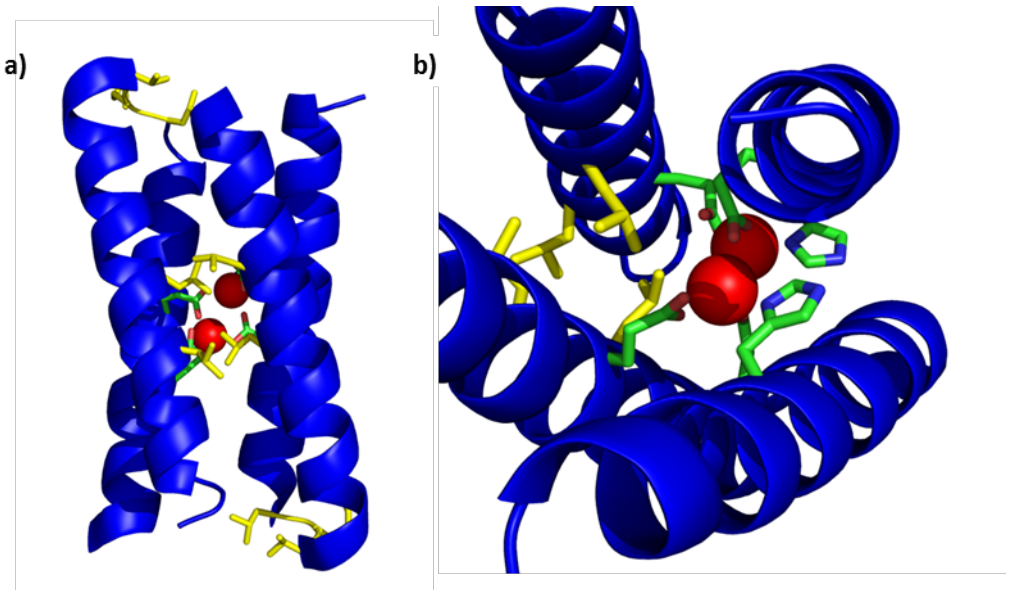

Figure 24. Cartoon representation of DF1 structures (PDB: 1EC5). Side view of the designed four helix bundles. Highlighted, in yellow, the amino acid mutations in the turn and in proximity of the active site, introduced to stabilize the protein scaffold and to allow substrates to approach the metal ions, respectively a). Zoom into the active site of Due Ferro protein. Iron centers are depicted in red. Coordinating residues (two His and four Glu) are represented as stick and coloured by element b).

DeGrado *et al.* repurposed a *de novo*-designed metalloprotein originally designed to

oxidize hydroquinones in order to catalyze selective *N*-hydroxylation of arylamines.[394] DFsc, a single-chain four-helix bundle protein from the dueferri family (PDB entry 2HZ8), was selected as template for the redesign. Four Ala → Gly mutations (analogous to the G_4-DF_{tet} construct) afforded a highly active hydroquinone oxidase (G4DFsc). Inspection of the crystal structure of AurF (PDB entry 2JCD), an *N*-oxygenase containing a di-iron catalytic center, inspired the incorporation of a third metal-binding His residue in the scaffold. Following the introduction of three additional stabilizing mutations, a functional *N*-hydroxylase was created (3His-G4DFsc, PDB entry 2LFD). Both enzymes displayed high affinity for Fe(II) (K_d = 70 ± 3 µM and 30 ± 2 µM for G4DFsc and 3His-G4DFsc respectively). G4DFsc had a high catalytic activity towards the oxidation of 4-aminophenol (**227**), whereas no *N*-hydroxylase activity was observed. The opposite trend was observed for 3His-G4DFsc. This construct showed high activity towards the selective *N*-hydroxylation of *p*-anisidine (**229**, Scheme 73) thus highlighting the flexibility of *de-novo* designed metalloproteins and the power to repurpose the reaction specificity by introduction of single mutations. Recently, DeGrado *et al.* identified the actual active species of the two due-ferri scaffolds (G4DFsc and 3His-G4DFsc) and suggested mechanisms explaining their different reactivities.[395]

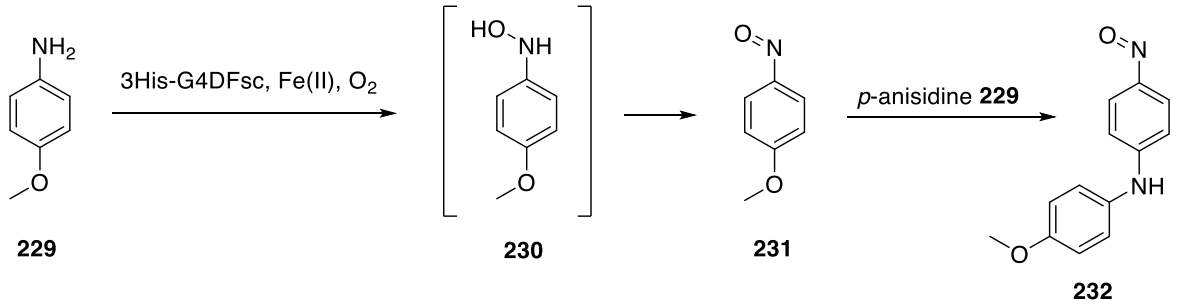

Scheme 73: Selective *N*-hydroxylation of *p*-anisidine (**229**) with the *de-novo* designed metalloprotein 3His-G4DFsc. The *N*-hydroxylated product (**230**) is thought to undergo disproportionation to form *p*-nitrosoanisole (**231**), which reacts with another molecule of *p*-anisidine (**229**) via a nucleophilic aromatic substitution to yield 4-nitroso-4`-

methoxydiphenylamine (**232**).

In 2008, Mahy and coworkers inserted the porphyrin [Fe(TpCCP)] (**213**) into xylanase A (Xln) via supramolecular interactions.[396] This protein possesses a hydrophobic pocket that may host a [M(TpCCP)]-complex. Even though modeling studies suggested that the porphyrin does not entirely fit into the cleft, the host-guest affinity was in the micromolar range (K_D = 0.5 μM), ensuring a high concentration of the desired ArM during catayltic experiments. The peroxidase activity of this ArM was determined via its ability to promote the oxidation *o*-dianisidine **210**, Scheme 63. Compared to **213** alone, **213**·Xln displayed an 1.8 fold higher k_{cat} but a 3-fold lower k_{cat}/K_M, arising from a lower affinity for the substrate (i.e. K_M 5 times higher) (Table 30, entries 1 and 2).

Table 30. Selected results for the peroxidase activity by **213**·Xln.

Entry	Cof.	Protein	Sub.	pH	T (°C)	[Cof] (μM)	[H_2O_2] (mM)	K_M (mM $^{-1}$)	k_{cat} (s $^{-1}$)	k_{cat}/K_M ($s^{-1}M^{-1}$)	Ref
1	**213**	–	**210**	7.5	20	1.2	2.4	0.16	0.49	3041	[396]
2	**213**	Xln	**210**	7.5	20	1.2	2.4	0.8	0.87	1083	[396]

In 2012, Itoh and Fujieda *et al.* prepared artificial dicopper oxidase by substitution of the di-zinc moiety of β-lactamase.[397] This artificial metalloenzyme catalyzed the oxidation of catechol under aerobic conditions. Based on molecular dynamics simulations, they redesigned the copper binding site to more closely mimic the dicopper active site of natural catechol oxidases (Figure 25). The resulting triple mutant displayed 87-fold higher k_{cat}/K_M values for the 4-*tert*-buthylcatecol **233** oxidation compared to the wild type β-lactamase (Scheme 74 and Table 31).

Table 31. Selected results for catechol oxidation by dicopper reconstituted β-lactamase.

Entry	Cofactor	Protein[a]	Sub.	pH	T (°C)	[ArM] (μM)	K_M (mM $^{-1}$)	k_{cat} (s $^{-1}$)	k_{cat}/K_M ($s^{-1}M^{-1}$)	Ref
1	Copper ion	β-lactamase (WT)	**233**	7.0	25	20	7.7	1.1–	1.4–	[397]
2	Copper ion	β-lactamase (D88G-S185H-	**233**	7.0	25	20	3.2	40	125	[397]

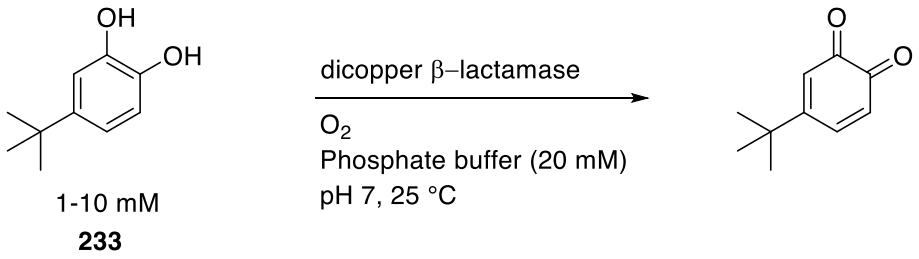

Scheme 74. Oxidation of catechol derivatives catalyzed by dicopper-reconstituted β-lactamases.

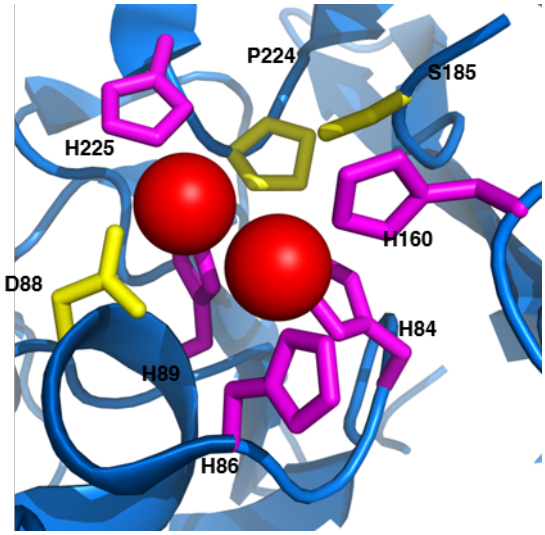

Figure 25. Active site structure of copper-substituted metallo β-Lactamase (PDB: 2FU7). Highlighted, in yellow, the amino acid position mutated to convert β-lactamase in catechol oxidase (D88G, S185H, P224G). In magenta the five coordinating histidine residues (displayed as spheres).

In 2015, Ward and coworkers constructed artificial copper oxidase by mining the pdb to identify proteins containing latent facial triad motifs, i.e. proteins would contain a metal binding site following a single point mutation. Following mutagenesis and metallation, the resulting ArMs might be expeted to possess radically different catalytic activity compared to the wild-type proteins. The algorithm “Search of Three-dimensional Atom Motifs in Protein Structure” (STAMPS)[398] was used to identify thirteen proteins with a putative facial triad motifs.[399] Among the identified proteins, only 6-phosphogluconolactonase (6-PGLac hereafter), afforded peroxidase activity toward *o*-dianisidine in the presence of H_2O_2 upon

metallation $CuSO_4$ (Scheme 75**)**. Using glucose oxidase with glucose and O_2 in the presence of Cu·6-PGLac led to slightly improved activity. A dramatic increase in activity was observed using *t*-BuOOH as oxidant. Michaelis-Menten kinetics were determined K_M = 11 μM, $k_{cat} = 78 \cdot 10^3 \cdot s^{-1}$, and the k_{cat} obtained was only four orders of magnitude lower than natural horseradish peroxidase ($7.7 \cdot 10^7$ $M^{-1}s^{-1}$). To identify the exact copper localization within 6-PGLac, crystals soaked with excess Cu^{2+} were subjected to X-ray analysis. Three copper binding sites were identified, one of which was the predicted triad (His67, His104, Asp131). However, only the two histidines were bound, while the Asp131 was rotated away (O⋯Cu = 6.6 Å) Mutation of the two surface histidines to alanines (H9A or H95A) revealed that, despite the copper electron density found in the X-ray analysis, these were not catalytically active.

a)

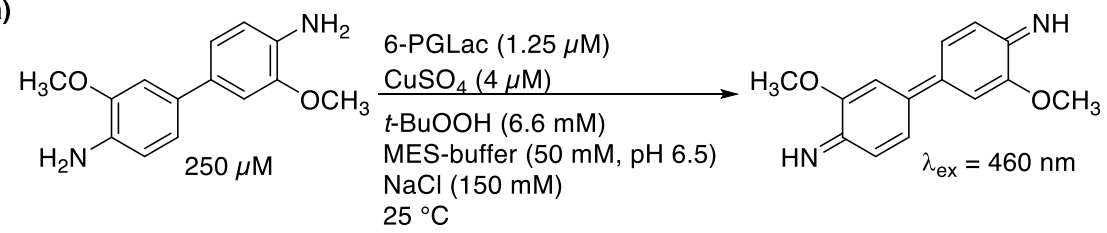

b)

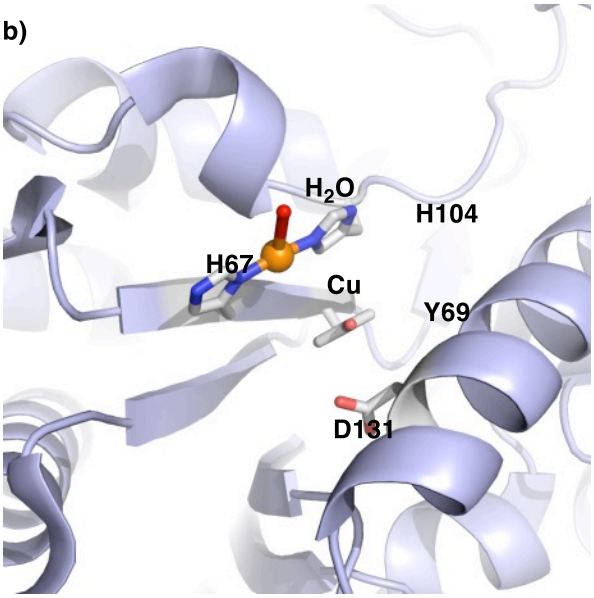

c)

Enzyme	k_{cat}/K_M x 10^3 ($M^{-1}s^{-1}$)
Cu-6-PGLac	
WT	6.9
H67F	N.D.
H104F	N.D.
D131A	7.7
Horseradish Peroxidase	71000

Scheme 75. A single point mutation of 6-phosphogluconolactonase yields a facial triad (H67-H104-N131D). Addition of $CuSO_4$ leads to an artificial peroxidase.[399] a) A colorimetric assay was applied to test peroxidase activity of Cu-PGLac in the presence of

t-BuOOH; b) the crystal structure of the artificial peroxidase (PDB code 4tm7) highlights copper coordination to only two histidines H67 and H104; c) mutagenesis highlights the requirement of both histidines but not of the aspartate D121.

In addition to supramolecular anchoring and dative anchoring, a non-natural ligand was directly introduced into the amino acid sequence. In 2008, Schultz and Lee incorporated the unnatural amino acid (2,2'-bipyridine-5-yl)alanine (Bpy-Ala, **237**, **Figure 26**) into the catabolite activator protein (CAP), a dsDNA binding protein of *E. coli* (**Figure 27**).[400] The engineered construct (CAP K26Bpy-Ala) showed a high affinity towards a 50-bp double-stranded DNA containing the 22-bp CAP recognition sequence (K_d = 1.90 nM vs. 0.85 nM for the wild type CAP). In the presence of Cu(II) or Fe(II), cAMP and 3-mercaptopropionic acid or ascorbic acid as a reducing agent, site specific DNA cleavage activity was observed. Thus, a DNA binding protein was repurposed into an artificial metalloenzyme. Additional DNA-cleaving ArMs are summarized in section 6.8.

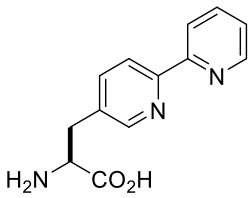

237

Figure 26: Unnatural metal binding amino acid (2,2'-bipyridine-5-yl)alanine (Bpy-Ala) (**237**) introduced in artificial zinc-finger domains.

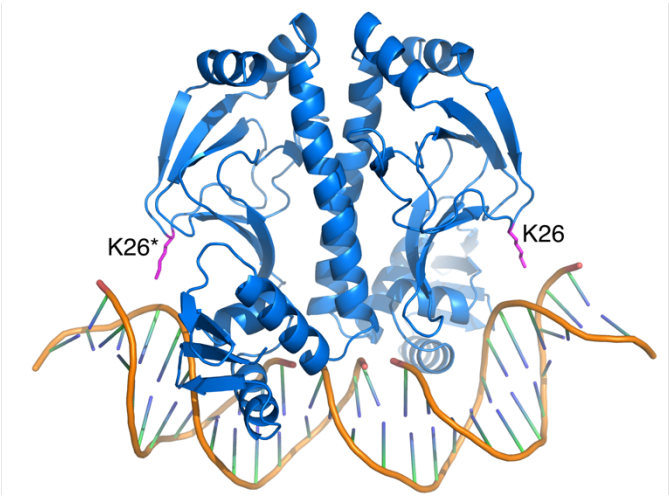

Figure 27. Catabolite activator protein CAP (PDB code 2CGP) was mutated to bear non-canonical amino acid bipyridyl-alanine in position 26. Upon addition of Cu^{2+} or Fe^{2+} and a reducing agent cleavage of the DNA substrate was achieved.

6.2 Sulfoxidation

Enantiopure sulfoxides are important building blocks for organic synthesis and have found applications as chiral auxiliaries and ligands in enantioselective catalysis.[401-403] Enantioselective oxidation of sulfides has gained considerable attention as an easy way of generating enantiopure sulfoxides.[402, 404-405] Most commonly used sulfoxidation catalysts rely on titanium, manganese, iron, or vanadium.[402, 406-407] The mechanism of asymmetric induction in these processes resembles that of several natural enzymes as the prochiral sulfide does not coordinate to the metal prior to its oxidation. Instead, a metal-activated oxygen moiety (e.g. a metal-oxo, -peroxo, etc.) is delivered to a suitably-positioned sulfide. Accordingly, sulfoxidation is an attractive reaction to scrutinize the role of second coordination sphere interactions that could be imparted by a host protein containing a suitable sulfoxidation catalyst. In this context, the asymmetric sulfoxidation of thioanisole-type substrates has become a benchmark reaction to evaluate the performance of artificial sulfoxidases (Scheme 76). Most of the ArMs previously described for their peroxidase activity have also been tested as sulfoxidases.

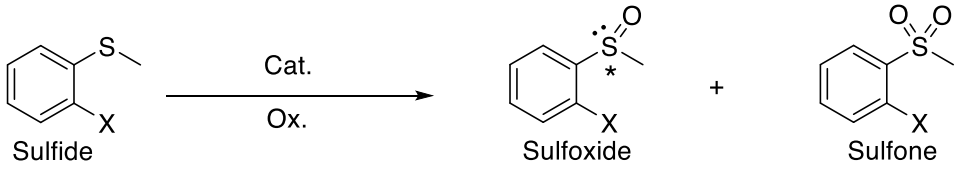

27: X = H
238: X = Cl
239: X = Br

28
240
241

242

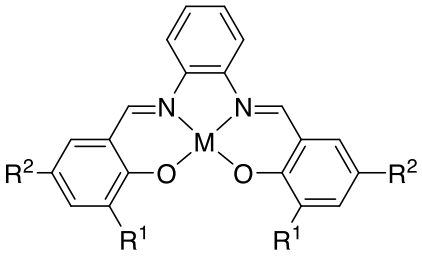

[M-salophen]

243: M = Cr, R^1 = H, R^2 = *t*-Bu
244: M = Mn, R^1 = Me, R^2 = H

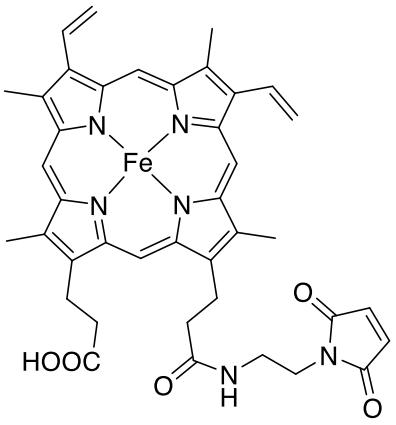

[Fe-Protoporphyrin IX] **252**

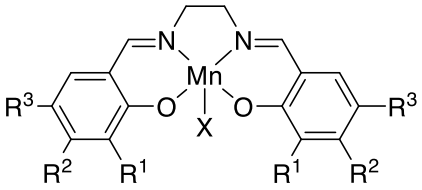

[Mn-salen]

245: R^1 = Me, R^2 = R^3 = H, no X
246: R^1 = Et, R^2 = R^3 = H, no X
247: R^1 = *n*-Pr, R^2 = R^3 = H, no X
248: X = Br, R^2 = $(CH_2)_3SS(O)_2Me$, R^1 = R^3 = H
249: X = Br, R^1 = R^2 = R^3 = H
250: X = Cl, R^3 = COOH, R^1 = R^2 = H

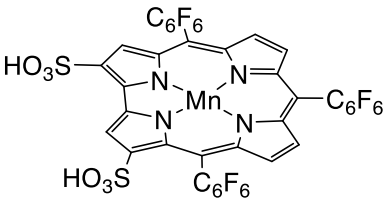

[Mn-corrole] **253**

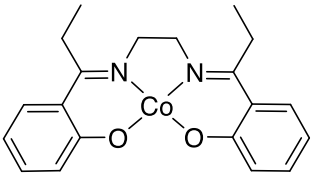

[Co-salen] **251**

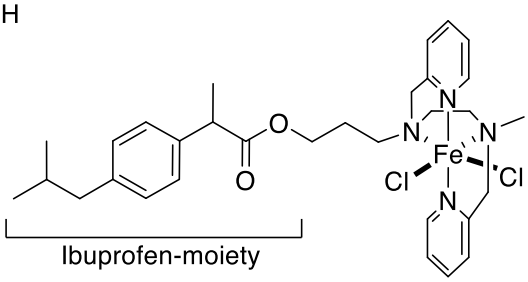

[$(Ibu\text{-}BPHMEN)FeCl_2$] **254**

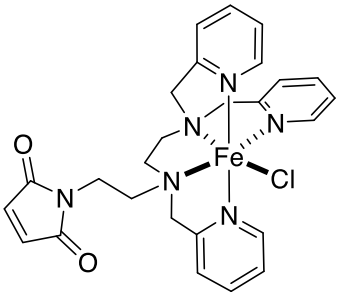

[$Fe(M\text{-}(Py)en(Py)_2)(L)$] **255**

Scheme 76. Thioanisole **27** is used as a benchmark substrate to evaluate the performance of artificial sulfoxidases. For reaction conditions and results, please refer to Table 32.

The first examples of ArM sulfoxidases were reported by the groups of Sheldon in 1998 and Keinan in 1999 (chapter 3 and Table 32, entries 1-2), and a similar antibody-based strategy was later used by Mahy and coworkers. Among the hemoabzymes that were investigated, **217**·Ab-3A3 displayed the highest peroxidase activity (Scheme 68). Mahy and coworkers later showed that this ArM catalyzes the sulfoxidation of thioanisole **27** in the presence of H_2O_2.[408] The ArM **217**·Ab-3A3 performed better than **217** alone, with 82 and 38 TON respectively (Table 32, entries 3-4). The ArM was also more enantioselective, with 45 % ee vs. 23 % ee in favor of the (*R*)-**28**. Those results were obtained in presence of 5 % *t*-BuOH, which significantly improved both activity and enantioselectivity of **217**, with and without Ab-3A3.

The hemoabzymes with anti-estradiol antibodies were also tested for the sulfoxidation of thioanisole **27** in presence of H_2O_2. First, **220**·Ab-7A3 was twice as active as **220** alone, and afforded for (*S*)-**28** with 8 % ee. (Table 32, entries 5-6).[384] Substitution of the *N*-methylpyridinium groups by *p*-sulfonatophenyl groups yielded an 25% less active artificial peroxidase affording similar enantioselectivity: up to 10 % ee for (*S*)-**28**.[409] Upon incorporation of the sulfonated cofactor within neocarzinostatin (NCS), the enantioselectivity slightly increased (i.e. 13 % ee), but was accompanied with a decrease in activity (i.e. 6 TON).[410]

Better results were obtained with the ArM resulting from incorporation of an iron porphyrin within xylanase, **213**·Xln instead of an antibody. Up to 40 % ee of (*S*)-**28** were achieved (Table 32, entries 7-8).[411-412] Addition of exogeneous imidazole to **213**·Xln, slightly increased the enantioselectivity, from 36 to 40 % ee, and significantly increased its activity,

from 42 to 145 TON. The authors speculate that the added imidazole mimics the effect of an axial histidine on catalysis, reminiscent of the activity observed with **217**·Ab-3A3. In summary, **213**·Xln and **217**·Ab-3A3 are the most active and enantioselective artificial sulfoxidases reported by the Mahy group and display enantioselectivities of 40 % ee (*S*)-**28** and 45 % (*R*)-**28**, respectively.

Watanabe, Ueno and coworkers reported the formation of an ArM sulfoxidase by incorporating an Fe-porphyrin cofactor into a $(gp27\text{-}gp5)_3$ (gp = gene product) scaffold from bacteriophage T4. The structure of this protein consists of a β-helical needle made of the gp5 trimer and a cup-shaped structure composed of the gp27 trimer. A cysteine residue was introduced at the bottom of the cup to react with a maleimide moiety of Fe-PPIX **252** (Scheme 76 and Figure 12).[413] The oxidation of the thioanisole **27** was investigated in the presence of hydrogen peroxide. The catalytic efficiency was enhanced tenfold in the presence of $(gp27\text{-}gp5)_3$, compared to the free cofactor **252** (Table 32, entries 9-10), which was attributed to the hydrophobic environment of the cup structure.

ArM sulfoxidases have also been generated using metal-salen and -salophen cofactors. For example, Watanabe and coworkers reconstituted myoglobin (Mb) with various Schiff-base complexes,[326] including Cr-salophen **243**, which has a similar size and shape to the native Fe-PPIX cofactor (**222**) of Mb. The reconstituted Mb ArM catalyzed enantioselective oxidation of thioanisole **27** (Scheme 76). Mutations H64D and A71G were introduced into the Mb scaffold to improve substrate access to the active site and to improve the affinity for **243**, respectively. The resulting ArM oxidized thioanisole **27** in the presence of hydrogen peroxide to afford **28** with 13% ee (Table 32, entries 11-12). A crystal structure of **244** · Mb A71G was obtained, and based on this structure, the salophen ligand was replaced with a salen ligand to create a larger substrate access pathway.[414] Modeling

suggested that the location of the metal complex in Mb depends on the nature of the 3, 3'-substituents of the salen moiety. Gratifyingly, the enantioselectivity for the thioanisole **27** oxidation was indeed influenced by the nature of the complexes **245-247**. The highest *ee* (32%) was obtained with **245**·Mb (Table 32, entry 13).

Lu later reported on a dual anchoring strategy to fix the orientation of a Mn(salen) cofactor bearing two methane thiosulfonate groups (**248**, Scheme 76) within an apo myoglobin scaffold containing two cysteine mutations L72C-Y103C. The resulting ArM catalyzed the sulfoxidation of thioanisole with higher enantioselectivity (51% ee) than an analogous system generated using the Y103C myoglobin mutant (12% ee) (Table 32, entries 14-15).[327] In both of these systems, sulfoxidation was accompanied by overoxidation to the corresponding sulfone **242**. By selecting alternate anchoring sites within Mb T39C-L72C, Lu also showed that ArMs could enhance the chemoselectivity of sulfoxidation.[328] Increased activity (52% yield), enantioselectivity (60% ee), and chemoselectivity (100% sulfoxide) were obtained for reactions catalyzed by **249**·Mb T39C-L72C (Scheme 76 and Table 32, entry 16 and Figure 15). Subsequent studies on this system suggested that polar residues in the ArM active site led to its improved activity, and the need for substrates to enter the active site via a hydrophobic region of the scaffold was believed to favor entry of sulfide over sulfoxide to impart chemoselectivity. In addition, residues in the secondary coordination sphere of the ArM active site were shown to impact the pH dependence of ArM catalysis relative to cofactor alone.[415]

In 2009, Ménage and coworkers inserted Mn−salen complexes (**250**, Scheme 76) into human serum albumin (HSA hereafter) to catalyze the oxidation of sulfide **27** to the corresponding sulfoxide **28**.[416] Serum albumins have been used in the past as host to catalyze a variety of reactions.[27, 91, 93] The choice of HSA as a host for ArM formation was

based on its ability to bind a variety of small hydrophobic molecules. Indeed, facile ArM formation was realized by incubating HSA with one equivalent of cofactor **250**, and 1:1 HSA:**250** binding stoichiometry was observed (K_D = 8 μM). The resulting ArM catalyzed oxidation of **27** in the presence of aqueous NaOCl (2 eq) at pH 5.2 to provide a mixture of sulfoxide **28** (7%) and sulfone **242** (31 %). The free Mn−salen complexes tested afforded almost exclusively the sulfone **242** (60 %). When combined with HSA, however, the resulting ArM (**250**·HSA) led to formation of sulfoxide **28** exclusively (97 %, i.e. 97 TON) (Table 32, entry 17), although racemic product was obtained. No catalysis was observed when hydrogen peroxide was used instead of hypochlorite, and addition of excess **250** relative to BSA led to decreased chemoselectivity. Interestingly, the ArM remained efficient (i.e. 95 % conversion) and chemoselective (i.e. 92 : 3 ratio for **28** : **242**) upon recycling the ArM up to four times. In contrast, HSA alone lost its selectivity upon recycling. In the absence of cofactor, HSA is unspecifically oxidized by HOCl as confirmed by SDS-PAGE, which led to a gradual erosion of the chemoselectivity.

Liang and coworkers also developed an ArM sulfoxidase by incorporating a cobalt-salen cofactor into a serum albumin scaffold,.[417] **251**·BSA (Scheme 76) achieved 98 TON for the sulfoxidation of thioanisole **27** with up to 50 % ee in favor of the (*R*)-**28** (Table 32, entry 18). Improved enantioselectivity was obtained with substrate **238**: up to 87 % ee was obtained for (*R*)-**240** (Table 32, entry 19). Unfortunately, the increase in enantioselectivity was accompanied with a loss of activity and chemoselectivity (sulfoxide vs sulfone).

Mn–corroles have also been combined with serum albumins to afford ArM sulfoxidases. In 2005, Gross and coworkers reported an enantioselective artificial sulfoxidase based on a sulfonated manganese corrole **253** inserted within various serum albumins, Scheme 76. Human serum albumin was shown to bind **253** with a dissociation constant in the

nanomolar range. In terms of catalysis, however, the best results were obtained with bovine serum albumin (BSA). In presence of hydrogen peroxide, **253**·BSA achieved 42 TON for thioanisole **27** sulfoxidation, with up to 52 % ee in favor of the (*S*)-**28** (Table 32, entry 20). The enantioselectivity increased with *o*-halogen-bearing substrates albeit at the cost of reduced activity: sulfoxidation of 2-bromo-thioanisole **239** proceeded in 74 % ee (*S*)-**241** but only 8 TON (Table 32, entry 21). The iron-containing corrole was also tested, but the corresponding ArMs had lower activity and selectivity. These same authors later evaluated ArMs generated from incorporation of metal-corrole complexes into other serum albumins. Interestingly, **253**·RSA (rabbit serum albumin) was used to complete the synthesis of armodafinil (**257**), a FDA-approved eugeroic drug: up to 70 % ee (*R*)-**257** could be achieved (Scheme 77 and Table 32, entry 22).[418]

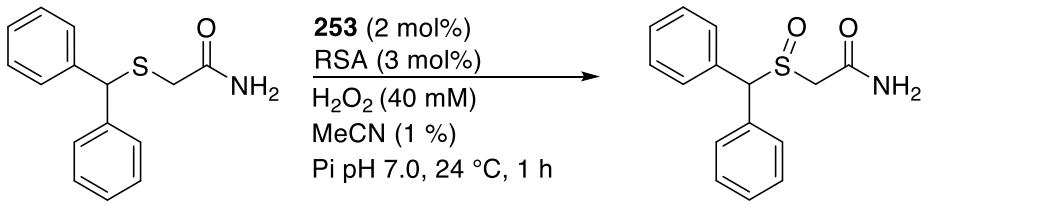

10 mM
256

up to 70 % ee for (*R*)-**257** (= armodafinil)

Scheme 77. Binding of a Mn-corrole to various serum albumins afford an artificial sulfoxidases for armodafinil synthesis.

Building on the **253**·BSA ArM reported by Gross and coworkers, Mahy and Gross later reported an ArM sulfoxidase that used water as an oxygen source.[419-420] Upon irradiation, a $[Ru(bpy)_3]^{2+}$–photosensitizer sequentially abstracts two electrons from [Mn(III)(Corrole)(OH_2)] to yield [Mn(V)(Corrole)(O)] in the presence of [Co(III) $(NH_3)_5Cl]^{2+}$ as an electron acceptor. The active [Mn(V)(Corrole)(O)] transfers its oxygen to thioanisole **27**. Isotope-labeling confirmed that water is indeed the oxygen source in the sulfoxide **28** (21 TON 16 % ee (*R*)-**28**, Table 32, entry 23). Strinkingly, when H_2O_2 was used as oxidant

in the presence of [Mn(metallocorrole)] · BSA, the opposite enantiomer (*S*)-**28** was produced. This clearly demonstrates that, depending on the oxidant, that the active species are not identical.[419]

Ward and coworkers investigated the propensity of vanadyl-loaded Sav to promote the asymmetric sulfoxidation of aryl-alkyl thioethers.[421] In the presence of the Sav scaffold (twofold excess of biotin-binding sites vs. VO^{2+}), vanadate sulfoxidase activity increased from 28 to 50 TON for thioanisole **27** (Scheme 78 and Table 32, entries 24 and 26). The Sav scaffold a 46 % ee in favor of (*R*)-**28**. While the VO^{2+} source did not influence the reaction, the oxidizing agent had a dramatic influence on the observed enantioselectivity. Only *t*-BuOOH afforded high activity and enantioselectivity, while H_2O_2 afforded (*rac*)-**28**) and cumylhydroperoxide yielded the opposite enantiomer (S)-**28** (15 % ee). Electron-rich aromatic thioethers yielded good to very good enantioselectivities: (*R*)-**258** and (*R*)-**259** were produced in 90 and 93 % ee respectively (Table 32, entries 27-28). Dialkyl thioethers **260** and **261** afforded moderate ee. In the presence of biotin, no enantioselectivity was obtained, suggesting that the vanadyl moiety is located within the biotin-binding site. This assumption was confirmed upon mutation of biotin-binding key residue Sav D128A to afford *rac*-**28**. The X-band EPR signal obtained with complex $VO(H_2O)_5$ · Sav is very similar to the free $VO(H_2O)_5$, suggesting that the protein binds the complex only via second coordination sphere interactions. It is interesting to note that, despite the poorly defined localization of the vanadyl moiety within Sav, the resulting sulfoxidase affords very good enantioselectivities, highlighting the flexibility of this facinating protein scaffold.

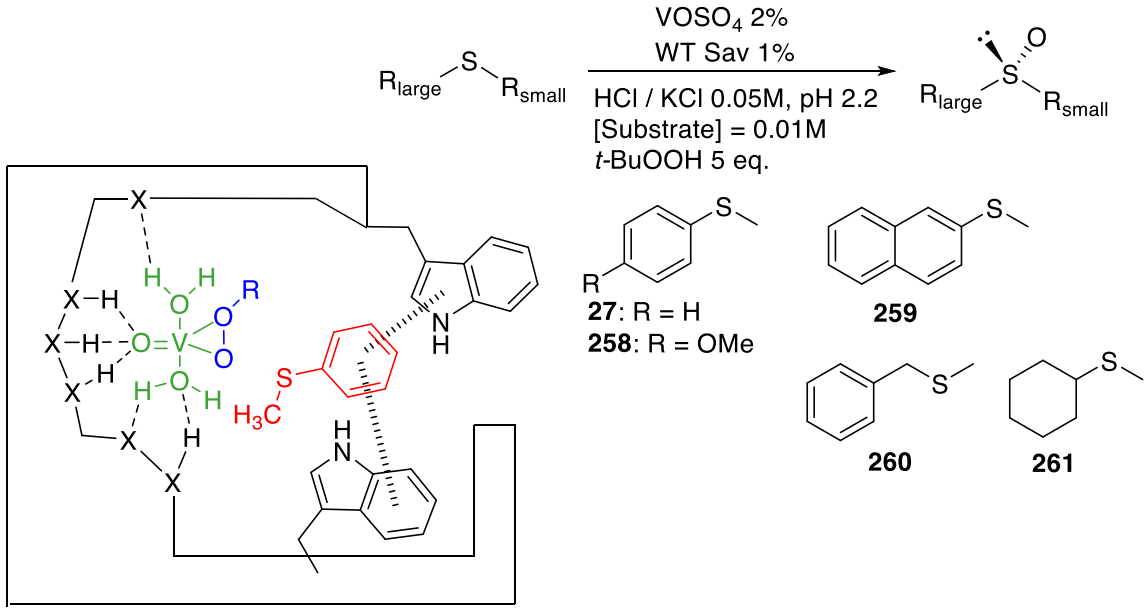

Scheme 78. Incorporation of $VOSO_4$ within Sav affords an artificial sulfoxidase. Adapted with permission from ref.[421] Copyright ACS Publication 2016.

Artificial sulfoxidases based on non-porphyrin iron complexes have been investigated by Ménage and coworkers. For example, Fe complexes **268, 254** (Scheme 79) were incorporated into NikA, a periplasmic nickel-binding protein.[422] Ménage and coworkers had previously reported on the incorporation of small iron complexes into the pocket of NikA: they characterized the complex · protein assembly as well as investigated the iron-mediated oxygen insertion in an aromatic C-H bond of the ligand.[423-424] The affinity of these complexes for NikA lies in the μM range. Based on the structure of the ArM, docking simulations of various substrates into the cofactor-loaded cavity were performed. The substrates evaluated all contained an R1-S-CH_2-X moiety. The main selection criterion was the Fe·····S distance, to favour an Fe····O····S transition state. The docking revealed that a family of molecules, containing an R_1-S-CH_2-C(O)-NH-R_2 motif (R_1, R_2 are aromatic), met this criterion. The simplest molecule, with R_1 = 3-amino-phenyl and R_2 = α-naphthyl, was selected as the starting point for substrate design. This skeleton is reminiscent of omeprazole and modafinil, drugs containing an enantiopure sulfoxide moiety. The

interaction of the docked molecule within the cavity is stabilized by a hydrogen-bond involving a glutamine side chain and the amide bond of the substrate. Six substrates derived from this skeleton were evaluated. In the absence of protein, oxidation of **262** yielded neither sulfoxide **264** nor sulfone. Instead, the dichlorinated sulfoxide species **265** was isolated. When **268**·NikA was added to a reaction mixture containing sulfide **262** (in a ratio ArM : substrate : NaOCl 1 : 255 : 600), it afforded 173 TON in 4 h and a selectivity of 87 % in favor of sulfoxide **264** of (Table 32, entry 29). **268**·NikA displayed the highest TOF (43 h^{-1}). Under similar conditions, sulfide **263** was selectively converted into sulfoxide with TON = 199 (Table 32, entry 30). Unfortunately these ArMs displayed only very modest enantioselectivity (i.e. ≤ 10 %).

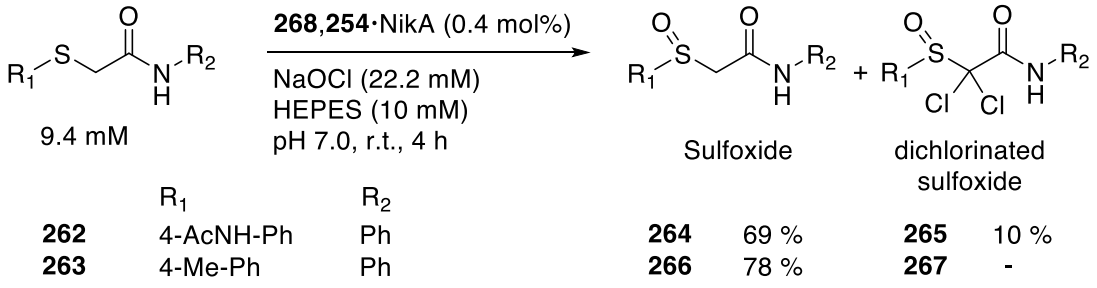

	R_1	R_2				
262	4-AcNH-Ph	Ph	**264**	69 %	**265**	10 %
263	4-Me-Ph	Ph	**266**	78 %	**267**	-

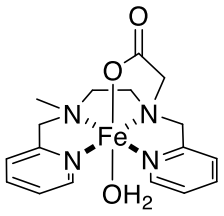

268

Scheme 79. Inserting iron complexes **268** into NikA yields an artificial sulfoxidase.

The same group subsequently reported another ArM sulfoxidase based on the supramolecular anchoring of **254** in human serum albumin (HSA).[425] To ensure a better defined localization within HSA, a “Trojan horse” known to interact specifically with HAS was used. The authors functionalized the abiotic cofactor [Fe(BPHMEN)Cl_2] with an ibuprofen anchor, resulting in **254** (Scheme 76). Ibuprofen is known to bind to HSA

preferentially in its “drug site 2” (IIIA domain). Correspondingly, **254** binds HSA with a ~27 μM affinity to afford **254**·HSA. When thioanisole **27** was dissolved in an acetate-buffered solution (pH 5.2, 2.4 equ. NaOCl), no oxidation was detected. If **254** alone was used, the sulfone **242** was produced exclusively (97% yield). When HSA alone was used as catalyst, a mixture of sulfoxide **28** and sulfone **242** were produced in 45 % and 12 % yield respectively. In the presence of **254**·HSA, the sulfoxide **28** and the sulfone **242** were produced in 62% and 10% yield respectively. Upon lowering the temperature to 4°C, 1367 TON were obtained with **254**·HSA, (TOF of 459 min^{-1}) (Table 32, entry 31). The main advantage brought by the incorporation of the cofactor into HSA was the stability and recyclability of the ArM: after four rounds of catalysis, **254**·HSA maintained its chemoselectivity for **28**. In contrast, HSA gradually lost its activity and selectivity upon recycling.[416] Despite the better defined localization of the cofactor within HSA, no enantioselectivity was observed for the sulfoxidation. Mutation of residues close to the “drug site 2” may allow to genetically improve the catalytic performance of this artificial sulfoxidase.

Finally, the groups of Mahy and Banse explored a covalent anchoring strategy for the generation of an artificial non-heme ArM sulfoxidase. β-lactoglobulin (β-LG) was used as a scaffold to covalently anchor the iron-cofactor **255** to Cys121, Scheme 76.[426] This ArM catalyzed the sulfoxidation of thioanisole, with a TON = 5.6 and a 20 % ee in favour of (*R*)-**28**. The selectivity eroded over the course of the reaction, suggesting a denaturation of the ArM.

Table 32. Selected results for artificial sulfoxidases.

Entry	Cof.	Protein	Sub.	Ox.	pH	T (°C)	[Cof] (μM)	[Ox.] (mM)	*ee* (%)	TON (t / h)	TOF (s^{-1})	Ref
1	**269**	Phytase	**27**	H_2O_2			10		66 (*S*)	550 (3)		[147]

2	TCPP-Ru(II)-CO	Ab-SN37.4	**27**	PhIO	9.0	4	0.5	0.5	43 (*S*)	~750		154
3	**217**	–	**27**	H_2O_2	7.5	r.t.	0.3	0.05	23 (*R*) [a]	38 (1.5) [a]		408
4	**217**	Ab-3A3	**27**	H_2O_2	7.5	r.t.	0.3	0.05	45 (*R*) [a]	82 (1.5) [a]		408
5	**220**	Ab-7A3	**27**	H_2O_2	4.4	r.t.	5	0.25	–	5.6 (2.6)		384
6	**220**	Ab-7A3	**27**	H_2O_2	4.4	r.t.	5	0.25	8 (*S*)	12 (2.6)		384
7	**213**	–	**27**	H_2O_2	7.4	r.t.	20	3.5	–	162 (2.3)[b]		412
8	**213**	Xln	**27**	H_2O_2	7.4	r.t.	20	3.5	40 (*S*)	145 (2.3)[b]		412
9	**252**	–	**27**	H_2O_2	8.0	18	2	0.5	–		0.0006	413
10	**252**	$(gp27\text{-}gp5)_3$	**27**	H_2O_2	8.0	18	2	0.5	–		0.006	413
11	**243**	–	**27**	H_2O_2	5.0	35	10	1	–		0.0002	326
12	**243**	Mb (H64D-A71G)	**27**	H_2O_2	5.0	35	10	1	13 (*S*)		0.001	326
13	**245**	Mb (H64D-A71G)	**27**	H_2O_2	5.0	35	10	1	32 (*S*)		0.008	414
14	**249**	–	**27**	H_2O_2	7.0	4	500	10	–	1.9 (0.17)		328
15	**248**	Mb(L72C/Y103C)	**27**	H_2O_2	5.1	4	130	6.5	51		0.007	327
16	**248**	Mb(T39C/L72C)	**27**	H_2O_2	7.0	4	500	10	60	5 (0.17)		328
17	**250**	HSA	**27**	NaOCl	5.2	r.t.	12.5	2.5	–	97 (0.17)		416
18	**251**	BSA	**27**	H_2O_2	5.1	0	2.7	0.4	50 (*R*)	98 (20)		417
19	**251**	BSA	**238**	H_2O_2	5.1	0	2.7	0.4	87 (*R*)	19 (20)		417
20	**253**	BSA	**27**	H_2O_2	7.0	24	200	15	52 (*S*)	42 (1.5)		419
21	**253**	BSA	**239**	H_2O_2	7.0	24	200	15	74 (*S*)	8 (1.5)		419
22	**253**	RSA	**256**	H_2O_2	7.0	r.t.	200	40	70 (*R*)	45 (1)		418
23	**253**	BSA	**27**	PS/hv [c]	7.4	r.t.	50	–	16 (*R*)	21 (0.2)		420
24	**–**	WT Sav	**27**	tBuOOH	2.2	r.t.	200	50	4 (*R*)	3.5 (4)		421
25	**$[VO]^{2+}$**	–	**27**	tBuOOH	2.2	r.t.	200	50	–	27.5 (4)		421
26	**$[VO]^{2+}$**	WT Sav	**27**	tBuOOH	2.2	r.t.	200	50	46 (*R*)	47 (4)		421
27	**$[VO]^{2+}$**	WT Sav	**258**	tBuOOH	2.2	r.t.	200	50	90 (*R*)	50 (4)		421
28	**$[VO]^{2+}$**	WT Sav	**259**	tBuOOH	2.2	r.t.	200	50	93 (*R*)	26.5 (4)		421
29	**268**	NikA	**262**	NaOCl	7.0	r.t.	37	22.2	≤10	173 (4)	0.012	422
30	**268**	NikA	**263**	NaOCl	7.0	r.t.	37	22.2	≤5	199 (4)		422
31	**254**	HSA	**27**	NaOCl	5.2	r.t.	38	45.7	–	1367	7.65	425

[a] with 5 % *t*-BuOH. [b] with 100 equivalents of imidazole. [c] irradiation at 450 nm in the presence of 0.4 mM $[Ru(bpy)_3]^{2+}$ and 12 mM $[Co(III)\ (NH_3)_5Cl]^{2+}$ as electron acceptor.

6.3 Alcohol Oxidation

Numerous natural enzymes, including laccases, glucose oxidases, and alcohol dehydrogenases, catalyze the alcohol oxidation.[427] Alcohol dehydrogenases are highly active and enantioselective NAD(P)H-dependent enzymes, but they often possess a narrow substrate scope. NAD(P)H cofactor recycling is an important economic issue and can be achived by enzymatic and non-enzymatic systems. Homogenous catalysts are of course widely used for alcohol oxidation.[428] Transition metal complexes of ruthenium,

palladium, or copper in combination with TEMPO/dioxygen or a peroxide such as H_2O_2 or *t*-BuOOH are typically applied for alcohol oxidation. Artificial metalloenzymes are potentially an attractive alternative for enantioselective alcohol oxidation. As elegantly demonstrated by Noyori, a pianostool-based asymmetric transfer hydrogenase catalyst, can act either in the reduction- or in the oxidation-direction, depending on the hydride donor : hydride acceptor ratio.[429] This is reminiscent of natural alcohol dehydrogenases.

To mimic such systems, Ward and coworkers investigated whether biotinylated transition metal piano stool complexes anchored within Sav could catalyze the (asymmetric) oxidation of primary and secondary aromatic alcohols.[430] Of the four biotinylated piano stool transition metal complexes tested [η^6-(benzene)Ru(**70**)Cl] displayed highest activity for the oxidation of phenethyl alcohol into acetophenone (200 TON) upon incorporation into WT Sav. On the other hand, no hydride acceptor (electron-deficient ketones, quinones etc.) proved efficient for the oxidation of phenetyl alcohol: only *t*-BuOOH led to oxidation, suggesting an alternative mechanism, different from the widely accepted concerted proton and hydride transfer via a six-membered transition state.[429]

6.4 Epoxidation

Olefin epoxidation is a powerful approach for introducing oxygen atoms into organic compounds due the stereospecificity of this reaction and the potential for subsequent ring opening reactions of epoxides.[431] While a wide range of olefin epoxidation catalysts have been developed,[432] high levels of enantioselectivity remain challenging for a number of olefin classes.[433] Several different ArMs have therefore been explored with the hope of controlling epoxidation selectivity.

For example, Kazlauskas[434] and Soumillion[435] independently reported that the active site Zn of carbonic anhydrase could be replaced with Mn to generate artificial epoxidases.

Specifically, incubating apo hCA II with Mn(II) salts (chloride or acetate) led to the formation of an hCA · Mn ArM that catalyzed the epoxidation of styrenes in the presence of hydrogen peroxide with a moderate conversion and enantioselectivity (up to 67% ee). The Kazlauskas system also provided modest enantioselectivity (52% ee) on an aliphatic olefin, albeit with low conversion (Scheme 80).

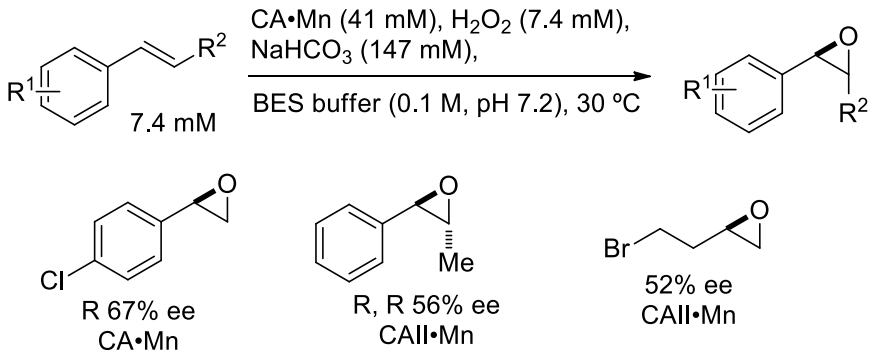

Scheme 80. Epoxidation catalyzed by Mn-substituted hCA II.

Manganese complexes with multidentate nitrogen ligands are robust catalysts for a range of oxygenation reactions. Reetz incorporated a maleimide-substituted Mn-salen cofactor **272** into papain via cysteine alkylation; the resulting ArM catalyzed the olefin epoxidation, but low enantioselectivity was observed (< 10% ee).[164] Lewis and coworkers also generated Mn-terpyridine ArMs by linking a maleimide-substituted terpyridine cofactor (**273**) to cysteine residues in nitrobindin and tHisF. Both benzylic oxidation and olefin epoxidation were catalyzed by these ArMs (Scheme 81).[200]

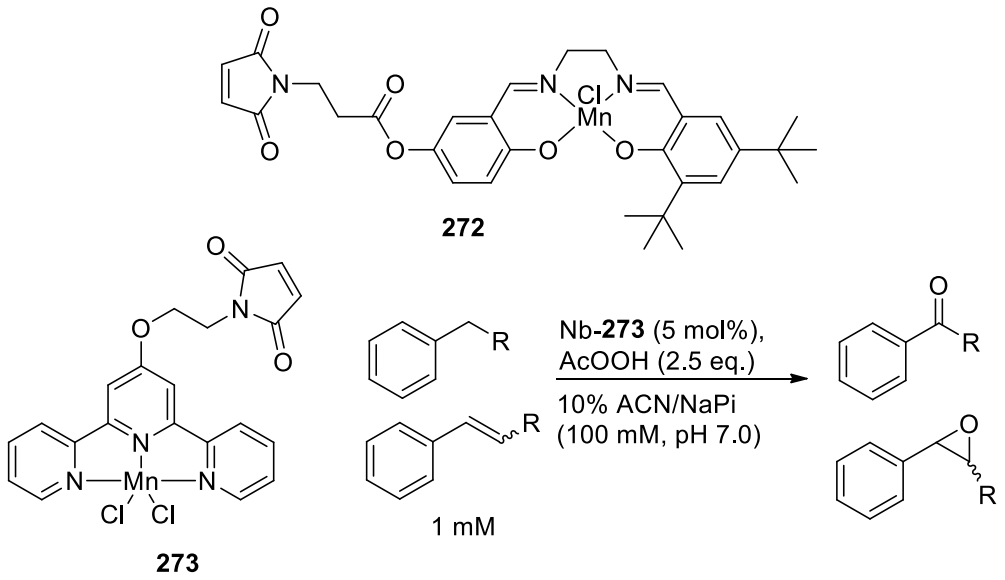

Scheme 81. Benzyl oxidation and olefin epoxidation catalyzed by Mn(salen) and Mn(terpy) ArMs.

Ab-7A3, an antibody that was raised against estradiol (K_D = 9.5 · 10^{-10} M) has been used as a scaffold for incorporating estradiol-substituted Mn(III)-porphyrins (Scheme 82).[409] The affinity of Ab-7A3 for **274** and **283** was lower byapproximately 3 orders of magnitude compared to the estradiol alone (K_D = 9.0 · 10^{-6} M and K_D = 1.9 · 10^{-6} M, respectively). Spectroscopic data suggested that the metal centers in these cofactors are not coordinated to any residues of the antibody scaffold. Nonetheless, **274**·Ab-7A3 and **283**·Ab-7A3 catalyzed the epoxidation of styrene, affording 425 and 100 turnovers respectively within one hour, in the presence of 0.2% ArM vs. the oxidant. Additional products **277** and **278** were also formed, however, and the chemoselectivity favored production of phenylacetaldehyde **277**: 25 % and 45 % using **274**·Ab-7A3 and **283**·Ab-7A3 respectively. As both cofactors were mostly located outside of the protein, the presence of the antibody only modestly influenced the catalytic performance of the resulting ArMs.

Mahy and coworkers demonstrated that Xylanase A (Xln hereafter) can host, deep in its pocket, the synthetic iron porphyrin [Fe(T*p*CPP)] **213** (K_D = 0.5 · 10^{-6} M).[396] The resulting ArM displays peroxidase and sulfoxidase catalytic activity (sections 6.1 and 6.2). Incorporation of [Mn(T*p*CPP)] **284** into Xln (K_D = 1.5 · 10^{-6} M) affords an ArM for the epoxidation of styrene.[436] The olefins **275** and **279** were converted to the aryloxirane compounds, **276** and **280** in 17% and 16% yields respectively (i.e. 23 and 21 TON). The chemoselectivity of the reaction was not affected by the protein scaffold, favouring **276** for styrene (65%). For the electron-rich **279** the carbonyl products **281** and **282** were formed preferentially (70%). Importantly, the Xln host protein was responsible for enantioselectivity in the **284**·Xln-catalyzed epoxidation, resulting in ee = 8.5% for (*S*)-**276** and 80% for (*R*)-**280**. In addition, an increase of yield was also observed when comparing **284** to **284** · Xln.

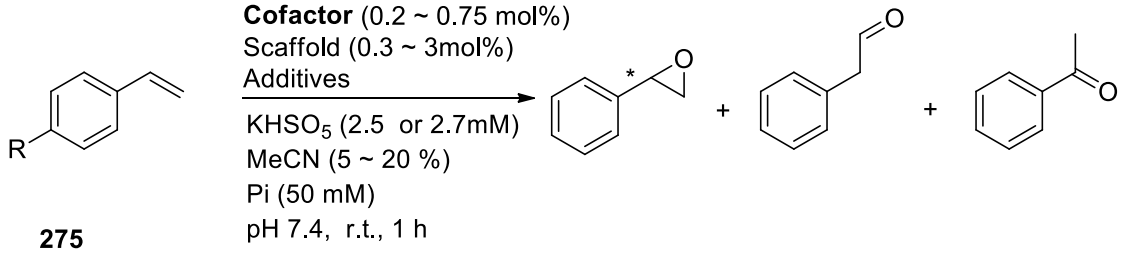

Substrate		Cofactor	276	277	278
		283	9 %, rac.	9 %	2 %
R = H	275	274	21 %, rac.	63 %	1 %
		284	17 % yield, up to 8.5 % ee (*S*)	9% combined yield	
			280	281	282
R = OMe	279	284	16 % yield, up to 80 % ee (*R*)	33.5 % combined yield	

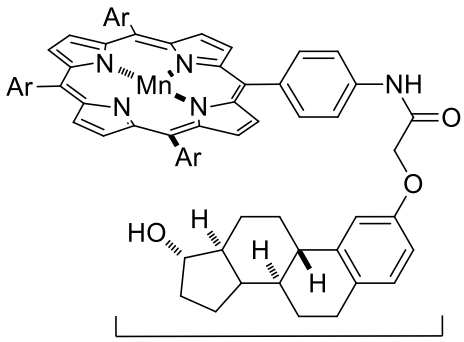

Ar = SO_3^-

[Mn(TpSPP)-est.] **283**

Ar = N^+

[Mn(TMPyP)-est.] **274**

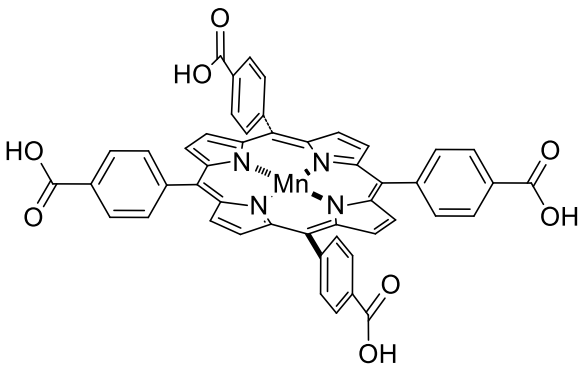

[Mn(T*p*CPP)] **284**

Scheme 82. Styrene epoxidation catalyzed by ArMs assembled with synthetic Mn(III)-porphyrins via a Trojan horse anchoring strategy and supramolecular incorporation. The catalyst loading is reported *vs.* the oxidant.

6.5 Dihydroxylation

Catalytic asymmetric dihydroxylation of olefins with osmium tetroxide and chiral ligands was discovered by Sharpless in the 1980s. As discussed in chapter 3, an ArM dihydroxylase was reported Kokubo.[116] Inspired by this report, Ward and coworkers

envisaged that the classic cinchona alkaloid ligands typically used for asymmetric dihydroxylation could be replaced with amino acid side chain functionality provided by Sav. X-ray analysis of a Sav crystal soaked with excess $K_2[OsO_2(OH)_4]$ revealed metal binding on most surface-exposed basic amino acid residues, including H87 and H127.[437] Incubating WT Sav with 1-2 eq. $K_2[OsO_2(OH)_4]$ yielded a highly enantioselective catalyst for the dihydroxylation of vinyl substrates, Table 33 and Scheme 83. (*R*)-1,2-dihydroxy-2-phenyl propane was obtained from substrate α-methylstyrene **10** with 95 % ee. To identify the position of the catalytic site, residues that had osmium-bound in the crystal structure were mutated to alanine. Surprisingly none of these mutants displayed a significantly eroded ee suggesting that the active osmium is not bound to any of these residues. In stark contrast, mutations within the biotin binding vestibule (e.g. S112, K121) and deep within the biotin binding pocket (e.g. D128) had a significant impact on the enantioselectivity of the artificial dihydroxylase. The ee for 1,2-dihydroxy-3-thiophenyl propane increased from 2 % (*R*)- to 71 % (*S*)-product when catalysis was performed with mutant S112Y. Mutant D128A afforded the same product with 71 % (*R*)-selectivity, Table 33.

Table 33. Incubation of Sav with $K_2[OsO_2(OH)_4]$ affords an asymmetric dihydroxylase.

Entry	Substrate	Sav mutant	$K_2[OsO_2(OH)_4]$ (mol%)	ee (%)	TON[a]
1	**10**	S112M	5.0	97 (*R*)	16
2	**285**	S112Y	5.0	82 (*S*)	14
3	**285**	D128A	2.5	77 (*R*)	21
4	**286**	S112Y	5.0	71 (*S*)	7
5	**286**	D128A	2.5	71 (*R*)	10
6	**287**	S112M	5.0	41 (1*R*, 2*S*)	12
7	**288**	WT	2.5	90 (1*R*, 2*S*)	26
8	**288**	S112T	2.5	92 (1*R*, 2*S*)	16
9	**289**	D128A	2.5	45 (1*R*, 2*S*)	13
10	**290**	S112T	2.5	68 (3*R*, 4*R*)	6

[a]Based on the amount of $K_2[OsO_2(OH)_4]$ employed.

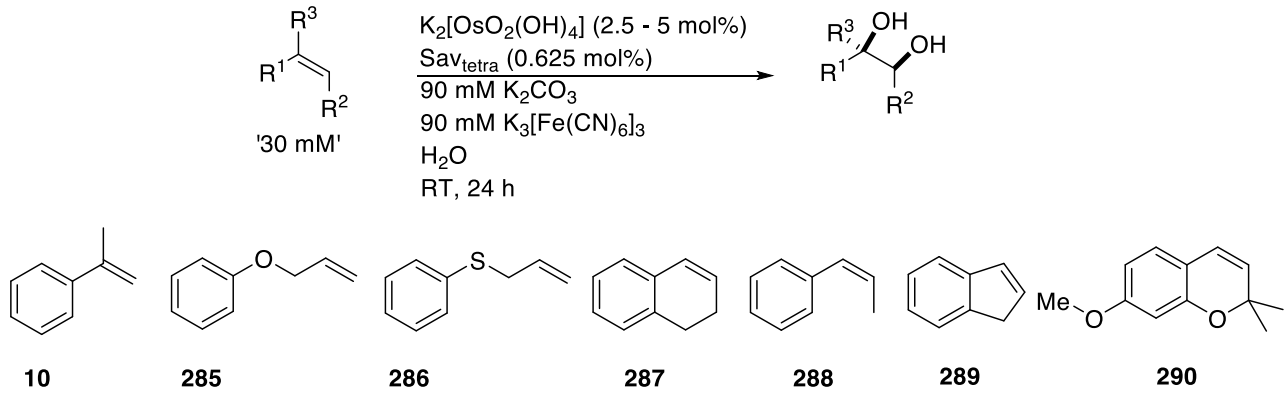

Scheme 83. Incubation of Sav with $K_2[OsO_2(OH)_4]$ affords an asymmetric dihydroxylase.

One of the most stringent requirements for ArMs is the preferred use of water as a reaction medium.[27] A few reports, however, outline efforts to create ArMs that operate in the presence of large amounts of organic solvents.[20, 174, 436, 438-439] To overcome the inherent tendency of proteins to denature in the presence of organic solvents, Tiller and co-worker have investigated the potential of organosoluble polymer enzyme conjugates (PECs hereafter,**294**) using poly(2-oxazoline) **291** for the creation of ArMs.[440-441] PEC formation was achieved by coupling anhydride intermediate **293** with the amino groups present on the surface of host proteins. (Scheme 84). The resulting ArMs are soluble in apolar solvents and display activity in both organic- and aqueous media.

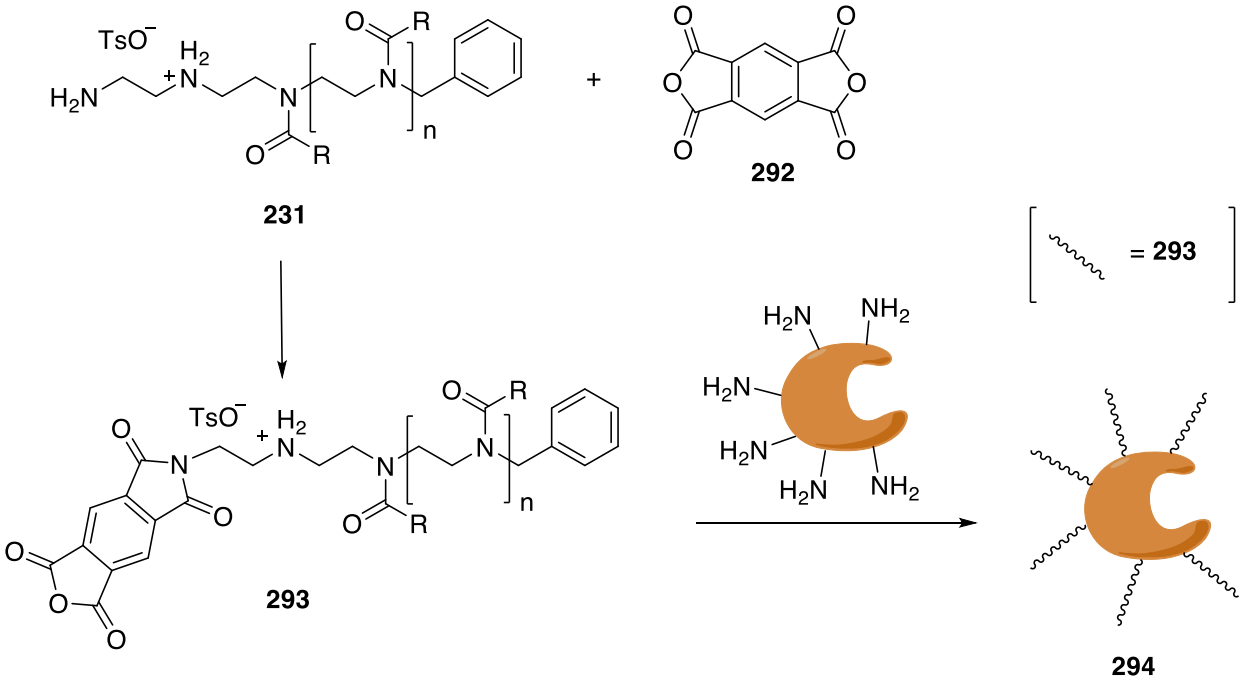

Scheme 84. The terminal amino group of poly(2-oxazoline) **291**, reacts with pyrometillic dianhydride **292** to afford the oligomer intermediate poly(2-oxazoline) anhydride **293**. PECs **294** are generated upon coupling of the anhydride **293** with the amino groups on the surface of the protein scaffold.

Building on the work of Kokubo[116] and Ward[437] on osmate-catalyzed dihydroxylation employing ArMs, Tiller and coworkers reported on the use of PECs (**294**) as chiral scaffolds for the dihydroxylation of alkenes in organic solvents.[442] The amphiphilic nature of PECs allowed formation of the osmate-PEC ArMs in fairly apolar media. PEC-derivatives from various proteins were evaluated in the asymmetric dihydroxylation of styrene **176** in water-saturated chloroform using hexacyanoferrate (III) as co-oxidizing agent.(Table 34 and Scheme 85).

Table 34. Selected results for the catalytic dihydroxylation of styrene **176** with PECs in chloroform.

Entry	Protein	co-oxidant	base	T (d)	Ratio [Os] / [Prot]	ee (%)	TON[a]
1	Lysozyme	$K_3[Fe(CN)_6]$ (300 mM)	K_2CO_3 (300 mM)	7	4.2	*rac.*	< 1
2	BSA	$K_3[Fe(CN)_6]$ (300 mM)	K_2CO_3 (300 mM)	7	18	*rac.*	< 1
3	α-chymotripsin	$K_3[Fe(CN)_6]$ (300 mM)	K_2CO_3 (300 mM)	7	7.5	19 (*S*)	< 1
4	Proteinase-K	$K_3[Fe(CN)_6]$ (300 mM)	K_2CO_3 (300 mM)	6	8.3	6 (*S*)	< 1
5	Lipase (*C. rugosa*)	$K_3[Fe(CN)_6]$ (300 mM)	K_2CO_3 (300 mM)	7	16.7	12 (*S*)	< 1
6	peroxidase	$K_3[Fe(CN)_6]$ (300 mM)	K_2CO_3 (300 mM)	7	12.5	12 (*S*)	< 1
7	ADH	$K_3[Fe(CN)_6]$ (300 mM)	K_2CO_3 (300 mM)	7	11	12 (*S*)	< 1
8	laccase	$K_3[Fe(CN)_6]$ (300 mM)	K_2CO_3 (300 mM)	7	7.7	15 (*R*)	< 1
9	laccase	$K_3[Fe(CN)_6]$ (300 mM)	K_2CO_3 (300 mM)	7	1.9	93 (*R*)	7
10[b]	laccase	$K_3[Fe(CN)_6]$ (300 mM)	K_2CO_3 (300 mM)	7	1.9	98 (*R*)	42
11	laccase	$K_3[Fe(CN)_6]$ (300 mM)	K_2CO_3 (300 mM)	3	3.8	99.4 (*R*)	<1
12[c]	laccase	*t*-BuOOH (110 mM)	K_2CO_3 (300 mM)	7	2	98 (*R*)	232
13[d]	laccase	*t*-BuOOH (110 mM)	KOH[e]	7	1	99.4 (*R*)	501

[a]Based on the amount of $K_2[OsO_2(OH)_4]$ employed. [b] PEC was dialyzed against 10mM EDTA for 24 h followed by further dialysis against water. [c]26 μM $K_2[OsO_2(OH)_4]$. [d]13 μM $K_2[OsO_2(OH)_4]$. [e]10 μL / mL of a saturated methanolic solution. BSA: bovine serum albumin, ADH: Alcohol dehydrogenases (ADH).

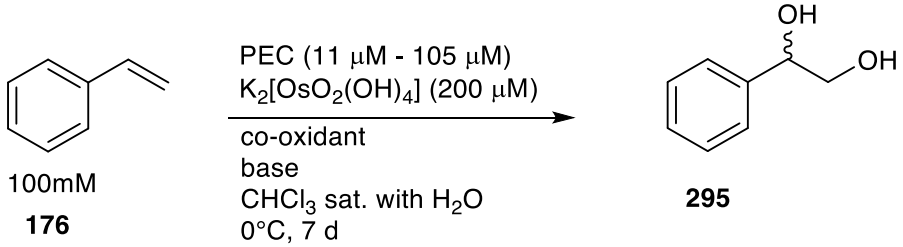

Scheme 85. Immobilized artificial dihydroxylase obtained as polymer enzyme conjugate using various protein hosts.

1-phenylethane-1,2-diol (**295**) was obtained in racemic form with enzyme conjugates derived from lysozyme or BSA (Table 34, entries 1 and 2). All other polymer-enzyme conjugates afforded enantioenriched product with (*S*)-configuration (Table 34, entries 3 and 7) except for laccase (Table 34, entry 8). Varying the osmate : laccase ratio from 7.7 to 1.9 improved the yield and ee substantially (7 TON and 93%) (Table 34, entry 9). Laccase contains four copper ions in its active site. Dialysis against EDTA and subsequent loading with osmate led to a further improvement in yield and ee for the dihydroxylation of styrene (98.4 % ee (*R*)-**295**, Table 34, entry 10).

In a subsequent study, alternative reaction conditions were investigated to overcome the poor solubility of the co-oxidant $K_3[Fe(CN)_6]$ in $CHCl_3$. *t*-BuOOH in combination with methanolic KOH as a base led to excellent results for dihydroxylation of styrene with a TON of 501 and even outcompeting the Sharpless system in terms of enantioselectivity (99.4% ee (*R*)) (Table 34, entries 12-13).[443] $KMnO_4$ and $FeCl_2$, respectively, were tested in the same study as alternatives to $K_2[OsO_2(OH)_4]$, but resulted in a sharp drop in TON (51 for $KMnO_4$ and 20 for $FeCl_2$) and enantioselectivity (26% ee (*R*) for $KMnO_4$ and 11% ee (*R*) for $FeCl_2$).

More challenging substrates were also tested with the $K_3[Fe(CN)_6]$ / K_2CO_3 system: 1-*H* indene **289**, 1,2-dihydronaphthalene **287**, and (allyloxy)benzene **285** yielded the corresponding vicinal diols in moderate to good ee. (Table 35, entries 1, 3 and 4 and Figure 28) The enantiomeric excess observed for substrates **289** and **287** is, however, the highest ever reported for osmium catalyzed dihydroxylation to the best of our knowledge. Strikingly, neither styrene derivative **10** nor **297** afforded the corresponding diol.[442] These result stand in contrast with those obtained by Ward and coworkers, relying on streptavidin as host protein.[437]

Table 35. Substrate scope for the catalytic dihydroxylation of alkenes with laccase based PEC.[a,b]

Entry	Protein	Sub.	T (d)	ee [c] (%)	TON[d]
1	laccase	**289**	7	71 (*R*)[e]	3
2	laccase	**10**	7	-	-
3	laccase	**285**	7	87 (*R*)	< 1
4	laccase	**287**	6	75 (*R*)[e]	11
5	laccase	**296**	7	-	-
6	laccase	**297**	7	*rac.*	1

[a] See Table MP1 for reaction conditions,[b] Ratio [Os] / [Prot] = 1.9, [c] positive *ee* values correspond to the (*R*)-enantiomer . [d] Based on the amount of $K_2[OsO_2(OH)_4]$ employed. [e] ee values of 1*R*,2*S* calculated by comparison of the amounts of the *cis* enantiomer (1*R*,2*S* and 1*S*,2*R*).

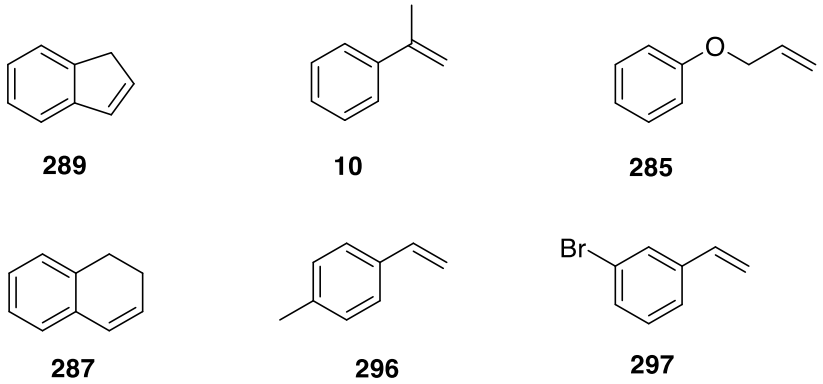

289 **10** **285**

287 **296** **297**

Figure 28. Substrates tested by Tiller in the catalytic dihydroxylation of alkenes with laccase based PEC.

6.6 Cco Oxidase

Lu designed and engineered a biosynthetic model of cytochrome *c* oxidase (C*c*O) by introducing a heme-copper center into Mb (Cu_bMb).[290] A tyrosine mutant in the active site (Cu_bMb F33Y or Cu_bMb G65Y) enabled its catalytic activity for the reduction of O_2 to H_2O and different reactive oxygen species (ROS) with high activity (TON > 1000).[444] Multiple approaches were used to fine-tune the ArM and thus increase the corresponding reduction rates. A point mutation (S92A) was introduced into Cu_bMb F33Y; this removed hydrogen bonds to the proximal His ligand and a heme propionate, created a more hydrophobic heme pocket, and increased the heme E^o from 95 to 123 mV. Reconstituting the scaffold with different heme derivatives (Figure 29, **222, 298-301**) led to the identification of ArMs with even higher E^o (up to 320 mV with **300**) and better activity (more than threefold TONs

after 9 h compared to Cu_bMb F33Y).[445] A series of different tyrosine analogs (Figure 30, **302-306**) were also introduced into the enzymes in *E. coli* via stop codon suppression methodology. **302** mimicked the Tyr-His crosslink in CcO, and the resulting ArM catalyzed the reduction of oxygen to water with eightfold more selectivity and threefold higher TON than Cu_bMb F33Y.[446] Tyrosine residues bearing different halogen substituents with decreased p*K*a also improved the selectivity and TON (up to 1200) of the ArM, suggesting the enhancement of proton donating ability of the phenol ring of the Tyr was beneficial.[447] More recently, 3-methoxytyrosine (**306**), a tyrosine analog with similar p*K*a but lower E^o, was incorporated into the ArM, the resulting ArM also showed higher oxidase activity (15.0 vs 6.5 μM min^{-1}) and selectivity (82% vs 51% to water).[448]

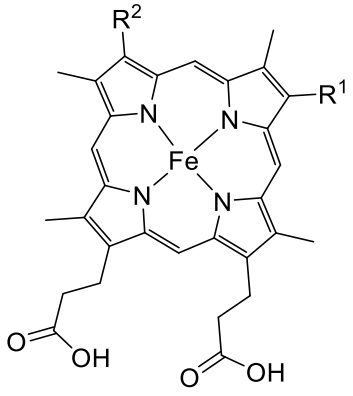

	R^1	R^2
222	vinyl	vinyl
298	acetyl	acetyl
299	vinyl	formyl
300	formyl	formyl
301	vinyl	$CH(OH)CH_2$(farnesyl)

Figure29. Various heme derivatives used to fine-tune the redox potential of the ArMs.

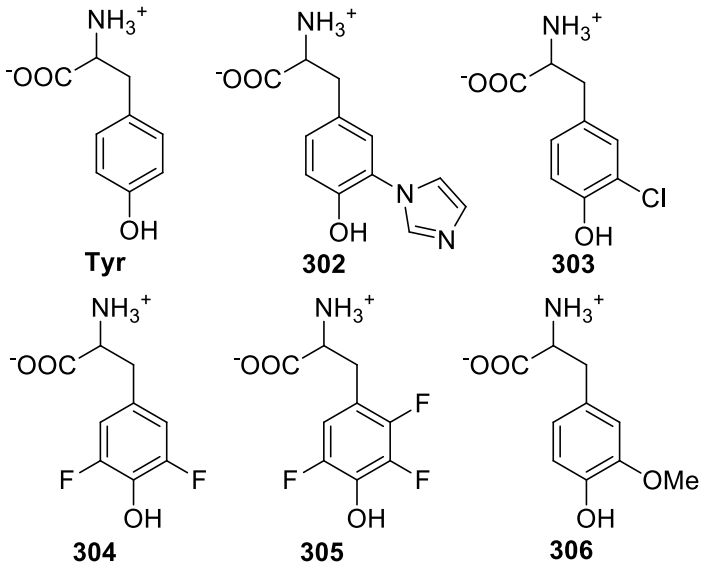

Figure 30. Various tyrosine analogs incorporated in the artificial oxidase to optimize the activity.

6.7 C-H oxidation

As noted in section 5.4, selective functionalization of C-H bonds remains a key challenge in catalysis, and ArMs have great potential to improve control over such processes. Toward this end, a Mn(terpy) cofactor (**307**) was covalently linked to the nitrobindin (Nb) scaffold, a heme protein with a β-barrel structure, as noted in section 5.5 (Scheme 81) to generate an ArM that catalyzed the oxidation of a broad range of hydrocarbons with good to excellent yields (up to 97%). Unfortunately, however selectivity identical to that of the free cofactor was observed (Scheme 86).[200]

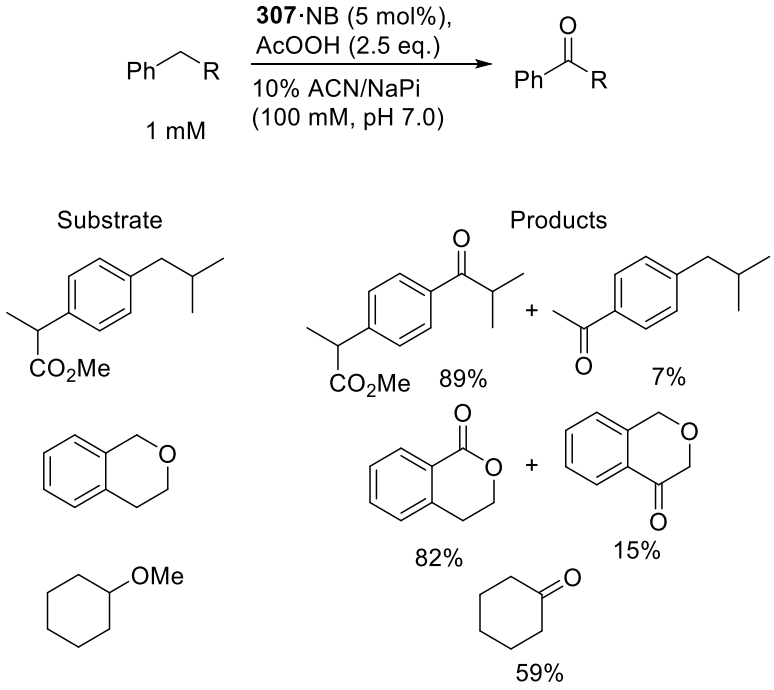

Scheme 86. Selected results for Mn(terpy) ArM catalyzed C-H oxidation.

In order to scrutinize the role of both the tetradentate ligand and the metal in Mb, Hayashi and coworkers tested the hydroxylation of ethylbenzene **308** by Mb reconstituted by Fe-porphycene **225** by Mn-protoporphyrin IX **309** and a Mn-porphycene **310** (Scheme 87).[449] Using hydrogen peroxide as oxidant, only **224**·Mb yielded phenylethanol **50** with TON =

13 and an *ee* = 14% (*S*))(Table 36, entries 1-4). No overoxidation to the corresponding acetophenone could be detected.

Table 36. The oxidation reaction by reconstituted Mbs with M-porphyrinoids

Entry	Cofactor	Protein	Sub.	pH	[Cof] (μM)	[H_2O_2] (mM)	TON	TOF (h^{-1})	Ref
1	**222**	Mb (WT)	**308**	8.0	20	10	0	0	[449]
2	**225**	Mb (WT)	**308**	8.0	20	10	0	0	[449]
3	**309**	Mb (WT)	**308**	8.0	20	10	0	0	[449]
4	**310**	Mb (WT)	**308**	8.0	20	10	13	33	[449]

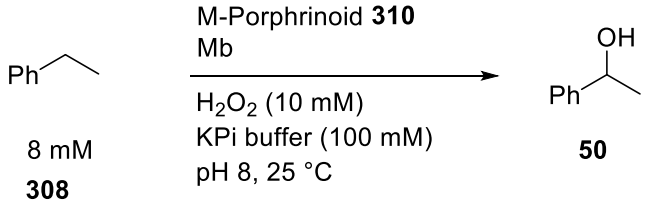

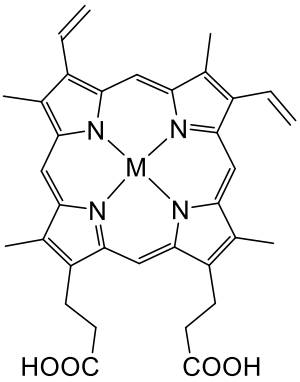

[M-Protoporphyrin IX]
222: M = Fe
309: M = Mn

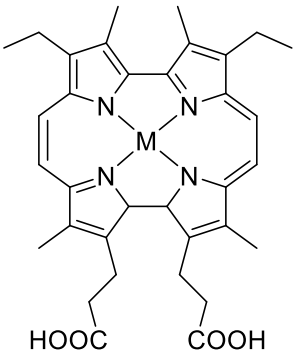

[M-Porphycene]
225: M = Fe
310: M = Mn

Scheme 87. Hydroxylation of ethylbenzene catalyzed by Mb reconstituted with metalloporphyrinoids.

6.8 Protein and Nucleic Acid Cleavage

ArMs have also been designed to catalyze site-selective cleavage of proteins and nucleic acids. Indeed, many of the earliest ArMs developed via covalent modification of protein scaffolds involved modification of protein- and DNA-binding scaffold proteins for this purpose. Unlike most of the systems described above, surface modification of the scaffold

is sufficient for selective biopolymer cleavage since the scaffold need only situate cofactors proximal to bound DNA. For example, following iminothiolane treatment, the surface lysine residues on the *E. coli* Trp repressor protein (*trp*) were used to install an iodoacetamide-substituted phenanthroline cofactor (Figure 22, **200**) that was metallated to generate an ArM nuclease.[125] Substrate DNA that contained the *aroH* transcription unit naturally recognized by the *trp* scaffold was selectively cleaved in the presence of tryptophan and 3-mercaptopropionic acid. A similar approach was used to link an Fe(III)-EDTA cofactor (**311**) to the σ^{70} subunit of *E. coli* RNAP complex. The resulting ArM catalyzed cleavage of nucleic acid and protein components of the RNAP complex near the σ^{70} binding sites.[450] Haloacetamide-substituted phenanthroline (Figure 22, **200**)[451] or EDTA ligands[452] and an Fe(III)-EDTA cofactor (Figure 31 **311**)[453] have been used to generate ArMs for selective biopolymer cleavage via alkylation of cysteine residues on scaffold proteins.[15] Related systems have been generated via disulfide exchange[454] and transesterification.[455] Finally, in order to bypass the need for the covalent scaffold modification, BpyAla was genetically encoded into catabolite activator protein (CAP) near the the DNA binding site of this scaffold.[400] The BpyAla **237** residue was selectively metallated with Fe(II) and Cu(II) to generate ArM nucleases.

Building on these studies, Nolte recently constructed an ArM containing a Mn-porphyrin cofactor ((Figure 31, **312**) that selectively and processively oxidized tri-adenine sites in double stranded DNA (dsDNA).[456] A trimeric, ring-shaped, DNA-binding clamp protein (gp45) was used as the scaffold, and cysteine residues on the clamp were alkylated with a maleimide substituted manganese-phorphyrin complex (**312**). Supercoiled DNA was quantitatively oxidized by **312** and the reactive position of dsDNA was turned into an aldehyde after oxidation, which was further modified with hydroxylamine-derived biotin. By the biotin-streptavidin interaction, the reaction site was then visualized in AFM. When

the gp45 was closed with an octapeptide, the activity of the ArM was decreased (55% conversion) and the site-selectivity was no longer existed, indicating the binding of gp45 to the DNA was the key to processive catalysis. The reaction direction of the ArM could also be guided by clamper-loader complex (gp44/62) like the native polymerase.

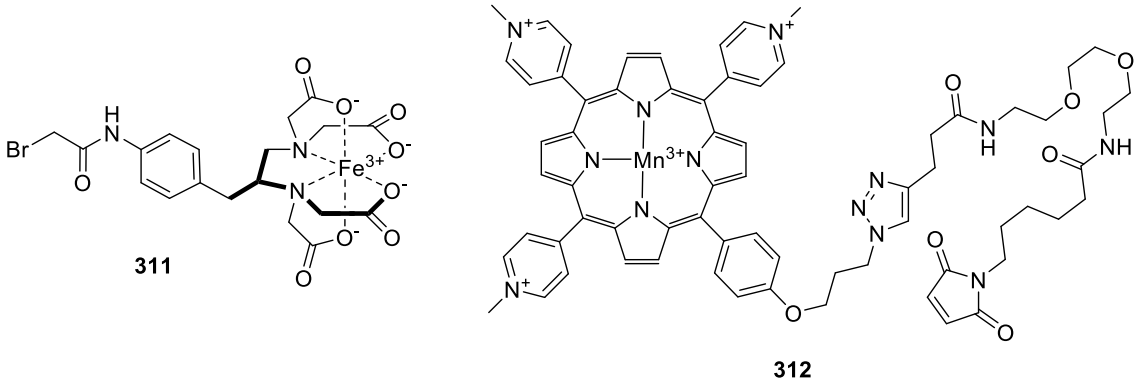

Figure 31. Selected cofactors used for construction of nucleic acid cleaving ArMs.

7. Hydration

A wide range of natural enzymes catalyze an equally diverse range of hydration reactions. Around one-third of the enzymes classified by the Nomenclature Committee of the International Union of Biochemistry and Molecular Biology (NC-IUBMB) are involved in the addition- or removal of a water molecule from a specific substrate, thus illustrating their importance in nature. Most of these enzymes are hydrolases (EC 3), but examples can also be found among the lyases (carbon-oxygen bond cleavage, EC 4.2).[457] Some of these enzymes (e.g. carbonic anhydrase, acetylcholinesterase or fumarase) belong to the fastest and most efficient enzymes known today, operating at the limit of substrate/product diffusion (with $k_{cat}/K_M \approx 10^8 – 10^9\ M^{-1} \cdot s^{-1}$).[458]

In addition to the large variety of natural hydrolytic (metallo)-enzymes, researchers have created ArMs to hydrolyze small model compounds (4-nitrophenyl acetate/phosphate), antibiotics (cefotaxime, ampicillin), or an analogue of the nerve agent cyclosarin. ArMs have also been applied for the hydration of CO_2 or α,β-unsaturated 2-acyl pyridines and were engineered to catalyze epoxide ring-opening reactions, Kemp eliminations, transesterifications, and RNA ligations. The applied metalloenzymes were created by placing a catalytically active metal center (often Zn(II)) either in existing proteins or in *de novo*-designed scaffolds. The catalytic performance and the selectivity of the constructs were subsequently improved by means of genetic engineering. The artificial hydrolases are presented below.

7.1 Hydrolytic Cleavage

In 2006, Kim and Benkovic *et al.* engineered an artificial β-lactamase for the hydrolysis of the antibiotic cefotaxime (**313**).[459] They repurposed the catalytic activity of an existing

protein scaffold by applying the SIAFE approach (simultaneous incorporation and adjustment of functional elements) in conjunction with directed evolution. Insertion, deletion, and substitution of active site loops led to β-lactamase activity in the αβ/βα metallo-hydrolase scaffold of glyoxalase II. Subsequent modification of the protein by point mutations resulted in a highly active engineered β-lactamase (evMBL8, PBD entry 2F50). The designed enzyme completely lost its native activity (hydrolysis of the thioester bond of (*S*)-D-lactoylglutathione), in favor of the hydrolysis of cefotaxime (**313**) (Scheme 88). The engineered enzyme, whose metal content was 1.63 ± 0.43 mol zinc and 0.46 ± 0.14 mol iron per mol of enzyme, displayed a catalytic efficiency (k_{cat}/K_M) of 184 $M^{-1} \cdot s^{-1}$.

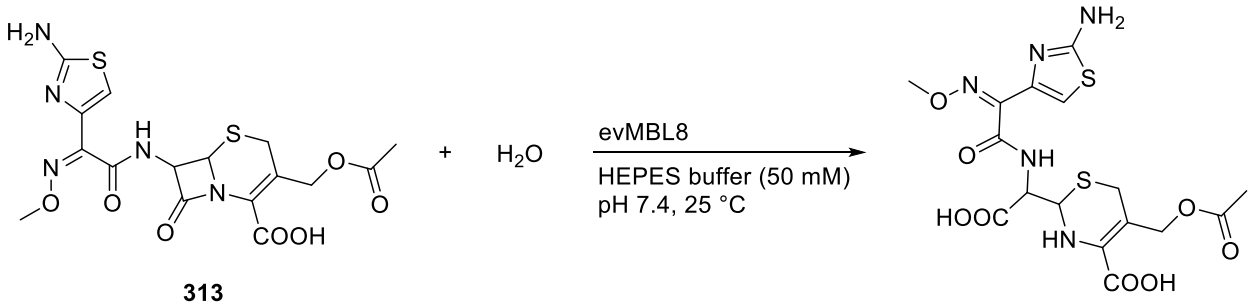

Scheme 88. An engineered β-lactamase evMBL8 catalyzes the hydrolysis of cefotaxime (**313**).

Beside antibiotics, small model compounds have also been examined as substrates for designed ArM hydrolases. For example, Pecoraro has engineered a variety of ArMs that catalyze hydrolysis of 4-nitrophenyl acetate (**315**).[460] The *de novo*-designed scaffolds consist of a coiled-coil motif with an engineered His_3 Zn(II) binding site. Metallation of this scaffold with Zn(II) led to an ArM that hydrolyzed **315** with a catalytic efficiency only ~100-fold lower than that of the natural human carbonic anhydrase II (hCAII) (Table 37). More generally, the ArM hydrolase ($[Hg(II)][Zn(II)(H_2O/OH^-)](TRIL9CL23H)_3^{n+}$) consists of a three-stranded coiled-coil motif based on the TRI peptide family. The α-helical monomers display the general amino acid sequence Ac-G(LKALEEK)$_4$G-NH_2 in which two leucine

residues were mutated to either histidine or cysteine. Upon metallation, this scaffold harbors a catalytically active tetrahedral Zn(II)$(His)_3OH_2$ site (mutation L23H) and a structure stabilizing trigonal planar Hg(II)$(Cys)_3$ site (mutation L9C) are formed (crystal structure of an analogue: PBD entry 3PBJ, Figure32).

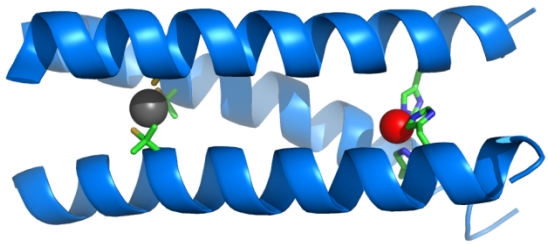

Figure 32. Cartoon representation of *de novo*-designed three helix bundle proteins. Side view of the trimer found in the asymmetric unit of the crystal structure in TRI peptide structure analogs (PDB:3PBJ). The three helix bundles contain Zn(II) (red) and Hg(II) (grey) metal centers coordinated with three His and three Cys, respectively.

Table 37. Kinetic constants of the artificial metallohydrolase [Hg(II)][Zn(II)(H_2O/OH^-)]$(TRIL9CL23H)_3^{n+}$ and human carbonic anhydrase II (hCAII) for the hydrolysis of 4-nitrophenyl acetate (**315**)[a]

Entry	Protein	pH	K_M (mM)	k_{cat} (s^{-1})	k_{cat}/K_M ($M^{-1} \cdot s^{-1}$)	Ref
1	[Hg(II)][Zn(II)(H_2O/OH^-)]$(TRIL9CL23H)_3^{n+}$	7.5	1.6 ± 0.4	2.2 ± 0.5 · 10^{-3}	1.38 ± 0.04	460
2	[Hg(II)][Zn(II)(H_2O/OH^-)]$(TRIL9CL23H)_3^{n+}$	8.0	1.7 ± 0.5	5.4 ± 1.5 · 10^{-3}	3.1 ± 0.1	460
3	[Hg(II)][Zn(II)(H_2O/OH^-)]$(TRIL9CL23H)_3^{n+}$	8.5	1.9 ± 0.6	12 ± 4 · 10^{-3}	6.0 ± 0.1	460
4	[Hg(II)][Zn(II)(H_2O/OH^-)]$(TRIL9CL23H)_3^{n+}$	9.0	2.1 ± 0.6	38 ± 10 · 10^{-3}	17.6 ± 0.3	460
5	[Hg(II)][Zn(II)(H_2O/OH^-)]$(TRIL9CL23H)_3^{n+}$	9.5	1.7 ± 0.5	40 ± 12 · 10^{-3}	23.3 ± 0.3	460
6	hCAII	7.4	30.5 ± 2.1	n.d.	2607 ± 85	461
7	hCAII	8.0	20.7	53 ± 10	2550	462
8	hCAII	9.0	23.9	56 ± 10	2320	462

[a] Reaction conditions: 10 µM [Hg(II)][Zn(II)(H_2O/OH^-)]$(TRIL9CL23H)_3^{n+}$ in 50 mM buffer (HEPES or CHES), 25°C.

Zastrow and Pecoraro subsequently investigated the influence of the active site location on the catalytic activity of TRI-based ArM hydrolases.[463] Four coiled-coil motifs were designed in which i) the positions of the Zn(II)-site and the Hg(II)-site were inverted (TRIL9CL23H and TRIL9HL23C, Table 38, entries 1-2 and 3-4), ii) the Zn(II)-site was moved closer to the *N*-terminus (TRIL9CL19H, Table 38, entries 5-6), iii) the Hg(II)-site was omitted (TRIL2WL23H, Table 38, entries 7-8). Analysis of these constructs revealed

that the maximal rate, the metal binding affinity and the substrate access depended on the position of the Zn(II)-site, whereas all designs showed similar maximal catalytic efficiencies for the hydrolysis of **315**.

Table 38. Kinetic analysis of four artificial metallohydrolases catalyzing the hydrolysis of 4-nitrophenyl acetate (**315**)[a]

Entry	Protein	pH	k_{cat} (s^{-1})	K_M (mM)	k_{cat}/K_M ($M^{-1} \cdot s^{-1}$)	$K_{d,app}$ (μM)	$(k_{cat})_{max}$ (s^{-1})[b]	$(k_{cat}/K_M)_{max}$ ($M^{-1} \cdot s^{-1}$)[b]
1	[Hg(II)][Zn(II)(H_2O/OH^-)](TRIL9CL23H)$_3^{n+}$ [c]	7.5	0.0022	1.6	1.38	0.8	~0.053	31
2	[Hg(II)][Zn(II)(H_2O/OH^-)](TRIL9CL23H)$_3^{n+}$ [c]	9.0	0.038	2.1	17.6	0.22		
3	[Zn(II)(H_2O/OH^-)][Hg(II)](TRIL9HL23C)$_3^{n+}$	7.5	0.0005	0.9	0.6	~8	~0.030	24
4	[Zn(II)(H_2O/OH^-)][Hg(II)](TRIL9HL23C)$_3^{n+}$	9.0	0.011	1.1	9.7	0.8		
5	[Hg(II)][Zn(II)(H_2O/OH^-)](TRIL9CL19H)$_3^{n+}$	7.5	0.0014	4.2	0.33	3.7	~0.076	27
6	[Hg(II)][Zn(II)(H_2O/OH^-)](TRIL9CL19H)$_3^{n+}$	9.0	0.010	2.3	4.5	0.4		
7	[Zn(II)(H_2O/OH^-)](TRIL2WL23H)$_3^{n+}$	7.5	0.0011	2.7	0.41	0.6	~0.055	25
8	[Zn(II)(H_2O/OH^-)](TRIL2WL23H)$_3^{n+}$	9.0	0.016	1.8	8.9	0.24		

[a] Reaction conditions: 10−20 μM active Zn(II)-bound peptide complex; values at pH 7.5 determined in 50 mM HEPES; values at pH 9.0 determined in 50 mM CHES; 25°C. The error range of the kinetic parameters is not displayed for clarity. [b] Determined at optimized pH. [c] Data reported by Pecoraro *et al.*[460]

Efficient and selective hydrolysis of organophosphates, especially those in nerve agents, has become increasingly important due the serious biological threat that these compounds pose. In 2012, Baker *et al.* repurposed a mouse adenosine deaminase to catalyze the hydrolysis of such an organophosphate.[464] A coumarinyl analogue **314** of the nerve agent cyclosarin was efficiently hydrolyzed by the engineered zinc dependent enzyme PT3.3 (Scheme 89), and a catalytic efficiency (k_{cat}/K_M) of ~10^4 $M^{-1} \cdot s^{-1}$ was determined. This ArM was engineered via a combination of computational design and directed evolution. Initially, the protein data base (PDB) was screened for enzymes containing mononuclear zinc sites. These enzymes are known to catalyze hydrolysis reactions in nature. A calculated model of the transition state for phosphate hydrolysis was subsequently docked into these scaffolds, beneficial hydrogen bonds in the active sites were engineered, and steric clashes were minimized. Out of a set of 12 designed enzymes, one showed a moderate catalytic activity (k_{cat}/K_M = 4 $M^{-1} \cdot s^{-1}$). Saturation mutagenesis of 12 residues

surrounding the active site led to the identification of a variant with a ~40-fold improved catalytic efficiency (PT3.1, PDB entry 3T1G). Random mutagenesis using error-prone PCR and a point mutation in the active site (based on analysis of the crystal structure) further increased the activity. Overall, the catalytic efficiency towards the hydrolysis of diethyl 7-hydroxycoumarinyl phosphate (**314**) was improved by a factor of 10^7. The designed artificial metalloenzyme (PT3.3) exceeded 140 turnovers. Based on a similar *in silico* design strategy relying on the Rosetta algorithm, Baker *et al.* have created artificial Diels-Alderases[465], Retro-Aldolases[466] and Kemp-Eliminases.[467] These engineered enzymes do not contain any catalytically active metal, are thus not included in this review. They do, however, demonstrate however the huge potential of computational enzyme design.

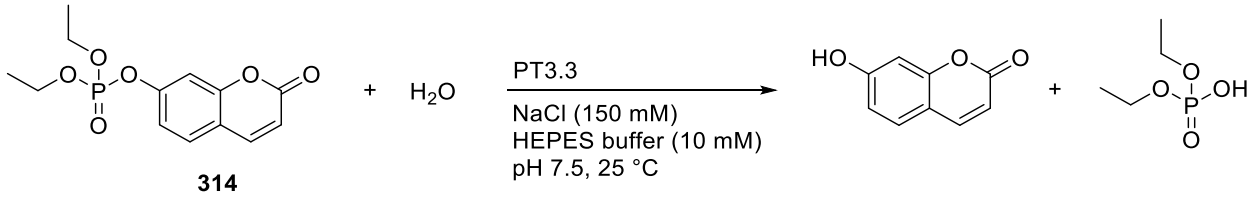

Scheme 89: Hydrolysis of a coumarinyl analogue of cyclosarin **314** catalyzed by an *in silico* designed artificial metallo-hydrolase PT3.3.

In 2012, Kuhlman reported an Zn(II)-dependent ArM that catalyzed hydrolysis of 4-nitrophenyl acetate/phosphate (**315/316**).[468] A 5 kDa helical hairpin monomer (Rab4-binding domain of rabenosyn) was used as a starting point to engineer a zinc-mediated homodimer (MID1-zinc). The construct bears two Zn(II)-binding sites at the protein interface. Analysis of the crystal structure (PDB entry 3V1C) revealed that only three out of the four designed histidine residues coordinate to zinc, thus suggesting a possible coordination site that may promote esterase activity. The $Zn(His)_3$ motif, located in a 6 · 4 Å protein cavity, indeed displayed hydrolase activity towards 4-nitrophenyl acetate (**315**, k_{cat}/K_M = 630 $M^{-1} \cdot s^{-1}$, max. TON = 50) and 4-nitrophenyl phosphate (**316**, k_{cat}/K_M = 14 M^{-}

$^{1} \cdot s^{-1}$) (Scheme 90). Mutagenesis of the three zinc-coordinating histidines to alanines led to a complete loss of esterase activity, suggesting that indeed the $Zn(His)_3$ motif is required for catalysis.

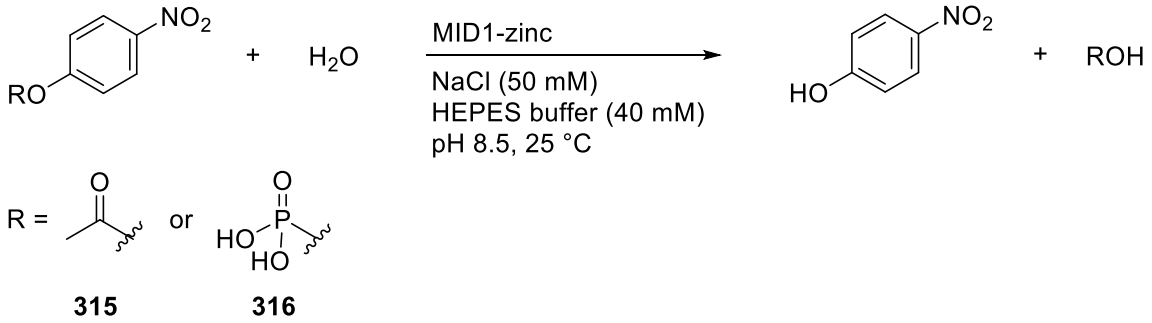

Scheme 90: Hydrolytic activity of MID1-zinc towards 4-nitrophenyl acetate (**315**) and 4-nitrophenyl phosphate (**316**).

Similar to the previous report from Kim and Benkovic *et al.*, Tezcan engineered an ArM β-lactamase to hydrolyze an antibiotic. The Tezcan system, however, involved Zn(II)-mediated self-assembly of four engineered cytochrome cb_{562} units (Figure 33).[469] To stabilize the resulting *D2* symmetric tetramer, a total of 16 surface mutations including the introduction of zinc-coordination sites, hydrophobic interactions, and disulfide bonds were introduced. The designed supramolecular protein assemblies harbor eight Zn(II)-ions (4 structural zinc sites and 4 catalytic zinc sites). Saturation mutagenesis of four individual amino acid positions surrounding the catalytic zinc sites led to the identification of a highly active variant (Zn_8:$^{A104/G57}AB3_4$, PDB entry 4U9E). This ArM β-lactamase catalyzed the hydrolysis of ampicillin (**317**) and 4-nitrophenyl acetate (**315**) with catalytic efficiencies (k_{cat}/K_M) of 35090 $M^{-1} \cdot min^{-1}$ and 296 $M^{-1} \cdot s^{-1}$ respectively (Scheme 91). *In vivo* β-lactamase activity was demonstrated by expression and secretion of this construct into the periplasm of *E. coli*. Colonies successfully grew on LB-agar plates containing ampicillin (0.8 mg/l).

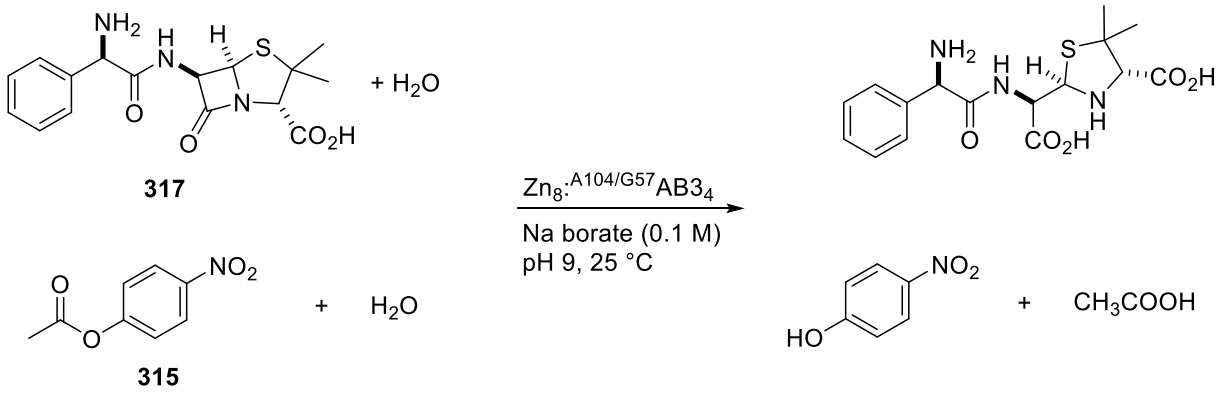

Scheme 91. An evolved artificial metallo β-lactamase Zn_8:$^{A104/G57}AB3_4$ catalyzes the hydrolysis of ampicillin (**317**) and 4-nitrophenyl acetate (**315**).

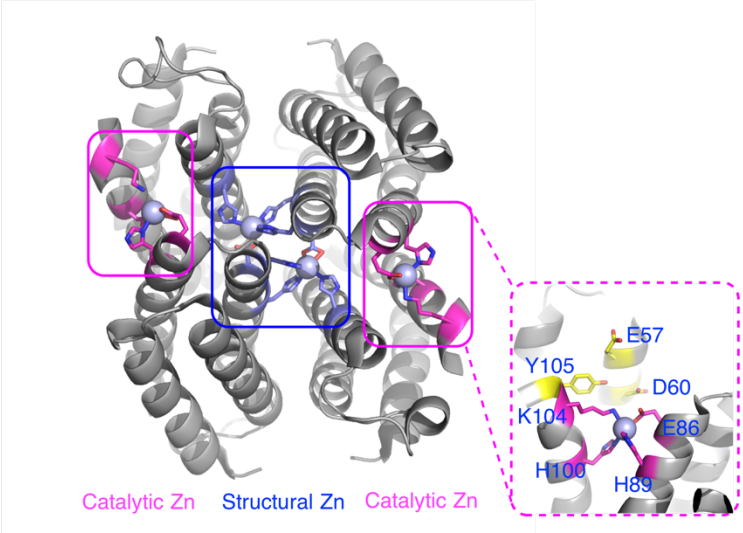

Figure 33. Cytochrome cb562 was engineered (PDB code 4U9E) to accommodate two structural and two catalytic zinc-binding sites affording β-lactamase activity.[469]

7.2 Ligation Reaction

In 2007, Szostak and Seelig introduced *de novo* RNA-ligase activity into human retinoid-X-receptor (hRXRα).[470] mRNA display-based screening of more than 10^{12} randomized two zinc-finger domains revealed highly active mutants towards the ligation of a 5'-triphosphorylated RNA with the terminal 3'-hydroxyl group of a second RNA (Scheme 92).[471] After 17 rounds of evolution, ligases performing several turnovers accompanied with a more than $2 \cdot 10^6$ fold rate enhancement were identified. Importantly, no initial

catalytic activity or knowledge of the reaction mechanism was required to engineer this ligase activity. Structure determination of a highly active variant (ligase 10C, PDB entry 2LZE) revealed substantial differences compared to the initial protein (hRXRα).[472] The helical DNA recognition domain was replaced by a long unstructured loop and the protein adopted a cyclic structure. The artificial ligase still contained two zinc-finger domains, although four of the eight initial cysteine coordination sites were replaced by aspartate, glutamate or histidine. The enzyme maintained its high activity even at temperatures up to 65°C (Figure 34).[473]

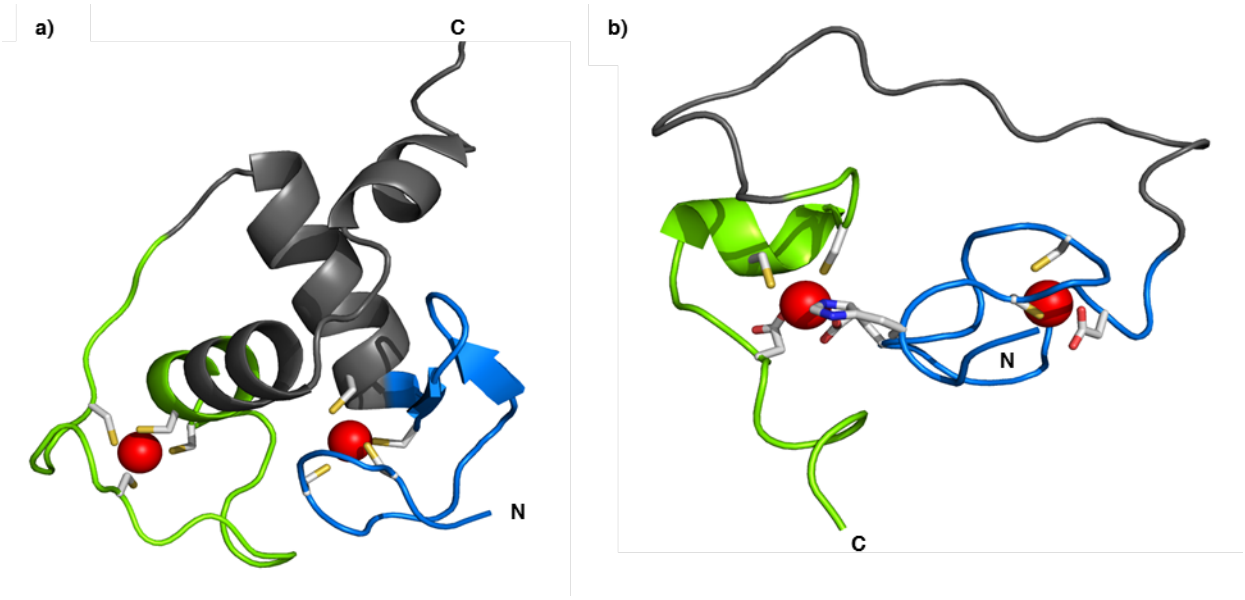

Figure 34. Cartoon representation of changes upon directed evolution of hXRXα (PDB: 1RXR) to the ligase C10 (PDB: 2LZE). a) Comparison of the 3D structure of hRXRα and b) the artificially evolved ligase. N and C termii omitted for clarity; the two zinc finger regions (Zn-I and Zn-II), in each scaffold, are highlighted in blue and green, respectively. Zinc-coordinating residues are shown as stick.

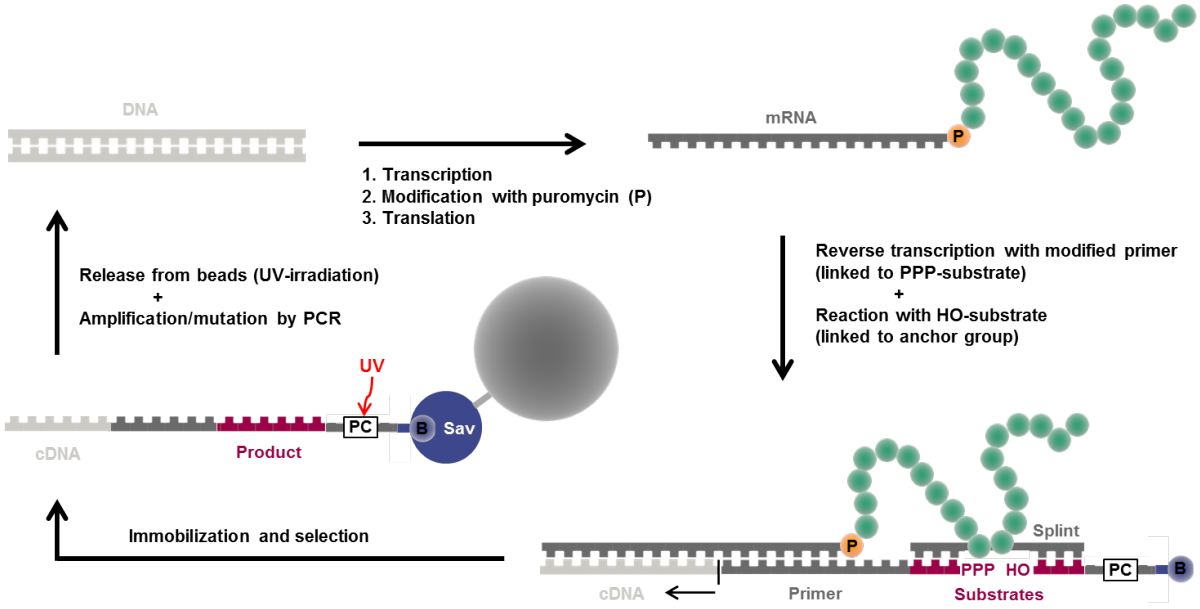

Scheme 92. *In vitro* selection of artificial ligase enzymes by mRNA display. A DNA library is transcribed and the corresponding mRNA modified with puromycin (P) followed by *in vitro* translation. The zinc-finger proteins (linked to their genotype) catalyze the ligation of a 5'-triphosphate-activated RNA (PPP-substrate) with the terminal 3'-hydroxyl group of a second RNA (HO-substrate) bearing a biotin anchor (B). The mRNA is reverse-transcribed and the linked strands (Product) are immobilized on streptavidin (Sav) coated beads. After selection, the constructs are released from the beads by UV-irradiation of a photocleavable linker (PC). DNA is amplified/mutated by PCR and subjected to the next round of selection. Adapted with permission from ref.[470] Copyright Macmillan Publishers Limited 2007.

7.3 Hydration of C=C and C=O Double Bonds

In 2013, Roelfes *et al.* applied their previously designed LmrR-Cu(phen) Diels-Alderase (section 5.8) in the hydration of α,β-unsaturated 2-acyl pyridine (Scheme 93).[366] Slightly lower conversion and enantiomeric excess (up to 84% ee) were observed compared to the Diels-Alder reaction. The point mutants of this ArM also suggested that the two residues (F93, D100) at the front entrance had a crucial impact on both the activity and the selectivity.

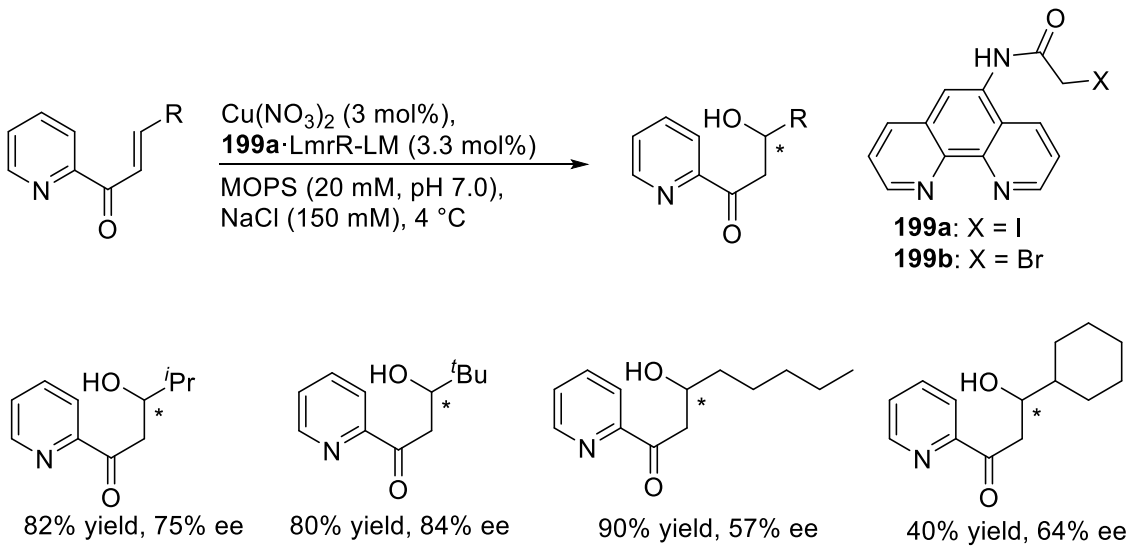

Scheme 93. Selected results for hydration of α,β-unsaturated 2-acyl pyridines.

A similar strategy was applied by Pecoraro *et al*. The previously designed ArM [Hg(II)][Zn(II)(H_2O/OH^-)](TRIL9CL23H)$_3^{n+}$ (section 7.1), a highly active hydrolase for 4-nitrophenyl acetate (**315**), displayed CO_2 hydration activity (Table 39, entry 1). In order to generalize their approach of *de novo*-designed ArMs, they switched from a three-stranded coiled-coil motif to a single-stranded antiparallel three-helix bundle (α_3D-motif, originally designed by DeGrado *et al.*[474]). Being single-stranded, this 73 amino acid protein allows the introduction of unique mutations (rather than mutations that are repeated with three-fold symmetry). The potential to improve the catalytic performance of ArMs derived from this scaffold is therefore expected to be higher. Indeed, Pecoraro *et al.* engineered CO_2 hydration activity into this scaffold by mutagenesis (4 mutations) and elongation of the C-terminus (4 residues).[475] Three leucine residues were replaced by histidines to form the catalytically active Zn(II)(His)$_3$O-site and an existing histidine was replaced by valine to avoid undesired Zn(II)-binding. The engineered protein (α_3DH_3) bound Zn(II) with nanomolar affinity (K_d = 59 ± 9 nM at pH 9.0) to form a highly active ArM (Table 39, entries 2-5 and Figure 35).

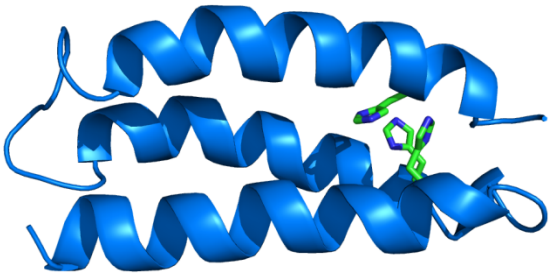

Figure 35. Side view of α_3DH_3 model built on α_3D peptide structure (PDB: 2A3D). Highlighted, in each single chain of the three helix bundle, the His introduced for the coordination with Zn(II) ion (not displayed). Coordinating residues are represented as stick and coloured by element.

Table 39. Kinetics for CO_2 hydration by natural and artificial metalloenzymes[a]

Entry	Protein	pH	K_M (mM)	k_{cat} (s^{-1})	k_{cat}/K_M ($M^{-1} \cdot s^{-1}$)	Ref
1	$[Hg(II)][Zn(II)(H_2O/OH^-)](TRIL9CL23H)_3^{n+}$	9.5	10.0 ± 2.4	$(1.8 \pm 0.4) \cdot 10^3$	$(1.8 \pm 0.3) \cdot 10^5$	460
2	$[Zn(II)]\alpha_3DH_3$	9.5	3.5 ± 0.6	134 ± 8	$(3.8 \pm 0.5) \cdot 10^4$	475
3	$[Zn(II)]\alpha_3DH_3$	9.0	4.9 ± 1.0	103 ± 8	$(2.1 \pm 0.3) \cdot 10^4$	475
4	$[Zn(II)]\alpha_3DH_3$	8.5	7.2 ± 1.1	82 ± 6	$(1.1 \pm 0.1) \cdot 10^4$	475
5	$[Zn(II)]\alpha_3DH_3$	8.0	6.2 ± 1.7	39 ± 4	$(0.63 \pm 0.1) \cdot 10^4$	475
6	hCAII	8.8	8.9	$8.2 \cdot 10^5$	$9.2 \cdot 10^7$	476
7	hCAIII	9.0	20	$8 \cdot 10^3$	$4 \cdot 10^5$	477

[a] Reaction conditions: 100 μM $[Zn(II)]\alpha_3DH_3$, 50 mM buffer / 25 μM indicator (TAPS/m-cresol purple (pH 8.0 and 8.5), AMPSO/thymol blue (pH 9.0), CHES/thymol blue (pH 9.5), 0.1 M ionic strength with Na_2SO_4, 25°C.

7.4 Lyases

In 2011, DeGrado *et al.* engineered Kemp-eliminase activity into the *C*-terminal domain (last 75 residues) of calmodulin (CaM), a Ca^{2+} binding EF-hand regulatory protein.[478] Although the artificial enzyme does not contain a catalytically active metal center, it will be highlighted in this review, since its activity is allosterically regulated by the addition of Ca^{2+} ions. Upon binding of Ca^{2+}, CaM undergoes a structural rearrangement and opens a hydrophobic pocket. De Grado *et al.* placed a general base (mutation F92E) at the bottom of the hydrophobic pocket (Figure 36), guided by computational design (i.e. docking of the substrate). This mutation afforded an active Kemp-eliminase (cCaM-F92E, PDB entry 2KZ2, Scheme 94). A catalytic efficiency (k_{cat}/K_M) of 5.8 ± 0.3 $M^{-1} \cdot s^{-1}$ was determined for

cCaM-F92E, whereas the natural CaM showed no activity. The engineered protein exceeded 40 turnovers.

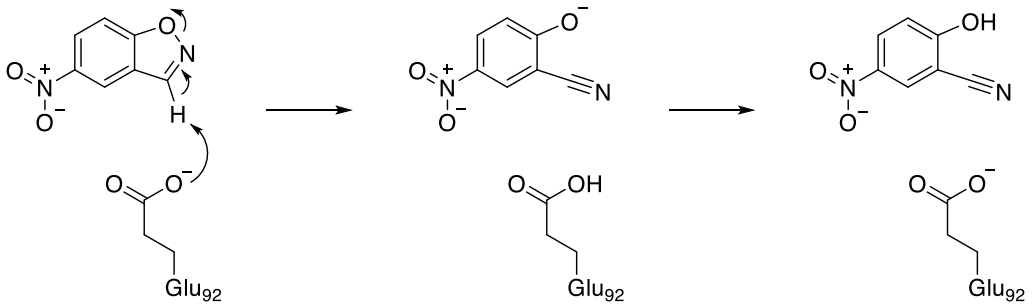

Scheme 94. Kemp elimination catalyzed by an engineered calmodulin variant cCaM-F92E.

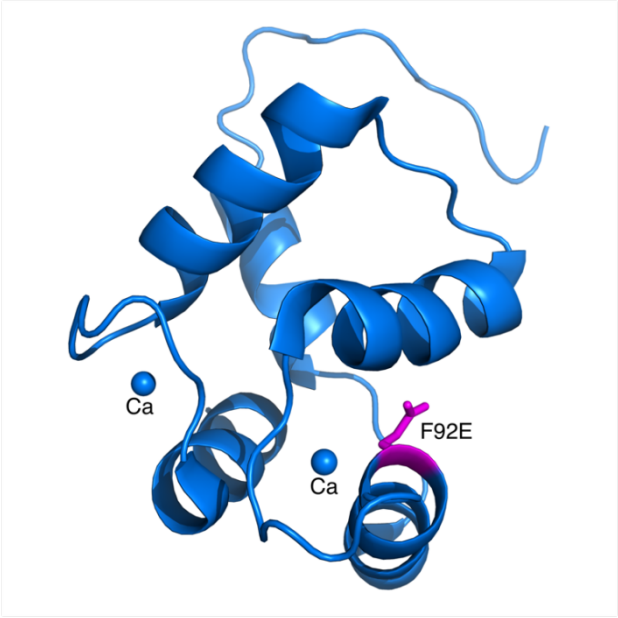

Figure 36. The C-terminal domain of calmodulin (PDB code 2KZ2) is a Ca^{2+}-dependent Kemp-Eliminase.[478]

Beside Kemp-eliminases, researchers have also designed ArMs to catalyze epoxide ring-opening reactions. In 2012, for example, Ueno *et al.* engineered such an artificial construct by covalently linking maleimide-substituted bipyridine cofactor **319** to a cysteine residue in $[(gp5\beta f)_3]_2$ (sections 5.9 and 6.2).[297] Metallation of this scaffold via addition of scandium ions led to the formation of **319**·$[(gp5\beta f)_3]_2$, which catalyzed the ring-opening of epoxide **316** with aniline as nucleophile. The reaction efficiency depended on the position of the bipyridine ligand **319** (Table 40). **319**·$[(gp5\beta f)_3]_2$ (G18C) gave the highest TON (8.4) and

ee (17%). In contrast, trace amounts of racemic aminoalcohol **318** were produced by the mixture of $[(gp5\beta f)_3]_2$ lacking the critical cysteine residue and **320** (Scheme 95).

Table 40. Selected results for the epoxide ring-opening reaction catalyzed by a Sc(bpy) complex anchored to $[(gp5\beta f)_3]_2$.[a]

Entry	Cofactor1	Protein	[Cof] (μM)	Sub1.	Sub2.	*ee* (%)	TON	Ref
1	**319**	$[(gp5\beta f)_3]_2$ (G18C)	200	**316**	**317**	17 (1*R*, 2*R*)	8.4	297
2	**319**	$[(gp5\beta f)_3]_2$ (L47C)	200	**316**	**317**	9 (1*S*, 2*S*)	2.6	297
3	**319**	$[(gp5\beta f)_3]_2$ (N51C)	200	**316**	**317**	1 (1*S*, 2*S*)	1.6	297
4	**320**	$[(gp5\beta f)_3]_2$	200	**316**	**317**	–	trace	297

[a] Reactions were carried out in solution of 1 : 9 acetonitrile/MOPS (10 mM, pH 7.5) at 40°C; $[[(gp5\beta f)_3]_2]$ = 33 μM; reaction time: 48 h.

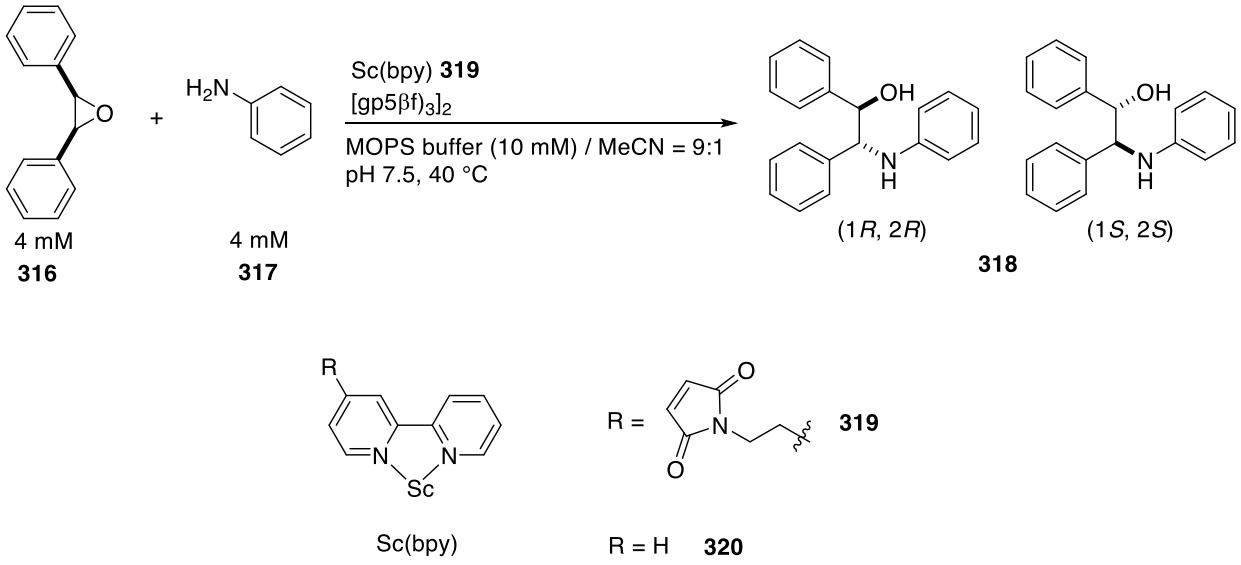

Scheme 95. Epoxide ring-opening reaction catalyzed by a Sc(bpy) complex covalently anchored to $[(gp5\beta f)_3]_2$.

As previously noted (section 4.1), Kamer has shown that a cysteine residue of photoactive yellow protein (PYP) can be selectively acylated with acylimidazole-substituted reagents, and this approach has been used to incorporate phosphine ligands into PYP (Figure 37 a).[479] The analogous reaction could also be achieved using the corresponding $[PdCl(\eta^3\text{-}C_3H_5)]_2$ complexes of phosphines **234** and **235** (Figure 37 b), and the resulting ArMs catalyzed allylic amination of 1,3-di-phenylprop-2-enyl acetate with benzylamine (Figure37 c). No enantioselectivity was observed in this transformation, but the authors also noted that no conversion was observed using PYP lacking phosphine modification in the presence of $[PdCl(\eta^3\text{-}C_3H_5)]_2$, showing that the observed amination reactions results

from intact ArM. Denaturation of the PYP scaffold in the presence of the organic solvent required for substrate solubility was suggested as an explanation for the lack of enantioselectivity in this transformation. These authors later reported a two-step procedure for incorporating phosphines into proteins, though no catalysis was reported.[480]

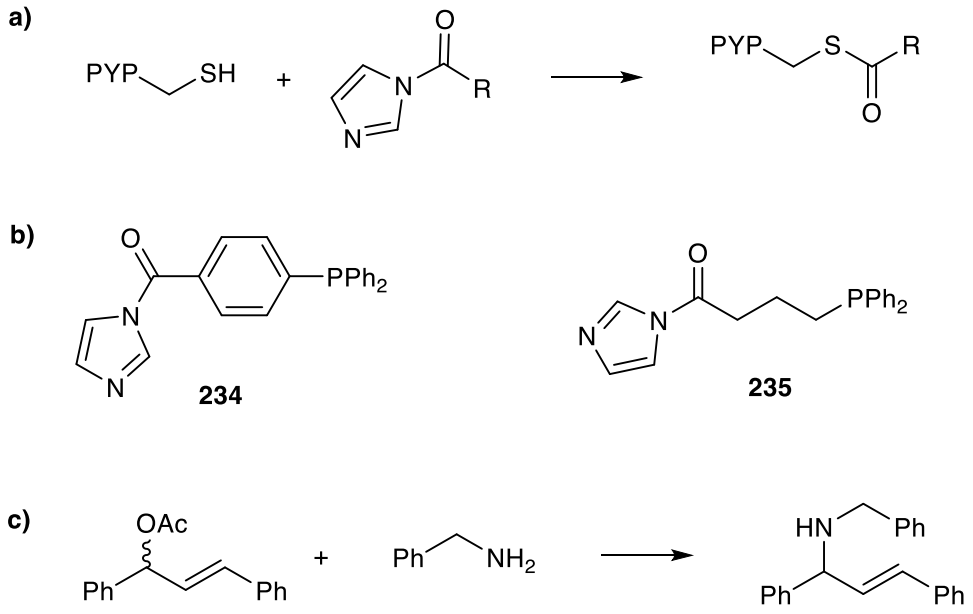

Figure 37. a) Covalent modification of PYP using acylimidazole reagents. b) Acyl-imidazole-substituted phosphine ligands used to generate Pd-allyl ArMs. c) Allylic amination catalyzed by PYP-phosphine Pd-allyl ArMs.[479]

In addition to the 20 natural amino acids, researchers have also incorporated a variety of unnatural amino acids[81] into designed ArM hydrolases. In 2013, Baker *et al.* designed an ArM relying on the unnatural amino acid (2,2'-bipyridin-5yl)alanine (Bpy-Ala, **237**, Figure 26, see also the work of Schultz *et al.* in section 6.1).[481] The engineered constructs bound divalent metal ions Co^{2+}, Zn^{2+}, Fe^{2+} and Ni^{2+}. The highest affinity was determined for Zn^{2+} (K_d ~ 40 pM). Analysis of the crystal structures of the nickel and cobalt-bound variants revealed an octahedral coordination provided by Bpy-Ala, a bidentate glutamate, an aspartate, and a water molecule. These constructs however do not display any catalytic activity.

Finally, an ArM transesterase that mimics the catalytic activity of an RNAse was generated by Mahy and coworkers using a “Trojan horse” strategy. The affinity of testosterone for variant 3.24 of neocarzinostatin (NCS hereafter) was previously exploited to anchor testosterone-linked metal cofactors to NCS.[410] A testosterone-substituted Zn complex, [Zn(N,N-(2-pyridylmethyl)$_2$)Cl] (**323**), was therefore prepared and used to generate an ArM transesterase upon binding to NCS (K_D = 4.0 μM).[482] The zinc-moiety of **323** is rapidly aquated and the Zn(II) ion reduces the pK_a of the bound water molecule, leading to nucleic acid hydrolase activity. Docking studies suggest that the testosterone-moiety of **323** could bind the site 2 of NCS in a fashion that is reminiscent to the interaction in the (unsubstituted) testosterone-NCS complex. The lowest energy docked **323** structure suggests that the catalytic-moiety is located in the site 1 of NCS, thus exerting a significant influence on the catalytic performance and paving the way for improvement through mutagenesis.

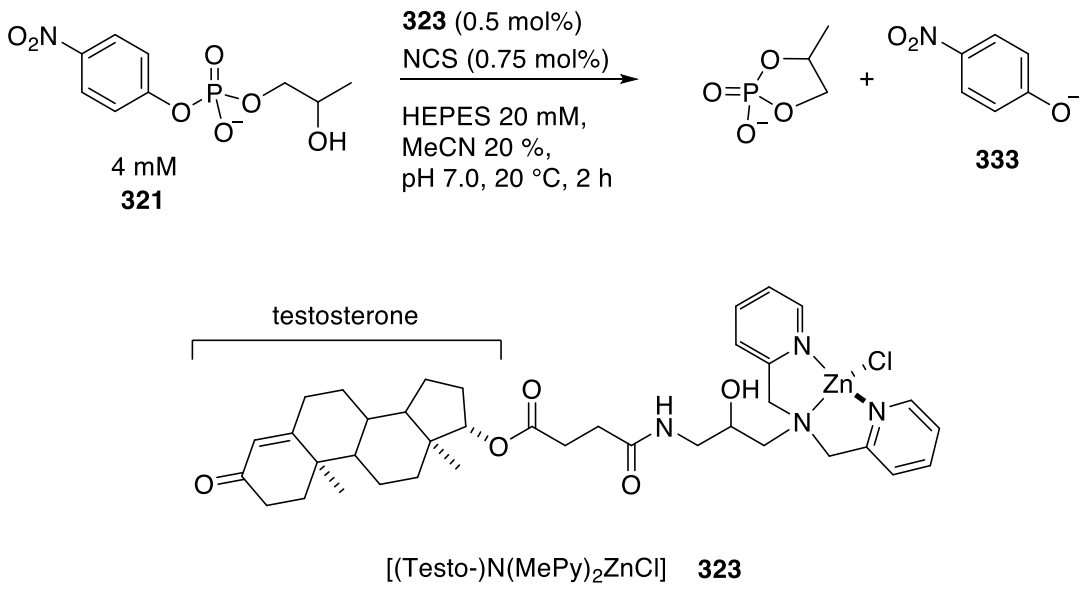

Scheme 96. Supramolecular anchoring of a [N(CH$_2$Py)$_2$ZnCl]-moiety, via a testosterone "Trojan Horse", into neocarzinostatin (NCS) affords an artificial metalloenzyme displaying RNAse-like activity.

The ArM **323**·NCS did not hydrolyze common DNA model compounds, such as bis(*p*-nitrophenyl)phosphate. It did, however, catalyze the transesterification of phosphate **321** into **322** (Scheme 96). The involvement of a vicinal hydroxy-moiety is reminiscent to the activity of RNAse enzymes. The highest activity achieved was TOF = $3 \cdot 10^{-4}$ s^{-1}, at pH 7.0. This is ~800 fold faster than the cofactor **323** alone, highlighting the positive influence of the NCS host protein. Saturation kinetics were determined for **323**·NCS: K_M = 22 μM and a $k_{cat} = 3 \cdot 10^{-4}$ s^{-1} resulting in an efficiency k_{cat}/K_M = 13.6 $M^{-1} \cdot s^{-1}$. Unfortunately, the protein rapidly denatures in solution, thus limiting the lifetime of **323**·NCS.

8. Outlook

The studies highlighted in this review showcase the wide range of metal complexes, protein scaffolds, and linkage strategies that have been used to generate ArMs to date. This diversity of components and methodologies has led to systems that catalyze an impressive range of challenging chemical reactions, many of which are not found in nature. Moreover, a range of approaches has been developed to optimize ArMs for chemo-, regio-, site-, and enantioselective catalysis. Early efforts toward this end involved altering cofactor linkage sites within scaffold proteins,[144] altering cofactor structure,[153] and exploring different scaffold/cofactor combinations to enable chemogenetic ArM optimization[176]. Point mutations were later introduced into putative ArM active sites of scaffold proteins to improve ArM selectivity,[172, 414] and iterative targeted mutagenesis was subsequently reported[483]. Despite these advances and many more since,[39] ArM catalysis remains rather underdeveloped when compared to homogeneous transition metal catalysis or enzyme catalysis. Because of this, Whitesides' pronouncement regarding the practicality of ArMs[2] remains true to this day.

As noted in the introduction, fundamental advances in protein engineering[484] and aqueous organometallic chemistry[485] contributed to a resurgence in ArM research around the year 2000. Further improvements in ArM efficiency will require innovations that specifically address and exploit the hybrid structures of ArMs.[87] For example, while many studies have demonstrated the potential for protein scaffolds to control the selectivity or organometallic catalysts, the catalysts used are typically well-known from the organometallic literature and remain unmodified upon incorporation into protein scaffolds. The activity and selectivity or cofactors designed to interact synergistically with scaffold proteins via ligand exchange,[319] electron transfer,[294] or other means could be more extensively tuned or even

uniquely activated via incorporation into proteins. Similarly, while a range of bioconjugation techniques have been used for cofactor incorporation, only a handful of these are compatible with complex media, including cell lysate (*in vitro*) or cytosol (*in vivo*). Transitioning to efficient bioorthogonal methods[352, 486] for covalent[352], non-covalent[349], dative[469], and substitutive[350] cofactor incorporation will ensure that ArM libraries can be readily generated as efficiently as for natural enzymes.

Just as methodology must be adapted to suit different aspects of the unique composition or ArMs, so too must our understanding of the structure and function of these catalysts, which currently lags far behind that of transition metal catalysts and enzymes. ArM characterization typically involves a battery of spectroscopy, mass spectrometry, and, in some cases, X-ray crystallography to ensure the desired composition. Evidence for specific scaffold-cofactor interactions (e.g. dative ligation of metal centers) is often presented,[255, 352] and many examples in which scaffold accelerated catalysis have been reported.[44, 319] On the other hand, the exact contributions to catalysis of the former and the origins of the latter remain unclear. Substrate binding interactions within ArM active sites remain almost completely unexplored. These are precisely the types of phenomena that natural enzymes have evolved to harness,[487] so understanding how they have emerged in ArMs (albeit to only a primordial extent at this point) could improve our ability to design and evolve comparably efficient systems. Given the importance of protein scaffolds to the activity of natural metal cofactors,[488] it is reasonable to hypothesize that large improvements in the activity and selectivity of synthetic catalysts could be achieved using properly designed protein scaffolds. Toward this end, far deeper biophysical studies into the nature of ArM catalysis, mirroring efforts in enzymology, are required. Similarly, significant improvements in computational approaches to design and simulate the structure and conformational dynamics or proteins containing synthetic metal catalysts will

be required to provide insight into the molecular level events that occur during ArM catalysis.[272, 481, 489]

Advances in cofactor design, activation, and bioconjugation, along with improved understanding of ArM catalysis would facilitate development of what is perhaps the most important methodological hurdle limiting ArM catalysis: directed evolution.[490] It is difficult to overstate the impact that directed evolution has had on biocatalysis using natural enzymes,[162] and yet such efforts toward ArMs remain in their infancy. Reports to date have demonstrated that iterative targeted mutagenesis of residues proximal to metal cofactors (or at least their presumed location during catalysis) can improve ArM selectivity and activity.[7] While similar approaches have of course been used to optimize natural enzymes, the true power of directed evolution and the great improvements and surprises in the activity of evolved enzymes have been realized not solely via mutation of active site residues but from functional screens and selections conducted on diverse populations of enzymes containing mutations throughout their structure.[490]

Unfortunately, random mutagenesis methods remain unexplored in part due to the small ArM library sizes that can be generated using existing cofactor incorporation methods,[491] while targeted mutagenesis (outside of the putative ArM active site) is hindered by a lack of fundamental understanding of how distal scaffold mutations impact cofactor selectivity. Toward the latter point, for example, it is not obvious that phylogenetic tools used to generate targeted "smart libraries" of natural enzymes are applicable to ArMs given that the function of the two are completely unrelated.[162] Nonetheless, adapting the full arsenal of library methodologies that are available for enzyme evolution, ranging from random mutagenesis and gene shuffling[484] to combinatorial codon mutagenesis[492] and chimeragenesis[493], to ArMs will ensure that the latter can be evolved with the efficiency of

the former. Genome mining to identify diverse homologues of relevant scaffolds and computations tools to identify new scaffolds based on sequence but (predicted) structural homology could also be highly beneficial for identifying new ArM scaffolds.[494-495] Based on the success of evolved enzymes for practical applications, this would go a long way to establish whether ArMs can in fact have practical utility.

Despite the need for significant advances in our ability to engineer and understand ArMs, hints of their potential utility have already begun to emerge. The many enantioselective transformations highlighted above have certainly proven their worth for fine chemical synthesis. The few studies reported on the activity of immobilized ArMs suggest that significant improvements in the practicality of ArM catalysis could be realized using different immobilization procedures.[257, 260, 314, 332] A key goal of future ArM research must be to develop such transformations that cannot be accomplished using small molecule or enzyme catalysts. In such cases, the added complexity of ArM formation relative to other systems might be offset by savings in other aspects of a process. Tandem processes involving enzyme and ArM catalysis have also been developed,[261] and these illustrate the unique ability of ArMs to shield transition metals from species that would otherwise lead to catalyst death. Taking this possibility to the extreme, ArM catalysis *in vivo*[349, 496] could ultimately be used to augment metabolic pathways with synthetic reactions to expand the scope of biosynthesis[497]. Obviously much work remains before these possibilities can be realized, but recent progress in ArM catalysis and other areas of protein engineering and organometallic chemistry should encourage those willing to take on the challenges that lie ahead.

References

1. Yamamura, K.; Kaiser, E. T., Studies on the Oxidase Activity of Copper(II) Carboxypeptidase A. *J. Chem. Soc., Chem. Commun.* **1976,** (20), 830-831.
2. Wilson, M. E.; Whitesides, G. M., Conversion of a Protein to a Homogeneous Asymmetric Hydrogenation Catalyst by Site-Specific Modification with a Diphosphinerhodium(I) Moiety. *J. Am. Chem. Soc.* **1978,** *100* (1), 306-307.
3. Chen, K.; Arnold, F. H., Tuning the Activity of an Enzyme for Unusual Environments: Sequential Random Mutagenesis of Subtilisin E for Catalysis in Dimethylformamide. *Proc. Natl. Acad. Sci. U. S. A.* **1993,** *90*, 5618-5622.
4. Stemmer, W. P. C., Rapid Evolution of a Protein in vitro by DNA Shuffling. *Nature* **1994,** *370*, 389-391.
5. Powell, K. A.; Ramer, S. W.; Cardayré, S. B. d.; Stemmer, W. P. C.; Tobin, M. B.; Longchamp, P. F.; Huisman, G. W., Directed Evolution and Biocatalysis. *Angew. Chem., Int. Ed.* **2001,** *40*, 3948-3959.
6. Bloom, J. D.; Arnold, F. H., In the Light of Directed Evolution: Pathways of Adaptive Protein Evolution. *Proc. Natl. Acad. Sci. U. S. A.* **2009,** *106*, 9995-10000.
7. Reetz, M. T., Biocatalysis in Organic Chemistry and Biotechnology: Past, Present, and Future. *J. Am. Chem. Soc.* **2013,** *135* (34), 12480-12496.
8. Savile, C. K.; Janey, J. M.; Mundorff, E. C.; Moore, J. C.; Tam, S.; Jarvis, W. R.; Colbeck, J. C.; Krebber, A.; Fleitz, F. J.; Brands, J., Biocatalytic Asymmetric Synthesis of Chiral Amines from Ketones Applied to Sitagliptin Manufacture. *Science* **2010,** *329* (5989), 305-309.
9. Hermanson, G. T., *Bioconjugate Techniques*. 3rd ed.; Elsevier: Oxford, 2013.
10. Yang, H.; Srivastava, P.; Zhang, C.; Lewis, J. C., A General Method for Artificial Metalloenzyme Formation through Strain-Promoted Azide-Alkyne Cycloaddition. *ChemBioChem* **2014,** *15* (2), 223-227.
11. Jing, Q.; Okrasa, K.; Kazlauskas, R. J., Manganese-Substituted Alpha-Carbonic Anhydrase as an Enantioselective Peroxidase. *Top. Organomet. Chem.* **2009,** *25*, 45-61.
12. Coelho, P. S.; Brustad, E. M.; Kannan, A.; Arnold, F. H., Olefin Cyclopropanation Via Carbene Transfer Catalyzed by Engineered Cytochrome P450 Enzymes. *Science* **2013,** *339* (6117), 307-310.
13. Renata, H.; Wang, Z. J.; Arnold, F. H., Expanding the Enzyme Universe: Accessing Non-Natural Reactions by Mechanism-Guided Directed Evolution. *Angew. Chem., Int. Ed.* **2015,** *54* (11), 3351-3367.
14. Bordeaux, M.; Tyagi, V.; Fasan, R., Highly Diastereoselective and Enantioselective Olefin Cyclopropanation Using Engineered Myoglobin-Based Catalysts. *Angew. Chem., Int. Ed.* **2015,** *54* (6), 1744-1748.
15. Qi, D.; Tann, C.-M.; Haring, D.; Distefano, M. D., Generation of New Enzymes Via Covalent Modification of Existing Proteins. *Chem. Rev.* **2001,** *101* (10), 3081-3111.
16. Thomas, C. M.; Ward, T. R., Design of Artificial Metalloenzymes. *Appl. Organomet. Chem.* **2005,** *19* (1), 35-39.
17. Thomas, C. M.; Ward, T. R., Artificial Metalloenzymes: Proteins as Hosts for Enantioselective Catalysis. *Chem. Soc. Rev.* **2005,** *34*, 337-346.
18. Letondor, C.; Ward, T. R., Artificial Metalloenzymes for Enantioselective Catalysis: Recent Advances. *ChemBioChem* **2006,** *7* (12), 1845-1852.
19. Creus, M.; Ward, T. R., Designed Evolution of Artificial Metalloenzymes: Protein Catalysts Made to Order. *Org. Biomol. Chem.* **2007,** *5*, 1835-1844.
20. Mao, J.; Ward, T. R., Artificial Metalloenzymes for Enantioselective Catalysis Based on the Biotin-Avidin Technology. *Chimia* **2008,** *62* (12), 956-961.
21. Heinisch, T.; Ward, T. R., Design Strategies for the Creation of Artificial Metalloenzymes. *Curr. Opin. Chem. Biol.* **2010,** *14* (2), 184-199.
22. Heinisch, T.; Ward, T. R., Latest Developments in Metalloenzyme Design and Repurposing. *Eur. J. Inorg. Chem.* **2015,** (21), 3406-3418.

23. Dürrenberger, M.; Ward, T. R., Recent Achievments in the Design and Engineering of Artificial Metalloenzymes. *Curr. Opin. Chem. Biol.* **2014,** *19*, 99-106.
24. Koehler, V.; Wilson, Y. M.; Lo, C.; Sardo, A.; Ward, T. R., Protein-Based Hybrid Catalysts-Design and Evolution. *Curr. Opin. Biotechnol.* **2010,** *21* (6), 744-752.
25. Pordea, A.; Ward, T. R., Artificial Metalloenzymes: Combining the Best Features of Homogeneous and Enzymatic Catalysis. *Synlett* **2009,** (20), 3225-3236.
26. Ringenberg, M. R.; Ward, T. R., Merging the Best of Two Worlds: Artificial Metalloenzymes for Enantioselective Catalysis. *Chem. Commun.* **2011,** *47* (30), 8470-8476.
27. Steinreiber, J.; T.R., W., Artificial Metalloenzymes as Selective Catalysts in Aqueous Media. *Coord. Chem. Rev.* **2008,** *252*, 751–766.
28. Steinreiber, J.; Ward, T. R., Artificial Metalloenzymes for Enantioselective Catalysis Based on the Biotin-Avidin Technology. In *Topics in Organometallic Chemistry*, Springer Berlin Heidelberg: 2008; Vol. 25, pp 93-112.
29. Ward, T. R., Artificial Metalloenzymes for Enantioselective Catalysis Based on the Noncovalent Incorporation of Organometallic Moieties in a Host Protein. *Chem. - Eur. J.* **2005,** *11* (13), 3798-3804.
30. Ward, T. R., Artificial Metalloenzymes: Enantioselective Catalysis and Beyond. *Chimia* **2010,** *64* (12), 850-852.
31. Ward, T. R., Artificial Metalloenzymes Based on the Biotin-Avidin Technology: Enantioselective Catalysis and Beyond. *Acc. Chem. Res.* **2011,** *44* (1), 47-57.
32. Ward, T. R.; Collot, J.; Gradinaru, J.; Loosli, A.; Skander, M.; Letondor, C.; Joseph, E.; Klein, G., Exploiting the Second Coordination Sphere: Proteins as Host for Enantioselective Catalysis. *Chimia* **2003,** *57*, 586-588.
33. Davies, C. L.; Dux, E. L.; Duhme-Klair, A. K., Supramolecular Interactions between Functional Metal Complexes and Proteins. *Dalton Trans.* **2009,** (46), 10141-10154.
34. Yu, F. T.; Cangelosi, V. M.; Zastrow, M. L.; Tegoni, M.; Plegaria, J. S.; Tebo, A. G.; Mocny, C. S.; Ruckthong, L.; Qayyum, H.; Pecoraro, V. L., Protein Design: Toward Functional Metalloenzymes. *Chem. Rev.* **2014,** *114* (7), 3495-3578.
35. Zastrow, M. L.; Pecoraro, V. L., Designing Functional Metalloproteins: From Structural to Catalytic Metal Sites. *Coord. Chem. Rev.* **2013,** *257* (17-18), 2565-2588.
36. Pamies, O.; Dieguez, M.; Bäckvall, J. E., Artificial Metalloenzymes in Asymmetric Catalysis: Key Developments and Future Directions. *Adv. Synth. Catal.* **2015,** *357* (8), 1567-1586.
37. Hoarau, M.; Hureau, C.; Gras, E.; Faller, P., Coordination Complexes and Biomolecules: A Wise Wedding for Catalysis Upgrade. *Coord. Chem. Rev.* **2016,** *308*, 445-459.
38. Heinisch, T.; Ward, T. R., Artificial Metalloenzymes Based on the Biotin-Streptavidin Technology: Challenges and Opportunities. *Acc. Chem. Res.* **2016,** *49* (9), 1711-1721.
39. Hyster, T. K.; Ward, T. R., Genetic Optimization of Metalloenzymes: Enhancing Enzymes for Non-Natural Reactions. *Angew. Chem., Int. Ed.* **2016,** *55* (26), 7344-7357.
40. Mao, J.; Ward, T. R., Proteins as Host for Enantioselective Catalysis: Artificial Metalloenzymes Based on the Biotin-Streptavidin Technology. John Wiley & Sons Ltd.: 2010; pp 361-376.
41. Praneeth, V. K. K.; Ward, T. R., Metal-Catalyzed Organic Transformations inside a Protein Scaffold Using Artificial Metalloenzymes. John Wiley & Sons, Inc.: 2013; pp 203-219.
42. Wilson, Y. M.; Duerrenberger, M.; Ward, T. R. In *Organometallic Chemistry in Protein Scaffolds*, Wiley-VCH Verlag GmbH & Co. KGaA: 2013; pp 215-241.
43. Chatterjee, A.; Ward, T. R., Recent Advances in the Palladium Catalyzed Suzuki-Miyaura Cross-Coupling Reaction in Water. *Catal. Lett.* **2016,** *146* (4), 820-840.
44. Collot, J.; Humbert, N.; Skander, M.; Klein, G.; Ward, T. R., Artificial Metalloenzymes for Enantioselective Catalysis: The Phenomenon of Protein Accelerated Catalysis. *J. Organomet. Chem.* **2004,** *689* (25), 4868-4871.
45. Creus, M.; Ward, T. R., Design and Evolution of Artificial Metalloenzymes: Biomimetic Aspects. *Prog. Inorg. Chem.* **2012,** *57*, 203-253.
46. Koehler, V.; Ward, T. R., Concurrent Cross Metathesis and Enzymatic Oxidation. Enabling Off-Equilibrium Transformations. *ChemCatChem* **2014,** *6* (8), 2191-2193.

47. Pordea, A.; Ward, T. R., Chemogenetic Protein Engineering: An Efficient Tool for the Optimization of Artificial Metalloenzymes. *Chem. Commun. (Cambridge, U. K.)* **2008,** (36), 4239-4249.
48. Quinto, T.; Koehler, V.; Ward, T. R., Recent Trends in Biomimetic NADH Regeneration. *Top. Catal.* **2014,** *57* (5), 321-331.
49. Ward, T. R., Artificial Enzymes Made to Order: Combination of Computational Design and Directed Evolution. *Angew. Chem., Int. Ed.* **2008,** *47* (41), 7802-7803.
50. Ward, T. R., Directed Evolution of Iridium-Substituted Myoglobin Affords Versatile Artificial Metalloenzymes for Enantioselective C-C Bond-Forming Reactions. *Angew. Chem., Int. Ed.* **2016,** *55* (48), 14909-14911.
51. Hayashi, T.; Hisaeda, Y., New Functionalization of Myoglobin by Chemical Modification of Heme-Propionates. *Acc. Chem. Res.* **2002,** *35* (1), 35-43.
52. Hayashi, T.; Sano, Y.; Onoda, A., Generation of New Artificial Metalloproteins by Cofactor Modification of Native Hemoproteins. *Isr. J. Chem.* **2015,** *55* (1), 76-84.
53. Inaba, H.; Kitagawa, S.; Ueno, T., Protein Needles as Molecular Templates for Artificial Metalloenzymes. *Isr. J. Chem.* **2015,** *55* (1), 40-50.
54. Maity, B.; Fujita, K.; Ueno, T., Use of the Confined Spaces of Apo-Ferritin and Virus Capsids as Nanoreactors for Catalytic Reactions. *Curr. Opin. Chem. Biol.* **2015,** *25*, 88-97.
55. Ueno, T.; Abe, S.; Yokoi, N.; Watanabe, Y., Coordination Design of Artificial Metalloproteins Utilizing Protein Vacant Space. *Coord. Chem. Rev.* **2007,** *251* (21-24), 2717-2731.
56. Yamaguchi, H.; Harada, A., Functionalized Antibodies as Biosensing Materials and Catalysts. *Chem. Lett.* **2008,** *37* (12), 1184-1189.
57. Artero, V.; Berggren, G.; Atta, M.; Caserta, G.; Roy, S.; Pecqueur, L.; Fontecave, M., From Enzyme Maturation to Synthetic Chemistry: The Case of Hydrogenases. *Acc. Chem. Res.* **2015,** *48* (8), 2380-2387.
58. Caserta, G.; Roy, S.; Atta, M.; Artero, V.; Fontecave, M., Artificial Hydrogenases: Biohybrid and Supramolecular Systems for Catalytic Hydrogen Production or Uptake. *Curr. Opin. Chem. Biol.* **2015,** *25*, 36-47.
59. Faiella, M.; Roy, A.; Sommer, D.; Ghirlanda, G., De Novo Design of Functional Proteins: Toward Artificial Hydrogenases. *Biopolymers* **2013,** *100* (6), 558-571.
60. Fukuzumi, S., Artificial Photosynthetic Systems for Production of Hydrogen. *Curr. Opin. Chem. Biol.* **2015,** *25*, 18-26.
61. Kandemir, B.; Chakraborty, S.; Guo, Y. X.; Bren, K. L., Semisynthetic and Biomolecular Hydrogen Evolution Catalysts. *Inorg. Chem.* **2016,** *55* (2), 467-477.
62. Mahy, J. P.; Marechal, J. D.; Ricoux, R., Various Strategies for Obtaining Oxidative Artificial Hemoproteins with a Catalytic Oxidative Activity: From "Hemoabzymes" to "Hemozymes"? *J. Porphyrins Phthalocyanines* **2014,** *18* (12), 1063-1092.
63. Mahy, J. P.; Marechal, J. D.; Ricoux, R., From "Hemoabzymes" to "Hemozymes": Towards New Biocatalysts for Selective Oxidations. *Chem. Commun. (Cambridge, U. K.)* **2015,** *51* (13), 2476-2494.
64. Marchi-Delapierre, C.; Rondot, L.; Cavazza, C.; Ménage, S., Oxidation Catalysis by Rationally Designed Artificial Metalloenzymes. *Isr. J. Chem.* **2015,** *55* (1), 61-75.
65. Mulfort, K. L.; Utschig, L. M., Modular Homogeneous Chromophore-Catalyst Assemblies. *Acc. Chem. Res.* **2016,** *49* (5), 835-843.
66. Onoda, A.; Hayashi, T., Artificial Hydrogenase: Biomimetic Approaches Controlling Active Molecular Catalysts. *Curr. Opin. Chem. Biol.* **2015,** *25*, 133-140.
67. Onoda, A.; Hayashi, T.; Salmain, M., Artificial Metalloenzymes Containing an Organometallic Active Site. In *Bioorganometallic Chemistry: Applications in Drug Discovery, Biocatalysis, and Imaging*, Wiley-VCH Verlag GmbH & Co. KGaA: Weinheim, 2014; pp 305-337.
68. Simmons, T. R.; Berggren, G.; Bacchi, M.; Fontecave, M.; Artero, V., Mimicking Hydrogenases: From Biomimetics to Artificial Enzymes. *Coord. Chem. Rev.* **2014,** *270*, 127-150.
69. Bailey, J. B.; Subramanian, R. H.; Churchfield, L. A.; Tezcan, F. A., Metal-Directed Design of Supramolecular Protein Assemblies. *Methods Enzymol.* **2016,** *580*, 223-250.
70. Ball, Z. T., Designing Enzyme-Like Catalysts: A Rhodium(II) Metallopeptide Case Study. *Acc. Chem. Res.* **2013,** *46* (2), 560-570.

71. Ball, Z. T., Molecular Recognition in Protein Modification with Rhodium Metallopeptides. *Curr. Opin. Chem. Biol.* **2015,** *25*, 98-102.
72. Chino, M.; Maglio, O.; Nastri, F.; Pavone, V.; DeGrado, W. F.; Lombardi, A., Artificial Diiron Enzymes with a De Novo Designed Four-Helix Bundle Structure. *Eur. J. Inorg. Chem.* **2015,** (21), 3371-3390.
73. Golynskiy, M. V.; Seelig, B., De Novo Enzymes: From Computational Design to mRNA Display. *Trends Biotechnol.* **2010,** *28* (7), 340-345.
74. Huang, P. S.; Boyken, S. E.; Baker, D., The Coming of Age of De Novo Protein Design. *Nature* **2016,** *537* (7620), 320-327.
75. Korendovych, I. V.; DeGrado, W. F., Catalytic Efficiency of Designed Catalytic Proteins. *Curr. Opin. Struct. Biol.* **2014,** *27*, 113-121.
76. Maglio, O.; Nastri, F.; de Rosales, R. T. M.; Faiella, M.; Pavone, V.; DeGrado, W. F.; Lombardi, A., Diiron-Containing Metalloproteins: Developing Functional Models. *C. R. Chim.* **2007,** *10* (8), 703-720.
77. Mocny, C. S.; Pecoraro, V. L., De Novo Protein Design as a Methodology for Synthetic Bioinorganic Chemistry. *Acc. Chem. Res.* **2015,** *48* (8), 2388-2396.
78. Nastri, F.; Chino, M.; Maglio, O.; Bhagi-Damodaran, A.; Lu, Y.; Lombardi, A., Design and Engineering of Artificial Oxygen-Activating Metalloenzymes. *Chem. Soc. Rev.* **2016,** *45* (18), 5020-5054.
79. Sontz, P. A.; Song, W. J.; Tezcan, F. A., Interfacial Metal Coordination in Engineered Protein and Peptide Assemblies. *Curr. Opin. Chem. Biol.* **2014,** *19*, 42-49.
80. Tebo, A. G.; Pecoraro, V. L., Artificial Metalloenzymes Derived from Three-Helix Bundles. *Curr. Opin. Chem. Biol.* **2015,** *25*, 65-70.
81. Xiao, H.; Schultz, P. G., At the Interface of Chemical and Biological Synthesis: An Expanded Genetic Code. *Cold Spring Harbor Perspect. Biol.* **2016,** *8* (9), 1-18.
82. Zastrow, M. L.; Pecoraro, V. L., Designing Hydrolytic Zinc Metalloenzymes. *Biochemistry* **2014,** *53* (6), 957-978.
83. Wieczorek, B.; Dijkstra, H. P.; Egmond, M. R.; Klein Gebbink, R. J. M.; van Koten, G., Incorporating ECE-pincer Metal Complexes as Functional Building Blocks in Semisynthetic Metalloenzymes, Supramolecular Polypeptide Hybrids, Tamoxifen Derivatives, Biomarkers and Sensors. *J. Organomet. Chem.* **2009,** *694* (6), 812-822.
84. Rosati, F.; Roelfes, G., Artificial Metalloenzymes. *ChemCatChem* **2010,** *2* (8), 916-927.
85. Bos, J.; Roelfes, G., Artificial Metalloenzymes for Enantioselective Catalysis. *Curr. Opin. Chem. Biol.* **2014,** *19*, 135-143.
86. Drienovská, I.; Roelfes, G., Artificial Metalloenzymes for Asymmetric Catalysis by Creation of Novel Active Sites in Protein and DNA Scaffolds. *Isr. J. Chem.* **2015,** *55* (1), 21-31.
87. Lewis, J. C., Artificial Metalloenzymes and Metallopeptide Catalysts for Organic Synthesis. *ACS Catal.* **2013,** *3* (12), 2954-2975.
88. Lewis, J. C., Metallopeptide Catalysts and Artificial Metalloenzymes Containing Unnatural Amino Acids. *Curr. Opin. Chem. Biol.* **2015,** *25*, 27-35.
89. Palomo, J. M.; Filice, M., New Emerging Bio-Catalysts Design in Biotransformations. *Biotechnol. Adv.* **2015,** *33* (5), 605-613.
90. Ilie, A.; Reetz, M. T., Directed Evolution of Artificial Metalloenzymes. *Isr. J. Chem.* **2015,** *55* (1), 51-60.
91. Reetz, M. T., Artificial Metalloenzymes as Catalysts in Stereoselective Diels-Alder Reactions. *Chem. Rec.* **2012,** *12* (4), 391-406.
92. Petrik, I. D.; Liu, J.; Lu, Y., Metalloenzyme Design and Engineering through Strategic Modifications of Native Protein Scaffolds. *Curr. Opin. Chem. Biol.* **2014,** *19*, 67-75.
93. Deuss, P. J.; den Heeten, R.; Laan, W.; Kamer, P. C. J., Bioinspired Catalyst Design and Artificial Metalloenzymes. *Chem. - Eur. J.* **2011,** *17* (17), 4680-4698.
94. Doble, M. V.; Ward, A. C. C.; Deuss, P. J.; Jarvis, A. G.; Kamer, P. C. J., Catalyst Design in Oxidation Chemistry; from $KMnO_4$ to Artificial Metalloenzymes. *Bioorg. Med. Chem.* **2014,** *22* (20), 5657-5677.
95. Kohler, V.; Ward, T. R., Design of a Functional Nitric Oxide Reductase within a Myoglobin Scaffold. *ChemBioChem* **2010,** *11* (8), 1049-1051.

96. Boersma, A. J.; Megens, R. P.; Feringa, B. L.; Roelfes, G., DNA-Based Asymmetric Catalysis. *Chem. Soc. Rev.* **2010,** *39* (6), 2083-2092.
97. Rioz-Martinez, A.; Roelfes, G., DNA-Based Hybrid Catalysis. *Curr. Opin. Chem. Biol.* **2015,** *25*, 80-87.
98. Park, S.; Sugiyama, H., DNA-Based Hybrid Catalysts for Asymmetric Organic Synthesis. *Angew. Chem., Int. Ed.* **2010,** *49* (23), 3870-3878.
99. Hoffmann, R.; Kabanov, A. A.; Golov, A. A.; Proserpio, D. M., Homo Citans and Carbon Allotropes: For an Ethics of Citation. *Angew. Chem., Int. Ed.* **2016,** *55* (37), 10962-10976.
100. Ward, T. R. Artificial Metalloenzymes: Update. http://www.chemie.unibas.ch/~ward/.
101. Kagan, H. B., Historical Perspective. In *Comprehensive Asymmetric Catalysis*, Pfaltz, A.; Jacobsen, E. N., Eds. Springer-Verlag: Berlin Heidelberg Germany, 1999; Vol. 1, pp 9-30.
102. Blaser, H. U.; Spindler, F.; Studer, M., Enantioselective Catalysis in Fine Chemicals Production. *Appl. Catal., A* **2001,** *221* (1-2), 119-143.
103. Akabori, S.; Sakurai, S.; Izumi, Y.; Fujii, Y., An Asymmetric Catalyst. *Nature* **1956,** *178* (4528), 323-324.
104. De Corte, S.; Hennebel, T.; De Gusseme, B.; Verstraete, W.; Boon, N., Bio-Palladium: From Metal Recovery to Catalytic Applications. *Microb. Biotechnol.* **2012,** *5* (1), 5-17.
105. Chankeshwara, S. V.; Indrigo, E.; Bradley, M., Palladium-Mediated Chemistry in Living Cells. *Curr. Opin. Chem. Biol.* **2014,** *21*, 128-135.
106. Yang, M.; Li, J.; Chen, P. R., Transition Metal-Mediated Bioorthogonal Protein Chemistry in Living Cells. *Chem. Soc. Rev.* **2014,** *43* (18), 6511-6526.
107. Cuatrecasas, P.; Fuchs, S.; Anfinsen, C. B., Catalytic Properties and Specificity of the Extracellular Nuclease of Staphylococcus Aureus. *J. Biol. Chem.* **1967,** *242* (7), 1541-1547.
108. Coleman, J. E., Metal Ion Dependent Binding of Sulphonamide to Carbonic Anhydrase. *Nature* **1967,** *214* (5084), 193-194.
109. Tainer, J. A.; Roberts, V. A.; Getzoff, E. D., Metal-Binding Sites in Proteins. *Curr. Opin. Biotechnol.* **1991,** *2* (4), 582-591.
110. Lu, Y.; Berry, S. M.; Pfister, T. D., Engineering Novel Metalloproteins: Design of Metal-Binding Sites into Native Protein Scaffolds. *Chem. Rev.* **2001,** *101* (10), 3047-3080.
111. Darnall, D. W.; Birnbaum, E. R., Rare Earth Metal Ions as Probes of Calcium Ion Binding Sites in Proteins: Neodynium(III) Acceleration of the Activation of Trypsinogen. *J. Biol. Chem.* **1970,** *245* (23), 6484-6486.
112. Gomez, J. E.; Birnbaum, E. R.; Darnall, D. W., The Metal Ion Acceleration of the Conversion of Trypsinogen to Trypsin. Lanthanide Ions as Calcium Ion Substitutes. *Biochemistry* **1974,** *13* (18), 3745-3750.
113. Sugimoto, T.; Kokubo, T.; Miyazaki, J.; Tanimoto, S.; Okano, M., Stereoselective Oxidation of Aromatic Sulfides and Sulfoxides in the Binding Domain of Bovine Serum Albumin. *Bioorg. Chem.* **1981,** *10* (3), 311-323.
114. Sugimoto, T.; Kokubo, T.; Miyazaki, J.; Tanimoto, S.; Okano, M., Stereoselective Formation of Aromatic Sulfoxides by Oxidation of Sulfides and Sulfoxides in the Presence of Bovine Serum Albumin. *J. Chem. Soc., Chem. Commun.* **1979,** (23), 1052-1053.
115. Sugimoto, T.; Kokubo, T.; Miyazaki, J.; Tanimoto, S.; Okano, M., Preparation of Optically Active Aromatic Sulfoxides of High Optical Purity by the Direct Oxidation of the Sulfides in the Presence of Bovine Serum Albumin. *J. Chem. Soc., Chem. Commun.* **1979,** (9), 402-404.
116. Kokubo, T.; Sugimoto, T.; Uchida, T.; Tanimoto, S.; Okano, M., The Bovine Serum Albumin-2-Phenylpropane-1,2-Diolatodioxo-Osmium(VI) Complex as an Enantioselective Catalyst for Cis-Hydroxylation of Alkenes. *J. Chem. Soc., Chem. Commun.* **1983,** (14), 769-770.
117. Hannemann, F.; Bichet, A.; Ewen, K. M.; Bernhardt, R., Cytochrome P450 Systems—Biological Variations of Electron Transport Chains. *Biochim. Biophys. Acta, Gen. Subj.* **2007,** *1770* (3), 330-344.
118. O'Reilly, E.; Kohler, V.; Flitsch, S. L.; Turner, N. J., Cytochromes P450 as Useful Biocatalysts: Addressing the Limitations. *Chem. Commun.* **2011,** *47* (9), 2490-2501.

119. Mieyal, J. J.; Ackerman, R. S.; Blumer, J. L.; Freeman, L. S., Characterization of Enzyme-Like Activity of Human Hemoglobin. Properties of the Hemoglobin-P-450 Reductase-Coupled Aniline Hydroxylase System. *J. Biol. Chem.* **1976,** *251* (11), 3436-3441.
120. Kokubo, T.; Sassa, S.; Kaiser, E. T., Flavohemoglobin: A Semisynthetic Hydroxylase Acting in the Absence of Reductase. *J. Am. Chem. Soc.* **1987,** *109* (2), 606-607.
121. Kuriyan, J.; Pahler, A.; Simon, R. J.; Kokubo, T.; Kaiser, E. T., The X-Ray Structure of Flavohemoglobin. A Semisynthetic Hydroxylase. *J. Am. Chem. Soc.* **1988,** *110* (18), 6261-6263.
122. Ilari, A.; Bonamore, A.; Farina, A.; Johnson, K. A.; Boffi, A., The X-Ray Structure of Ferric *Escherichia coli* Flavohemoglobin Reveals an Unexpected Geometry of the Distal Heme Pocket. *J. Biol. Chem.* **2002,** *277* (26), 23725-23732.
123. Corey, D.; Schultz, P., Generation of a Hybrid Sequence-Specific Single-Stranded Deoxyribonuclease. *Science* **1987,** *238* (4832), 1401-1403.
124. Sluka, J.; Horvath, S.; Bruist, M.; Simon, M.; Dervan, P., Synthesis of a Sequence-Specific DNA-Cleaving Peptide. *Science* **1987,** *238* (4830), 1129-1132.
125. Chen, C. H.; Sigman, D. S., Chemical Conversion of a DNA-Binding Protein into a Site-Specific Nuclease. *Science* **1987,** *237* (4819), 1197-1201.
126. Ebright, R. H.; Ebright, Y. W.; Pendergrast, P. S.; Gunasekera, A., Conversion of a Helix-Turn-Helix Motif Sequence-Specific DNA Binding Protein into a Site-Specific DNA Cleavage Agent. *Proc. Natl. Acad. Sci. U. S. A.* **1990,** *87* (8), 2882-2886.
127. Mazzarelli, J. M.; Ermacora, M. R.; Fox, R. O.; Grindley, N. D. F., Mapping Interactions between the Catalytic Domain of Resolvase and Its DNA Substrate Using Cysteine-Coupled EDTA-Iron. *Biochemistry* **1993,** *32* (12), 2979-2986.
128. Tullius, T. D., Physical Studies of Protein-DNA Complexes by Footprinting. *Annu. Rev. Biophys. Biophys. Chem.* **1989,** *18* (1), 213-237.
129. Hilvert, D., Critical Analysis of Antibody Catalysis. *Annu. Rev. Biochem.* **2000,** *69*, 751-793.
130. Iverson, B. L.; Lerner, R. A., Sequence-Specific Peptide Cleavage Catalyzed by an Antibody. *Science* **1989,** *243* (4895), 1184-1188.
131. Sasaki, T.; Kaiser, E. T., Helichrome: Synthesis and Enzymic Activity of a Designed Hemeprotein. *J. Am. Chem. Soc.* **1989,** *111* (1), 380-381.
132. Cochran, A.; Schultz, P., Antibody-Catalyzed Porphyrin Metallation. *Science* **1990,** *249* (4970), 781-783.
133. Cochran, A. G.; Schultz, P. G., Peroxidase-Activity of an Antibody Heme Complex. *J. Am. Chem. Soc.* **1990,** *112* (25), 9414-9415.
134. Harada, A.; Fukushima, H.; Shiotsuki, K.; Yamaguchi, H.; Oka, F.; Kamachi, M., Peroxidation of Pyrogallol by Antibody-Metalloporphyrin Complexes. *Inorg. Chem.* **1997,** *36* (26), 6099-6102.
135. Keinan, E.; Sinha, S. C.; Sinha-Bagchi, A.; Benory, E.; Ghozi, M. C.; Eshhar, Z.; Green, B. S., Towards Antibody-Mediated Metallo-Porphyrin Chemistry. *Pure Appl. Chem.* **1990,** *62* (10), 2013-2019.
136. Germanas, J. P.; Kaiser, E. T., Autoxidation of Ascorbic Acid Catalyzed by a Semisynthetic Enzyme. *Biopolymers* **1990,** *29* (1), 39-43.
137. Wuttke, D. S.; Gray, H. B.; Fisher, S. L.; Imperiali, B., Semisynthesis of Bipyridyl-Alanine Cytochrome C Mutants: Novel Proteins with Enhanced Electron-Transfer Properties. *J. Am. Chem. Soc.* **1993,** *115* (18), 8455-8456.
138. Wade, W. S.; Ashley, J. A.; Jahangiri, G. K.; McElhaney, G.; Janda, K. D.; Lerner, R. A., A Highly Specific Metal-Activated Catalytic Antibody. *J. Am. Chem. Soc.* **1993,** *115* (11), 4906-4907.
139. Martell, A. E., Vitamin B6-Catalyzed Reactions of Alpha-Amino and Alpha-Keto Acids: Model Systems. *Acc. Chem. Res.* **1989,** *22* (4), 115-124.
140. Imperiali, B.; Roy, R. S., Coenzyme-Amino Acid Chimeras: New Residues for the Assembly of Functional Proteins. *J. Am. Chem. Soc.* **1994,** *116* (26), 12083-12084.
141. Roy, R. S.; Imperiali, B., Pyridoxamine-Amino Acid Chimeras in Semisynthetic Aminotransferase Mimics. *Protein Eng.* **1997,** *10* (6), 691-698.
142. Davies, R. R.; Distefano, M. D., A Semisynthetic Metalloenzyme Based on a Protein Cavity That Catalyzes the Enantioselective Hydrolysis of Ester and Amide Substrates. *J. Am. Chem. Soc.* **1997,** *119* (48), 11643-11652.

143. Ory, J. J.; Mazhary, A.; Kuang, H.; Davies, R. R.; Distefano, M. D.; Banaszak, L. J., Structural Characterization of Two Synthetic Catalysts Based on Adipocyte Lipid-Binding Protein. *Protein Eng.* **1998,** *11* (4), 253-261.
144. Davies, R. R.; Kuang, H.; Qi, D.; Mazhary, A.; Mayaan, E.; Distefano, M. D., Artificial Metalloenzymes Based on Protein Cavities: Exploring the Effect of Altering the Metal Ligand Attachment Position by Site Directed Mutagenesis. *Bioorg. Med. Chem. Lett.* **1999,** *9* (1), 79-84.
145. Kuang, H.; Davies, R. R.; Distefano, M. D., Modulation of the Rate, Enantioselectivity, and Substrate Specificity of Semisynthetic Transaminases Based on Lipid Binding Proteins Using Site Directed Mutagenesis. *Bioorg. Med. Chem. Lett.* **1997,** *7* (15), 2055-2060.
146. Qi, D.; Kuang, H.; Distefano, M. D., Effects of Metal Ions on the Rates and Enantioselectivities of Reactions Catalyzed by a Series of Semisynthetic Transaminases Created by Site Directed Mutagenesis. *Bioorg. Med. Chem. Lett.* **1998,** *8* (7), 875-880.
147. van de Velde, F.; Konemann, L.; van Rantwijk, F.; Sheldon, R. A., Enantioselective Sulfoxidation Mediated by Vanadium-Incorporated Phytase: A Hydrolase Acting as a Peroxidase. *Chem. Commun. (Cambridge, U. K.)* **1998,** (17), 1891-1892.
148. van de Velde, F.; Arends, I. W. C. E.; Sheldon, R. A., Vanadium-Catalysed Enantioselective Sulfoxidations: Rational Design of Biocatalytic and Biomimetic Systems. *Top. Catal.* **2000,** *13* (3), 259-265.
149. van de Velde, F.; Könemann, L.; van Rantwijk, F.; Sheldon, R. A., The Rational Design of Semisynthetic Peroxidases. *Biotechnol. Bioeng.* **2000,** *67* (1), 87-96.
150. Finn, M. G.; Lerner, R. A.; Barbas, C. F., Cofactor-Induced Refinement of Catalytic Antibody Activity: A Metal-Specific Allosteric Effect. *J. Am. Chem. Soc* **1998,** *120* (12), 2963-2964.
151. Barbas, C. F.; Heine, A.; Zhong, G.; Hoffmann, T.; Gramatikova, S.; Björnestedt, R.; List, B.; Anderson, J.; Stura, E. A.; Wilson, I. A. et al, Immune Versus Natural Selection: Antibody Aldolases with Enzymic Rates but Broader Scope. *Science* **1997,** *278* (5346), 2085-2092.
152. Wagner, J.; Lerner, R. A.; Barbas, C. F., Efficient Aldolase Catalytic Antibodies That Use the Enamine Mechanism of Natural Enzymes. *Science* **1995,** *270* (5243), 1797-1800.
153. Lin, C.-C.; Lin, C.-W.; Chan, A. S. C., Catalytic Hydrogenation of Itaconic Acid in a Biotinylated Pyrphos–Rhodium(I) System in a Protein Cavity. *Tetrahedron: Asymmetry* **1999,** *10* (10), 1887-1893.
154. Nimri, S.; Keinan, E., Antibody−Metalloporphyrin Catalytic Assembly Mimics Natural Oxidation Enzymes. *J. Am. Chem. Soc.* **1999,** *121* (39), 8978-8982.
155. Marchetti, M.; Mangano, G.; Paganelli, S.; Botteghi, C., A Protein-Rhodium Complex as an Efficient Catalyst for Two-Phase Olefin Hydroformylation. *Tetrahedron Lett.* **2000,** *41* (19), 3717-3720.
156. Bertucci, C.; Botteghi, C.; Giunta, D.; Marchetti, M.; Paganelli, S., Aqueous Biphasic Hydroformylation Catalysed by Protein-Rhodium Complexes. *Adv. Synth. Catal.* **2002,** *344* (5), 556-562.
157. Eckl, R. W.; Priermeier, T.; Herrmann, W. A., IX. ^{1}mono- and Biphasic Asymmetric Hydroformylation with Rhodium Catalysts of the Diphosphine Ligand Naphos and Its Sulfonated Derivatives. *J. Organomet. Chem.* **1997,** *532* (1–2), 243-249.
158. Nicholas, K. M.; Wentworth, P., Jr.; Harwig, C. W.; Wentworth, A. D.; Shafton, A.; Janda, K. D., A Cofactor Approach to Copper-Dependent Catalytic Antibodies. *Proc. Natl. Acad. Sci. U. S. A.* **2002,** *99* (5), 2648-2653.
159. Smith, M., Synthetic DNA and Biology (Nobel Lecture). *Angew. Chem., Int. Ed.* **1994,** *33* (12), 1214-1221.
160. Mullis, K. B., The Polymerase Chain Reaction (Nobel Lecture). *Angew. Chem., Int. Ed.* **1994,** *33* (12), 1209-1213.
161. Kuchner, O.; Arnold, F. H., Directed Evolution of Enzyme Catalysts. *Trends Biotechnol.* **1997,** *15* (12), 523-530.
162. Bornscheuer, U. T.; Huisman, G. W.; Kazlauskas, R. J.; Lutz, S.; Moore, J. C.; Robins, K., Engineering the Third Wave of Biocatalysis. *Nature* **2012,** *485* (7397), 185-194.
163. Kiss, G.; Çelebi-Ölçüm, N.; Moretti, R.; Baker, D.; Houk, K. N., Computational Enzyme Design. *Angew. Chem., Int. Ed.* **2013,** *52* (22), 5700-5725.

164. Reetz, M. T.; Rentzsch, M.; Pletsch, A.; Maywald, M., Towards the Directed Evolution of Hybrid Catalysts. *Chimia* **2002,** *56* (12), 721-723.
165. Reetz, M. T., Directed Evolution of Selective Enzymes and Hybrid Catalysts. *Tetrahedron* **2002,** *58* (32), 6595-6602.
166. Kennedy, M. L.; Gibney, B. R., Metalloprotein and Redox Protein Design. *Curr. Opin. Struct. Biol.* **2001,** *11* (4), 485-490.
167. Case, M. A.; McLendon, G. L., Metal-Assembled Modular Proteins: Toward Functional Protein Design. *Acc. Chem. Res.* **2004,** *37* (10), 754-762.
168. Hill, R. B.; Raleigh, D. P.; Lombardi, A.; DeGrado, W. F., De Novo Design of Helical Bundles as Models for Understanding Protein Folding and Function. *Acc. Chem. Res.* **2000,** *33* (11), 745-754.
169. Osborn, J. A.; Jardine, F. H.; Young, J. F.; Wilkinson, G., Preparation and Properties of Tris(Triphenylphosphine)Halorhodium(I) and Some Reactions Thereof Including Catalytic Homogeneous Hydrogenation of Olefins and Acetylenes and Their Derivatives. *J. Chem. Soc., A* **1966,** (12), 1711-1732.
170. Mazurek, S.; Ward, T. R.; Novic, M., Counter Propagation Artificial Neural Networks Modeling of an Enantioselectivity of Artificial Metalloenzymes. *Mol. Diversity* **2007,** *11* (3), 141-152.
171. Skander, M.; Malan, C.; Ivanova, A.; Ward, T. R., Chemical Optimization of Artificial Metalloenzymes Based on the Biotin-Avidin Technology: (S)-Selective and Solvent-Tolerant Hydrogenation Catalysts Via the Introduction of Chiral Amino Acid Spacers. *Chem. Commun. (Cambridge, U. K.)* **2005,** (38), 4815-4817.
172. Skander, M.; Humbert, N.; Collot, J.; Gradinaru, J.; Klein, G.; Loosli, A.; Sauser, J.; Zocchi, A.; Gilardoni, F.; Ward, T. R., Artificial Metalloenzymes: (Strept)Avidin as Host for Enantioselective Hydrogenation by Achiral Biotinylated Rhodium-Diphosphine Complexes. *J. Am. Chem. Soc.* **2004,** *126* (44), 14411-14418.
173. Rusbandi, U. E.; Skander, M.; Ivanova, A.; Malan, C.; Ward, T. R., Second-Generation Artificial Hydrogenases Based on the Biotin-Avidin Technology: Improving Selectivity and Organic Solvent Tolerance by Introduction of an (R)-Proline Spacer. *C. R. Chim.* **2007,** *10* (8), 678-683.
174. Rusbandi, U. E.; Lo, C.; Skander, M.; Ivanova, A.; Creus, M.; Humbert, N.; Ward, T. R., Second Generation Artificial Hydrogenases Based on the Biotin-Avidin Technology: Improving Activity, Stability and Selectivity by Introduction of Enantiopure Amino Acid Spacers. *Adv. Synth. Catal.* **2007,** *349* (11-12), 1923-1930.
175. Klein, G.; Humbert, N.; Gradinaru, J.; Ivanova, A.; Gilardoni, F.; Rusbandi, U. E.; Ward, T. R., Tailoring the Active Site of Chemzymes by Using a Chemogenetic-Optimization Procedure: Towards Substrate-Specific Artificial Hydrogenases Based on the Biotin-Avidin Technology. *Angew. Chem., Int. Ed.* **2005,** *44* (47), 7764-7767.
176. Collot, J.; Gradinaru, J.; Humbert, N.; Skander, M.; Zocchi, A.; Ward, T. R., Artificial Metalloenzymes for Enantioselective Catalysis Based on Biotin-Avidin. *J. Am. Chem. Soc.* **2003,** *125* (30), 9030-9031.
177. Kruithof, C. A.; Casado, M. A.; Guillena, G.; Egmond, M. R.; van der Kerk-van Hoof, A.; Heck, A. J.; Klein Gebbink, R. J. M.; van-Koten, G., Lipase Active-Site-Directed Anchoring of Organometallics: Metallopincer/Protein Hybrids. *Chem. - Eur. J.* **2005,** *11* (23), 6869-6877.
178. Rutten, L.; Wieczorek, B.; Mannie, J.-P. B. A.; Kruithof, C. A.; Dijkstra, H. P.; Egmond, M. R.; Lutz, M.; Klein Gebbink, R. J. M.; Gros, P.; van-Koten, G., Solid-State Structural Characterization of Cutinase–ECE-pincer–Metal Hybrids. *Chem. - Eur. J.* **2009,** *17* (15), 4270 – 4280.
179. Wieczorek, B.; Snelders, D. J. M.; Dijkstra, H. P.; Versluis, K.; Lutz, M.; Spek, A. L.; Egmond, M. R.; Klein Gebbink, R. J. M.; van-Koten, G., Coordination Chemistry in Water of a Free and a Lipase-Embedded Cationic NCN-pincer Platinum Center with Neutral and Ionic Triarylphosphines. *Organometallics* **2012,** *31* (7), 2810-2820.
180. Basauri-Molina, M.; Riemersma, C. F.; Wurdemann, M. A.; Kleijn, H.; Klein Gebbink, R. J. M., Lipase Active Site Covalent Anchoring of Rh(NHC) Catalysts: Towards Chemoselective Artificial Metalloenzymes. *Chem. Commun. (Cambridge, U. K.)* **2015,** *51* (31), 6792-6795.
181. Syska, H.; Herrmann, W. A.; Kühn, F. E., Water-Soluble Carbene Complexes as Catalysts for the Hydrogenation of Acetophenone under Hydrogen Pressure. *J. Organomet. Chem.* **2012,** *703*, 56-62.

182. Wieczorek, B.; Träff, A.; Krumlinde, P.; Dijkstra, H. P.; Egmond, M. R.; van-Koten, G.; Bäckvall, J.-E.; Klein Gebbink, R. J. M., Covalent Anchoring of a Racemization Catalyst to Calb-Beads: Towards Dual Immobilization of Dkr Catalysts. *Tetrahedron Lett.* **2011,** *52* (14), 1601-1604.
183. Shang, G.; Li , W.; Zhang, X., *Catalytic Asymmetric Synthesis,Transition Metal-Catalyzed Homogeneous Asymmetric Hydrogenation*. John Wiley & Sons, Inc.: 2010; p 343.
184. Panella, L.; Broos, J.; Jin, J.; Fraaije, M. W.; Janssen, D. B.; Jeronimus-Stratingh, M.; Feringa, B. L.; Minnaard, A. J.; de Vries, J. G., Merging Homogeneous Catalysis with Biocatalysis; Papain as Hydrogenation Catalyst. *Chem. Commun.* **2005,** (45), 5656-5658.
185. den Heeten, R.; Munoz, B. K.; Popa, G.; Laan, W.; Kamer, P. C. J., Synthesis of Hybrid Transition-Metalloproteins Via Thiol-Selective Covalent Anchoring of Rh-Phosphine and Ru-Phenanthroline Complexes. *Dalton Trans.* **2010,** *39* (36), 8477-8483.
186. Yamaguchi, H.; Hirano, T.; Kiminami, H.; Taura, D.; Harada, A., Asymmetric Hydrogenation with Antibody-Achiral Rhodium Complex. *Org. Biomol. Chem.* **2006,** *4* (19), 3571-3573.
187. Jing, Q.; Okrasa, K.; Kazlauskas, R. J., Stereoselective Hydrogenation of Olefins Using Rhodium-Substituted Carbonic Anhydrase-a New Reductase. *Chem. - Eur. J.* **2009,** *15* (6), 1370-1376.
188. Reiner, T.; Jantke, D.; Marziale, A. N.; Raba, A.; Eppinger, J., Metal-Conjugated Affinity Labels: A New Concept to Create Enantioselective Artificial Metalloenzymes. *ChemistryOpen* **2013,** *2*, 50-54.
189. Yan, T.; Feringa, B. L.; Barta, K., Iron Catalysed Direct Alkylation of Amines with Alcohols. *Nat. Commun.* **2014,** *5*, 5602.
190. Merel, D. S.; Gaillard, S.; Ward, T. R.; Renaud, J.-L., Achiral Cyclopentadienone Iron Tricarbonyl Complexes Embedded in Streptavidin: An Access to Artificial Iron Hydrogenases and Application in Asymmetric Hydrogenation. *Catal. Lett.* **2016,** *146* (3), 564-569.
191. Berggren, G.; Adamska, A.; Lambertz, C.; Simmons, T. R.; Esselborn, J.; Atta, M.; Gambarelli, S.; Mouesca, J. M.; Reijerse, E.; Lubitz, W. et al, Biomimetic Assembly and Activation of [FeFe]-Hydrogenases. *Nature* **2013,** *499* (7456), 66-69.
192. Esselborn, J.; Lambertz, C.; Adamska-Venkatesh, A.; Simmons, T.; Berggren, G.; Nothl, J.; Siebel, J.; Hemschemeier, A.; Artero, V.; Reijerse, E. et al, Spontaneous Activation of [FeFe]-Hydrogenases by an Inorganic [2Fe] Active Site Mimic. *Nat. Chem. Biol.* **2013,** *9* (10), 607-609.
193. Shima, S.; Chen, D. F.; Xu, T.; Wodrich, M. D.; Fujishiro, T.; Schultz, K. M.; Kahnt, J.; Ataka, K.; Hu, X. L., Reconstitution of [Fe]-Hydrogenase Using Model Complexes. *Nat. Chem.* **2015,** *7* (12), 995-1002.
194. Siebel, J. F.; Adamska-Venkatesh, A.; Weber, K.; Rumpel, S.; Reijerse, E.; Lubitz, W., Hybrid [FeFe]-Hydrogenases with Modified Active Sites Show Remarkable Residual Enzymatic Activity. *Biochemistry* **2015,** *54* (7), 1474-1483.
195. Utschig, L. M.; Soltau, S. R.; Tiede, D. M., Light-Driven Hydrogen Production from Photosystem I-Catalyst Hybrids. *Curr. Opin. Chem. Biol.* **2015,** *25*, 1-8.
196. Sano, Y.; Onoda, A.; Hayashi, T., A Hydrogenase Model System Based on the Sequence of Cytochrome c: Photochemical Hydrogen Evolution in Aqueous Media. *Chem. Commun. (Cambridge, U. K.)* **2011,** *47* (29), 8229-8231.
197. Onoda, A.; Kihara, Y.; Fukumoto, K.; Sano, Y.; Hayashi, T., Photoinduced Hydrogen Evolution Catalyzed by a Synthetic Diiron Dithiolate Complex Embedded within a Protein Matrix. *ACS Catal.* **2014,** *4* (8), 2645-2648.
198. Sauer, D. F.; Himiyama, T.; Tachikawa, K.; Fukumoto, K.; Onoda, A.; Mizohata, E.; Inoue, T.; Bocola, M.; Schwaneberg, U.; Hayashi, T. et al, A Highly Active Biohybrid Catalyst for Olefin Metathesis in Water: Impact of a Hydrophobic Cavity in a Beta-Barrel Protein. *ACS Catal.* **2015,** *5* (12), 7519-7522.
199. Onoda, A.; Fukumoto, K.; Arlt, M.; Bocola, M.; Schwaneberg, U.; Hayashi, T., A Rhodium Complex-Linked Beta-Barrel Protein as a Hybrid Biocatalyst for Phenylacetylene Polymerization. *Chem. Commun. (Cambridge, U. K.)* **2012,** *48* (78), 9756-9758.
200. Zhang, C.; Srivastava, P.; Ellis-Guardiola, K.; Lewis, J. C., Manganese Terpyridine Artificial Metalloenzymes for Benzylic Oxygenation and Olefin Epoxidation. *Tetrahedron* **2014,** *70* (27–28), 4245-4249.
201. Saintmartin, P.; Lespinat, P. A.; Fauque, G.; Berlier, Y.; Legall, J.; Moura, I.; Teixeira, M.; Xavier, A. V.; Moura, J. J. G., Hydrogen-Production and Deuterium-Proton Exchange-Reactions Catalyzed by

Desulfovibrio Nickel(II)-Substituted Rubredoxins. *Proc. Natl. Acad. Sci. U. S. A.* **1988,** *85* (24), 9378-9380.
202. Slater, J. W.; Shafaat, H. S., Nickel-Substituted Rubredoxin as a Minimal Enzyme Model for Hydrogenase. *J. Phys. Chem. Lett.* **2015,** *6* (18), 3731-3736.
203. Artero, V.; Bacchi, M.; Berggren, G.; Fontecave, M., Artificial Hydrogenases Based on Cobaloxime and Sperm-Whale Myoglobin. *J. Biol. Inorg. Chem.* **2014,** *19*, 8071-8082.
204. Hawecker, J.; Lehn, J. M.; Ziessel, R., Efficient Homogeneous Photochemical Hydrogen Generation and Water Reduction Mediated by Cobaloxime or Macrocyclic Cobalt Complexes. *Nouv. J. Chim.* **1983,** *7* (5), 271-277.
205. Kellett, R. M.; Spiro, T. G., Cobalt(I) Porphyrin Catalysts of Hydrogen Production from Water. *Inorg. Chem.* **1985,** *24* (15), 2373-2377.
206. Kleingardner, J. G.; Kandemir, B.; Bren, K. L., Hydrogen Evolution from Neutral Water under Aerobic Conditions Catalyzed by Cobalt Microperoxidase-11. *J. Am. Chem. Soc.* **2014,** *136* (1), 4-7.
207. Sommer, D. J.; Vaughn, M. D.; Ghirlanda, G., Protein Secondary-Shell Interactions Enhance the Photoinduced Hydrogen Production of Cobalt Protoporphyrin IX. *Chem. Commun. (Cambridge, U. K.)* **2014,** *50* (100), 15852-15855.
208. Sommer, D. J.; Vaughn, M. D.; Clark, B. C.; Tomlin, J.; Roy, A.; Ghirlanda, G., Reengineering cyt b_{562} for Hydrogen Production: A Facile Route to Artificial Hydrogenases. *Biochim. Biophys. Acta, Bioenerg.* **2016,** *1857* (5), 598-603.
209. Bediako, D. K.; Solis, B. H.; Dogutan, D. K.; Roubelakis, M. M.; Maher, A. G.; Lee, C. H.; Chambers, M. B.; Hammes-Schiffer, S.; Nocera, D. G., Role of Pendant Proton Relays and Proton-Coupled Electron Transfer on the Hydrogen Evolution Reaction by Nickel Hangman Porphyrins. *Proc. Natl. Acad. Sci. U. S. A.* **2014,** *111* (42), 15001-15006.
210. Helm, M. L.; Stewart, M. P.; Bullock, R. M.; DuBois, M. R.; DuBois, D. L., A Synthetic Nickel Electrocatalyst with a Turnover Frequency above 100,000 S^{-1} for H_2 Production. *Science* **2011,** *333* (6044), 863-866.
211. Bacchi, M.; Veinberg, E.; Field, M. J.; Niklas, J.; Matsui, T.; Tiede, D. M.; Poluektov, O. G.; Ikeda-Saito, M.; Fontecave, M.; Artero, V., Artificial Hydrogenases Based on Cobaloximes and Heme Oxygenase. *ChemPlusChem* **2016,** *81*, 1083-1089.
212. Utschig, L. M.; Silver, S. C.; Mulfort, K. L.; Tiede, D. M., Nature-Driven Photochemistry for Catalytic Solar Hydrogen Production: A Photosystem I-Transition Metal Catalyst Hybrid. *J. Am. Chem. Soc.* **2011,** *133* (41), 16334-16337.
213. Silver, S. C.; Niklas, J.; Du, P. W.; Poluektov, O. G.; Tiede, D. M.; Utschig, L. M., Protein Delivery of a Ni Catalyst to Photosystem I for Light-Driven Hydrogen Production. *J. Am. Chem. Soc.* **2013,** *135* (36), 13246-13249.
214. Soltau, S. R.; Dahlberg, P. D.; Niklas, J.; Poluektov, O. G.; Mulfort, K. L.; Utschig, L. M., Ru-Protein-Co Biohybrids Designed for Solar Hydrogen Production: Understanding Electron Transfer Pathways Related to Photocatalytic Function. *Chem. Sci.* **2016,** *7*, 7068-7078.
215. Soltau, S. R.; Niklas, J.; Dahlberg, P. D.; Poluektov, O. G.; Tiede, D. M.; Mulfort, K. L.; Utschig, L. M., Aqueous Light Driven Hydrogen Production by a Ru-Ferredoxin-Co Biohybrid. *Chem. Commun. (Cambridge, U. K.)* **2015,** *51* (53), 10628-10631.
216. Sano, Y.; Onoda, A.; Hayashi, T., Photocatalytic Hydrogen Evolution by a Diiron Hydrogenase Model Based on a Peptide Fragment of Cytochrome c_{556} with an Attached Diiron Carbonyl Cluster and an Attached Ruthenium Photosensitizer. *J. Inorg. Biochem.* **2012,** *108*, 159-162.
217. Marshall, N. M.; Garner, D. K.; Wilson, T. D.; Gao, Y. G.; Robinson, H.; Nilges, M. J.; Lu, Y., Rationally Tuning the Reduction Potential of a Single Cupredoxin Beyond the Natural Range. *Nature* **2009,** *462* (7269), 113-116.
218. Sandoval, C. A.; Noyori, R.; Zhou, Q. L.; Pfaltz, A.; Hou, X. L.; Yamamoto, H., An Overview of Recent Developments in Metal-Catalyzed Asymmetric Transformations In *Organic Chemistry - Breakthroughs and Perspectives*, Wiley-VCH Verlag GmbH & Co. KGaA: Weinheim, Germany, 2012; pp 335-366.
219. Kitamura, M.; Noyori, R., Hydrogenation and Transfer Hydrogenation. In *Ruthenium in Organic Synthesis*, Wiley-VCH Verlag GmbH & Co. KGaA: Weinheim, FRG. , 2004.

220. Gladiali, S.; Alberico, E., Asymmetric Transfer Hydrogenation: Chiral Ligands and Applications. *Chem. Soc. Rev.* **2006,** *35* (3), 226-236.
221. Xue, D.; Chen, Y.-C.; Cui, X.; Wang, Q.-W.; Zhu, J.; Deng, J.-G., Transfer Hydrogenation of Activated C=C Bonds Catalyzed by Ruthenium Amido Complexes: Reaction Scope, Limitation and Enantioselectivity. *J. Org. Chem.* **2005,** *70*, 3584-3591.
222. Everaere, K.; Mortreux, A.; Carpentier, J.-F., Ruthenium(II)-Catalyzed Asymmetric Transfer Hydrogenation of Carbonyl Compounds with 2-Propanol and Ephedrine-Type Ligands. *Adv. Synth. Catal.* **2003,** *345*, 67-77.
223. Nixon, T. D.; Whittlesey, M. K.; Williams, J. M. J., Ruthenium-Catalysed Transfer Hydrogenation Reactions with Dimethylamine Borane. *Tetrahedron Lett.* **2011,** *52* (49), 6652-6654.
224. Lee, S.-H.; Nikonov, G. I., Transfer Hydrogenation of Ketones, Nitriles, and Esters Catalyzed by a Half-Sandwich Complex of Ruthenium. *ChemCatChem* **2015,** *7* (1), 107-113.
225. Mai, V. H.; Nikonov, G. I., Transfer Hydrogenation of Nitriles, Olefins, and N-Heterocycles Catalyzed by an N-Heterocyclic Carbene-Supported Half-Sandwich Complex of Ruthenium. *Organometallics* **2016,** *35* (7), 943-949.
226. Ratovelomanana-Vidal, V.; Phansavath, P.; Echeverria, P.-G.; Ayad, T., Recent Developments in Asymmetric Hydrogenation and Transfer Hydrogenation of Ketones and Imines through Dynamic Kinetic Resolution. *Synthesis* **2016,** *48* (16), 2523-2539.
227. Wang, D.; Astruc, D., The Golden Age of Transfer Hydrogenation. *Chem. Rev.* **2015,** *115* (13), 6621-6686.
228. Hashiguchi, S.; Fujii, A.; Takehara, J.; Ikariya, T.; Noyori, R., Asymmetric Transfer Hydrogenation of Aromatic Ketones Catalyzed by Chiral Ruthenium (II) Complexes. *J. Am. Chem. Soc.* **1995,** *117*, 7562-7563.
229. Noyori, R.; Hashiguchi, S., Asymmetric Transfer Hydrogenation Catalyzed by Chiral Ruthenium Complexes. *Acc. Chem. Res.* **1997,** *30* (2), 97-102.
230. Ikariya, T.; Murata, K.; Noyori, R., Bifunctional Transition Metal-Based Molecular Catalyst for Asymmetric Syntheses. *Org. Biomol. Chem.* **2006,** *4* (3), 393-406.
231. Zhou, X.; Wu, X.; Yang, B.; Xiao, J., Varying the Ratio of Formic Acid to Triethylamine Impacts on Asymmetric Transfer Hydrogenation of Ketones. *J. Mol. Catal. A: Chem.* **2012,** *357*, 133-140.
232. Wang, C.; Li, C.; Wu, X.; Pettman, A.; Xiao, J., pH-Regulated Asymmetric Transfer Hydrogenation of Quinolines in Water. *Angew. Chem., Int. Ed.* **2009,** *48* (35), 6524-6528.
233. Wu, X.; Xiao, J., Hydrogenation and Transfer Hydrogenation in Water. In *Metal-Catalyzed Reactions in Water*, first ed.; Wiley-VCH Verlag GmbH & Co. KGaA, : Weinheim, Germany., 2013; pp 173-242.
234. Pollard, D. J.; Kosjek, B.; Devine, P. N.; Moore, J. C., Advances in the Enzymatic Reduction of Ketones. *Acc. Chem. Res.* **2007,** *40*, 1412–1419.
235. Stuermer, R.; Hauer, B.; Hall, M.; Faber, K., Asymmetric Bioreduction of Activated C=C Bonds Using Enoate Reductases from the Old Yellow Enzyme Family. *Curr. Opin. Chem. Biol.* **2007,** *11* (2), 203-213.
236. Mitsukura, K.; Suzuki, M.; Shinoda, S.; Kuramoto, T.; Yoshida, T.; Nagasawa, T., Purification and Characterization of a Novel (R)-Imine Reductase from *Streptomyces Sp.* GF3587. *Biosci., Biotechnol., Biochem.* **2011,** *75* (9), 1778-1782.
237. Hussain, S.; Leipold, F.; Man, H.; Wells, E.; France, S. P.; Mulholland, K. R.; Grogan, G.; Turner, N. J., An (R)-Imine Reductase Biocatalyst for the Asymmetric Reduction of Cyclic Imines. *ChemCatChem* **2015,** *7* (4), 579-583.
238. Scheller, P. N.; Fademrecht, S.; Hofelzer, S.; Pleiss, J.; Leipold, F.; Turner, N. J.; Nestl, B. M.; Hauer, B., Enzyme Toolbox: Novel Enantiocomplementary Imine Reductases. *ChemBiochem* **2014,** *15* (15), 2201-2204.
239. Letondor, C.; Pordea, A.; Humbert, N.; Ivanova, A.; Mazurek, S.; Novic, M.; Ward, T. R., Artificial Transfer Hydrogenases Based on the Biotin-(Strept)Avidin Technology: Fine Tuning the Selectivity by Saturation Mutagenesis of the Host Protein. *J. Am. Chem. Soc.* **2006,** *128* (25), 8320-8328.

240. Creus, M.; Pordea, A.; Rossel, T.; Sardo, A.; Letondor, C.; Ivanova, A.; LeTrong, I.; Stenkamp, R. E.; Ward, T. R., X-Ray Structure and Designed Evolution of an Artificial Transfer Hydrogenase. *Angew. Chem., Int. Ed.* **2008,** *47* (8), 1400-1404.
241. Haquette, P.; Salmain, M.; Svedlung, K.; Martel, A.; Rudolf, B.; Zakrzewski, J.; Cordier, S.; Roisnel, T.; Fosse, C.; Jaouen, G., Cysteine-Specific, Covalent Anchoring of Transition Organometallic Complexes to the Protein Papain from *Carica papaya*. *ChemBioChem* **2007,** *8* (2), 224-231.
242. Haquette, P.; Talbi, B.; Canaguier, S.; Dagorne, S.; Fosse, C.; Martel, A.; Jaouen, G.; Salmain, M., Functionalized Cationic ($H^{(6)}$-Arene)Ruthenium(II) Complexes for Site-Specific and Covalent Anchoring to Papain from *Papaya latex*. Synthesis, X-Ray Structures and Reactivity Studies. *Tetrahedron Lett.* **2008,** *49* (31), 4670-4673.
243. Madern, N.; Talbi, B.; Salmain, M., Aqueous Phase Transfer Hydrogenation of Aryl Ketones Catalysed by Achiral Ruthenium(II) and Rhodium(III) Complexes and Their Papain Conjugates. *Appl. Organomet. Chem.* **2013,** *27* (1), 6-12.
244. Chevalley, A.; Salmain, M., Enantioselective Transfer Hydrogenation of Ketone Catalysed by Artificial Metalloenzymes Derived from Bovine Beta-Lactoglobulin. *Chem. Commun. (Cambridge, U. K.)* **2012,** *48* (98), 11984-11986.
245. Chevalley, A.; Cherrier, M. V.; Fontecilla-Camps, J. C.; Ghasemia, M.; Salmain, M., Artificial Metalloenzymes Derived from Bovine B-Lactoglobulin for the Asymmetric Transfer Hydrogenation of an Aryl Ketone - Synthesis, Characterization and Catalytic Activity. *Dalton Trans.* **2014,** *43* (14), 5482-5489.
246. Cherrier, M. V.; Engilberge, S.; Amara, P.; Chevalley, A.; Salmain, M.; Fontecilla-Camps, J. C., Structural Basis for Enantioselectivity in the Transfer Hydrogenation of a Ketone Catalyzed by an Artificial Metalloenzyme. *Eur. J. Inorg. Chem.* **2013,** *2013* (21), 3596-3600.
247. Tabe, H.; Abe, S.; Hikage, T.; Kitagawa, S.; Ueno, T., Porous Protein Crystals as Catalytic Vessels for Organometallic Complexes. *Chem. Asian J.* **2014,** *9* (5), 1373-1378.
248. McNae, I. W.; Fishburne, K.; Habtemariam, A.; Hunter, T. M.; Melchart, M.; Wang, F.; Walkinshaw, M. D.; Sadler, P. J., Half-Sandwich Arene Ruthenium(II)-Enzyme Complex. *Chem. Commun. (Cambridge, U. K.)* **2004,** (16), 1786-1787.
249. Durrenberger, M.; Heinisch, T.; Wilson, Y. M.; Rossel, T.; Nogueira, E.; Knorr, L.; Zimbron, M. J.; Pierron, J.; Mutschler, A.; Kersten, K. et al, Artificial Transfer Hydrogenases for the Enantioselective Reduction of Cyclic Imines. *Angew. Chem., Int. Ed.* **2011,** *50* (13), 3026-3029.
250. Schwizer, F.; Kohler, V.; Durrenberger, M.; Knorr, L.; Ward, T. R., Genetic Optimization of the Catalytic Efficiency of Artificial Imine Reductases Based on Biotin-Streptavidin Technology. *ACS Catal.* **2013,** *3* (8), 1752-1755.
251. Munoz Robles, V.; Vidossich, P.; Lledos, A.; Ward, T. R.; Marechal, J.-D., Computational Insights on an Artificial Imine Reductase Based on the Biotin-Streptavidin Technology. *ACS Catal.* **2014,** *4* (3), 833-842.
252. Munoz Robles, V.; Durrenberger, M.; Heinisch, T.; Lledos, A.; Schirmer, T.; Ward, T. R.; Marechal, J.-D., Structural, Kinetic, and Docking Studies of Artificial Imine Reductases Based on Biotin-Streptavidin Technology: An Induced Lock-and-Key Hypothesis. *J. Am. Chem. Soc.* **2014,** *136* (44), 15676-15683.
253. Facchetti, G.; Gandolfi, R.; Fusè, M.; Zerla, D.; Cesarotti, E.; Pellizzoni, M. M.; Rimoldi, I., Simple 1,3-Diamines and Their Application as Ligands in Ruthenium(II) Catalysts for Asymmetric Transfer Hydrogenation of Aryl Ketones. *New J. Chem.* **2015,** *39* (5), 3792-3800.
254. Pellizzoni, M. M.; Gandolfi, R.; Fusè, M.; Facchetti, G.; Contini, A.; Isabella, R., Evaluation of Chemical Diversity of Biotinylated Chiral 1,3-Diamines as a Catalytic Moiety in Artificial Imine Reductase. *ChemCatChem* **2016**, 1665–1670.
255. Zimbron, J. M.; Heinisch, T.; Schmid, M.; Hamels, D.; Nogueira, E. S.; Schirmer, T.; Ward, T. R., A Dual Anchoring Strategy for the Localization and Activation of Artificial Metalloenzymes Based on the Biotin-Streptavidin Technology. *J. Am. Chem. Soc.* **2013,** *135* (14), 5384-5388.
256. Quinto, T.; Schwizer, F.; Zimbron, J. M.; Morina, A.; Koehler, V.; Ward, T. R., Expanding the Chemical Diversity in Artificial Imine Reductases Based on the Biotin-Streptavidin Technology. *ChemCatChem* **2014,** *6* (4), 1010-1014.

257. Hestericova, M.; Correro, M. R.; Lenz, M.; Corvini, P. F. X.; Shahgaldian, P.; Ward, T. R., Immobilization of an Artificial Imine Reductase within Silica Nanoparticles Improves Its Performance. *Chem. Commun. (Cambridge, U. K.)* **2016,** *52* (60), 9462-9465.
258. Fahey, R. C.; Brown, W. C.; Adams, W. B.; Worsham, M. B., Occurrence of Glutathione in Bacteria. *J. Bacteriol.* **1978,** *133* (3), 1126-1129.
259. Wilson, Y. M.; Durrenberger, M.; Nogueira, E. S.; Ward, T. R., Neutralizing the Detrimental Effect of Glutathione on Precious Metal Catalysts. *J. Am. Chem. Soc.* **2014,** *136* (25), 8928-8932.
260. Mallin, H.; Hestericova, M.; Reuter, R.; Ward, T. R., Library Design and Screening Protocol for Artificial Metalloenzymes Based on the Biotin-Streptavidin Technology. *Nat. Protoc.* **2016,** *11* (5), 835-852.
261. Kohler, V.; Wilson, Y. M.; Durrenberger, M.; Ghislieri, D.; Churakova, E.; Quinto, T.; Knorr, L.; Haussinger, D.; Hollmann, F.; Turner, N. J., Synthetic Cascades Are Enabled by Combining Biocatalysts with Artificial Metalloenzymes. *Nat. Chem.* **2013,** *5* (2), 93-99.
262. Haquette, P.; Talbi, B.; Barilleau, L.; Madern, N.; Fosse, C.; Salmain, M., Chemically Engineered Papain as Artificial Formate Dehydrogenase for NAD(P)H Regeneration. *Org. Biomol. Chem.* **2011,** *9* (16), 5720-5727.
263. Okamoto, Y.; Kohler, V.; Paul, C. E.; Hollmann, F.; Ward, T. R., Efficient in Situ Regeneration of NADH Mimics by an Artificial Metalloenzyme. *ACS Catal.* **2016,** *6* (6), 3553-3557.
264. Quinto, T.; Haussinger, D.; Kohler, V.; Ward, T. R., Artificial Metalloenzymes for the Diastereoselective Reduction of NAD^+ to $NADH_2$. *Org. Biomol. Chem.* **2015,** *13* (2), 357-360.
265. Okamoto, Y.; Kohler, V.; Ward, T. R., An NAD(P)H-Dependent Artificial Transfer Hydrogenase for Multienzymatic Cascades. *J. Am. Chem. Soc.* **2016,** *138* (18), 5781-5784.
266. Liu, Z.; Lebrun, V.; Kitanosono, T.; Mallin, H.; Koehler, V.; Haeussinger, D.; Hilvert, D.; Kobayashi, S.; Ward, T. R., Upregulation of an Artificial Zymogen by Proteolysis. *Angew. Chem., Int. Ed.* **2016,** *55* (38), 11587-11590.
267. Mayer, C.; Hilvert, D., A Genetically Encodable Ligand for Transfer Hydrogenation. *Eur. J. Org. Chem.* **2013,** (17), 3427-3431.
268. Genz, M.; Koehler, V.; Krauss, M.; Singer, D.; Hoffmann, R.; Ward, T. R.; Straeter, N., An Artificial Imine Reductase Based on the Ribonuclease S Scaffold. *ChemCatChem* **2014,** *6* (3), 736-740.
269. Krishnamurthy, V. M.; Kaufman, G. K.; Urbach, A. R.; Gitlin, I.; Gudiksen, K. L.; Weibel, D. B.; Whitesides, G. M., Carbonic Anhydrase as a Model for Biophysical and Physical-Organic Studies of Proteins and Protein−Ligand Binding. *Chem. Rev.* **2008,** *108* (3), 946−1051.
270. Monnard, F. W.; Heinisch, T.; Nogueira, E. S.; Schirmer, T.; Ward, T. R., Human Carbonic Anhydrase II as a Host for Piano-Stool Complexes Bearing a Sulfonamide Anchor. *Chem. Commun. (Cambridge, U. K.)* **2011,** *47* (29), 8238-8240.
271. Monnard, F. W.; Nogueira, E. S.; Heinisch, T.; Schirmer, T.; Ward, T. R., Human Carbonic Anhydrase II as Host Protein for the Creation of Artificial Metalloenzymes: The Asymmetric Transfer Hydrogenation of Imines. *Chem. Sci.* **2013,** *4* (8), 3269-3274.
272. Heinisch, T.; Pellizzoni, M.; Durrenberger, M.; Tinberg, C. E.; Kohler, V.; Klehr, J.; Haussinger, D.; Baker, D.; Ward, T. R., Improving the Catalytic Performance of an Artificial Metalloenzyme by Computational Design. *J. Am. Chem. Soc.* **2015,** *137* (32), 10414-10419.
273. Watanabe, M.; Murata, K.; Ikariya, T., Enantioselective Michael Reaction Catalyzed by Well-Defined Chiral Ru Amido Complexes: Isolation and Characterization of the Catalyst Intermediate, Ru Malonato Complex Having a Metal-Carbon Bond. *J. Am. Chem. Soc.* **2003,** *125* (25), 7508-7509.
274. Heinisch, T.; Langowska, K.; Tanner, P.; Reymond, J.-L.; Meier, W.; Palivan, C.; Ward, T. R., Fluorescence-Based Assay for the Optimization of the Activity of Artificial Transfer Hydrogenase within a Biocompatible Compartment. *ChemCatChem* **2013,** *5* (3), 720-723.
275. Palivan, C. G.; Goers, R.; Najer, A.; Zhang, X. Y.; Car, A.; Meier, W., Bioinspired Polymer Vesicles and Membranes for Biological and Medical Applications. *Chem. Soc. Rev.* **2016,** *45* (2), 377-411.
276. Franke, R.; Selent, D.; Börner, A., Applied Hydroformylation. *Chem. Rev.* **2012,** *112* (11), 5675-5732.
277. Breit, B.; Seiche, W., Recent Advances on Chemo-, Regio- and Stereoselective Hydroformylation. *Synthesis* **2001,** (1), 1-36.

278. Bertini, I.; Luchinat, C.; Scozzafava, A., Carbonic Anhydrase: An Insight into the Zinc Binding Site and into the Active Cavity through Metal Substitution. In *Biochemistry*, Springer Berlin, Heidelberg, 1982; pp 45-92.
279. Jing, Q.; Kazlauskas, R. J., Regioselective Hydroformylation of Styrene Using Rhodium-Substituted Carbonic Anhydrase. *ChemCatChem* **2010,** *2*, 953-957.
280. Key, H. M.; Clark, D. S.; Hartwig, J. F., Generation, Characterization, and Tunable Reactivity of Organometallic Fragments Bound to a Protein Ligand. *J. Am. Chem. Soc.* **2015,** *137*, 8261-8268.
281. Shimahara, H.; Yoshida, T.; Shibata, Y.; Shimizu, M.; Kyogoku, Y.; Sakiyama, F.; Nakazawa, T.; Tate, S.-I.; Ohki, S.-Y.; Kato, T. et al, Tautomerism of Histidine 64 Associated with Proton Transfer in Catalysis of Carbonic Anhydrase. *J. Biol. Chem.* **2007,** *282* (13), 9646-9656.
282. Romao, C. V.; Vicente, J. B.; Borges, P. T.; Frazao, C.; Teixeira, M., The Dual Function of Flavodiiron Proteins: Oxygen and/or Nitric Oxide Reductases. *J. Biol. Inorg. Chem.* **2016,** *21* (1), 39-52.
283. McQuarters, A. B.; Wirgau, N. E.; Lehnert, N., Model Complexes of Key Intermediates in Fungal Nitric Oxide Reductase (P450nor). *Curr. Opin. Chem. Biol.* **2014,** *19*, 82-89.
284. Hino, T.; Nagano, S.; Sugimoto, H.; Tosha, T.; Shiro, Y., Molecular Structure and Function of Bacterial Nitric Oxide Reductase. *Biochim. Biophys. Acta, Bioenerg.* **2012,** *1817* (4), 680-687.
285. Peterson, R. L.; Kim, S.; Karlin, K. D., Copper Enzymes. In *Comprehensive Inorganic Chemistry II*, Second ed.; Elsevier: Amsterdam, 2013; pp 149-177.
286. Maia, L. B.; Moura, J. J. G., Nitrite Reduction by Molybdoenzymes: A New Class of Nitric Oxide-Forming Nitrite Reductases. *J. Biol. Inorg. Chem.* **2015,** *20* (2), 403-433.
287. Kirk, M. L.; Stein, B., Molybdenum Enzymes. In *Comprehensive Inorganic Chemistry II* Second ed.; Elsevier: Amsterdam, 2013; pp 263-293.
288. Hu, Y. L.; Ribbe, M. W., Nitrogenases-a Tale of Carbon Atom(s). *Angew. Chem., Int. Ed.* **2016,** *55* (29), 8216-8226.
289. Pessoa, J. C.; Garribba, E.; Santos, M. F. A.; Santos-Silva, T., Vanadium and Proteins: Uptake, Transport, Structure, Activity and Function. *Coord. Chem. Rev.* **2015,** *301*, 49-86.
290. Sigman, J. A.; Kwok, B. C.; Lu, Y., From Myoglobin to Heme-Copper Oxidase: Design and Engineering of a Cub Center into Sperm Whale Myoglobin. *J. Am. Chem. Soc.* **2000,** *122* (34), 8192-8196.
291. Zhao, X.; Yeung, N.; Russell, B. S.; Garner, D. K.; Lu, Y., Catalytic Reduction of NO to N_2O by a Designed Heme Copper Center in Myoglobin: Implications for the Role of Metal Ions. *J. Am. Chem. Soc.* **2006,** *128* (21), 6766-6767.
292. Lu, Y.; Yeung, N.; Sieracki, N.; Marshall, N. M., Design of Functional Metalloproteins. *Nature* **2009,** *460*, 855-862.
293. Lin, Y.-W.; Yeung, N.; Gao, Y.-G.; Miner, K. D.; Lei, L.; Robinson, H.; Lu, Y., Introducing a 2-His-1-Glu Nonheme Iron Center into Myoglobin Confers Nitric Oxide Reductase Activity. *J. Am. Chem. Soc.* **2010,** *132* (29), 9970-9972.
294. Ueno, T.; Yokoi, N.; Unno, M.; Matsui, T.; Tokita, Y.; Yamada, M.; Ikeda-Saito, M.; Nakajima, H.; Watanabe, Y., Design of Metal Cofactors Activated by a Protein-Protein Electron Transfer System. *Proc. Natl. Acad. Sci. U. S. A.* **2006,** *103* (25), 9416-9421.
295. Yokoi, N.; Miura, Y.; Huang, C. Y.; Takatani, N.; Inaba, H.; Koshiyama, T.; Kanamaru, S.; Arisaka, F.; Watanabe, Y.; Kitagawa, S. et al, Dual Modification of a Triple-Stranded Beta-Helix Nanotube with Ru and Re Metal Complexes to Promote Photocatalytic Reduction of CO_2. *Chem. Commun. (Cambridge, U. K.)* **2011,** *47* (7), 2074-2076.
296. Yokoi, N.; Inaba, H.; Terauchi, M.; Stieg, A. Z.; Sanghamitra, N. J. M.; Koshiyama, T.; Yutani, K.; Kanamaru, S.; Arisaka, F.; Hikage, T. et al, Construction of Robust Bio-Nanotubes Using the Controlled Self-Assembly of Component Proteins of Bacteriophage T4. *Small* **2010,** *6* (17), 1873-1879.
297. Inaba, H.; Kanamaru, S.; Arisaka, F.; Kitagawa, S.; Ueno, T., Semi-Synthesis of an Artificial Scandium(III) Enzyme with a Beta-Helical Bio-Nanotube. *Dalton Trans.* **2012,** *41* (37), 11424-11427.
298. Tegoni, M.; Yu, F. T.; Bersellini, M.; Penner-Hahn, J. E.; Pecoraro, V. L., Designing a Functional Type 2 Copper Center That Has Nitrite Reductase Activity within Alpha-Helical Coiled Coils. *Proc. Natl. Acad. Sci. U. S. A.* **2012,** *109* (52), 21234-21239.

299. Butt, N. A.; Zhang, W., Transition Metal-Catalyzed Allylic Substitution Reactions with Unactivated Allylic Substrates. *Chem. Soc. Rev.* **2015,** *44* (22), 7929-7967.
300. Christianson, D. W., Structural Biology and Chemistry of the Terpenoid Cyclases. *Chem. Rev. (Washington, DC, U. S.)* **2006,** *106* (8), 3412-3442.
301. Voelker, T.; Dempwolff, F.; Graumann, P. L.; Meggers, E., Progress Towards Bioorthogonal Catalysis with Organometallic Compounds. *Angew. Chem., Int. Ed.* **2014,** *53* (39), 10536-10540.
302. Tomas-Gamasa, M.; Martinez-Calvo, M.; Couceiro, J. R.; Mascarenas, J. L., Transition Metal Catalysis in the Mitochondria of Living Cells. *Nat. Commun.* **2016,** *7*, 12538.
303. Hsu, H.-T.; Trantow, B. M.; Waymouth, R. M.; Wender, P. A., Bioorthogonal Catalysis: A General Method to Evaluate Metal-Catalyzed Reactions in Real Time in Living Systems Using a Cellular Luciferase Reporter System. *Bioconjugate Chem.* **2016,** *27* (2), 376-382.
304. Pierron, J.; Malan, C.; Creus, M.; Gradinaru, J.; Hafner, I.; Ivanova, A.; Sardo, A.; Ward, T. R., Artificial Metalloenzymes for Asymmetric Allylic Alkylation on the Basis of the Biotin-Avidin Technology. *Angew. Chem., Int. Ed.* **2008,** *47* (4), 701-705.
305. Suzuki, A., Cross-Coupling Reactions of Organoboranes: An Easy Way to Construct C-C Bonds (Nobel Lecture). *Angew. Chem., Int. Ed.* **2011,** *50* (30), 6722-6737.
306. Yusop, R.; Broceta, A. U.; Johansson, E.; Sanchez-Martin, R.; Bradley, M., Palladium-Mediated Intracellular Chemistry. *Nat. Chem.* **2011,** *3*, 239-243.
307. Li, J.; Chen, P. R., Moving Pd-Mediated Protein Cross Coupling to Living Systems. *ChemBioChem* **2012,** *13* (12), 1728-1731.
308. Gao, Z.; Gouverneur, V.; Davis, B. G., Enhanced Aqueous Suzuki-Miyaura Coupling Allows Site-Specific Polypeptide 18F-Labeling. *J. Am. Chem. Soc.* **2013,** *135* (37), 13612-13615.
309. Li, N.; Lim, R. K. V.; Edwardraja, S.; Lin, Q., Copper-Free Sonogashira Cross-Coupling for Functionalization of Alkyne-Encoded Proteins in Aqueous Medium and in Bacterial Cells. *J. Am. Chem. Soc.* **2011,** *133* (39), 15316-15319.
310. Abe, S.; Niemeyer, J.; Abe, M.; Takezawa, Y.; Ueno, T.; Hikage, T.; Erker, G.; Watanabe, Y., Control of the Coordination Structure of Organometallic Palladium Complexes in an Apo-Ferritin Cage. *J. Am. Chem. Soc.* **2008,** *130* (32), 10512-10514.
311. Abe, S.; Hirata, K.; Ueno, T.; Morino, K.; Shimizu, N.; Yamamoto, M.; Takata, M.; Yashima, E.; Watanabe, Y., Polymerization of Phenylacetylene by Rhodium Complexes within a Discrete Space of Apo-Ferritin. *J. Am. Chem. Soc.* **2009,** *131* (20), 6958-6960.
312. Wang, Z. Y.; Takezawa, Y.; Aoyagi, H.; Abe, S.; Hikage, T.; Watanabe, Y.; Kitagawa, S.; Ueno, T., Definite Coordination Arrangement of Organometallic Palladium Complexes Accumulated on the Designed Interior Surface of Apo-Ferritin. *Chem. Commun. (Cambridge, U. K.)* **2011,** *47* (1), 170-172.
313. Chatterjee, A.; Mallin, H.; Klehr, J.; Vallapurackal, J.; Finke, A. D.; Vera, L.; Marsh, M.; Ward, T. R., An Enantioselective Artificial Suzukiase Based on the Biotin-Streptavidin Technology. *Chem. Sci.* **2016,** *7* (1), 673-677.
314. Filice, M.; Romero, O.; Aires, A.; Guisan, J. M.; Rumbero, A.; Palomo, J. M., Preparation of an Immobilized Lipase-Palladium Artificial Metalloenzyme as Catalyst in the Heck Reaction: Role of the Solid Phase. *Adv. Synth. Catal.* **2015,** *357* (12), 2687-2696.
315. Davies, H. M. L.; Du Bois, J.; Yu, J.-Q., C-H Functionalization in Organic Synthesis. *Chem. Soc. Rev.* **2011,** *40* (4), 1855-1856.
316. Lewis, J. C.; Coelho, P. S.; Arnold, F. H., Enzymatic Functionalization of Carbon-Hydrogen Bonds. *Chem. Soc. Rev.* **2011,** *40* (4), 2003-2021.
317. Souillart, L.; Cramer, N., Catalytic C-C Bond Activations Via Oxidative Addition to Transition Metals. *Chem. Rev. (Washington, DC, U. S.)* **2015,** *115* (17), 9410-9464.
318. Fagnou, K.; Lautens, M., Rhodium-Catalyzed Carbon-Carbon Bond Forming Reactions of Organometallic Compounds. *Chem. Rev. (Washington, DC, U. S.)* **2003,** *103* (1), 169-196.
319. Hyster, T. K.; Knorr, L.; Ward, T. R.; Rovis, T., Biotinylated Rh(III) Complexes in Engineered Streptavidin for Accelerated Asymmetric C-H Activation. *Science* **2012,** *338* (6106), 500-503.
320. Che, C.-M.; Lo, V. K.-Y.; Zhou, C.-Y.; Huang, J.-S., Selective Functionalisation of Saturated C-H Bonds with Metalloporphyrin Catalysts. *Chem. Soc. Rev.* **2011,** *40* (4), 1950-1975.

321. Leak, D. J.; Sheldon, R. A.; Woodley, J. M.; Adlercreutz, P., Biocatalysts for Selective Introduction of Oxygen. *Biocatal. Biotransform.* **2009,** *27* (1), 1-26.
322. Svastits, E. W.; Dawson, J. H.; Breslow, R.; Gellman, S. H., Functionalized Nitrogen Atom Transfer Catalyzed by Cytochrome P-450. *J. Am. Chem. Soc.* **1985,** *107* (22), 6427-6428.
323. Wang, Z. J.; Peck, N. E.; Renata, H.; Arnold, F. H., Cytochrome P450-Catalyzed Insertion of Carbenoids into N-H Bonds. *Chem. Sci.* **2014,** *5* (2), 598-601.
324. Sreenilayam, G.; Fasan, R., Myoglobin-Catalyzed Intermolecular Carbene N-H Insertion with Arylamine Substrates. *Chem. Commun.* **2015,** *51* (8), 1532-1534.
325. Key, H. M.; Dydio, P.; Clark, D. S.; Hartwig, J. F., Abiological Catalysis by Artificial Haem Proteins Containing Noble Metals in Place of Iron. *Nature* **2016,** *534* (7608), 534-537.
326. Ohashi, M.; Koshiyama, T.; Ueno, T.; Yanase, M.; Fujii, H.; Watanabe, Y., Preparation of Artificial Metalloenzymes by Insertion of Chromium(III) Schiff Base Complexes into Apomyoglobin Mutants. *Angew. Chem., Int. Ed.* **2003,** *42* (9), 1005-1008.
327. Carey, J. R.; Ma, S. K.; Pfister, T. D.; Garner, D. K.; Kim, H. K.; Abramite, J. A.; Wang, Z. L.; Guo, Z. J.; Lu, Y., A Site-Selective Dual Anchoring Strategy for Artificial Metalloprotein Design. *J. Am. Chem. Soc.* **2004,** *126* (35), 10812-10813.
328. Zhang, J. L.; Garner, D. K.; Liang, L.; Chen, Q.; Lu, Y., Protein Scaffold of a Designed Metalloenzyme Enhances the Chemoselectivity in Sulfoxidation of Thioanisole. *Chem. Commun.* **2008,** (14), 1665-1667.
329. Hayashi, T.; Hitomi, Y.; Ando, T.; Mizutani, T.; Hisaeda, Y.; Kitagawa, S.; Ogoshi, H., Peroxidase Activity of Myoglobin Is Enhanced by Chemical Mutation of Heme-Propionates. *J. Am. Chem. Soc.* **1999,** *121* (34), 7747-7750.
330. Sato, H.; Hayashi, T.; Ando, T.; Hisaeda, Y.; Ueno, T.; Watanabe, Y., Hybridization of Modified-Heme Reconstitution and Distal Histidine Mutation to Functionalize Sperm Whale Myoglobin. *J. Am. Chem. Soc.* **2004,** *126* (2), 436-437.
331. Hayashi, T.; Murata, D.; Makino, M.; Sugimoto, H.; Matsuo, T.; Sato, H.; Shiro, Y.; Hisaeda, Y., Crystal Structure and Peroxidase Activity of Myoglobin Reconstituted with Iron Porphycene. *Inorg. Chem.* **2006,** *45* (26), 10530-10536.
332. Dydio, P.; Key, H. M.; Nazarenko, A.; Rha, J. Y.-E.; Seyedkazemi, V.; Clark, D. S.; Hartwig, J. F., An Artificial Metalloenzyme with the Kinetics of Native Enzymes. *Science* **2016,** *354* (6308), 102-106.
333. Grubbs, R. H., *Handbook of Metathesis*. Wiley-VCH: Weinheim, 2003; Vol. 3.
334. Herbert, M. B.; Grubbs, R. H., Z-Selective Cross Metathesis with Ruthenium Catalysts: Synthetic Applications and Mechanistic Implications. *Angew. Chem., Int. Ed.* **2015,** *54* (17), 5018-5024.
335. Koh, M. J.; Khan, R. K. M.; Torker, S.; Yu, M.; Mikus, M. S.; Hoveyda, A. H., High-Value Alcohols and Higher-Oxidation-State Compounds by Catalytic Z-Selective Cross-Metathesis. *Nature* **2015,** *517* (7533), 181-186.
336. Nguyen, T. T.; Koh, M. J.; Shen, X.; Romiti, F.; Schrock, R. R.; Hoveyda, A. H., Kinetically Controlled E-Selective Catalytic Olefin Metathesis. *Science* **2016,** *352* (6285), 569-575.
337. Lin, Y. A.; Chalker, J. M.; Floyd, N.; Bernardes, G. J. L.; Davis, B. G., Allyl Sulfides Are Privileged Substrates in Aqueous Cross-Metathesis: Application to Site-Selective Protein Modification. *J. Am. Chem. Soc.* **2008,** *130* (30), 9642-9643.
338. Ai, H. W.; Shen, W. J.; Brustad, E.; Schultz, P. G., Genetically Encoded Alkenes in Yeast. *Angew. Chem., Int. Ed.* **2010,** *49* (5), 935-937.
339. Lo, C.; Ringenberg, M. R.; Gnandt, D.; Wilson, Y.; Ward, T. R., Artificial Metalloenzymes for Olefin Metathesis Based on the Biotin-(Strept)Avidin Technology. *Chem. Commun.* **2011,** *47* (44), 12065-12067.
340. Mayer, C.; Gillingham, D. G.; Ward, T. R.; Hilvert, D., An Artificial Metalloenzyme for Olefin Metathesis. *Chem. Commun.* **2011,** *47* (44), 12068-12070.
341. Matsuo, T.; Yoshida, T.; Fujii, A.; Kawahara, K.; Hirota, S., Effect of Added Salt on Ring-Closing Metathesis Catalyzed by a Water-Soluble Hoveyda-Grubbs Type Complex to Form N-Containing Heterocycles in Aqueous Media. *Organometallics* **2013,** *32* (19), 5313-5319.
342. Kajetanowicz, A.; Chatterjee, A.; Reuter, R.; Ward, T. R., Biotinylated Metathesis Catalysts: Synthesis and Performance in Ring Closing Metathesis. *Catal. Lett.* **2014,** *144* (3), 373-379.

343. Matsuo, T.; Imai, C.; Yoshida, T.; Saito, T.; Hayashi, T.; Hirota, S., Creation of an Artificial Metalloprotein with a Hoveyda-Grubbs Catalyst Moiety through the Intrinsic Inhibition Mechanism of Alpha-Chymotrypsin. *Chem. Commun.* **2012,** *48* (11), 1662-1664.
344. Basauri-Molina, M.; Verhoeven, D. G. A.; van Schaik, A. J.; Kleijn, H.; Klein Gebbink, R. J. M., Ring-Closing and Cross-Metathesis with Artificial Metalloenzymes Created by Covalent Active Site-Directed Hybridization of a Lipase. *Chem. - Eur. J.* **2015,** *21* (44), 15676-15685.
345. Zhao, J. M.; Kajetanowicz, A.; Ward, T. R., Carbonic Anhydrase II as Host Protein for the Creation of a Biocompatible Artificial Metathesase. *Org. Biomol. Chem.* **2015,** *13* (20), 5652-5655.
346. Philippart, F.; Arlt, M.; Gotzen, S.; Tenne, S. J.; Bocola, M.; Chen, H. H.; Zhu, L. L.; Schwaneberg, U.; Okuda, J., A Hybrid Ring-Opening Metathesis Polymerization Catalyst Based on an Engineered Variant of the Beta-Barrel Protein FhuA. *Chem. - Eur. J.* **2013,** *19* (41), 13865-13871.
347. Sauer, D. F.; Bocola, M.; Broglia, C.; Arlt, M.; Zhu, L. L.; Brocker, M.; Schwaneberg, U.; Okuda, J., Hybrid Ruthenium ROMP Catalysts Based on an Engineered Variant of Beta-Barrel Protein FhuA Delta Cvftev : Effect of Spacer Length. *Chem. Asian J.* **2015,** *10* (1), 177-182.
348. Osseili, H.; Sauer, D. F.; Beckerle, K.; Arlt, M.; Himiyama, T.; Polen, T.; Onoda, A.; Schwaneberg, U.; Hayashi, T.; Okuda, J., Artificial Diels-Alderase Based on the Transmembrane Protein FhuA. *Beilstein J. Org. Chem.* **2016,** *12*, 1314-1321.
349. Jeschek, M.; Reuter, R.; Heinisch, T.; Trindler, C.; Klehr, J.; Panke, S.; Ward, T. R., Directed Evolution of Artificial Metalloenzymes for *in vivo* Metathesis. *Nature* **2016,** *537* (7622), 661-665.
350. Reynolds, E. W.; McHenry, M. W.; Cannac, F.; Gober, J. G.; Snow, C. D.; Brustad, E. M., An Evolved Orthogonal Enzyme/Cofactor Pair. *J. Am. Chem. Soc.* **2016,** *138* (38), 12451-12458.
351. Deuss, P. J.; Popa, G.; Slawin, A. M. Z.; Laan, W.; Kamer, P. C. J., Artificial Copper Enzymes for Asymmetric Diels-Alder Reactions. *ChemCatChem* **2013,** *5*, 1184-1191.
352. Srivastava, P.; Yang, H.; Ellis-Guardiola, K.; Lewis, J. C., Engineering a Dirhodium Artificial Metalloenzyme for Selective Olefin Cyclopropanation. *Nat. Commun.* **2015,** *6*, 7789.
353. Harris, M. N.; Madura, J. D.; Ming, L. J.; Harwood, V. J., Kinetic and Mechanistic Studies of Prolyl Oligopeptidase from the Hyperthermophile Pyrococcus Furiosus. *J. Biol. Chem.* **2001,** *276* (22), 19310-19317.
354. Fukumoto, K.; Onoda, A.; Mizohata, E.; Bocola, M.; Inoue, T.; Schwaneberg, U.; Hayashi, T., Rhodium-Complex-Linked Hybrid Biocatalyst: Stereo-Controlled Phenylacetylene Polymerization within an Engineered Protein Cavity. *ChemCatChem* **2014,** *6* (5), 1229-1235.
355. Sigg, S. J.; Seidi, F.; Renggli, K.; Silva, T. B.; Kali, G.; Bruns, N., Horseradish Peroxidase as a Catalyst for Atom Transfer Radical Polymerization. *Macromol. Rapid Commun.* **2011,** *32* (21), 1710-1715.
356. Renggli, K.; Nussbaumer, M. G.; Urbani, R.; Pfohl, T.; Bruns, N., A Chaperonin as Protein Nanoreactor for Atom-Transfer Radical Polymerization. *Angew. Chem.,Int. Ed.* **2014,** *53* (5), 1443-1447.
357. Nicolaou, K. C.; Snyder, S. A.; Montagnon, T.; Vassilikogiannakis, G., The Diels–Alder Reaction in Total Synthesis. *Angew. Chem., Int. Ed.* **2002,** *41* (10), 1668-1698.
358. Fringuelli, F.; Piermatti, O.; Pizzo, F.; Vaccaro, L., Recent Advances in Lewis Acid Catalyzed Diels−Alder Reactions in Aqueous Media. *Eur. J. Org. Chem.* **2001,** *2001* (3), 439-455.
359. Podtetenieff, J.; Taglieber, A.; Bill, E.; Reijerse, E. J.; Reetz, M. T., An Artificial Metalloenzyme: Creation of a Designed Copper Binding Site in a Thermostable Protein. *Angew. Chem., Int. Ed.* **2010,** *49*, 5151-5155.
360. Kuo, C.-H.; Fruk, L.; Niemeyer, C. M., Addressable DNA-Myoglobin Photocatalysis. *Chem. Asian J.* **2009,** *4*, 1064-1069.
361. Ghattas, W.; Cotchico-Alonso, L.; Marechal, J. D.; Urvoas, A.; Rousseau, M.; Mahy, J. P.; Ricoux, R., Artificial Metalloenzymes with the Neocarzinostatin Scaffold: Toward a Biocatalyst for the Diels-Alder Reaction. *ChemBioChem* **2016,** *17* (5), 433-440.
362. Talbi, B.; Haquette, P.; Martel, A.; de Montigny, F.; Fosse, C.; Cordier, S.; Roisnel, T.; Jaouen, G.; Salmain, M., (Eta^6-Arene) Ruthenium(II) Complexes and Metallo-Papain Hybrid as Lewis Acid Catalysts of Diels-Alder Reaction in Water. *Dalton Trans.* **2010,** *39* (24), 5605-5607.

363. Himiyama, T.; Sauer, D. F.; Onoda, A.; Spaniol, T. P.; Okuda, J.; Hayashi, T., Construction of a Hybrid Biocatalyst Containing a Covalently-Linked Terpyridine Metal Complex within a Cavity of Aponitrobindin. *J. Inorg. Biochem.* **2016,** *158*, 55-61.
364. Filice, M.; Romero, O.; Gutierrez-Fernandez, J.; de las Rivas, B.; Hermoso, J. A.; Palomo, J. M., Synthesis of a Heterogeneous Artificial Metallolipase with Chimeric Catalytic Activity. *Chem. Commun.* **2015,** *51* (45), 9324-9327.
365. Bos, J.; Fusetti, F.; Driessen, A. J. M.; Roelfes, G., Enantioselective Artificial Metalloenzymes by Creation of a Novel Active Site at the Protein Dimer Interface. *Angew. Chem., Int. Ed.* **2012,** *51*, 7472-7475.
366. Bos, J.; García-Herraiz, A.; Roelfes, G., An Enantioselective Artificial Metallo-Hydratase. *Chem. Sci.* **2013,** *4* (9), 3578-3582.
367. Reetz, M. T.; Jiao, N., Copper–Phthalocyanine Conjugates of Serum Albumins as Enantioselective Catalysts in Diels–Alder Reactions. *Angew. Chem., Int. Ed.* **2006,** *45* (15), 2416-2419.
368. Ueno, T.; Tabe, H.; Tanaka, Y., Artificial Metalloenzymes Constructed from Hierarchically-Assembled Proteins. *Chem. Asian J.* **2013,** *8* (8), 1646-1660.
369. Rueping, M.; Nachtsheim, B. J., A Review of New Developments in the Friedel-Crafts Alkylation - from Green Chemistry to Asymmetric Catalysis. *Beilstein J. Org. Chem.* **2010,** *6* (6), 1-24.
370. Lu, H. H.; Tan, F.; Xiao, W. J., Enantioselective Organocatalytic Friedel-Crafts Alkylations. *Curr. Org. Chem.* **2011,** *15* (24), 4022-4045.
371. Qiu, R. H.; Chen, Y.; Yin, S. F.; Xu, X. H.; Au, C. T., A Mini-Review on Air-Stable Organometallic Lewis Acids: Synthesis, Characterization, and Catalytic Application in Organic Synthesis. *RSC Adv.* **2012,** *2* (29), 10774-10793.
372. Drienovska, I.; Rioz-Martinez, A.; Draksharapu, A.; Roelfes, G., Novel Artificial Metalloenzymes by *in vivo* Incorporation of Metal-Binding Unnatural Amino Acids. *Chem. Sci.* **2015,** *6* (1), 770-776.
373. Bos, J.; Browne, W. R.; Driessen, A. J. M.; Roelfes, G., Supramolecular Assembly of Artificial Metalloenzymes Based on the Dimeric Protein LmrR as Promiscuous Scaffold. *J. Am. Chem. Soc.* **2015,** *137*, 9796-9799.
374. Kurtz Jr, D. M., Dioxygen-Binding Proteins. In *Comprehensive Coordination Chemistry II*, Pergamon: Oxford, 2003.
375. Schultz, P. G.; Lerner, R. A., Antibody Catalysis of Difficult Chemical-Transformations. *Acc. Chem. Res.* **1993,** *26* (8), 391-395.
376. Takagi, M.; Kohda, K.; Hamuro, T.; Harada, A.; Yamaguchi, H.; Kamachi, M.; Imanaka, T., Thermostable Peroxidase-Activity with a Recombinant Antibody L-Chain-Porphyrin Fe(III) Complex. *FEBS Lett.* **1995,** *375* (3), 273-276.
377. Quilez, R.; deLauzon, S.; Desfosses, B.; Mansuy, D.; Mahy, J. P., Artificial Peroxidase-Like Hemoproteins Based on Antibodies Constructed from a Specifically Designed Ortho-Carboxy Substituted Tetraarylporphyrin Hapten and Exhibiting a High Affinity for Iron-Porphyrins. *FEBS Lett.* **1996,** *395* (1), 73-76.
378. Kawamura-Konishi, Y.; Fujie, Y.; Suzuki, H., Kinetics of Formation of Antibody-Ferric Porphyrin Complex with Peroxidase Activity. *J. Protein Chem.* **1999,** *18* (7), 741-745.
379. Mahy, J. P.; Desfosses, B.; de Lauzon, S.; Quilez, R.; Desfosses, B.; Lion, L.; Mansuy, D., Hemoabzymes - Different Strategies for Obtaining Artificial Hemoproteins Based on Antibodies. *Appl. Biochem. Biotechnol.* **1998,** *75* (1), 103-127.
380. Yamaguchi, H.; Tsubouchi, K.; Kawaguchi, K.; Horita, E.; Harada, A., Peroxidase Activity of Cationic Metalloporphyrin-Antibody Complexes. *Chem. - Eur. J.* **2004,** *10* (23), 6179-6186.
381. de Lauzon, S.; Mansuy, D.; Mahy, J. P., Coordination Chemistry of Iron(III)-Porphyrin-Antibody Complexes - Influence on the Peroxidase Activity of the Axial Coordination of an Imidazole on the Iron Atom. *Eur. J. Biochem.* **2002,** *269* (2), 470-480.
382. Ricoux, R.; Sauriat-Dorizon, H.; Girgenti, E.; Blanchard, D.; Mahy, J. P., Hemoabzymes: Towards New Biocatalysts for Selective Oxidations. *J. Immunol. Methods* **2002,** *269* (1-2), 39-57.
383. Ricoux, R.; Boucher, J. L.; Mansuy, D.; Mahy, J. P., Microperoxidase 8 Catalyzed Nitration of Phenol by Nitrogen Dioxide Radicals. *Eur. J. Biochem.* **2001,** *268* (13), 3783-3788.

384. Raffy, Q.; Ricoux, R.; Mahy, J. P., Synthesis of a New Estradiol-Iron Metalloporphyrin Conjugate Used to Build up a New Hybrid Biocatalyst for Selective Oxidations by the 'Trojan Horse' Strategy. *Tetrahedron Lett.* **2008,** *49* (11), 1865-1869.
385. Raffy, Q.; Ricoux, R.; Sansiaume, E.; Pethe, S.; Mahy, J. P., Coordination Chemistry Studies and Peroxidase Activity of a New Artificial Metalloenzyme Built by the "Trojan Horse" Strategy. *J. Mol. Catal. A: Chem.* **2010,** *317* (1-2), 19-26.
386. Girgenti, E.; Ricoux, R.; Mahy, J. P., Design and Synthesis of a Mn(III)-Porphyrin Steroid Conjugate Used as a New Cleavable Affinity Label: On the Road to Semi-Synthetic Catalytic Antibodies. *Tetrahedron* **2004,** *60* (44), 10049-10058.
387. de Lauzon, S.; Desfosses, B.; Mansuy, D.; Mahy, J. P., Studies of the Reactivity of Artificial Peroxidase-Like Hemoproteins Based on Antibodies Elicited against a Specifically Designed Ortho-Carboxy Substituted Tetraarylporphyrin. *FEBS Lett.* **1999,** *443* (2), 229-234.
388. Matsuo, T.; Fukumoto, K.; Watanabe, T.; Hayashi, T., Precise Design of Artificial Cofactors for Enhancing Peroxidase Activity of Myoglobin: Myoglobin Mutant H64D Reconstituted with a "Single-Winged Cofactor" Is Equivalent to Native Horseradish Peroxidase in Oxidation Activity. *Chem. Asian J.* **2011,** *6* (9), 2491-2499.
389. Matsuo, T.; Murata, D.; Hisaeda, Y.; Hori, H.; Hayashi, T., Porphyrinoid Chemistry in Hemoprotein Matrix: Detection and Reactivities of Iron(IV)-Oxo Species of Porphycene Incorporated into Horseradish Peroxidase. *J. Am. Chem. Soc.* **2007,** *129* (43), 12906-12907.
390. Matsuo, T.; Hayashi, A.; Abe, M.; Matsuda, T.; Hisaeda, Y.; Hayashi, T., Meso-Unsubstituted Iron Corrole in Hemoproteins: Remarkable Differences in Effects on Peroxidase Activities between Myoglobin and Horseradish Peroxidase. *J. Am. Chem. Soc.* **2009,** *131* (42), 15124-15125.
391. Kaplan, J.; DeGrado, W. F., De Novo Design of Catalytic Proteins. *Proc. Natl. Acad. Sci. U. S. A.* **2004,** *101* (32), 11566-11570.
392. Faiella, M.; Andreozzi, C.; de Rosales, R. T.; Pavone, V.; Maglio, O.; Nastri, F.; DeGrado, W. F.; Lombardi, A., An Artificial Di-Iron Oxo-Protein with Phenol Oxidase Activity. *Nat. Chem. Biol.* **2009,** *5* (12), 882-884.
393. Lombardi, A.; Summa, C. M.; Geremia, S.; Randaccio, L.; Pavone, V.; DeGrado, W. F., Retrostructural Analysis of Metalloproteins: Application to the Design of a Minimal Model for Diiron Proteins. *Proc. Natl. Acad. Sci. U. S. A.* **2000,** *97* (12), 6298-6305.
394. Reig, A. J.; Pires, M. M.; Snyder, R. A.; Wu, Y.; Jo, H.; Kulp, D. W.; Butch, S. E.; Calhoun, J. R.; Szyperski, T.; Solomon, E. I. et al, Alteration of the Oxygen-Dependent Reactivity of De Novo Due Ferri Proteins. *Nat. Chem.* **2012,** *4* (11), 900-906.
395. Snyder, R. A.; Butch, S. E.; Reig, A. J.; DeGrado, W. F.; Solomon, E. I., Molecular-Level Insight into the Differential Oxidase and Oxygenase Reactivities of De Novo Due Ferri Proteins. *J. Am. Chem. Soc.* **2015,** *137* (29), 9302-9314.
396. Ricoux, R.; Dubuc, R.; Dupont, C.; Marechal, J. D.; Martin, A.; Sellier, M.; Mahy, J. P., Hemozymes Peroxidase Activity of Artificial Hemoproteins Constructed from the Streptomyces Lividans Xylanase a and Iron(III)-Carboxy-Substituted Porphyrins. *Bioconjugate Chem.* **2008,** *19* (4), 899-910.
397. Fujieda, N.; Hasegawa, A.; Ishihama, K.; Itoh, S., Artificial Dicopper Oxidase: Rational Reprogramming of Bacterial Metallo-Beta-Lactamase into a Catechol Oxidase. *Chem. Asian J.* **2012,** *7* (6), 1203-1207.
398. Amrein, B.; Schmid, M.; Collet, G.; Cuniasse, P.; Gilardoni, F.; Seebeck, F. P.; Ward, T. R., Identification of Two-Histidines One-Carboxylate Binding Motifs in Proteins Amenable to Facial Coordination to Metals. *Metallomics* **2012,** *4* (4), 379-388.
399. Fujieda, N.; Schatti, J.; Stuttfeld, E.; Ohkubo, K.; Maier, T.; Fukuzumi, S.; Ward, T. R., Enzyme Repurposing of a Hydrolase as an Emergent Peroxidase Upon Metal Binding. *Chem. Sci.* **2015,** *6* (7), 4060-4065.
400. Lee, H. S.; Schultz, P. G., Biosynthesis of a Site-Specific DNA Cleaving Protein. *J. Am. Chem. Soc.* **2008,** *130* (40), 13194-13195.
401. Fernandez, I.; Khiar, N., Recent Developments in the Synthesis and Utilization of Chiral Sulfoxides. *Chem. Rev.* **2003,** *103* (9), 3651-3705.

402. Pellissier, H., Recent Advances in Enantioselective Vanadium-Catalyzed Transformations. *Coord. Chem. Rev.* **2015,** *284*, 93-110.
403. Sipos, G.; Drinkel, E. E.; Dorta, R., The Emergence of Sulfoxides as Efficient Ligands in Transition Metal Catalysis. *Chem. Soc. Rev.* **2015,** *44* (11), 3834-3860.
404. Legros, J.; Dehli, J. R.; Bolm, C., Applications of Catalytic Asymmetric Sulfide Oxidations to the Syntheses of Biologically Active Sulfoxides. *Adv. Synth. Catal.* **2005,** *347* (1), 19-31.
405. Wojaczynska, E.; Wojaczynski, J., Enantioselective Synthesis of Sulfoxides: 2000-2009. *Chem. Rev.* **2010,** *110* (7), 4303-4356.
406. Correa, A.; Mancheno, O. G.; Bolm, C., Iron-Catalysed Carbon-Heteroatom and Heteroatom-Heteroatom Bond Forming Processes. *Chem. Soc. Rev.* **2008,** *37* (6), 1108-1117.
407. Licini, G.; Conte, V.; Coletti, A.; Mba, M.; Zonta, C., Recent Advances in Vanadium Catalyzed Oxygen Transfer Reactions. *Coord. Chem. Rev.* **2011,** *255* (19-20), 2345-2357.
408. Ricoux, R.; Lukowska, E.; Pezzotti, F.; Mahy, J. P., New Activities of a Catalytic Antibody with a Peroxidase Activity - Formation of Fe(II)-RNO Complexes and Stereoselective Oxidation of Sulfides. *Eur. J. Biochem.* **2004,** *271* (7), 1277-1283.
409. Sansiaume, E.; Ricoux, R.; Gori, D.; Mahy, J. P., Oxidation of Organic Molecules in Homogeneous Aqueous Solution Catalyzed by Hybrid Biocatalysts (Based on the Trojan Horse Strategy). *Tetrahedron: Asymmetry* **2010,** *21* (11-12), 1593-1600.
410. Sansiaume-Dagousset, E.; Urvoas, A.; Chelly, K.; Ghattas, W.; Marechal, J. D.; Mahy, J. P.; Ricoux, R., Neocarzinostatin-Based Hybrid Biocatalysts for Oxidation Reactions. *Dalton Trans.* **2014,** *43* (22), 8344-8354.
411. Mahy, J. P.; Raffy, Q.; Allard, M.; Ricoux, R., Various Strategies for Obtaining Artificial Hemoproteins: From "Hemoabzymes" to "Hemozymes". *Biochimie* **2009,** *91* (10), 1321-1323.
412. Ricoux, R.; Allard, M.; Dubuc, R.; Dupont, C.; Marechal, J. D.; Mahy, J. P., Selective Oxidation of Aromatic Sulfide Catalyzed by an Artificial Metalloenzyme: New Activity of Hemozymes. *Org. Biomol. Chem.* **2009,** *7* (16), 3208-3211.
413. Koshiyama, T.; Yokoi, N.; Ueno, T.; Kanamaru, S.; Nagano, S.; Shiro, Y.; Arisaka, F.; Watanabe, Y., Molecular Design of Heteroprotein Assemblies Providing a Bionanocup as a Chemical Reactor. *Small* **2008,** *4* (1), 50-54.
414. Ueno, T.; Koshiyama, T.; Ohashi, M.; Kondo, K.; Kono, M.; Suzuki, A.; Yamane, T.; Watanabe, Y., Coordinated Design of Cofactor and Active Site Structures in Development of New Protein Catalysts. *J. Am. Chem. Soc.* **2005,** *127* (18), 6556-6562.
415. Zhang, J. L.; Garner, D. K.; Liang, L.; Barrios, D. A.; Lu, Y., Noncovalent Modulation of pH-Dependent Reactivity of a Mn-Salen Cofactor in Myoglobin with Hydrogen Peroxide. *Chem. Eur. J.* **2009,** *15* (30), 7481-7489.
416. Rousselot-Pailley, P.; Bochot, C.; Marchi-Delapierre, C.; Jorge-Robin, A.; Martin, L.; Fontecilla-Camps, J. C.; Cavazza, C.; Ménage, S., The Protein Environment Drives Selectivity for Sulfide Oxidation by an Artificial Metalloenzyme. *ChemBioChem* **2009,** *10* (3), 545-552.
417. Tang, J.; Huang, F. P.; Wei, Y.; Bian, H. D.; Zhang, W.; Liang, H., Bovine Serum Albumin-Cobalt(II) Schiff Base Complex Hybrid: An Efficient Artificial Metalloenzyme for Enantioselective Sulfoxidation Using Hydrogen Peroxide. *Dalton Trans.* **2016,** *45* (19), 8061-8072.
418. Nigel-Etinger, I.; Mahammed, A.; Gross, Z., Covalent Versus Non-Covalent (Biocatalytic) Approaches for Enantioselective Sulfoxidation Catalyzed by Corrole Metal Complexes. *Catal. Sci. Technol.* **2011,** *1* (4), 578-581.
419. Mahammed, A.; Gross, Z., Albumin-Conjugated Corrole Metal Complexes: Extremely Simple yet Very Efficient Biomimetic Oxidation Systems. *J. Am. Chem. Soc.* **2005,** *127* (9), 2883-2887.
420. Herrero, C.; Quaranta, A.; Ricoux, R.; Trehoux, A.; Mahammed, A.; Gross, Z.; Banse, F.; Mahy, J. P., Oxidation Catalysis Via Visible-Light Water Activation of a $[Ru(Bpy)_3]^{2+}$ Chromophore BSA-Metallocorrole Couple. *Dalton Trans.* **2016,** *45* (2), 706-710.
421. Pordea, A.; Creus, M.; Panek, J.; Duboc, C.; Mathis, D.; Novic, M.; Ward, T. R., Artificial Metalloenzyme for Enantioselective Sulfoxidation Based on Vanadyl-Loaded Streptavidin. *J. Am. Chem. Soc.* **2008,** *130* (25), 8085-8088.

422. Esmieu, C.; Cherrier, M. V.; Amara, P.; Girgenti, E.; Marchi-Delapierre, C.; Oddon, F.; Iannello, M.; Jorge-Robin, A.; Cavazza, C.; Ménage, S., An Artificial Oxygenase Built from Scratch: Substrate Binding Site Identified Using a Docking Approach. *Angew. Chem., Int. Ed.* **2013,** *52* (14), 3922-3925.
423. Cherrier, M. V.; Girgenti, E.; Amara, P.; Iannello, M.; Marchi-Delapierre, C.; Fontecilla-Camps, J. C.; Ménage, S.; Cavazza, C., The Structure of the Periplasmic Nickel-Binding Protein NikA Provides Insights for Artificial Metalloenzyme Design. *J. Biol. Inorg. Chem.* **2012,** *17* (5), 817-829.
424. Cavazza, C.; Bochot, C.; Rousselot-Pailley, P.; Carpentier, P.; Cherrier, M. V.; Martin, L.; Marchi-Delapierre, C.; Fontecilla-Camps, J. C.; Ménage, S., Crystallographic Snapshots of the Reaction of Aromatic C-H with O_2 Catalysed by a Protein-Bound Iron Complex. *Nat. Chem.* **2010,** *2* (12), 1069-1076.
425. Rondot, L.; Girgenti, E.; Oddon, F.; Marchi-Delapierre, C.; Jorge-Robin, A.; Ménage, S., Catalysis without a Headache: Modification of Ibuprofen for the Design of Artificial Metalloenzyme for Sulfide Oxidation. *J. Mol. Catal. A: Chem.* **2016,** *416*, 20-28.
426. Buron, C.; Senechal-David, K.; Ricoux, R.; Le Caer, J. P.; Guerineau, V.; Mejanelle, P.; Guillot, R.; Herrero, C.; Mahy, J. P.; Banse, F., An Artificial Enzyme Made by Covalent Grafting of an Fe-II Complex into Beta-Lactoglobulin: Molecular Chemistry, Oxidation Catalysis, and Reaction-Intermediate Monitoring in a Protein. *Chem. - Eur. J.* **2015,** *21* (34), 12188-12193.
427. Faber, K., *Biotransformations in Organic Chemistry*. 6th ed.; Springer: 2011.
428. Baeckvall, J.-E., *Modern Oxidation Methods, 2nd Completely Revised*. Wiley-VCH Verlag GmbH & Co. KGaA: 2010.
429. Hashiguchi, S.; Fujii, A.; Haack, K.-J.; Matsumura, K.; Ikariya, T.; Noyori, R., Kinetic Resolution of Racemic Secondary Alcohols by Ru-Catalyzed Hydrogen Transfer. *Angew. Chem., Int. Ed.* **1997,** *36* (3), 288-290.
430. Thomas, C. M.; Letondor, C.; Humbert, N.; Ward, T. R., Aqueous Oxidation of Alcohols Catalyzed by Artificial Metalloenzymes Based on the Biotin-Avidin Technology. *J. Organomet. Chem.* **2005,** *690* (20), 4488-4491.
431. Smith, J. G., Synthetically Useful Reactions of Epoxides. *Synthesis* **1984,** (8), 629-656.
432. Xia, Q. H.; Ge, H. Q.; Ye, C. P.; Liu, Z. M.; Su, K. X., Advances in Homogeneous and Heterogeneous Catalytic Asymmetric Epoxidation. *Chem. Rev.* **2005,** *105* (5), 1603-1662.
433. Diez, D.; Nunez, M. G.; Anton, A. B.; Garcia, P.; Moro, R. F.; Garrido, N. M.; Marcos, I. S.; Basabe, P.; Urones, J. G., Asymmetric Epoxidation of Electron-Deficient Olefins. *Curr. Org. Synth.* **2008,** *5* (3), 186-216.
434. Okrasa, K.; Kazlauskas, R. J., Manganese-Substituted Carbonic Anhydrase as a New Peroxidase. *Chem. - Eur. J.* **2006,** *12*, 1587-1596.
435. Fernández-Gacio, A.; Codina, A.; Fastrez, J.; Riant, O.; Soumillion, P., Transforming Carbonic Anhydrase into Epoxide Synthase by Metal Exchange. *ChemBioChem* **2006,** *7*, 1013-1016.
436. Allard, M.; Dupont, C.; Munoz Robles, V.; Doucet, N.; Lledos, A.; Marechal, J. D.; Urvoas, A.; Mahy, J. P.; Ricoux, R., Incorporation of Manganese Complexes into Xylanase: New Artificial Metalloenzymes for Enantioselective Epoxidation. *ChemBioChem* **2012,** *13* (2), 240-251.
437. Koehler, V.; Mao, J.; Heinisch, T.; Pordea, A.; Sardo, A.; Wilson, Y. M.; Knoerr, L.; Creus, M.; Prost, J.-C.; Schirmer, T. et al, Oso_4·Streptavidin: A Tunable Hybrid Catalyst for the Enantioselective Cis-Dihydroxylation of Olefins. *Angew. Chem., Int. Ed.* **2011,** *50* (46), 10863-10866.
438. Colonna, S.; Manfredi, A.; Spadoni, M., The Effect of Organic Cosolvents on the Enantioselectivity in the Bovine Serum Albumin Catalyzed Weitz-Scheffer Condensation *Tetrahedron Lett.* **1987,** *28* (14), 1577-1580.
439. Laan, W.; Munoz, B. K.; den Heeten, R.; Kamer, P. C., Artificial Metalloenzymes through Cysteine-Selective Conjugation of Phosphines to Photoactive Yellow Protein. *ChemBioChem* **2010,** *11* (9), 1236-1239.
440. S. Konieczny; C. P. Fik; N. J. Averesch; Tiller, J. C., Organosoluble Enzyme Conjugates with Poly(2-Oxazoline)S Via Pyromellitic Acid Dianhydride. *J. Biotechnol.* **2012,** *159* (3), 195-203.
441. S. Konieczny; C. Krumm; D. Doert; K. Neufeld; Tiller, J. C., Investigations on the Activity of Poly(2-Oxazoline) Enzyme Conjugates Dissolved in Organic Solvents. *J. Biotechnol.* **2014,** *181*, 55-63.

442. S. Konieczny; M. Leurs; Tiller, J. C., Polymer Enzyme Conjugates as Chiral Ligands for Sharpless Dihydroxylation of Alkenes in Organic Solvents. *ChemBioChem* **2015,** *16* (1), 83-90.
443. Leurs, M.; Spiekermann, P. S.; Tiller, J. C., Optimization of and Mechanistic Considerations for the Enantioselective Dihydroxylation of Styrene Catalyzed by Osmate-Laccase-Poly(2-Methyloxazoline) in Organic Solvents. *ChemCatChem* **2016,** *8* (3), 593-599.
444. Miner, K. D.; Mukherjee, A.; Gao, Y.-G.; Null, E. L.; Petrik, I. D.; Zhao, X.; Yeung, N.; Robinson, H.; Lu, Y., A Designed Functional Metalloenzyme That Reduces O_2 to H_2o with over One Thousand Turnovers. *Angew. Chem., Int. Ed.* **2012,** *51* (23), 5589-5592.
445. Bhagi-Damodaran, A.; Petrik, I. D.; Marshall, N. M.; Robinson, H.; Lu, Y., Systematic Tuning of Heme Redox Potentials and Its Effects on O_2 Reduction Rates in a Designed Oxidase in Myoglobin. *J. Am. Chem. Soc.* **2014,** *136* (34), 11882-11885.
446. Liu, X.; Yu, Y.; Hu, C.; Zhang, W.; Lu, Y.; Wang, J., Significant Increase of Oxidase Activity through the Genetic Incorporation of a Tyrosine–Histidine Cross-Link in a Myoglobin Model of Heme–Copper Oxidase. *Angew. Chem., Int. Ed.* **2012,** *51* (18), 4312-4316.
447. Yu, Y.; Lv, X.; Li, J.; Zhou, Q.; Cui, C.; Hosseinzadeh, P.; Mukherjee, A.; Nilges, M. J.; Wang, J.; Lu, Y., Defining the Role of Tyrosine and Rational Tuning of Oxidase Activity by Genetic Incorporation of Unnatural Tyrosine Analogs. *J. Am. Chem. Soc.* **2015,** *137* (14), 4594-4597.
448. Yu, Y.; Zhou, Q.; Wang, L.; Liu, X.; Zhang, W.; Hu, M.; Dong, J.; Li, J.; Lv, X.; Ouyang, H. et al, Significant Improvement of Oxidase Activity through the Genetic Incorporation of a Redox-Active Unnatural Amino Acid. *Chem. Sci.* **2015,** *6* (7), 3881-3885.
449. Oohora, K.; Kihira, Y.; Mizohata, E.; Inoue, T.; Hayashi, T., C(sp3)-H Bond Hydroxylation Catalyzed by Myoglobin Reconstituted with Manganese Porphycene. *J. Am. Chem. Soc.* **2013,** *135* (46), 17282-17285.
450. Traviglia, S. L.; Datwyler, S. A.; Meares, C. F., Mapping Protein−Protein Interactions with a Library of Tethered Cutting Reagents: The Binding Site of σ^{70} on *Escherichia coli* RNA Polymerase. *Biochemistry* **1999,** *38* (14), 4259-4265.
451. Bruice, T. W.; Wise, J. G.; Rosser, D. S. E.; Sigman, D. S., Conversion of λ Phage Cro into an Operator-Specific Nuclease. *J. Am. Chem. Soc.* **1991,** *113* (14), 5446-5447.
452. Rana, T. M.; Meares, C. F., Specific Cleavage of a Protein by an Attached Iron Chelate. *J. Am. Chem. Soc.* **1990,** *112* (6), 2457-2458.
453. Greiner, D. P.; Miyake, R.; Moran, J. K.; Jones, A. D.; Negishi, T.; Ishihama, A.; Meares, C. F., Synthesis of the Protein Cutting Reagent Iron (S)-1-(P-Bromoacetamidobenzyl)Ethylenediaminetetraacetate and Conjugation to Cysteine Side Chains. *Bioconjugate Chem.* **1997,** *8* (1), 44-48.
454. Platis, I. E.; Ermacora, M. R.; Fox, R. O., Oxidative Polypeptide Cleavage Mediated by EDTA-Iron Covalently Linked to Cysteine Residues. *Biochemistry* **1993,** *32* (47), 12761-12767.
455. Erlanson, D. A.; Chytil, M.; Verdine, G. L., The Leucine Zipper Domain Controls the Orientation of AP-1 in the NFAT·AP-1·DNA Complex. *Chem. Biol.* **1996,** *3* (12), 981-991.
456. van Dongen, S. F. M.; Clerx, J.; Nørgaard, K.; Bloemberg, T. G.; Cornelissen, J. J. L. M.; Trakselis, M. A.; Nelson, S. W.; Benkovic, S. J.; Rowan, A. E.; Nolte, R. J. M., A Clamp-Like Biohybrid Catalyst for DNA Oxidation. *Nat. Chem.* **2013,** *5* (11), 945-951.
457. McDonald, A. G.; Tipton, K. F., Fifty-Five Years of Enzyme Classification: Advances and Difficulties. *FEBS J.* **2014,** *281* (2), 583-592.
458. Fersht, A. R., *Structure and Mechanism in Protein Science: A Guide to Enzyme Catalysis and Protein Folding*. W. H. Freeman and Company: New York, 1999.
459. Park, H. S.; Nam, S. H.; Lee, J. K.; Yoon, C. N.; Mannervik, B.; Benkovic, S. J.; Kim, H. S., Design and Evolution of New Catalytic Activity with an Existing Protein Scaffold. *Science* **2006,** *311* (5760), 535-538.
460. Zastrow, M. L.; Peacock, A. F. A.; Stuckey, J. A.; Pecoraro, V. L., Hydrolytic Catalysis and Structural Stabilization in a Designed Metalloprotein. *Nat. Chem.* **2012,** *4* (2), 118-123.
461. Innocenti, A.; Scozzafava, A.; Parkkila, S.; Puccetti, L.; De Simone, G.; Supuran, C. T., Investigations of the Esterase, Phosphatase, and Sulfatase Activities of the Cytosolic Mammalian Carbonic

Anhydrase Isoforms I, II, and XIII with 4-Nitrophenyl Esters as Substrates. *Bioorg. Med. Chem. Lett.* **2008,** *18* (7), 2267-2271.
462. Verpoorte, J. A.; Mehta, S.; Edsall, J. T., Esterase Activities of Human Carbonic Anhydrases B and C. *J. Biol. Chem.* **1967,** *242* (18), 4221-4229.
463. Zastrow, M. L.; Pecoraro, V. L., Influence of Active Site Location on Catalytic Activity in De Novo-Designed Zinc Metalloenzymes. *J. Am. Chem. Soc.* **2013,** *135* (15), 5895-5903.
464. Khare, S. D.; Kipnis, Y.; Greisen, P., Jr.; Takeuchi, R.; Ashani, Y.; Goldsmith, M.; Song, Y.; Gallaher, J. L.; Silman, I.; Leader, H. et al, Computational Redesign of a Mononuclear Zinc Metalloenzyme for Organophosphate Hydrolysis. *Nat. Chem. Biol.* **2012,** *8* (3), 294-300.
465. Siegel, J. B.; Zanghellini, A.; Lovick, H. M.; Kiss, G.; Lambert, A. R.; St Clair, J. L.; Gallaher, J. L.; Hilvert, D.; Gelb, M. H.; Stoddard, B. L. et al, Computational Design of an Enzyme Catalyst for a Stereoselective Bimolecular Diels-Alder Reaction. *Science* **2010,** *329* (5989), 309-313.
466. Jiang, L.; Althoff, E. A.; Clemente, F. R.; Doyle, L.; Rothlisberger, D.; Zanghellini, A.; Gallaher, J. L.; Betker, J. L.; Tanaka, F.; Barbas, C. F. et al, De Novo Computational Design of Retro-Aldol Enzymes. *Science* **2008,** *319* (5868), 1387-1391.
467. Rothlisberger, D.; Khersonsky, O.; Wollacott, A. M.; Jiang, L.; DeChancie, J.; Betker, J.; Gallaher, J. L.; Althoff, E. A.; Zanghellini, A.; Dym, O. et al, Kemp Elimination Catalysts by Computational Enzyme Design. *Nature* **2008,** *453* (7192), 190-195.
468. Der, B. S.; Edwards, D. R.; Kuhlman, B., Catalysis by a De Novo Zinc-Mediated Protein Interface: Implications for Natural Enzyme Evolution and Rational Enzyme Engineering. *Biochemistry* **2012,** *51* (18), 3933-3940.
469. Song, W. J.; Tezcan, F. A., A Designed Supramolecular Protein Assembly with in vivo Enzymatic Activity. *Science* **2014,** *346* (6216), 1525-1528.
470. Seelig, B.; Szostak, J. W., Selection and Evolution of Enzymes from a Partially Randomized Non-Catalytic Scaffold. *Nature* **2007,** *448* (7155), 828-831.
471. Seelig, B., mRNA Display for the Selection and Evolution of Enzymes from *in vitro*-Translated Protein Libraries. *Nat. Protoc.* **2011,** *6* (4), 540-552.
472. Chao, F. A.; Morelli, A.; Haugner, J. C.; Churchfield, L.; Hagmann, L. N.; Shi, L.; Masterson, L. R.; Sarangi, R.; Veglia, G.; Seelig, B., Structure and Dynamics of a Primordial Catalytic Fold Generated by *in vitro* Evolution. *Nat. Chem. Biol.* **2013,** *9* (2), 81-83.
473. Morelli, A.; Haugner, J.; Seelig, B., Thermostable Artificial Enzyme Isolated by *in vitro* Selection. *Plos One* **2014,** *9* (11), e112028.
474. Bryson, J. W.; Desjarlais, J. R.; Handel, T. M.; DeGrado, W. F., From Coiled Coils to Small Globular Proteins: Design of a Native-Like Three-Helix Bundle. *Protein Sci.* **1998,** *7* (6), 1404-1414.
475. Cangelosi, V. M.; Deb, A.; Penner-Hahn, J. E.; Pecoraro, V. L., A De Novo Designed Metalloenzyme for the Hydration of CO_2. *Angew. Chem., Int. Ed.* **2014,** *53* (30), 7900-7903.
476. Jackman, J. E.; Merz, K. M.; Fierke, C. A., Disruption of the Active Site Solvent Network in Carbonic Anhydrase II Decreases the Efficiency of Proton Transfer. *Biochemistry* **1996,** *35* (51), 16421-16428.
477. Jewell, D. A.; Tu, C. K.; Paranawithana, S. R.; Tanhauser, S. M.; Lograsso, P. V.; Laipis, P. J.; Silverman, D. N., Enhancement of the Catalytic Properties of Human Carbonic Anhydrase-III by Site-Directed Mutagenesis. *Biochemistry* **1991,** *30* (6), 1484-1490.
478. Korendovych, I. V.; Kulp, D. W.; Wu, Y.; Cheng, H.; Roder, H.; DeGrado, W. F., Design of a Switchable Eliminase. *Proc. Natl. Acad. Sci. U. S. A.* **2011,** *108* (17), 6823-6827.
479. Laan, W.; Munoz, B. K.; den Heeten, R.; C., K. P., Artificial Metalloenzymes through Cysteine-Selective Conjugation of Phosphines to Photoactive Yellow Protein. *ChemBioChem* **2010,** *11* (9), 1236-1239.
480. Deuss, P. J.; Popa, G.; Botting, C. H.; Laan, W.; Kamer, P. C. J., Highly Efficient and Site-Selective Phosphane Modification of Proteins through Hydrazone Linkage: Development of Artificial Metalloenzymes. *Angew. Chem. Int. Edit.* **2010,** *49* (31), 5315-5317.
481. Mills, J. H.; Khare, S. D.; Bolduc, J. M.; Forouhar, F.; Mulligan, V. K.; Lew, S.; Seetharaman, J.; Tong, L.; Stoddard, B. L.; Baker, D., Computational Design of an Unnatural Amino Acid Dependent Metalloprotein with Atomic Level Accuracy. *J. Am. Chem. Soc.* **2013,** *135* (36), 13393-13399.

482. Urvoas, A.; Ghattas, W.; Marechal, J. D.; Avenier, F.; Bellande, F.; Mao, W.; Ricoux, R.; Mahy, J. P., Neocarzinostatin-Based Hybrid Biocatalysts with a RNase Like Activity. *Bioorg. Med. Chem.* **2014,** *22* (20), 5678-5686.
483. Reetz, M. T.; Peyralans, J. J. P.; Maichele, A.; Fu, Y.; Maywald, M., Directed Evolution of Hybrid Enzymes: Evolving Enantioselectivity of an Achiral Rh-Complex Anchored to a Protein. *Chem. Commun.* **2006,** (41), 4318-4320.
484. Arnold, F. H., Design by Directed Evolution. *Acc. Chem. Res.* **1998,** *31* (3), 125-131.
485. Joó, F.; Kathó, Á., Recent Developments in Aqueous Organometallic Chemistry and Catalysis. *J. Mol. Catal. A: Chem.* **1997,** *116* (1), 3-26.
486. Sletten, E. M.; Bertozzi, C. R., Bioorthogonal Chemistry: Fishing for Selectivity in a Sea of Functionality. *Angew. Chem., Int. Ed.* **2009,** *48* (38), 6974-6998.
487. Garcia-Viloca, M.; Gao, J.; Karplus, M.; Truhlar, D. G., How Enzymes Work: Analysis by Modern Rate Theory and Computer Simulations. *Science* **2004,** *303* (5655), 186-195.
488. Ragsdale, S. W., Metals and Their Scaffolds to Promote Difficult Enzymatic Reactions. *Chem. Rev.* **2006,** *106* (8), 3317-3337.
489. Muñoz Robles, V.; Ortega-Carrasco, E.; Alonso-Cotchico, L.; Rodriguez-Guerra, J.; Lledós, A.; Maréchal, J.-D., Toward the Computational Design of Artificial Metalloenzymes: From Protein–Ligand Docking to Multiscale Approaches. *ACS Catal.* **2015,** *5* (4), 2469-2480.
490. Romero, P. A.; Arnold, F. H., Exploring Protein Fitness Landscapes by Directed Evolution. *Nat. Rev. Mol. Cell Biol.* **2009,** *10* (12), 866-876.
491. Reetz, M. T.; Rentzsch, M.; Pletsch, A.; Taglieber, A.; Hollmann, F.; Mondiere, R. J.; Dickmann, N.; Hocker, B.; Cerrone, S.; Haeger, M. C. et al, A Robust Protein Host for Anchoring Chelating Ligands and Organocatalysts. *ChemBioChem* **2008,** *9*, 552-564.
492. Belsare, K.; Andorfer, M. C.; Cardenas, F.; Chael, J.; Park, H.-J.; Lewis, J. C., A Simple Combinatorial Codon Mutagenesis Method for Targeted Protein Engineering. In *submitted*, 2016.
493. Landwehr, M.; Carbone, M.; Otey, C. R.; Li, Y.; Arnold, F. H., Diversification of Catalytic Function in a Synthetic Family of Chimeric Cytochrome P450s. *Chem. Biol.* **2007,** *14* (3), 269-278.
494. Heins, R. A.; Cheng, X.; Nath, S.; Deng, K.; Bowen, B. P.; Chivian, D. C.; Datta, S.; Friedland, G. D.; D' Haeseleer, P.; Wu, D. et al, Phylogenomically Guided Identification of Industrially Relevant Gh1 Β-Glucosidases through DNA Synthesis and Nanostructure-Initiator Mass Spectrometry. *ACS Chem. Biol.* **2014,** *9* (9), 2082-2091.
495. Sardo, A.; Wohlschlager, T.; Lo, C.; Zoller, H.; Ward, T. R.; Creus, M., Burkavidin: A Novel Secreted Biotin-Binding Protein from the Human Pathogen Burkholderia Pseudomallei. *Protein Expression Purif.* **2011,** *77* (2), 131-139.
496. Sasmal, P. K.; Streu, C. N.; Meggers, E., Metal Complex Catalysis in Living Biological Systems. *Chem. Commun.* **2013,** *49* (16), 1581-1587.
497. Wallace, S.; Balskus, E. P., Opportunities for Merging Chemical and Biological Synthesis. *Curr. Opin. Biotechnol.* **2014,** *30*, 1-8.